Volume 33 JNSChE ISSN
No. 2 Sep/Oct 2018 0794-6759

JOURNAL OF THE NIGERIAN SOCIETY OF CHEMICAL ENGINEERS

Published by,
THE NIGERIAN SOCIETY OF CHEMICAL ENGINEERS
National Secretariat: Infinite Grace House, Plot 4, Oyetubo Street,
Off Obafemi Awolowo Way, Ikeja, Lagos State, Nigeria.
E-mail: nationalhqtrs@nsche.org, nsche_headquarters@yahoo.com
Website: http:www.nsche.org.ng
Submission of Manuscripts: nschejournal@yahoo.com and copy: stevmomoh@yahoo.com

JOURNAL OF THE NIGERIAN SOCIETY OF CHEMICAL ENGINEERS
A Publication on the Science and Technology of Chemical Engineering

EDITORIAL BOARD

2018 NIGERIAN SOCIETY OF CHEMICAL ENGINEERS

BOARD OF DIRECTORS AND OFFICIALS

Prof. Sam S. Adefila, *FNSChE*	National President
Engr. O. A. Anyaoku, *FNSChE*	Deputy National President
Prof. E. N. Wami A, *FNSChE*	Immediate Past President
Engr. D. Uweh, *MNSChE*	Publicity Secretary
Engr. Ben Akaakar, *FNSChE*	Asst. Publicity Secretary
Engr. Anthony Ogheneovo, *MNSChE*	National Treasurer
Engr. (Mrs.) Edith A. Alagbe, *MNSChE*	Asst. National Treasurer
S. O. Bosoro, *MNSChE*	Executive Secretary

INTERNAL AUDITORS

Engr. Dr. Mrs. G. Akujobi-Emetuche, *FNSChE*
Engr. Edwin N.Ikezue, *FNSChE*

SUBSCRIPTION

a.	**Individual Readers**	₦3,000.00
b.	**Overseas Subscribers**	US$100.00
c.	**Institution, Libraries, etc**	₦5,000.00

CHAPTER CHAIRMEN

Engr. G. H. Abubakar, *MNSChE*	Kogi
Engr. (Mrs.) Rosemary O. Imhanwa, *MNSChE*	Edo/Delta
Engr. I. A. Dirani, *MNSChE*	ABBYGOT
Prof. I. A. Mohammed-Dabo, *MNSChE*	Kaduna
Dr. M. S. Nwakaudu, *FNSChE*	Imo/Abia
Prof. G. O. Mbah, *FNSChE*	Anambra/Enugu/ Ebonyi
Dr. A. A. Ujile,*FNSChE*	RIVBAY
Engr. N. A. Akanji,*MNSChE*	Niger
Engr. O. O. Onugu, *MNSChE*	FCT/Nasarawa
Prof. F. A. Akeredolu, *FNSChE*	Oyo/Osun/Kwara
Dr. K. F. K. Oyedeko, *FNSChE*	Lagos/Ogun
Engr. T. S. Soom, *MNSChE*	Benue Industrial
Dr. I. O. Oboh , *MNSChE*	Akwa Ibom/Cross River
Dr. E. I. Dada, *FNSChE*	USA

CONTROL SYSTEM DESIGN FOR MULTIVARIABLE NONLINEAR SYSTEMS GUARANTEEING GOOD PERFORMANCE OVER WIDE OPERATING RANGES

***Taiwo, O., Adeyemo, S. O. and Sorinolu A.**

Process Systems Engineering Laboratory, Obafemi Awolowo University, Ile-Ife, Nigeria
(E-mails:femtaiwo@yahoo.com, ftaiwo@oauife.edu.ng, adeyesam@yahoo.com, adeolasorinolu@yahoo.com)

ABSTRACT:

It is sometimes necessary that a process plant operates over a wide range while satisfying desired performance and stipulated constraints**.** This paper proposes a method based on computing a mean (nominal) plant, uncertainty weight based on the deviations of the extreme plants from the mean plant and performance weights capturing desired performance. The work considers simple multi-loop and centralized controllers and their parameter determination using optimization. In order to expeditiously compute the centralized controller parameters, its initial parameters are determined using the parameterization based on the multivariable internal model controller (MIMC) of the p/q Pade approximant of the mean plant. The order of magnitude of the MIMC filter is determined by noting the magnitude of a suitably computed multiloop controller which, at least, stabilizes the closed loop system. In this work, desired metrics for the closed loop system include robust performance, minimization of the closed loop system integral of squared error (ISE) and limiting the maximum controller outputs over the full operating range. It is demonstrated that the new method facilitates the computation of simple centralized controllers yielding closed loop systems with favorable characteristics.

Keywords: Nonlinear systems, uncertainty, robust performance, centralized controllers, optimization.

1. INTRODUCTION

A typical control engineering problem entails the design of a control system subject to closed-loop stability and certain performance requirements (Oloomi and Shafai, 2011). The requirements may include the figures of merit such as gain/phase margin, bandwidth, and tracking error to a reference command. The robust control theory attempts to address the question of stability and performance of multivariable systems in the face of modelling errors and unknown disturbances (Zhou et al., 1996, Skogestad and Postlethwaite, 2005).

Un-modelled dynamics, non linearity of systems and the existence of disturbances are largely responsible for the inability of linear control systems theory to reach the ideal solution. For this, Fard et al (2013) identified several targets that are often attended to in a control system namely: robust stability, nominal performance, robust performance, operating limitation on controlling signal and minimized disturbance effect.

In robust control theory, the question concerning the achievable performance limits is generally posed as an optimization problem in an appropriate mathematical setting. A major benefit of this approach is that it provides a means to optimize the system performance by trading off various stringent, and often conflicting, specifications against each other.

Gu et al (2005) synthesized robust controllers for some physical and chemical systems using H∞ synthesis, H∞ Loop-shaping Design Procedures (LSDP), and μ synthesis. Oloomi and Shafai (2011) specifically worked on optimizing the tracking performance in robust process control by deriving expressions relating the tracking error specifications to various parameters of the weighting functions used in the mixed S/T sensitivity design.

In some other works, different optimization procedures have been combined to obtain a single robust controller. For instance, Fard et al (2013) carried out a combination of two methods: μ and H_2/H_∞. Similarly McKernan et al (2009) combined the method of inequalities (MoI) with McFarlane and Glover's H_∞ LSDP in a mixed-optimization approach.

In this work simple controllers such as PI(D) are parameterized using internal model control (IMC) theory for multi-loop and centralized structures. After determining initial controller parameters on observing closed loop responses, MATLAB optimization toolbox is exploited in computing optimal values satisfying multiple objectives such as stability, minimum integral of the squared error, robust performance measure as well as minimizing the peak controller outputs.

In section 2, we give a brief background description of the design techniques used in this work while applications of these methods to typical nonlinear multivariable systems are presented in section 3. The performances of the resulting control systems were compared based on integral squared error values, the structured singular values for robust performance and ability to minimize the peak controller outputs. A discussion of the results and conclusions from the work are considered in section 4.

2. METHODOLOGY

2.1 Uncertainty Modelling

We consider the average plant (going by the Nyquist plots of different operating points) as the nominal model. Then the deviation of the models of the other operating points from this nominal model was plotted as a function of frequency, and the upper bounds of these deviations were captured by curve fitting to give the relation for the uncertainty weight.

2.2 Controller Design and Optimization

Well known IMC tuning relations for single input single output (SISO) systems (see, for example, Seborg, et al., 2014, Table 12.1) and multivariable (MIMC) systems, introduced here, are used respectively to parameterize PI(D) multiloop and centralized multivariable controllers. The quality of the closed loop responses are used to fix the initial values of these controllers. Thereafter, optimal controller parameters are computed using MATLAB optimization toolbox.

2.2.1 Computation of p/q Pade approximant and parameterization of the centralized controller using MIMC

If it is desired to use the new method to design a simple feedback controller for the plant then the p/q Pade approximant of the mean plant should be computed. This is undertaken as follows: Expand the plant model G(s) in infinite series about a real point a:

$$G(s) = \sum_{i=0}^{\infty} G_i (s-a)^i \tag{1}$$

Here, without loss of generality, we elect to express its reduced model R(s) in the right matrix fraction form, (Taiwo and Krebs, 1995, Kailath, 1980):

$$R(s) = \left(\sum_{i=0}^{p} V_i s^i \right) \left(\sum_{i=0}^{q} T_i s^i \right)^{-1}, \quad (T_q = I) \tag{2}$$

R(s) is a p/q Pade approximant at s=a if R(s) is asymptotically stable and

$$\sum_{i=0}^{q-1} G_{r-i} T_i = -G_{r-q} \quad (q \le r \le p+q) \tag{3}$$

$$V_\mu = \sum_{i=0}^{r} G_{r-i} T_i \quad (0 \le r \le p) \tag{4}$$

In (3) and (4), $G_r = 0$, $r < 0$. A unique solution exists and

$$R(s) = G(s) + O((s-a)^{p+q+1}) \tag{5}$$

where the notation means that the power series expansion on both sides exists and agree up to terms of degree (p+q) inclusive. However, if expansion about s=a does not furnish a stable p/q Pade approximant, Taiwo and Krebs (1995) have shown how, generically, a stable approximant may be obtained by resorting to matching moments about more than the single point s=a. All the controllers designed in this work were based on parameterizing a classical feedback controller from the MIMC controller computed from the 0/1 Pade approximant of the original mean plant. Consequently, for space economy, we limit discussion to this case in the sequel.

Assume that the PI controller is desired, then the 0/1 reduced model R(s) given by

$$R(s) = V_o(Is + T_o)^{-1} \tag{6}$$

will be computed. In order to obtain the MIMC controller $\bar{Q}$, invert (6), giving,

$$\bar{Q} = R^{-1} = (Is + T_o)V_o^{-1} \tag{7}$$

also, $Q = \bar{Q}f$ where f is the filter given by

$$f = 1/(\lambda s + 1) \tag{8}$$

The conventional feedback controller C(s) is given by

$$C(s) = \bar{Q}f(I - fI)^{-1} \tag{9}$$

For illustration purposes, suppose G(s) is 3*3 and $\bar{Q}f = (q_{ij})/(\lambda s + 1)$, (9) simplifies to

$$C(s) = \frac{1}{\lambda s}\begin{bmatrix} q_{11} & q_{12} & q_{13} \\ q_{21} & q_{22} & q_{23} \\ q_{31} & q_{32} & q_{33} \end{bmatrix} \tag{10}$$

where $q_{ij} = \hat{V}_{oij} s + \hat{G}_{oij}$ (11)

and $\hat{V}_{oij}$, $\hat{G}_{oij}$ respectively denotes the (i,j)th element of V_o^{-1} and G_o^{-1}.

The next issue is the choice of λ. One way to determine a preliminary value is to compute the multi-loop controllers for the original plant. The order of magnitude observed here should be used to estimate the starting value of λ in order to optimize the parameters of the feedback controller, C(s). Usually it is advisable to start with a λ which gives a closed loop stable system. A detailed exposition of this procedure will be given in the next Section. If it is desired to use a PID controller, then either a ½ or 0/2 Pade approximant of mean plant would be used for feedback controller parameterization.

3. ILLUSTRATIVE EXAMPLES

.3.1 Example 1: Six-Spherical Tank Plant

The six-spherical tank system (Figure 1) is a theoretical case study that was posited by Escobar and Trierweiler (2013).

The control objective is to maintain the lower levels h_3 and h_6 at their reference values (set points) by manipulating the opening of the two valves (x_1, x_2), with $0 \leq x_1, x_2 \leq 1$, and defining the flow rates as F_1 and F_2.

The following set of differential equations was derived as model describing the system:

$$A_1 \frac{dh_1}{dt} = x_1 F_1 - R_1\sqrt{h_1}$$

$$A_2 \frac{dh_2}{dt} = R_1\sqrt{h_1} - R_2\sqrt{h_2}$$

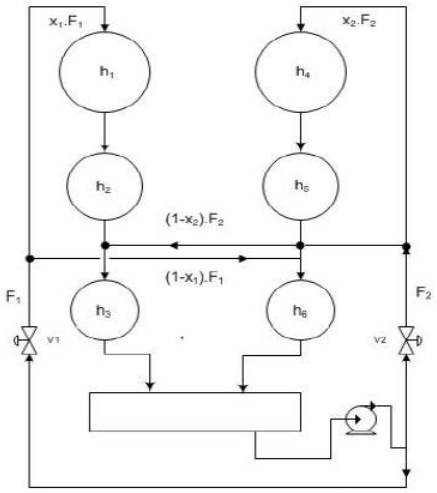

Figure 1: Schematic Diagram of Six-Tank System

$$A_3 \frac{dh_3}{dt} = (1 - x_2)F_2 + R_2\sqrt{h_2} - R_3\sqrt{h_3}$$

$$A_4 \frac{dh_4}{dt} = x_2 F_2 - R_4\sqrt{h_4}$$

$$A_5 \frac{dh_5}{dt} = R_4\sqrt{h_4} - R_5\sqrt{h_5}$$

$$A_6 \frac{dh_6}{dt} = (1 - x_1)F_1 + R_5\sqrt{h_5} - R_6\sqrt{h_6} \qquad (6)$$

where A_i denotes the tank i cross-sectional area, g is the acceleration due to gravity, R_i is the tank i discharge coefficient, a_i is the cross-sectional area of the tank i discharge pipe, and D_i is the tank i diameter.

$$A_i = \pi(D_i h_i - h_i^2) \quad \text{and} \quad R_i = a_i\sqrt{2g}$$

Four operating conditions are considered (Tables1 & 2).

Table 1: Process Parameters for Six-tank System

Parameters	Value
D_1 D_4 [cm]	35
D_2 D_5 [cm]	30
D_3 D_6 [cm]	25
R_1 R_4 [$cm^{2.5}min^{-1}$]	1690
R_2 R_5 [$cm^{2.5}min^{-1}$]	1830
R_3 R_6 [$cm^{2.5}min^{-1}$]	2000

Table 2: Operating Points of Six-tank System

Variables	OP1	OP2	OP3	OP4
$h_{1s}[\boldsymbol{cm}]$	2.7450	9.6504	2.7450	9.6504
$h_{2s}[\boldsymbol{cm}]$	2.3411	3.2303	2.3411	8.2303
$h_{3s}[\boldsymbol{cm}]$	4.8400	17.0156	8.4100	11.7306
$h_{4s}[\boldsymbol{cm}]$	2.0167	7.0901	7.0901	2.0167
$h_{5s}[\boldsymbol{cm}]$	1.7200	6.0468	6.0468	1.7200
$h_{6s}[\boldsymbol{cm}]$	3.2400	11.3906	8.1225	5.4056
$F_{1s}[L\ min^{-1}]$	4	7.5	4	7.5
$F_{2s}[L\ min^{-1}]$	4	7.5	7.5	4
x_1, x_2	0.7, 0.6	0.7, 0.6	0.7, 0.6	0.7, 0.6

$$\begin{bmatrix} h_3(s) \\ h_6(s) \end{bmatrix} = \begin{bmatrix} \frac{x_1 c_1 e^{-0.9s}}{\prod_{i=1}^{3}(\tau_i s+1)} & \frac{(1-x_2)c_1 e^{-0.3s}}{(\tau_3 s+1)} \\ \frac{(1-x_1)c_2 e^{-0.3s}}{(\tau_6 s+1)} & \frac{x_1 c_1 e^{-0.9s}}{\prod_{i=4}^{6}(\tau_i s+1)} \end{bmatrix} \begin{bmatrix} F_1(s) \\ F_2(s) \end{bmatrix} \qquad (7)$$

where $c_1 = \frac{2\sqrt{h_{3s}}}{R_3}$, $c_2 = \frac{2\sqrt{h_{6s}}}{R_6}$ and $\tau_i = \frac{2A_i\sqrt{h_{is}}}{R_i}$

The nominal model considered for controller design and optimization is given as

$$G_{nom} = \begin{bmatrix} \frac{2.215(1-0.9s)}{(0.5454s+1)(0.0883s+1)(2.3s+1)} & \frac{1.265(1-0.3s)}{(1.2175s+1)} \\ \frac{0.77625(1-0.3s)}{(1.02115s+1)} & \frac{1.5525(1-0.9s)}{(0.0712s+1)(1.2227s+1)(1.20s+1)} \end{bmatrix} \qquad (8)$$

which corresponds to the nominal linearized model of operating point 2 (OP2). In Figure 2, we show how well this plant represents the average plant of the four operating points. The multiplicative input uncertainty modelled for this system to cover all the operating points is given by:

$$W_i = \text{diag}(w_i, w_i);\ w_i(s) = \frac{1.7395(s+0.0422)(s+0.2550)}{(s+0.4816)(s+0.1268)} \qquad (9)$$

w_i increases from a magnitude of about 30% at low frequencies to approximately 175% at high frequency reaching 100% uncertainty at about 0.25rad/min

3.1.1 Controller Design and Optimization

The classical feedback structure has been used in this work. Relative gain array, RGA was calculated for the above approximated transfer function and we obtained $\begin{pmatrix} 1.3997 & -0.3997 \\ -0.3997 & 1.3997 \end{pmatrix}$. This suggests a diagonal pairing. IMC tuning relation was employed to obtain the initial controller parameters after the diagonal elements in (8) were approximated as first order plus time delay (FOPTD) and final values obtained after optimization using MATLAB Optimization Toolbox which facilitates constraints handling (fmincon) to minimize ISE and satisfy the constraint of structured singular value for robust performance $\mu_{RP} < 1$ using MATLAB robust control Toolbox. For robust performance analyses, we consider the performance weight

$$W_P = diag(w_p, w_p) \quad , \quad w_p = \frac{0.4s+0.02}{s} \qquad (10)$$

With this, we have specified maximum sensitivity, Ms=2.5 (with an implication that gain margin $GM \geq 1.67$, phase margin $PM \geq 23.07^o$) and bandwith $\omega_B^* = 0.02$rad/s. The best parameters obtained for the multi-loop controller for the controller K(s)=diag(p1+p2/s,p3+p4/s) are given by

p=[0.1882 0.03634 0.08559 0.03739], with an initial controller parameters p_0 = [0.1206 0.03285 0.17488 0.05999]. This corresponds to using an IMC tuning parameter of λ=1.8.

In designing the centralized controller, following the development in Section 2, the values of V_0^{-1} and G_0^{-1}

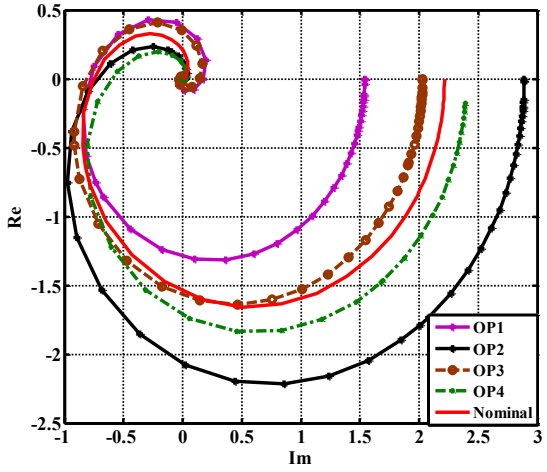

2(a) Element (1,1)

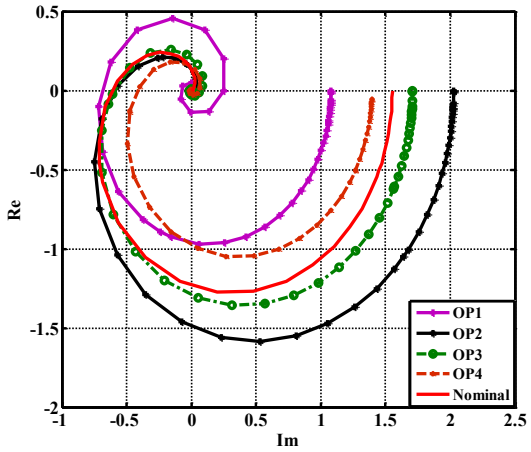

2(b) Element (2,2)

Figure 2: Nyquist Plots of diagonal elements of different Ops for six-tank system

calculated from the 0/1 Pade approximant of the nominal plant at s=0, and the magnitude of the elements of the multi-loop controller, λ is taken as 100. The final multivariable controller computed using MATLAB Optimization Tollbox fmincon and the robust analysis toolbox is given by p =[0.1910 0.0325 -0.0115 -0.0089 -0.0039 0.0056 0.0822 0.0376]. The performances of these controllers are assessed by tabulating the structured singular values when they are implemented in the closed loop system (Table 3). The performance of the nonlinear closed loop system over the entire operating range was also tested by simulation using both the multi-loop and multivariable and two other controllers obtained using μ-synthesis, namely the full 22nd order (Mu-22) and the reduced 2nd order Mu-2) controllers. The simulation starts with the process operating in OP2 and the process moves to OP4, OP1, OP3 and OP4 in succession, until 500min have elapsed as given in Fig 3. The ISE and maximum controller outputs over this simulation scenario are given in Table 3, indicating that the controller yielded by the new method outperforms Mu-2 of the same (second) order. It was impossible to compare our results with those of Escobar and Trierweiler (2013) as their controller parameters were not given.

Table 3. Performance Metrics of Controllers

Controller	μ_{RP}	ISE	Max|U|	
			U1	U2
Mu-22	0.95	1012	7.94	7.62
Mu-2	0.90	1411	7.86	7.63
Proposed(centralized)	0.94	1188	7.95	7.50
Proposed(decentralized)	0.96	1155	8.00	7.50

The closeness between the performances of the system with the multi-loop and centralized controllers is due to the transfer function being essentially diagonally dominant and the system being non-minimum phase, thus limiting transient performance via control means.

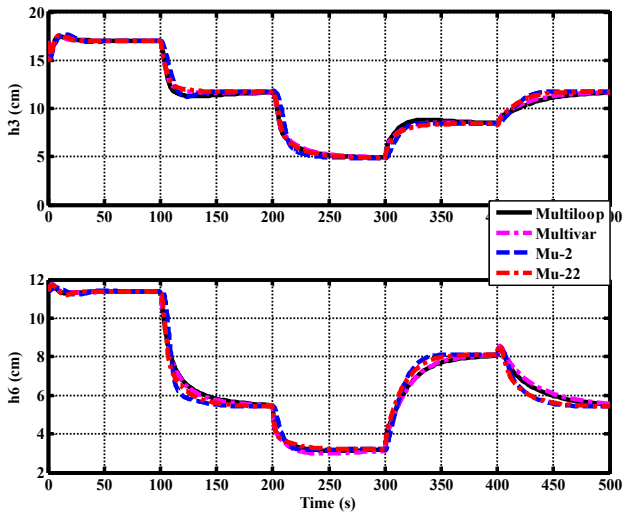

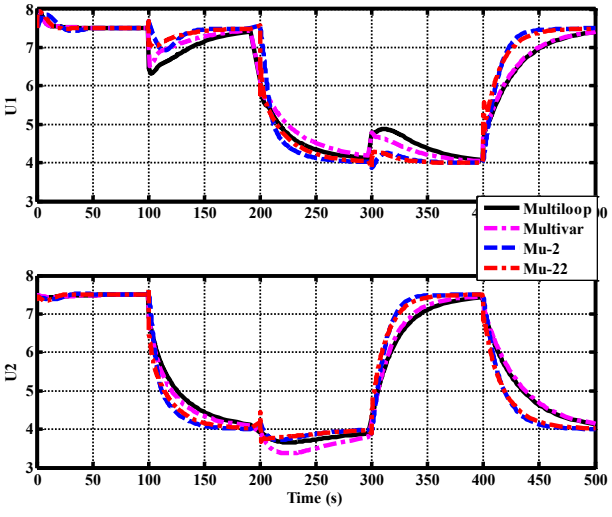

Figure 3. Response of the nonlinear closed loop system to a scenario of changes in operating points.

3.2 Example 2. Nonlinear Boiler-Turbine Alternator

The differential equations for this process (Garrido et al 2012) are:

$$\dot{x}_1 = -0.0018u_2x_1^{9/8} + 0.9u_1 - 0.15u_3$$
$$\dot{x}_2 = (0.073u_2 - 0.016)x_1^{9/8} - 0.15x_2$$
$$\dot{x}_3 = \frac{(141u_3 - (1.1u_2 - 0.19)x_1)}{85}$$
$$y_1 = x_1$$
$$y_2 = x_2$$
$$y_3 = 0.05(0.13073x_3 + 100a_{cs} + \frac{q_e}{9} - 67.975)$$
$$a_{cs} = \frac{(1-0.001538x_3)(0.8x_1 - 25.6)}{x_3(1.0394 - 0.0012304x_1)}$$
$$q_e = (0.854u_2 - 0.147)x_1 + 45.59u_1 - 2.514u_3 - 2.096$$

where state variables x_1, x_2 and x_3 denote the drum pressure (kg/cm^2), power output (MW) and fluid density (kg/m^3), respectively. The output y_3 is the drum water level (m) and a_{cs} and q_e are steam quality and evaporation rate (kg/s), respectively. The inputs u_1, u_2 and u_3 are the valve positions for fuel flow, steam control, and feed-water flow, respectively. Because of actuator limitations, the control inputs are subjected to the constraints given by

$0 \le u_i \le 1$ (i = 1, 2, 3)

$|\dot{u}_1| \le 0.007$

$-2 \le \dot{u}_2 \le 0.02$

$|\dot{u}_3| \le 0.05$

However, the linear control design for the plant found in the literature usually takes the linearized model at the operating point 4: x_s = [108 66.65 428]^T, u_s = [0.34 0.69 0.433]^T and y_s = [108 66.65 0]^T.

3.2.1 Nominal model

Following previous investigators, operating point 4 has been chosen as the nominal model and has been found to be a good average plant of the four (4) operating points considered here. It has the following transfer function matrix.

$$G_{OP4} = \begin{bmatrix} g_{11}(s) & g_{12}(s) & g_{13}(s) \\ g_{21}(s) & g_{22}(s) & g_{23}(s) \\ g_{31}(s) & g_{32}(s) & g_{33}(s) \end{bmatrix}$$

where $g_{11}(s) = \frac{358.7}{398.6s+1}$, $g_{12}(s) = \frac{-139.1}{398.6s+1}$, $g_{13} = \frac{-59.79}{398.6s+1}$,

$g_{22}(s) = \frac{44.96(1255.3s+1)}{(398.6s+1)(10s+1)}$, $g_{23}(s) = \frac{-41.49}{(398.6s+1)(10s+1)}$

$g_{21}(s) = 249.1/((398.6s+1)(10s+1))$

$g_{31} = \frac{0.0113(34.58s+1)(258.33s-1)}{(398.6s+1)s}$

$g_{32} = (0.0022(1428.6s+1)(65.15s-1))/(398.6s+1)s$

$g_{33}(s) = \frac{-0.0097(282.57s+1)(2.03s-1)}{(398.6s+1)s}$

3.2.2 Control Objectives

Following previous workers, the goal is to obtain a single controller such that the closed loop system will be stable and have good performance over the operating points 3, 4, 5 and 6.

The simulation began with OP4 (y = [108 66.7 0]'), and then moves on to OP3 (y = [97.2 50.5 -0.32]'), OP5 (y = [119 85.1 0.32]'), OP4 (y = [108 66.7 0]') and finally OP6 (y = [130 105 0.64]').

Figure 4 shows the plot of the magnitude of the relative deviation of the different operating points considered from the nominal model. The uncertainty weight that captures the upper bound of these deviations is given by the equation

$$W_I = diag(w_i, w_i, w_i);\ w_i = \frac{0.5791s+0.1393}{s+0.3134}$$

In the same figure is shown how the fitted uncertainty weight captures the upper bound of these deviations at all frequencies. The uncertainty under consideration increases in magnitude from about 45 – 58% as the frequency increases.

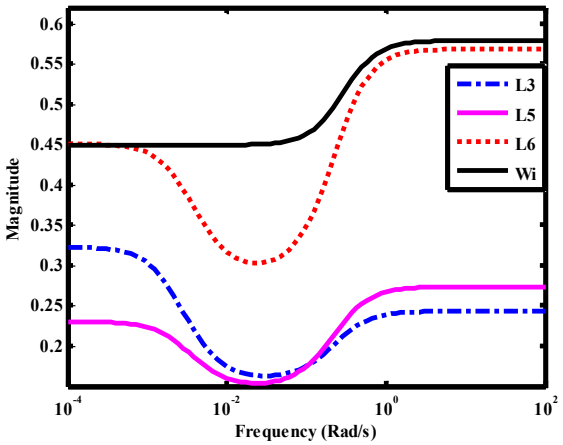

Figure 4: Uncertainty Weight and Relative Deviations of OPs 3, 5 and 6 from Nominal OP4

3.2.3 Controller Design

Although a multi-loop control structure was determined, it soon became clear that it would lead to a closed loop system with severe interaction. Hence only the centralized controller will be discussed further here.

As this plant is open loop unstable, a reduced Pade approximant was calculated from Taylor series expansion about s=0.001 (because $G_{op4}(0)$ is null and hence is not analytic at s=0 for series expansion), yielding

$$V_0^{-1} = \begin{bmatrix} 0.5917 & 0.2185 & 5.31 \\ -0.0186 & 0.069 & -0.0036 \\ -0.444 & 1.1507 & 31.867 \end{bmatrix}, G_0^{-1} = \begin{bmatrix} 0.001 & 0.0037 & 0.0106 \\ -0.0049 & 0.0071 & 0 \\ -0.0008 & 0.0057 & 0.0638 \end{bmatrix}$$

From observing the magnitudes of the terms in the multi-loop controller designed for this system, (not reported here for the sake of brevity) λ=100 was used. After some iterations and with an emphasis to compute a robust controller, the following controller parameters were obtained:

$$C(s)=\begin{bmatrix}0.16 & -0.12 & 1.096\\ 0.05 & 0.17 & -0.001\\ 0.2 & -0.2 & 5.85\end{bmatrix}+\frac{1}{s}\begin{bmatrix}0.18 & 0.18 & 0.08\\ 0.17 & 0.16 & 0.06\\ 0.012 & 0.2 & 0.135\end{bmatrix}$$

Fig.5 shows the controller's excellent performance over the operation envelope while its metrics are given in Table 4. The switching between OPs begins with OP4 before moving to OP3, OP5, OP4 and finally OP6 for period of 100 each. The original 27th order μ-synthesis controller was reduced to 5th order (Mu-5). It is observed that the third order simple PI controller compares well with other more complex controllers. Although the Garrido centralized controller includes a derivative term, its ISE is much larger.

Table 4. Performance Metrics of Controllers

Controller	μ_{RP}	ISE	Max |U|		
			U1	U2	U3
Mu-27	1.04	3470	6.74	6.28	14.19
Mu- 5	1.09	1034	46.90	11.40	18.88
Proposed	0.91	5627	7.76	8.34	22.83
Garrido	1.02	33953	1.49	1.00	1.92

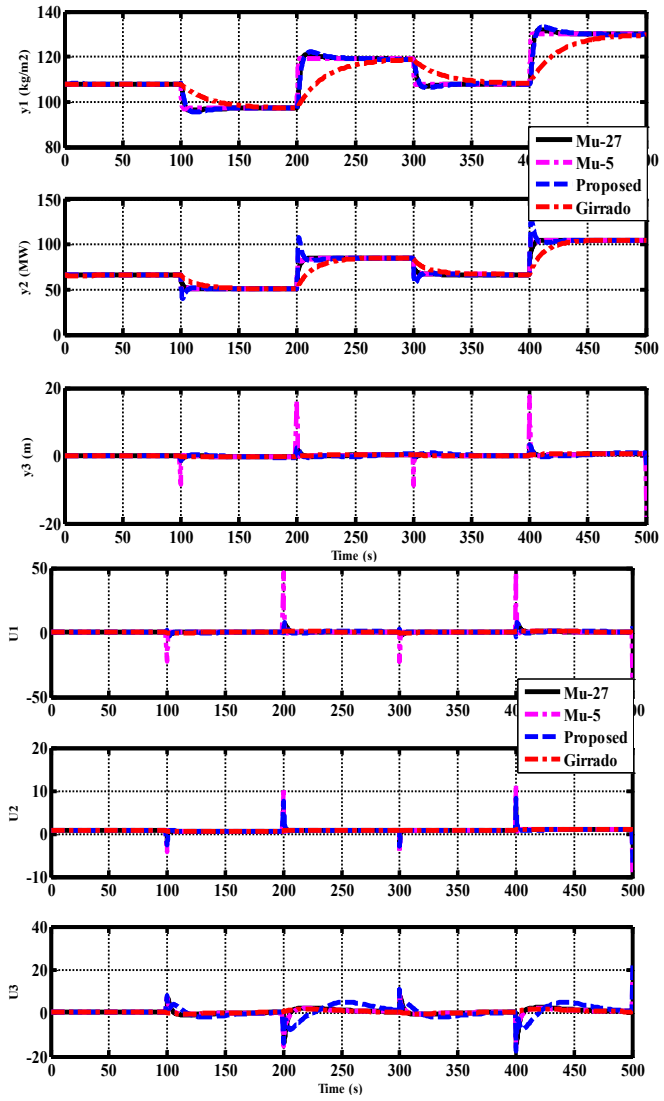

Fig.5. Response of the nonlinear closed loop system to a scenario of changes in operating points.

4. CONCLUSIONS

The paper considers the design of simple effective controllers for multivariable systems subject to wide operating range. After determining a mean plant, the uncertainty weight is computed from fitting a simple least upper bound or supremal function over the extreme multiplicative uncertainties of the neighbouring plants. Thereafter, the desired performance is characterized by the performance weight. Controllers with minimum ISE subject to ensuring $\mu_{RP} \prec 1$as well as minimizing maximum controller outputs are then designed for the closed loop system involving the nominal plant. The new procedure of centralized controller design which entails its parametrization using MIMC and the determination of the initial values of controller parameters using the method of Section 2.2.1 is powerful. Imagine, otherwise, having to arbitrarily determine the 18 parameters of a centralized PI controller for a 3*3 plant. The new method facilitates the design of simple controllers meeting several objectives with the closed loop systems operating within the stipulated constraints over the envelope of wide operating points.

5. REFERENCES

Escobar, M., and Trierweiler, J. O. (2013). Multivariable PID controller design for chemical processes by frequency response approximation. *Chemical Engineering Science* 88, 1–15

Fard, J. M., Nekoui, M. A., Sedigh, A. K. and Amjadifard, R. (2013). Robust Controller Design by Multi-Objective Optimization With H_2/H∞/μ Combination. *International Journal of Computer Science And Technology* Vol. 4, Issue 1.

Garrido, J., Vazquez, F. and Morilla, F. (2012). Centralized multivariable control by simplified decoupling. *Journal of process control*, (22):1044-1062.

Gu, W. D., Petkov, P. H. and Konstantinov, M. M. (2005). *Robust Control Design with MATLAB*. British Library Catalogue

Kailath, T. (1980). *Linear Systems*, Prentice Hall, Englewood Cliffs, New Jersey.

McKernan, J., Whidborne, J. F. and Papadakis, G. (2009) Poiseuille Flow Controller Design via the Method of Inequalities. *Int. J. Automation & Comp.* 6, 23-30

Oloomi, H. and Shafai, B. (2011). 'Optimizing The Tracking Performance In Robust Control Systems'. Recent Advances In Robust Control – Theory And Applications In Robotics And Electromechanics. Andreas Mueller. (Ed), 103-114.

Seborg, D. E., Edgar, T. F. and Mellichamp, D. A. (2004): *Process Dynamics and Control*. John Wiley and sons Inc. New York.

Skogestad, S. and Postlethwaite, I. (2005) *Multivariable Feedback Control, Analysis and Design* John Wiley and sons Inc. New York.

Taiwo, O. and Krebs, V. (1995) Multivariable system simplification using moment matching an.d optimization. *IEE Proc. Control Theory Application*, Vol.142 pp103-110.

Zhou, K., Doyle, J. C. and Glover, K. (1996). *Robust and Optimal Control.* Prentice Hall, Englewood Cliffs, New Jerse

IMPACT OF OIL EXPLORATION AND ENVIRONMENTAL POLLUTION ON GROUND WATER QUALITY IN SELECTED LOCAL GOVERNMENT AREA OF RIVERS STATE

***Ojirika, E. C. [1] and Joel, O. F. [2]**
[1]World Bank African Centre of Excellence, Centre for Oilfield Chemicals Research, University of Port Harcourt, Nigeria.
[2]Department of Petroleum & Gas Engineering, University of Port Harcourt, Nigeria.
Corresponding Author: fomida2005@yahoo.com

ABSTRACT

Groundwater remains one of the most important and reliable sources of water supply for man's use. In its natural form, groundwater is considered pure and unpolluted. However, anthropogenic activities such as crude oil and natural gas exploitation and production introduce foreign materials (contaminants) to groundwater which render it unfit for use. In this study, groundwater quality in oil bearing LGAs of Khana and Obio-Akpor in Rivers State was assessed. Water samples from existing boreholes were analyzed in the laboratory to ascertain their physicochemical characteristics. Results show that groundwater in the study areas are acidic and do not meet the World Health Organization (WHO) standard for drinking water which is a pH range of 6.5 – 8.5. While Khana has a pH range of 4.72 – 6.16 with a mean value of 5.23, Obio-Akpor recorded a pH range of 4.31 – 6.18 and a mean value of 4.79. The study traced the acid contamination to severe environmental pollution of the study areas as well as poor effluent and waste management practices. The study recommends adequate treatment of groundwater in the study areas before use to eliminate water borne diseases and corrosion/clogging of water facilities. It further recommends regular assessment and monitoring of groundwater in these areas to ascertain level of contamination and the likely method and technique for treatment and remediation.

1.0 INTRODUCTION

Groundwater is an important source of water for agricultural and domestic use in developing countries like Nigeria (Agbalagba, et al, 2011). Groundwater naturally contains dissolved minerals/salts/gases and other substances but only in concentrations that fall within the tolerable limits for human use. These substances are picked up as water flows from the surface through soil and rock strata/formations into the underground aquifer. When harvested in its natural form through drilling of wells/boreholes, groundwater is generally considered pure and uncontaminated.

However, groundwater does not exist in isolation. Hydrological cycle studies show that while groundwater can be recharged from surface water bodies – lakes, streams, swamps, rivers, seas and oceans, it can equally discharge into these bodies depending on the prevailing circumstances. This interaction is a major source through which groundwater can be contaminated. In the Niger Delta region water table is shallow and vulnerable to pollution from anthropogenic activities, mainly crude oil and natural gas exploitation and production. Groundwater can also be contaminated through salt water intrusion as well as other activities of man in Agriculture, industrial manufacturing, waste disposal, mining activities and oil exploration.

Rivers State is a coastal state which has a direct contact with the Atlantic Ocean (saline water). Fresh surface water, generally, is difficult to come by (about 0.3% of the earth's total fresh water) and even when available is highly vulnerable to pollution due to numerous industrial activities within the area. Potable water, therefore, must be sourced from groundwater which accounts for 30.1% of the earth's total fresh water. This scenario, therefore, puts so much pressure on groundwater resources in Rivers State including the areas of our case study – Khana and Obio-Akpor LGAs.

Rivers State is highly endowed with crude oil and natural gas reserves with a lot of upstream, midstream and downstream activities in the sector**.** High level of oil/gas exploitation, exploration, production, processing, distribution and utilization take place in the state all year round with their concomitant environmental hazards.

Oil spills, gas flaring, industrial effluent discharges into the environment are some of the consequences of oil exploration activities, which have impacted negatively on the environment and the quality of both surface and groundwater in the study areas. The famous UNEP Report of the devastation of Ogoni land by oil production activities is a case in point. The story is not different in the other parts of the state and indeed the entire Niger Delta region.

The ugly situation is made worse by recent developments in which angry youths of the region (Rivers State inclusive) by way of protests are engaging in crude oil theft, pipeline vandalization and illegal refining of stolen crude oil, causing even more pollution and degradation of the ecosystem. Remote sensing revealed the rapid proliferation in the past two years of artisanal refining whereby crude oil is distilled in makeshift facilities *(UNEP Report on Ogoni land, 2011).* The study found out that this illegal activity is causing pockets of environmental devastation in Ogoni land and neighbouring areas and endangering lives. Groundwater, no doubt, is among the victims of this environmental pollution and devastation.

Gas flaring is still a regular feature in the landscape of Rivers State including the study areas of Khana and Obio-Akpor Local Governments. Gases such as carbon dioxide, oxides of sulphur and nitrogen which are usually injected into the atmosphere produce *acid rain* in a state that records heavy rainfall for most of the year.

Rivers State has two refineries with a total installed/production capacity of 210,000 barrels of crude oil per day representing about 47% of Nigeria's total refining capacity, a petrochemical plant, a fertilizer plant that is presently moribund but that has left in its wake tremendous environmental damage; not less than four gas plants, two very busy sea ports in Onne and Port Harcourt, numerous active oilfields/wells including offshore, many industrial/manufacturing companies, all of which exert environmental pressure on the state by way of pollution. It is instructive to note that the two refineries, the petrochemical plant, the moribund fertilizer plant, the Onne sea port, and quite a number of oil fields/wells are sandwiched between Khana and Obio-Akpor LGAs which are our study areas.

Water is an indispensable and essential requirement for the existence of any form of life, just like air. The availability of a water supply adequate in terms of both quantity and quality is essential to human existence (Peavy, et al, 1985).The importance of water can, therefore, not be over emphasized. While man can survive for a long time without food, he can hardly do the same for the same period of time without water. Water is needed by man for domestic purposes including cooking, washing, drinking and sanitation. Water is also required by man for agricultural activities - irrigation, growing of crops and processing his farm products; industrial manufacture of goods and production of power for energy. Water quality, therefore, must be ascertained to ensure it meets the required standard that can guarantee its safe use for both domestic and industrial/agricultural purposes.

2.0. STUDY AREA

This study was carried out in two local government areas of Rivers State namely Khana and Obio-Akpor. Rivers State is located in the oil rich Niger Delta Region, South-South geopolitical zone of Nigeria. It is bounded on the south by the Atlantic Ocean, on the north by Anambra, Imo and Abia states, on the east by Akwa Ibom state and on the west by Bayelsa and Delta states. It has a topography of flat plains with a network of rivers and tributaries. These include New Calabar, Orashi, Bonny, Sombreiro, and Bartholomew rivers.

2.1. Khana Local Government Area.

Khana is one of the 23 Local Government Areas of Rivers State. It is situated on the coordinates $4^0$42'N, 7^0 21'E. Bori serves as its administrative headquarters as well as the traditional headquarters of the Ogoni ethnic nationality spread across four LGAs namely Khana, Gokana, Tai and Eleme. It also serves as the commercial nerve centre for the Ogoni, Andoni, Opobo, Nkoro, Anang and other ethnic nationalities of the Niger Delta region of Nigeria.

Khana people are spread across 560 square kilometres with a population of 294,217 according to 2006 census figures. It shares boundaries with Oyigbo in the north, Tai and Gokana in the west, Andoni and Opobo/Nkoro in the south and the Atlantic Ocean in the east. Khana has a very rich arable land and is surrounded by rivers, creeks, and marshland. The traditional occupation of the people is farming, fishing and petty trading all at the level of mere subsistence.

2.2 Obio/Akpor Local Government Area.

Obio-Akpor has a total land mass of approximately 260 square kilometres and shares boundaries with Emohua (west), Ikwerre & Etche (north), Oyibo & Eleme (east) and Port Harcourt (south). By 2006 census records,

Obio-Akpor had a total population of 878,890. Based on the national average population growth rate of 2.82%, Obio-Akpor's current population is projected at over one million people.

Obio-Akpor is rich with natural resources such as oil and gas, clay, sand, and gravel. It is one of the major centres of economic activities in Nigeria. Obio-Akpor has a high industrial base location as most of the companies in the state including key oil and gas companies are located in parts of the Local Government Area. It has a vast arable land, forest reserves and forest based resources such as fruits and vegetables and is surrounded by rivers, creeks, marshland, and semi-forest zones from where various fishes and other sea foods are sourced mainly for subsistence.

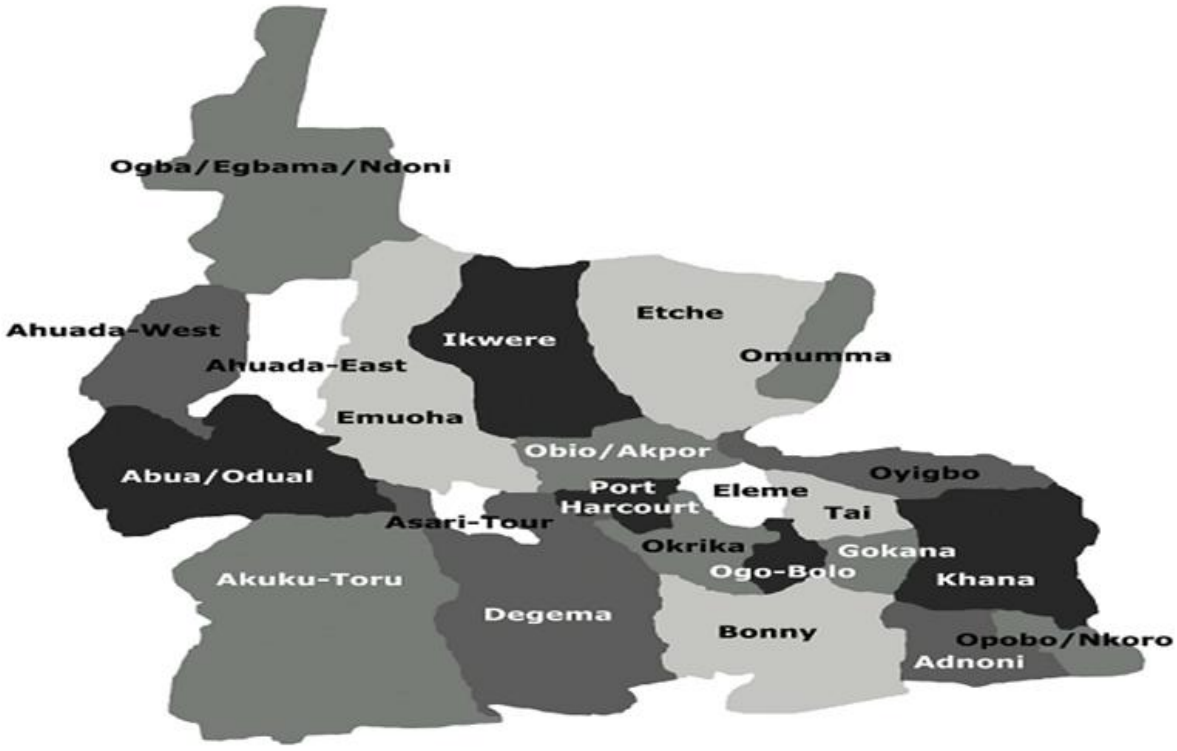

Fig.1. Physical map of Rivers State showing the 23 LGAs including Khana&Obio-Akpor.

3.0 RESEARCH METHODOLOGY

3.1 Field Collection of Samples

Groundwater samples were collected from different boreholes from different locations/communities in both Local Governments according to international best practice for sampling protocols. All collected samples were preserved in coolers and taken to the laboratory for analysis within 24 hours of collection to minimize interference and contamination of the physico-chemical properties of the samples.

3.2 Laboratory Analysis of Collected Water Samples

All the samples collected were analysed using internationally accepted standard laboratory methods as indicated in Table 1.

Table1. Laboratory Analytical Methods Used for the Physico-chemical Analyses.

Parameter	pH	Temp	Elect. Cond.	TDS	Cl	Fe	Ca	Mg	Pb	Cu	Zn
Analytical Method	ASTM D3921	ASTM D3921	Electro metric	APHA 208D	APHA 408C	APHA 301A	APHA 301A	APHA 301A	APHA 301A	APHA 301A	APHA 301A

4.0 RESULTS AND DISCUSSION

4.1 Results

The results show that all the groundwater samples analyzed are acidic with their pH below WHO's limit of >6.5 < 8.5 for potable water (Fig.2). However, all the physico-chemical properties analyzed and heavy metal presence in the samples are within WHO's permissible limit and are, therefore, acceptable for drinking and other domestic, commercial and agricultural purposes (Figs. 3 – 9)

4.2 Discussions

The acid contamination of the analyzed groundwater samples can be attributed to severe environmental pollution and degradation of the study area and the entire Niger Delta region as a result of oil exploration and production activities. Both Khana and Obio-Akpor have heavy presence of oil production activities including gas flaring which injects acidic gases - carbon dioxide, sulphur dioxide, oxides of nitrogen among others into the atmosphere. Nigeria is reported to flare more natural gas associated with oil extraction than any country in the world. Wikipedia Report (2007), show that natural gas in Nigeria's Niger Delta is flared into the environment at a rate of 70 million cubic metres per annum. Being a zone of heavy rainfall almost throughout the year, these gases are washed down to the soil as *acid rain*. Consequently these acid rain seep through the soil and percolate into the underground aquifer and contaminate groundwater.

Nwankwoala & Walter (2012), stated this much in their assessment of groundwater quality in Okrika Local Government Area of Rivers State: *Gas flaring in the area generates CO_2 which could have been dissolved in precipitation which percolates into the groundwater to reduce the pH.* Similar study by Nwankwoala &Amadi (2013) for groundwater in Port Harcourt, Eastern Niger Delta, showed that pH in Rumuolumeni and Elelenwo were respectively 5.90 and 5.93 and acidic. This study confirms the acidic nature of the groundwater in these areas and in fact indicate a deterioration of the acid contamination to pH of 4.50 and 4.90 respectively. This is an indication of three things:

a) No remediation actions have taken place since the 2013 study

b) The activities that lead to increase in pH are still continuing

c) The situation will get even worse if no remediation actions are taken.

The simple reason for the deterioration is that there have not been any coordinated effort by any government agency or the private sector to address the issue of environmental pollution and in particular water contamination and degradation. The much publicized UNEP Report of Environmental Assessment of Ogoni land is still gathering dust in Government files without any concerted effort to address the issue by implementing the recommendations. Instead, the matter has been politicized with the various stakeholders trading blames, accusations and counter accusations on each other and in the process abandoning the task of cleaning the environment and water supply sources to alleviate the challenges of the people.

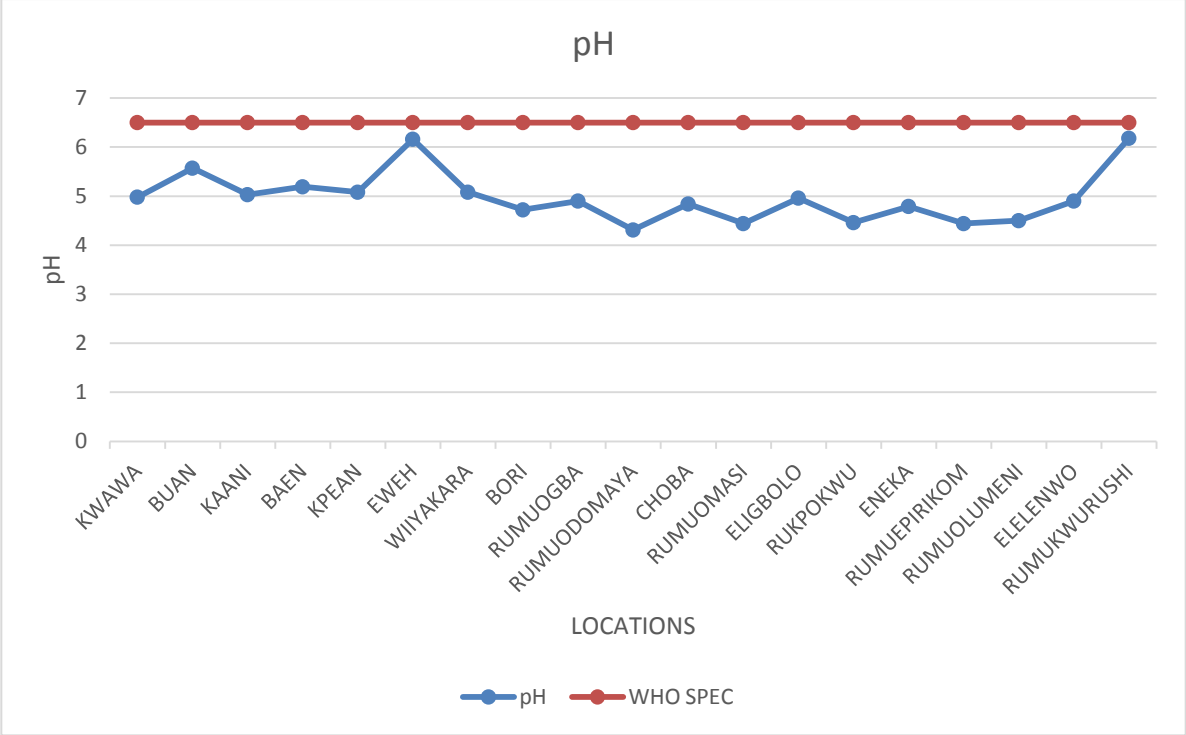

Fig. 2. Sample pH compared with WHO standards

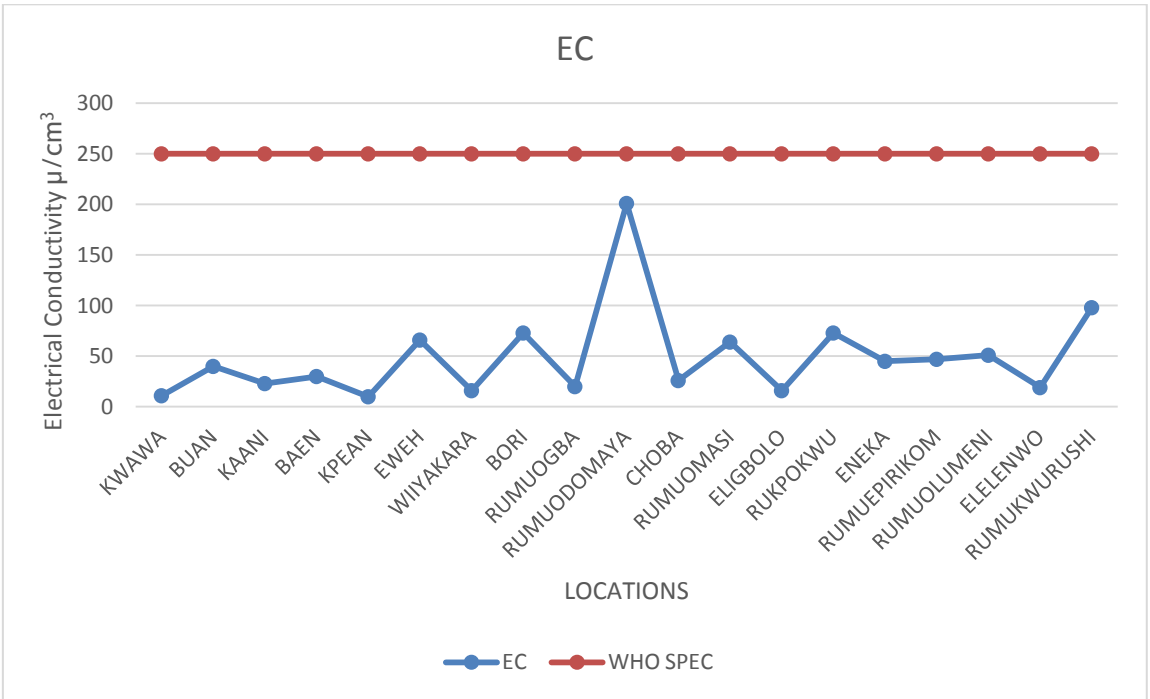

Fig. 3: Electrical Conductivity of Sample compared with WHO standards

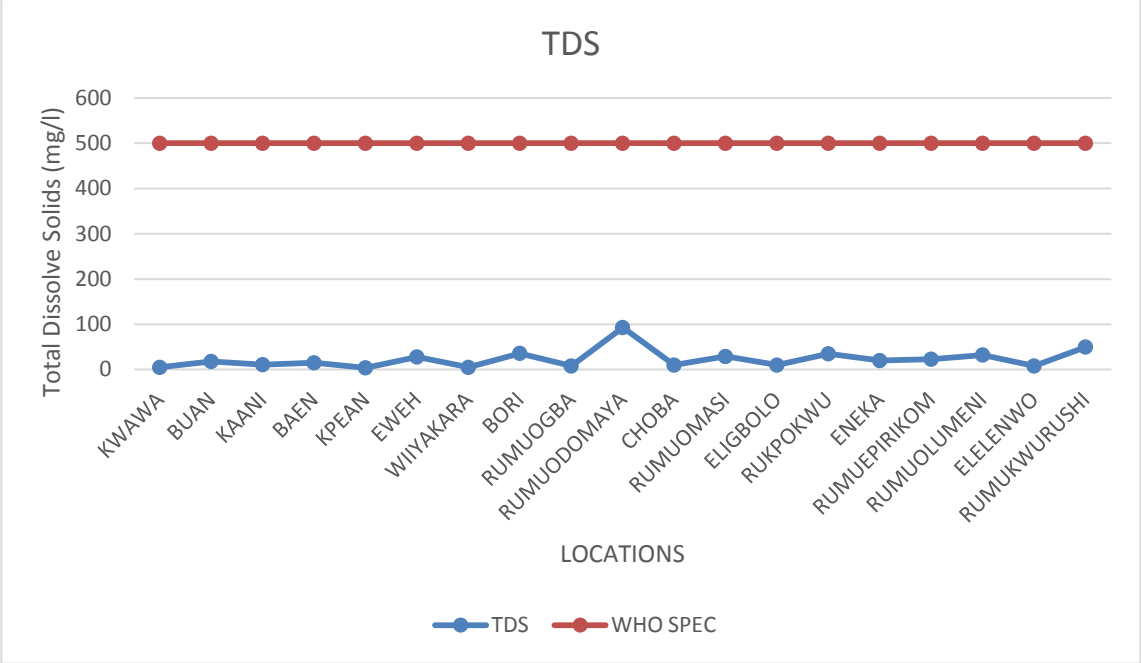

Fig. 4: Total Dissolved Solid of Sample compared with WHO Standards

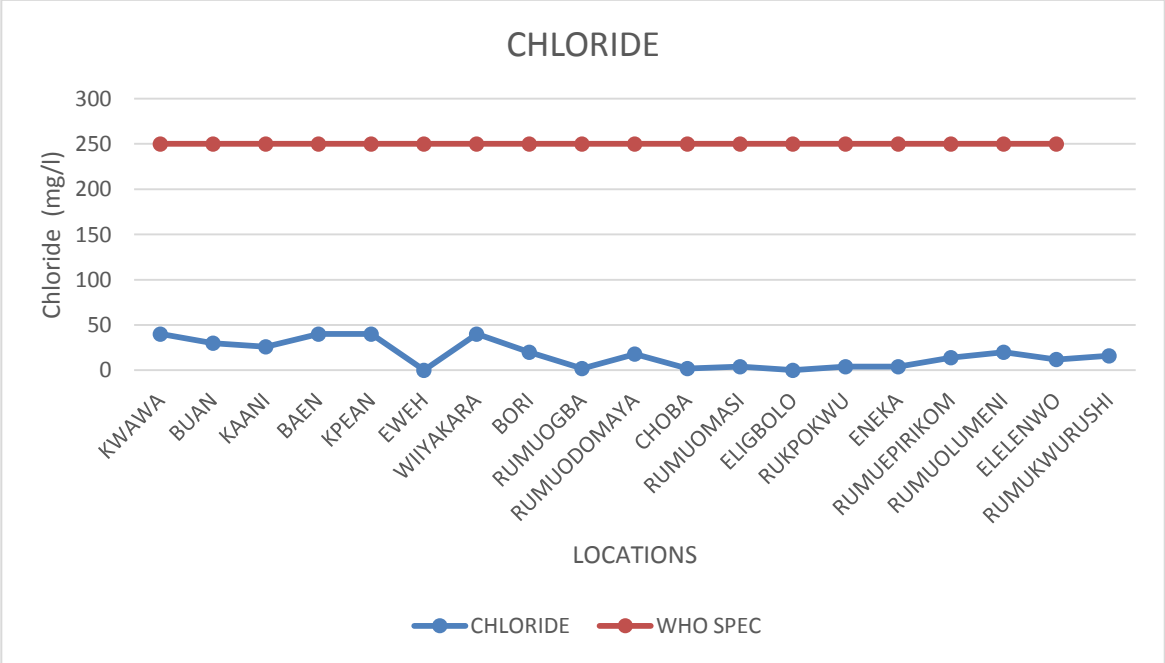

Fig. 5: Chloride Ion Concentration of Sample Compared with WHO Standards

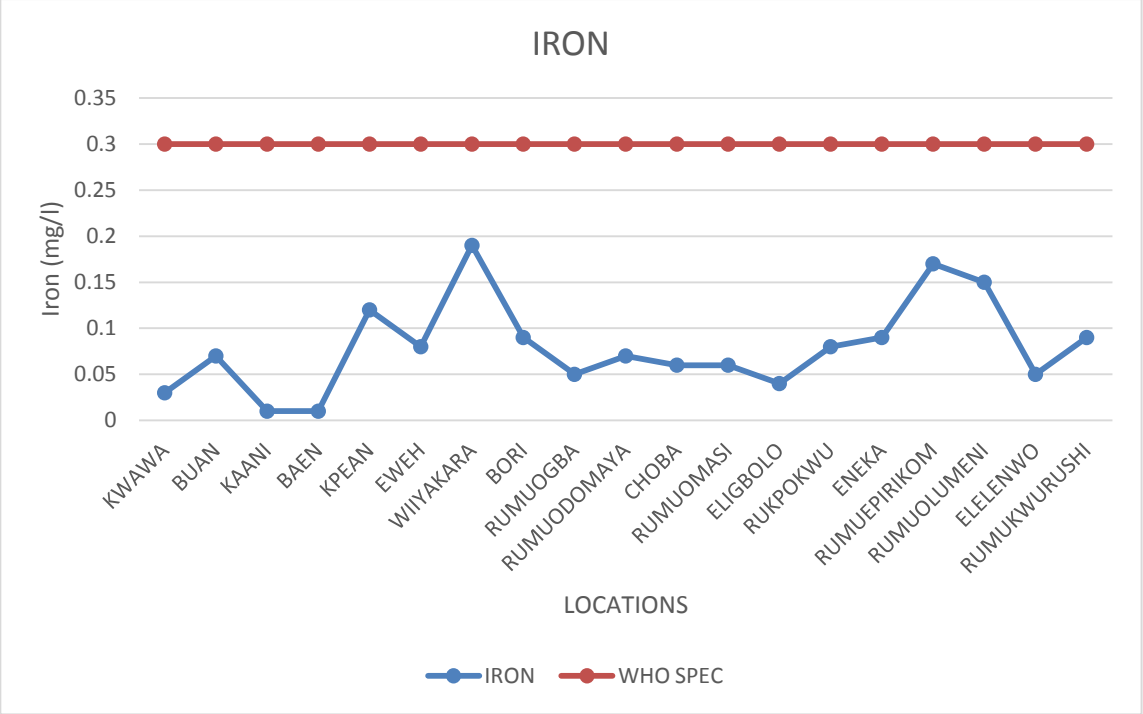

Fig. 6: Iron Concentration of Sample Compared with WHO Standards

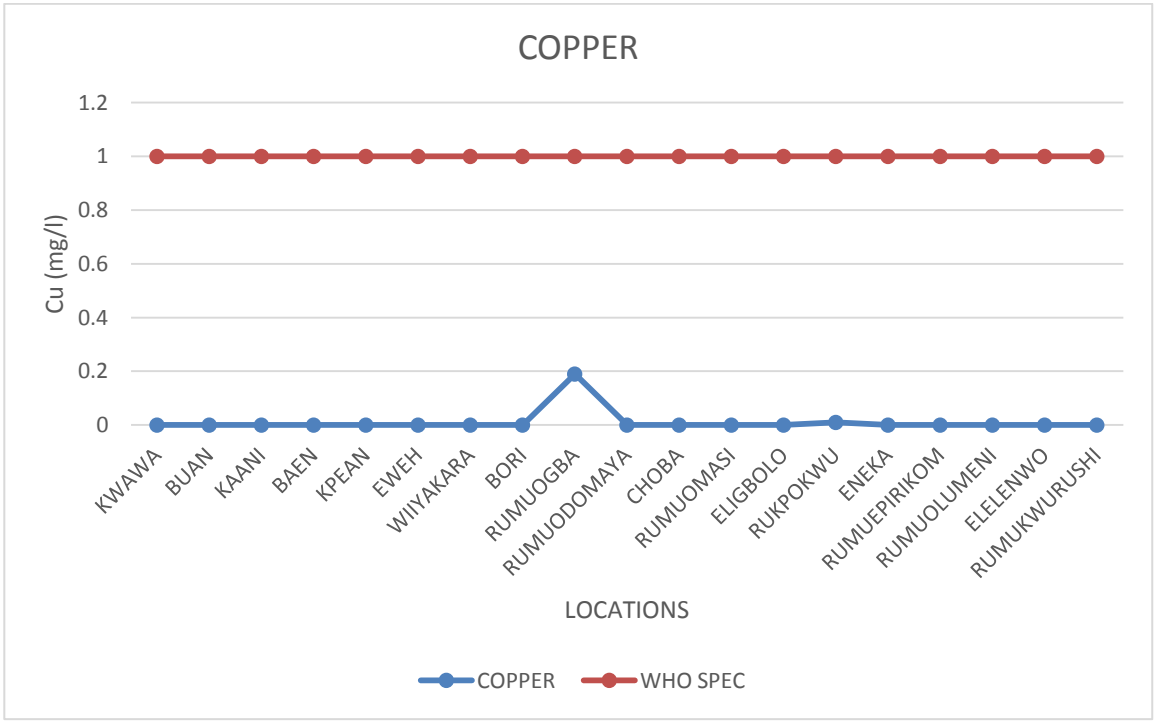

Fig. 7. Copper Concentration of Sample Compared with WHO Standards

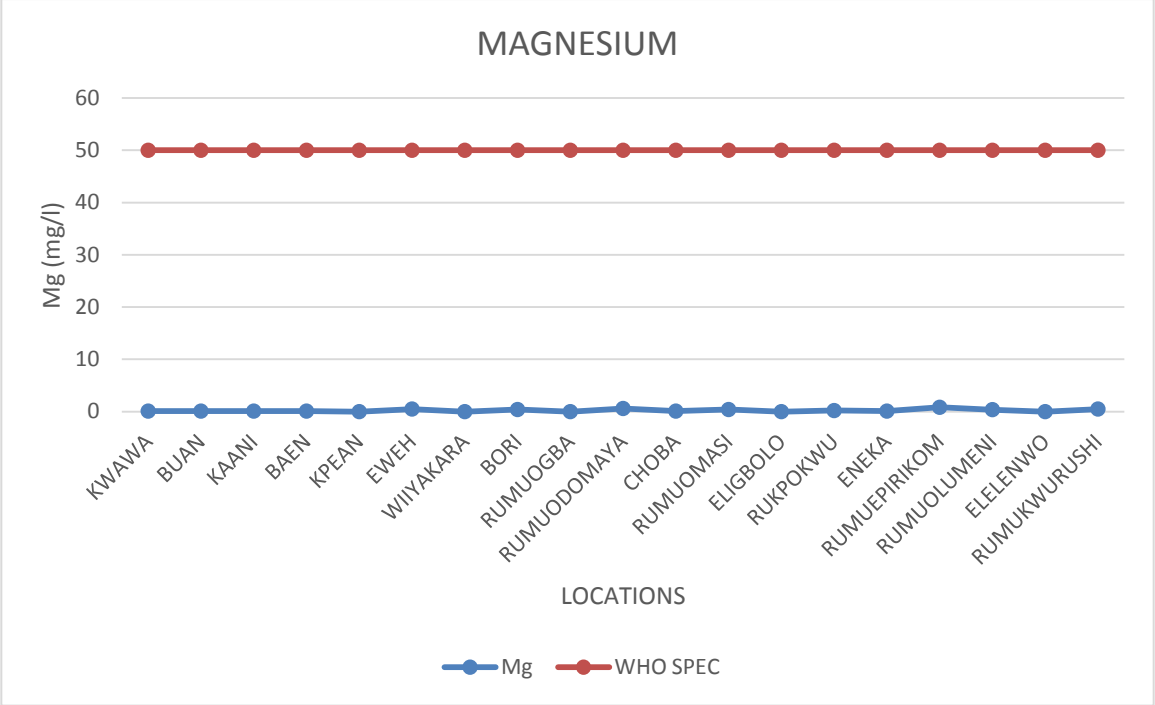

Fig. 8: Magnesium Concentration of Sample Compared with WHO Standards

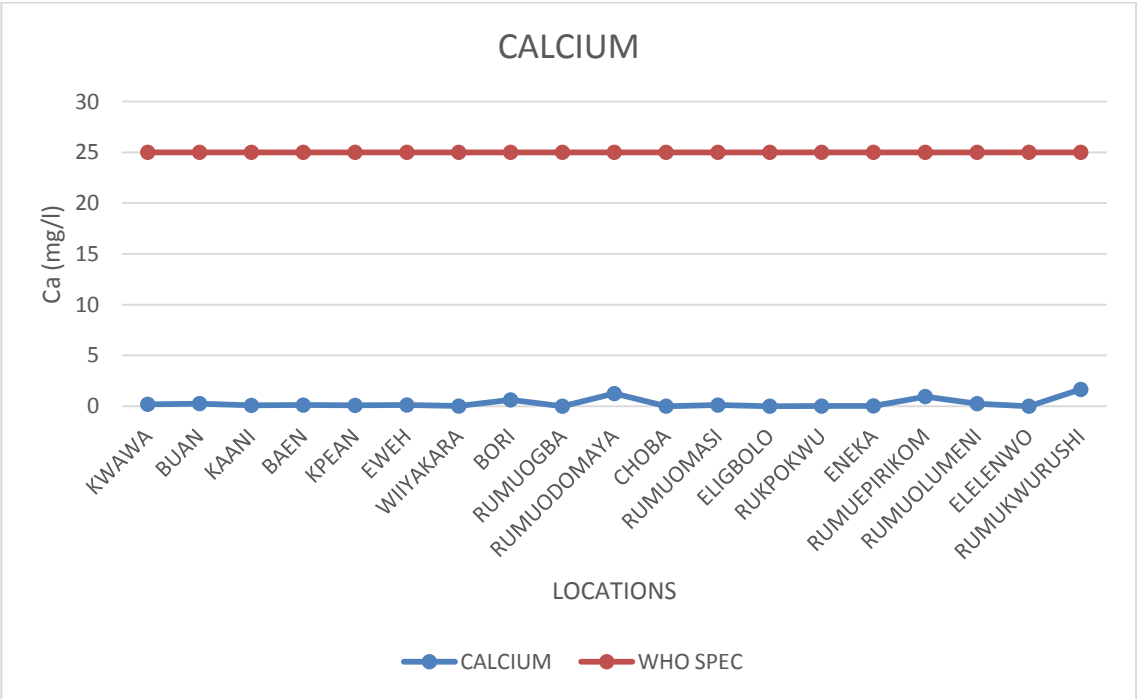

Fig. 9: Calcium Concentration of Sample Compared with WHO Standard

Besides oil and gas exploration activities, lots of other anthropogenic activities in the study area are contributing to excessive injection of carbon dioxide into the atmosphere without a commensurate amount of carbon sink available to absorb them and mitigate their environmental impact. Some of these include automobile exhaust systems, fossil fuel combustion, forest fires and objectionable agricultural practices such as bush burning among others which are predominant in the study area.

While these activities of man produce and inject CO_2 into the atmosphere, green vegetation (a natural carbon sink) is disappearing at an alarming rate due to deforestation arising from population explosion and rapid urbanization. Apart from the environmental hazard of contributing to global warming/climate change (being a greenhouse gas), CO_2 combines with moisture/rain water in the atmosphere to form carbonic acid (H_2CO_3) a major contributor to groundwater contamination.

$$H_2O + CO_2 \rightarrow H_2CO_3 \quad (4.1)$$

Some of the carbonic acid in the rain water disassociates or break down to form bicarbonate (HCO_3^-) and hydrogen ion H^+.

$$H_2CO_3 \rightarrow HCO_3^- + H^+ \quad (4.2)$$

The hydrogen ion produced in reaction 4.2 lowers the pH of rain water. The more CO_2 present in the atmosphere, the more acidic is rain water (Nelson, 2002). Again through seepage and percolation, this acidic rain water get in contact with groundwater causing contamination.

Another factor that may have influenced the acidification of groundwater in the study area is poor waste management practices within the area. A comparison of the groundwater assessment in Khana and Obio-Akpor indicates higher acidic values in Obio-Akpor than in Khana. Obio-Akpor is densely populated (probably the highest in the Niger Delta Region) with very high rate of municipal waste/refuse generation which are equally poorly managed. In most cases these wastes are dumped in open spaces including road medians and are not removed for disposal by waste disposal contractors for upwards of 4 to 5 days or even weeks.

When rain falls the already decomposing wastes are washed off by rain water and the leachate seep through the soil and percolate into the underground aquifer causing contamination of groundwater. Even when the wastes are removed and taken to approved disposal or dump sites, the disposal practices at such sites leave much to be desired. There are usually no liners, membranes or any form of protection of the adjourning areas from leachate seepage and eventual percolation into the underground aquifer. Dumpsites at Rumuolumeni, Eneka, Eliozu, all in Obio-Akpor among others are eye sores and constitute real environmental danger to groundwater in the area. A sizeable chunk of these wastes are disused and discarded lead-acid batteries which can be a source of lead contamination of groundwater.

Khana on the other hand has better results in terms of groundwater acidity. This may, among other factors, be attributed to the fact that it is more of a rural setting than Obio-Akpor; has far less population density and generates wastes far below that of Obio-Akpor. Bori which is a semi urban area in the zone and the headquarters of the LGA has the least pH level in Khana and therefore more acid contamination. Lead and other heavy metal concentration in the area fall within WHO standards for drinking water. This again may be attributed to the fact that waste generation/disposal which follows the same trend as in Obio-Akpor is more in Bori than the other areas indicated in the study in Khana Local Government Area.

Domestic sewage can also be a source of acid contamination of groundwater. Due to anaerobic fermentation processes that take place in septic tanks, carbon dioxide and hydrogen sulphide (a pungent and toxic gas) are usually produced. These gases are acidic and can be a source of production of acid in septic tanks. Most homes in the study area have privately constructed septic tanks for their domestic sewage disposal. Unfortunately, most of these septic tanks are poorly designed and are not linked to any central sewage treatment facility. Permits from municipal authorities are usually not obtained nor any form of inspection from them before citing and constructing such tanks. These poorly designed tanks are in most cases located very close to water boreholes, particularly in Obio-Akpor where the population density is very high. This therefore can be a major source of contamination of groundwater in the study area.

Whatever is the source of acid contamination of groundwater, the truth remains that acidic water is unfit for domestic, agricultural, industrial and commercial

use. World Health Organization (WHO) and Nigerian Standard for Drinking Water Quality (NSDWQ) recommend pH range for potable water as 6.5 to 8.5. For our study area the closest to this range is 6.18 (Rumuokwurusi – Obio-Akpor) which falls short of the standard by WHO. For figures below or above this range it is recommended that such water be subjected to treatment/remediation and certified fit before use. Acidic water results in corrosion of iron and steel materials (pipes) and plumbing fixtures, clogging of distribution pipes and cause objectionable tastes of drinks and food and may stain clothes and rust cooking utensils (Jones, 1998). WHO guidelines for drinking water equally states that exposure to extreme pH values results in irritation to eyes, skin, mucous membranes; and exposure to low pH can result to redness and irritation of the eyes among other health and medical implications. Bertills & Sundlof (1995) further posit that acid groundwater can corrode plumbing systems and solubilize metals in the soil or in the plumbing systems. They further state that since the soluble forms of some of these metals are toxic, this trend has raised concerns regarding the effects of groundwater acidification on human health.

Acidic water increases the overall cost of provision of potable water for the citizens. Apart from the direct cost of treatment/remediation of contaminated water, there could be further cost that may arise from maintenance/replacement of materials and equipment that get damaged or deteriorated as a result of corrosion. In industrial plants, equipment like boilers, heat exchangers and water storage tanks can suffer serious damage if acidic water is used for operations without prior treatment/remediation. This again can increase the cost of production and provision of goods and services to the populace.

Solution to this deteriorating trend in acidity of our groundwater lies in remediation/treatment and improving seriously on our overall environmental management and waste disposal practices. Otherwise the trend may get to alarming proportions in the next few decades with a corresponding increase in water borne diseases and ailments.

5.0 CONCLUSION AND RECOMMENDATIONS

5.1 Conclusion

This study has shown that groundwater in the study areas is acidic [(pH of between 4.72 – 6.16 for Khana LGA) and (4.31 – 6.18 for Obio-Akpor LGA)]. Comparatively Obio-Akpor with average pH of 4.79 suffered more acid contamination than Khana with an average of 5.23. This is probably because the environmental pollution in the highly urbanized Obio-Akpor is more than in Khana. Interestingly, all the other physico-chemical properties analyzed fall within the WHO's limit for potable water.

The acidity of groundwater in the study areas is attributable to serious environmental pollution arising mainly from oil and gas production activities which are prevalent in the area and other parts of the Niger Delta region of Nigeria. The frequent rainfall in the area results in frequent *acid rain* which when dropped on the soil gradually seep into the ground and thereafter into the underground aquifer and contaminate groundwater. Fashola et al, (2013) in their study agrees with this finding when they posited that *acidity arises from gas flaring in most parts of the Niger Delta as well as the presence of organic matter in the soil.* Poor waste management and sanitation habits of the study areas may have also contributed to this high acidic groundwater. A lot of acidic liquids are regularly leached from decomposing wastes from the ubiquitous refuse dumpsites in the area and washed down the soil during rain falls and subsequently contaminate groundwater sources.

Another interesting finding from the study is that over time the pH values of the groundwater has deteriorated. Similar research work carried out around several locations in the Niger Delta region in the last decade produced the same result – *acidic groundwater*. But there has been a downward trend of pH values from average of 6.5 in the last decade to less than 5.0 as this study indicates. This trend may continue in the years ahead if no remediation measures are initiated and sustained and efforts made to eliminate or curtail the rate of environmental pollution identified in the study.

5.2 Recommendations

The research work, therefore, recommends as follows:

a) Regular recharging and dosing of groundwater sources in the area with alkaline solutions – limestone, dolomite or caustic soda. This can be done by Government in partnership with the private sector.

b) Drastic reduction in environmental pollution through gas flaring, oil spills and poor waste management and disposal practices. Government can achieve this by enforcing the relevant environmental laws and guidelines,

and meting out appropriate punishments to offenders where applicable.

c) Rehabilitation of public water supply stations at Elelenwo, Rumuokwurusi, Rumuola, Rumuogba, Bori and others all located in the study areas but which have since gone moribund and install relevant water treatment units. With this in place Government can place a ban on the use of poorly constructed private boreholes as source of drinking water.

d) Enactment of a law banning the sinking of private boreholes without a mini water treatment facility. This is to ensure that only properly treated water is consumed by the public.

e) Laws should be enacted against deforestation and environmentally harmful agricultural practices such as bush burning, while the crusade for tree planting should be sustained to enhance the capacity of green vegetation to absorb excess carbon dioxide from the atmosphere.

f) Central sewage treatment systems/facilities should be built in the cities/towns/residential areas to avoid the present situation where poorly constructed private septic tanks discharge sewage to the underground aquifer and in the process contaminate groundwater.

g) Government should as a matter of urgency begin to construct properly designed sanitary landfills for efficient and effective disposal of municipal wastes.

h) Research studies such as this should regularly be embarked upon to monitor groundwater contamination and deterioration.

ACKNOWLEDGEMENT

The authors wish to acknowledge with deep gratitude the Nigerian Content Development and Monitoring Board (NCDMB) for their support and sponsorship of this research work. We would also like to thank all individuals and corporate bodies who allowed us access to their water boreholes and facilities as well as the relevant information required for this study.

REFERENCES

Agbalagba, O.E; Agbalagba, O.H; Ononugbo, C.P; Alao, A.A. (2011): Investigation into the physico-chemical properties &hydrochemical processes of groundwater from commercial boreholes in Yenegoa, Bayelsa State, Nigeria. African Journal of *Environmental Science and Technology*. Vol. 5(7), pp 473 – 481.

Bertills, U &Sundlof, B. (1995). Methods for Treating Acid Groundwater Results and Evaluation of Long-Term Tests. *Water, Air & Soil Pollution December (III), Vol.85, Issue 3, pp 1849 – 1854.*

Chilton, J (1996): Water Quality Assessments-A guide to Use of Biota Sediments & Water in Environmental Monitoring, UNESCO, WHO, UNEP Report, 2nd Edition.

Drinking Water Standards, United States Environmental Protection Agency Report, 2012.

Edet, A.E &Okereke, C.S. (2001). A Regional Study of Saltwater Intrusion inSouth Eastern Nigeria based on the analysis of geo-electrical & hydro-chemical data. *Environmental Geology 40, pp 1278 – 1289.*

Edet, A; Nganje, T.N; Ukpong, A.J; Ekwere, A.S. (2011). Groundwater Chemistry and Quality on Nigeria. A status review. *African Journal of Env. Sc. & Tech. Vol.5(13) pp 1152-1169.*

Environmental Issues in the Niger Delta (2007). Retrieved from: http://en.wikipedia.org/wiki/environmental in the Niger Delta.

Environmental Protection Agency (USA) Report (2012). Water Monitoring and Assessment. Retrieved from http://water.epa.gov/type/rsl/monitoring.

Fashola, F.I., Nwankwoala, H.O &Tse, A.C. (2013). Physico-chemical Characteristics of groundwater in Old Port Harcourt Township, Eastern Niger Delta. *International Journal of Physical Sciences* Vol.1(3). pp.047-055.

Frank-Briggs, I.B. (2003). Hydrogeology of some Island Towns of Eastern Niger Delta, Nigeria. Ph.D Thesis, Uniport, Nigeria. Pp 283

Guidelines for Drinking Water Quality Criteria, Second Edition, WHO Geneva, 2006. pp 281 – 308.

Kensas Geological Survey (2001): Geohydrology of Reno County. A Report Retrieved from http://www.kgs. Ku . edu/General/ Geology/Reno/gw 01.html.

Minnesota Dept. of Health, USA: Iron in Well Water: Retrieved from http://www.health.state.mn.us/divs/eh/wells/waterquality/iron.html. Thursday Feb.26, 2015.

Mohammed, I.S.A; Najam U.I.H; Magbool, A. (2015). Preventive Measures and Remedial Techniques For Groundwater Contamination. Royal Commission Environmental Project. Pp 26.

Nelson, D. (2002). Natural Variations in the Composition of Groundwater. Oregon Dept. of Human Services, Springfield, Oregon. Pp8.

Nwankwoala, H.O.; Amadi, A.N; Oborie, E; Ushie, F.A. (2014): Hydrochemical Factors and Correlation Analysis in Groundwater Quality in Yenegoa, Bayelsa State, Nigeria. *Applied Ecology & Environmental Sciences 2.4(2014); pp 100 – 105.*

Nwankwoala, H.O.; Walter I. O (2012): Assessment of Groundwater Quality in Shallow Aquifer of Okrika Island, Eastern Niger Delta, Nigeria.*Ife Journal of Sc. (2) Vol. 14.*

Park, C.H. (2004): Salt Water Intrusion in Coastal Aquifers. A Ph.D Thesis Presented to Civil & Environmental Engineering Dept., Georgia Institute of Technology, Georgia, USA.

Peavy, H. S, Rowe, D. R, Tchobanoglous, G: (1985). Environmental Engineering. (Int. Edition). Quality Water Treatment Inc, USA. (2009)

Rao, C. S. (2006): Environmental Pollution Control Engineering, Second Edition (Revised), New Age International (P) Ltd, Publishers.

Safe Drinking Water Foundation (SDWF) (2009). A Report Retrieved from www.safewater.org.

Todd, D. K (1980): Groundwater Hydrology, Second Edition, John Wiley & Sons, New York Chichester.

Todd, D. K. (1980): The Water Encyclopedia, Water Information Centre, Port Washington, New York.

UNEP Report (2011). Environmental Assessment of Ogoniland. pp 257.

Uzoije, A. P., Onunkwo, A. A., Uche, C. C., Ashiegbu, D. (2014): Evaluation of Groundwater Quality of Coastal Aquifer Systems in Buguma City, Rivers State, South-South Nigeria. Civil & Environmental Research. ISSN 2225-0514. (7) Vol. 6.

RECYCLING OF RIGID POLYURETHANE WASTE – A COST REDUCTION STRATEGY IN RIGID POLYURETHANE FOAM PRODUCTION

Akintayo, K. A.
Vitapur Nigeria Limited
Kehinde.akintayo@gmail.com; 08123877585; 08060100121

ABSTRACT

With the surging demand for rigid polyurethane in worldwide as insulation material against increasing temperature, a large number of polyurethane foam wastes need to be disposed. There are mainly four types of disposal technology, landfill, incineration and recycling in the world. This research work presents recycling of rigid polyurethane foam waste as an input in the production of sandwich panels. This method ensures a huge cost saving in the rigid polyurethane sandwich panel production process while waste reduction is also achieved in large volume.
Key words - Rigid Polyurethane Foam, production waste

1. INTRODUCTION

According to Behrendth and Naber, 2009, Polyurethane are major plastic material with annual world production capacity of over 12 million tons. They are polymers consisting of chains of organic units joined by urethane links. Rigid polyurethane foam is currently one of the best thermal insulating materials avail-able, according to Plastemart, Rigid polyurethane foam accounted for 28% of Polyurethane foam worldwide production in 2006 and 39% in 2006, which is sign of surging interest in Energy conservation, while onces again rigid polyurethane foam products accounted for the Largest share of 6.5 billion ibs of polyurethane produced in NAFTA. The figure reflects the relative strength in demand for rigid polyurethane as an insulation material. As a result, thermal insulation is a key feature of almost all its applications. The possibility of combining rigid polyurethane foam with different facing materials to produce composites also gives it an important role as a construction material. The principal areas of use for rigid polyurethane foam are:

Domestic appliances

- Thermal insulation for domestic and commercial refrigerators and freezers, hot water tanks

The building industry

- Sandwich panels with rigid facings as wall and roofing panels
- Insulating boards with flexible facings for roofs, walls, ceilings and floors
- Insulating and construction material as cutto-size pieces from slabstock
- Spray-in-place foam for insulation and sealing

Industrial thermal insulation

- Insulation of tanks and containers, pipelines, district heating pipes and cold stores

The automotive industry

- Thermal insulation of refrigerated vehicles for road and rail including containers

Rigid polyurethane foam has a number of particular advantages:

- It can be produced in a wide range of densities.
- It adheres to various facings without the use of adhesives.
- It can also be produced in complex cavities.

Polyurethane foam materials are used widely, inevitably leading to a large number of polyurethane foam wastes production. Polyurethane foam wastes mainly come from the production process of leftover materials and product scraps. In addition, polyurethane foam products more than use fixed number of year, because of the performance will be decimated and scrap, with home appliance, furniture and other consumer goods in the most obvious scrap. According to Wenqing Yang et al, with present economic level and traditional habit in china, every year there will be 14.66 million refrigerators of scrap. Recycling of post-consumer polyurethane product is still a challenge in some part of the world (Yanyin 2002; Knight 2006; Behrendth and Naber, 2009). The form of polyurethane recycling existing in Nigeria considering its huge foam manufacturing factories is that used in the production process

According to Wenqing Yang et al, Polyurethane foam wastes belong to the white pollution, and affect the living environment. At the same time, because polyurethane foam plastics pile-up density is small,

about 30 kg/m³, stockpiling will take up a lot of area. Because of its difficult to degradation of ecological environment will cause adverse effect.

2. PRODUCTION PROCESS OF RIGID POLYURETHANE FOAM

The production of rigid polyurethane foam requires two main liquid components - a polyol and a polyisocyanate - and a blowing agent. The blowing agent is usually added to the polyol together with further auxiliary components such as activators (reaction accelerators), foam stabilizers and flame retardants. The polyaddition reaction that takes place when the polyol and polyisocyanate are mixed together results in macromolecules with urethane structures (polyurethanes).

During the reaction a considerable amount of heat is released which is used partly to evaporate readily volatile liquids (blowing agents). As a result, the reaction mix is expanded to form a foam.

Various quantities of water are normally added to the polyol. The water reacts with the polyisocyanate to form polyurea and carbon dioxide, which serves as a co-blowing agent but can also be the sole blowing agent.

In the presence of certain activators, isocyanates can react with one another to form macromolecules with isocyanurate structures (polyisocyanurate = PIR). Reactions between isocyanates and polyols and isocyanates can take place simultaneously or in direct succession, forming macromolecules with urethane and isocyanurate structures (PIR-PUR). Rigid polyisocyanurate-polyurethane foams are used, for example, when a high level of fire performance is required

3. HAND MIXING METHOD

Mixing of the raw materials with the aid of a stirring rod was originally referred to as the hand mixing method. Nowadays this term is also used when the components placed in a mixing vessel are mixed with an electrically driven stirrer.

The hand mixing method is used mainly for developing and checking raw material systems on a laboratory scale and producing smaller rigid foam buns

4. PRODUCTION OF RIGID POLYURETHANE FOAM BY MACHINE

Foaming machines and foaming lines

The hand mixing process only plays a subordinate role in the production of rigid polyurethane foams.

Normally polyurethane raw materials are processed into foams with the aid of machines. Foaming plant for processing two or more components consists of at least one foaming machine and one molding device. The foaming machine can be seen as the heart of a plant.

It receives the liquid components, brings the components to a state in which they can be processed and keeps them there, meters them in the correct proportions, thoroughly mixes the components and dispenses the reaction mix. The following diagram shows the individual process stages.

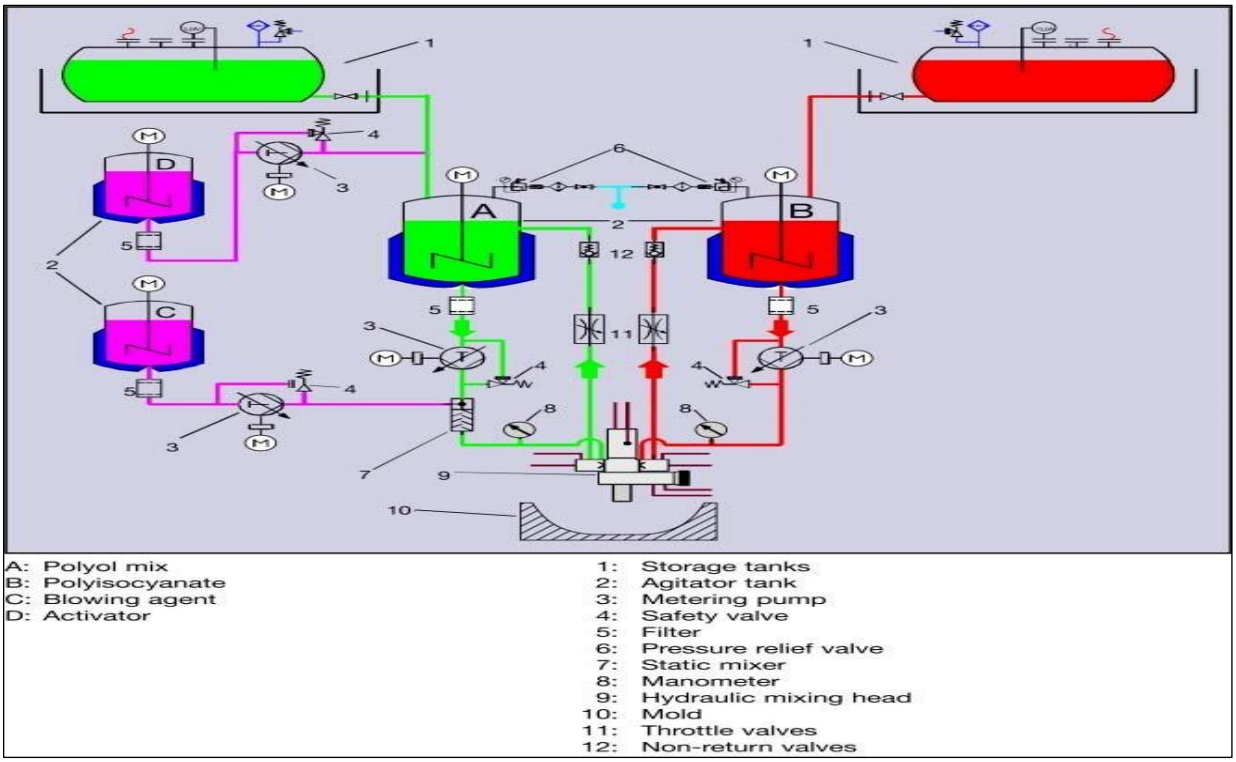

Figure 1.0 – Flow diagram for Production Rigid Polyurethane Foam

The two main components, polyol and polyisocyanate, are transferred from their storage containers into day tanks. In many cases, processing involves two-component systems, i.e. all the additives which are important for the reaction such as activators, stabilizers, blowing agents or flame retardants are already contained in the main components. However, individual mixing operations can also be carried out at pre-mixing stations or the additional components can be added directly into the metering lines of the pump units. The components are introduced into the day tanks in a process able state, i.e. temperature controlled and homogenized, and are kept in them. Dispensing units now convey the components in a set mixing ratio from the day tanks to the mixing head. The reactants meet here and are combined to form the reaction mix. This is discharged and then expands.

In general, a distinction is made between two machine systems: low-pressure and high-pressure machines. The two systems are simple to define. On low-pressure machines the component streams at a pressure of 3 to 40 bar are conveyed to agitator mixing chambers, and on high-pressure machines the components are compressed to 150 to 300 bar by piston pumps and are then mixed by impingement injection. The high kinetic energy of the component streams as they enter the mixing chamber is used for mixing.

5.RIGID POLYURETHANE WASTE RECYCLING

There are two ways, physical recycling and chemical recycling, for recycling polyurethane foam wastes .Physical recycling is directly reusing polyurethane wastes without chemical treatment. Chemical recycling is following the degradation principle. Polyurethane wastes will gradually depolymerize for original reactant or other oligomer and even small molecule organic compound.

6. PHYSICAL RECYCLING

Physical recycling method is crushing polyurethane foam wastes, only changing physical form. The smashing solid particles have no reactive activity, but directly make new polyurethane products as recovery processing of raw materials. Through mixed with adhesives, they can make all kinds of mold products by the compression molding method. This is currently the most widely used method. The usage of waste polyurethane powder can be as high as 90%. Physical recycling method is simple and convenient, with low cost, but there are still certain technical limitations at various physical recycling method processing. Performance of recovery products is poor, which only apply to some of the cheap products, and limit the market.

7. BONDING PROCESS

This method is the most common physical recycling method. The key points are: first the polyurethane foam wastes are shattered into fine flake, coating with adhesive, which is commonly MDI or MDI-Based prepolymer, about 5%-10%. Direct access to water vapor of high temperature, make polyurethane adhesive melting or dissolved. And then press solidified into a certain shape of foam. According to Jiang et al, regenerated a kind of waste rigid polyurethane foam plastic and produced insulation board. The present invention had simple process, low cost and environmentally friendly. But the largest defect is that performance of regenerated foam product was declining, which only applied to furniture, car lining and cheap components.

8. HOT PRESS MOLDING PROCESS

This method makes polyurethane softening, self-bonding under heat and pressure, without adhesive. Almost all kinds of polyurethane, due to it's contain soft segment which has thermoplastic in the 150-220 range, when heated to such temperature and pressure, can make to mutual bonding. Different polyurethane foam wastes and reworked material final products have different conditions of molding. For some low degree of crosslinking thermosetting polyurethane wastes, there is certain between thermal softening plasticity in the 100-220 deg C. Wastes can directly bond together in the range of temperature. The product is suitable for the low elongation and the poor surface performance requirements, such as damping tablet, fender, etc. Because of the limitation of processing temperature, this kind of method applies only to component known cases (Ge ZQ, et al, 2008). The polyurethane foam composite waste produced in the automotive roof lining production was press-formed into artificial board. The influence of the pressing parameter on the properties of the board was studied. The test results showed that the board formed under the temperature of above 150^{o}C, had flexural strength of 15-28 MPa, water absorptivity of 0-2 % and density of 1.0-1.2 g/cm3. The flexural strength is similar to that of the fiber board with medium density. The density is higher and the water absorptivity is much lower than that of the fiber board. The board with this feature could be used for the application situations which need resistance to water and high density such as furnishings in park and acoustics area (Zhong SY, et al, 2011).

Usage for filler Polyurethane wastes, shattered into fritter or powder, can be used as filler to join a new polyurethane product, dosage of which can reach 20%. Within the scope of certainty and not affecting the product properties (Wang & Chen, 2003), it can be applied to make elastomer, energy absorption foam and sound insulation foam as the main products. Lin [2008] shattered rigid polyurethane foam plastics into powder, removed impurities, mixed with polyether polyol and isocyanate, and made product. In the construction industry, the rigid polyurethane foam powder can be directly added to concrete, in order to improve concrete adiabatic effects. The polyurethane wastes should be grinded to a certain particle size as construction materials of packing, such as roof heat insulating layer. The cement, sand, water and waste rigid polyurethane foam were mixed in the shop roof. As a result, the thermal insulation performance is good, with light quality, and still can ingot nail advantages. In Japan, it has been already used for mortar of light aggregate [Cao and Cao, 2005]. Toyota [Xu WC, et al, 2008] made mudguard by addition 10% powder RIM as packing in polyhydric alcohol. It can reduce 4 % -5 % cost. Amor [7] studied the reduction of concrete density and increased pore by addition of the rigid polyurethane foam plastics. In the same volume, adding polyurethane foam wastes can make concrete weight by 29 % -36 % reductions.

9. EXPERIMENTAL

Process Description For The Recycling Process

The feed to the process is the waste rigid polyurethane block from the conversion of rigid block to pipe section.

The waste is crumbed in the hammer mill into particles.

The rigid PU particles are feed to the mixer for proper mixing and then blended in a drum with water and MDI-based Prepolymer.

The blended composite is transferred to Jig and subjected to hydraulic press pressure of over 150 bar.

The hydraulic press is then disengaged after 120 minutes.

Recycling Process

The recycling process adopted for this process is as presented Figure 2.0 below

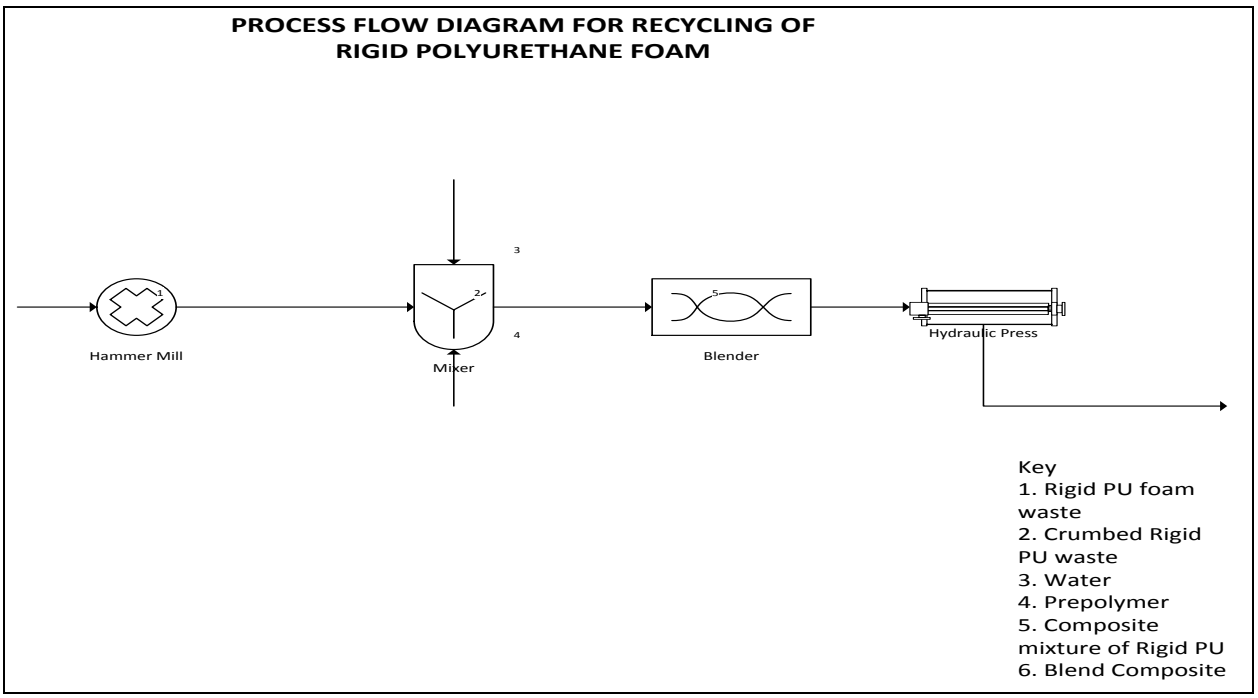

Figure 2.0 – Process Flow diagram for the recycling of rigid polyurethane foam

Result and Analysis

Table 1. Result of blending of rigid PU waste

	UOM	A		B		C		D	
Description		**Mass**	**% Composition**	**Mass**	**% Composition**	**Mass**	**% Composition**	**Mass**	**% Composition**
PU crumb	g	10	54%	10.43	78%	10	72%	40	67%
Prepolymer	g	6.11	33%	1.91	14%	2.95	21%	10	17%
Water	g	2.29	12%	1.07	8%	1.03	7%	10	17%
Mass	g	16.29		13		13.14		54.06	
Ratio of PU/Prepolymer		1.6367		5.4607		3.3898		4	
Density	g/ml	0.4715		0.2113		0.2227		0.1515	
Cutting with Saw-blade		ok		ok		ok		ok	

As it can be observed from the table, the various product obtained from the blend of the rigid PU waste showed good sign of being used as spacer in the production of sandwich panel and infill in other hollow structures.

10. CONCLUSION

In view of the difficulty in managing rigid polyurethane waste, the product of this research works is a cost saving approach in the production of rigid polyurethane products. The saving cuts across the waste management, reduced operational cost and raw material management. The product of this research work has been tested to observe its effect on the quality of rigid polyurethane foam produced, it has proven not to compromise the quality rather, it enhanced the mechanical strength while it also saves cost on waste disposal.

REFERENCES

Behrendt, G and Naber, B, W (2009), Chemical Recycling of Polyurethanes; *Journal of University of Chemical Technology and Metallurgy, 4(1): 3- 23*

Cao MG, Cao XR. Recycling and Disposing Methods for Rigid Polyurethane *Foamed Plastic Wastes. Plastics*, 2005, 34(14): 14-18

Ge ZQ, Xu HX, Li ZY, et al. Treatment and Recovery Methods for Polyurethane Wastes. *Chemical Propellants & Polymeric Materials*, 2008, 6(1): 65-68

Jiang BX, Xue HW, Xu B, et al. Waste rigid polyurethane foam plastics recycling regenerative production insulation board. CN1631631, 2005. 06. 29

Knight, J (2006), Recycling Post Consumer Polyurethane Foam in New Zealand, online, www.zerowaste.conz;Accessed on 12/7/2010

Lin YF. Waste rigid polyurethane foam plastics recycling method. CN101096426, 2008.01.02.

Wang JR, Chen DJ. The chemical and physical recycling methods for polyurethane wastes. *China Elastomerics*, 2003, 13(6): 61-65

Wenqing Y, Qingyin D, Shili L, Henghua , Lili L and Jinhui Lib (2012), "Recycling and disposal methods for polyurethane foam wastes", The 7th International Conference on Waste Management and Technology, Procedia Environmental Sciences 16 (2012) 167 – 175

www.plastemart.com/plastic-technical-article/Global-Polyurethane-market-to-reach-9-6-mln-ton-by-2015/1674

Xu WC, Song WS, Zhu CC, et al. The recycle and reuse of the polyurethane. *China Elastomerics*, 2008, 18(2): 65-68.

Yan Yin,H (2002), Recycling as a sustainable wastes management strategy for Singapore; An Investigation to find ways to promote Singapore Household waste Recycling Behavior; Lund university online;www.lumes.lu.se/database/alumni/01/ho_yanyin.pdf accessed 18/06/2010

Zhong SY, Li DF, Wang GS, et al. Recycling of Polyurethane Foam Composite Waste as Boards. China Plastics, 2011, 15(11): 67-70

STUDY OF BLEND OF PLANT SEED OILS AS POUR POINT DEPRESSANT IN NIGERIAN WAXY CRUDE OIL

***Akinyemi O. P. [1], Udonne J.D. [2] and Oyedeko K. F. K. [3]**

[1-3]Chemical and Polymer Engineering Department, Lagos State University, Epe, Lagos

poakinyemi@yahoo.com, udonne.joseph@gmail.com, kfkoyedeko@yahoo.com

ABSTRACT

Finding solution to the problem of paraffin wax deposition in crude oil production facilities is of the major concerns in the oil industry. Chemical treatment had been most convenient and economical method for tackling this problem. This paper considered the study of blend of plant seed oils as pour point depressant in Nigerian waxy crude oil. Two waxy crude oil samples obtained from Niger Delta region of Nigeria were characterized to determine their pour point, American Petroleum Institute gravity (APIg), wax content and viscosity using standard methods. The impacts of the blend of Jatropha seed oil and castor seed oil on the pour points of the crude oil samples were determined using a portable Pour Point Tester PPT 45150 by PSL Systemtechnik. The results obtained showed that blend of castor seed oil with 40% Jatropha seed oil gave the highest depression of about 10^{O}C on the pout points of the crude oil samples at concentration of 0.1%v/v of additive with crude oil. Also, using copper strip test, the blend of the seed oils was found not to have corrosive effect on crude oil facilities. The appropriate blend of castor and Jatropha seed oils can be used as a pour point depressant in crude oil facilities.

***Keywords**: Blend of plant seed oil, pour point depressant, waxy crude oil*

1.0 INTRODUCTION

The risk of wax deposition is one of the most important challenges in the production of crude oils and handling of fuels (Misra *et al*, 1995; Lorge *et al*,. 1997; Garcia, 2001; Bello *et al*,. 2005; Fadairo *et al.*, 2010; Oseghale *et al.*, 2012, Akinyemi *et al.*, 2016a). Summarily, problems associated with wax deposition may result in production shutdown and hazardous conditions and will require extensive workovers, production losses, and possibly irreparable damage requiring equipment abandonment and replacement (Koshel and Kapoor, 1999; Adewusi, 1997; Kok and Saracoglu, 2000).

To reduce the operating cost during production of waxy crude oil and for lowering the energy consumption and ensuring safety and cost effectiveness in pipeline transportation of waxy crude, an extensive study of the rheological characteristics of crude oil is indispensible (Mahto and Singh, 2013). One of the most important rheological properties impacting on the flow behaviour of wax bearing crude oils is Pour point. Many of the problems associated with wax deposition in crude oil facilities can be effectively resolved by the appropriate application of pour point depressing chemicals (Akinyemi *et al.*, 2016b). Crude oil pour point depression is significant in eliminating paraffin wax deposition (Adewusi, 1997) and is crucial for assessment of flow behavior and storage of crude samples. This study is therefore designed to investigate the use of blend natural non-edible plant seed oils as pour point depressants for Nigeria waxy crude oil and compare their effectiveness with the impacts of the previously tested triethanolamine-xylene blend on the crude oil. The plant seeds oil considered in this study are from: *Jatropha* plant (*Jatropha curcas*), castor plant (*Ricinus communis*) and rubber plant (*Hevea brasiliensis*).

2.0 MATERIALS AND METHODS

The seed oils were extracted from seeds obtained from farm locations within the western region of Nigeria. The xylene and triethanolamine used were analytical grade products of BDH Chemical Ltd, Poole England. Two crude oil samples A and B, obtained through the Department of Petroleum Resources (DPR) from oil fields in Niger Delta region of Nigeria were used in the study. Solvent extraction was used to extract the oil from the seeds using a Soxhlet extractor with *n*-hexane (800 ml) as the solvent as described by Akinyemi *et al* (2016a) and fatty acid composition analysed using gas chromatography. Each crude oil sample was reconditioned by heating it to a temperature of about

60^{o}C for nearly 10hr, with hand-rocking occasionally during heating in the laboratory prior to experiments to erase any previous history that might exist in such sample. Reconditioning the samples ensured that all pre-crystallized wax got re-dissolved into the oil, thereby erasing any thermal and shear history and producing homogenous sample for testing. The specific gravity (S.G.) and API (American Petroleum Institute) gravity of the crude oil samples were determined using the ASTM D287 standard while the wax content was determined using precipitation method reported by Mahto and Singh (2013). Their pour points were determined by using the portable Pour Point Tester PPT 45150 by PSL SystemTechnik, which is a compact lab-instrument for measuring the pour point of oils and oil products. PPT 45150 which has the accuracy of ± 0.1^{o}C at high repeatability, measures according to the rotational method ASTM D5985 like the Herzog Pour Point Apparatus MC 850.

For each run of the experiment the pour points of samples were obtained by heating each sample to 35^{o}C and then poured into the hollow tubing connected to the internal cooling device. The pour points were identified based on the flow-temperature characteristics of the fluid. A sensing head for crude oil and inhibited crude oil determined the pour point temperature. The procedure was carried out on the pure crude oil samples as the reference point. To produce a binary blend of seed oil as chemical additive, the seed oil were blended in ratio 1:4, 1:3, 2:3, 1:1, 3:2 and 4:1 by volume in separate bottles. The blended mixtures were shaken together enough to ensure homogenous liquid was obtained for each binary mixture. Each chemical additive was added to crude oil sample at the concentrations of 0.1%v/v for subsequent tests of the additives on the pour points of the crude oil samples. The seed oils tested were rubber seed oil (RSO), jatropha seed oil (JSO) and castor seed oil (CSO). Impact of triethanolamine (TEA) blended with 90% xylene (being the percentage observed by previous researchers to be most effective on Nigerian waxy crude oil – Taiwo *et al.*, 2009, 2012) on the samples pour points was also tested for comparative purpose. Corrosive tendency of the blended seed oil on crude oil facilities was investigated using ASTM130 method with copper strip test apparatus.

3.0 RESULTS

The specific gravity of the extracted seed oils were found to be 0.91, 0.93 and 0.96 for CSO, RSO and JSO respectively. The results obtained showed that the specific gravity of sample A is 0.8777 and that of sample B is 0.8497while their API^{o} are 29.7^{o} for A and 35^{o} for B. Sample A has the higher wax content of 30.71% and higher viscosity of 18.67mPa.s at 40^{o}C. The pour point of sample B which is 10^{o}C, is however higher than that of A (Table 1). Thus, high API gravity does not necessary depict low pour point for a particular crude oil sample. This is in agreement with the findings of previous researchers (Miadonye and Puttagunta, 1998; Adewusi 1997; Koshel and Kapoor, 1999; Bello *et. al.*, 2005; Akinyemi *et al.*, 2016a). Both crude oil samples have low sulphur content. The results obtained from the copper strip test carried out on the plant seed oils blends showed that the colour of the copper strip was not altered after been dipped in the additive for 3hours (recorded as 1a in the result rating).

Table 1. Characteristic Properties of Crude oil Samples

Samples	S.G	APIg	Viscosity at 40^{o}C (mPa.s)	Wax content (%)	Sulphur content (wt%)	Pour point (^{o}C)
A	0.8777	29.7	18.67	30.71	0.11	7
B	0.8497	35.0	2.86	8.44	0.08	10

It was observed from Figure 1 that blending of the seed oils tend to improve the pour point depression ability for all the seed oils on sample A. The blend of CSO with little proportion of JSO (20% of JSO), increased its ability as a pour point depressant for sample A. Also, blend of CSO with little proportion of RSO caused a slight increase in its pour point depression ability. It was further observed that the mixture containing 40% and 50% of JSO in JSO/CSO blend gave similar and the highest pour point depression of sample A from 7 to -3^{o}C (pour point depression of 10^{o}C). The resultant effect of the combination of the interaction of oleic acid and ricinoleic acid in the mixture with the higher paraffin molecules in the crude oil sample may have been contributed to this.

From the results shown in Figure 2 it was observed that blending of the seed oils tend to improve the pour point depression ability for all the seed oils on sample B. The blend of CSO with little proportion of JSO (20% of

JSO), increased its ability as a pour point depressant for sample B. Also, blend of CSO with little proportion of RSO caused a slight increase in its pour point depression ability. It was further observed that the mixture containing 25%, 40% and 50% of JSO in JSO/CSO gave similar and the highest depression of the sample B pour point from 10 to 2.5°C. This may have been due to the resultant effect of the combination of the interaction of oleic acid and ricinoleic acid in the mixture with the higher paraffin molecules in the crude oil sample.

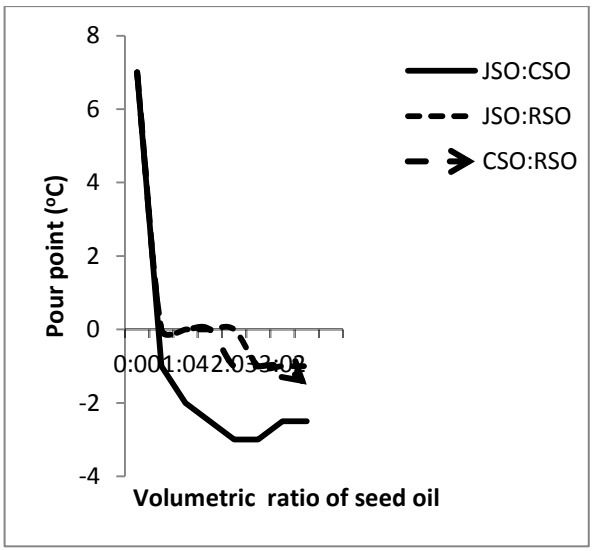

Figure 1. Effects of blends of seed oils on pour point of Sample A

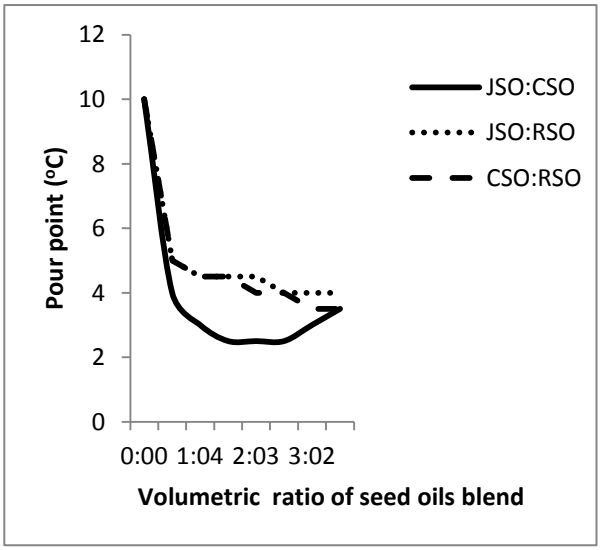

Figure 2 Effects of blends of seed oils on pour point of Sample B

The effects of addition of blend of xylene with TEA on pour points of samples A and B are shown in Figure 3.

The TEA-XY additive mixture contained 10% of TEA and 0.1% of the mixture was added to the crude oil samples tested. From the results obtained, addition of the blended xylene with TEA on both crude oil samples A and B depressed their pour points appreciably in agreement with the findings of the previous researchers (Taiwo *et al.*, 2009; 2012; Popoola *et al.*, 2015). However, comparing the performance of the TEA-XY with those of the plant seed oils blends, especially for sample A, all the plant seed oils blend performed better than the TEA-XY blend. CSO blended with 40% JSO performed better than TEA-XY as pour depressant in sample B while the TEA-XY performed better than CSO/RSO and JSO/RSO blends for the crude oil sample. The observed performance of the CSO/JSO blend was as a result of the synergy between the ricinoleic acid in CSO and oleic acid in the JSO in interacting with the higher paraffin molecules in the waxy crude oil.

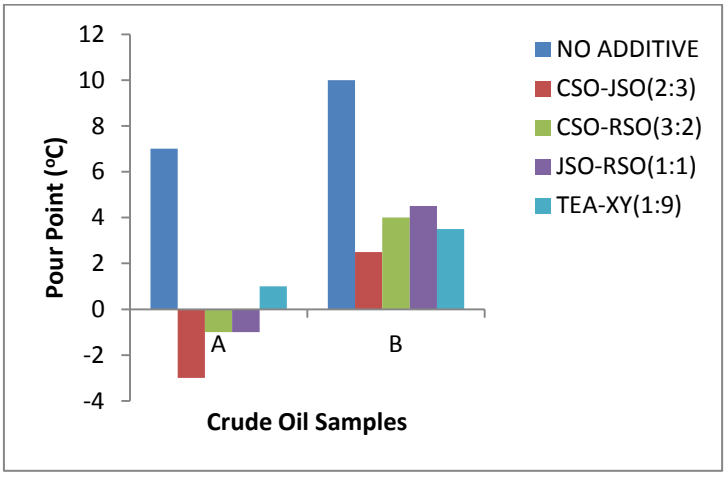

Figure 3. Comparison of effects of blend of seed oils and TEA-XY on pour points of crude oil samples

4.0 CONCLUSION

The impacts of blend plant seed oils and triethanolamine-xylene blend on the pour points of two waxy crude oil samples were investigated. The blended seed oils in binary formulations depressed the pour points of the crude oil samples appreciably better than the TEA-XY blend. 40% of JSO in CSO gave the optimum ratio of combination of plant seed oils blend with best performance on the waxy crude oil as our depressant. The JSO-CSO blend was able to depressed pour point of the waxy crude oil with about 10°C. The blend of the seed oils will not give any corrosion problem the crude oil facilities based on the result obtained from the copper strip test. Thus, appropriate blend of CSO with JSO could be used as pour point

depressant for waxy crude oil at low concentration of additives.

5.0 REFERENCES

Adewusi, V. A. (1997). *Prediction of wax deposition potential of hydrocarbon systems from viscosity-pressure correlation*. Elsevier fuel journal, vol. 76, No. 12, Pp. 1079 - 1083.

Akinyemi O. P., Udonne J. D., Efeovbokhan V. E., Ayoola A. A., (2016a). *A study on the use of plant seed oils, triethanolamine and xylene as flow improvers of Nigerian waxy crude oil*. *Journal of Applied Research and Technology*, 14(2016), 195-205

Akinyemi O. P., Udonne J.D., Oyedeko K.F.K. (2016b). *Study of utilisation of Plant seed oils as Pour Point Depressant for Nigerian waxy crude oil.* Proceedings of 46th Nigerian Society of Chemical Engineers (NSChE) Annual Conference and General Meeting. Nov. 17 – 19. Abuja, Nigeria. 45, pp. 225 – 230

Bello O. O., Fasesan S. O., Akinyemi P. O., Macaulay S. R. A., Latinwo G. K. (2005). *Study of the influence of xylene-based chemical additive on crude oil flow properties and paraffin deposition inhibition, Engineering Journal of the University of Qatar,* 18, 15-28

Fadairo A., Ameloko A., Ako C., Duyilemi A. (2010). *Modeling a wax deposition during oil production using a two-phase flash calculation*. *Petroleum & Coal* 52 (3) 193 -202.

Garcia M. C. (2001). *Paraffin deposition in oil production*. SPE 64992, presented at the 2001 *SPE International Symposium on Oilfield Chemistry* (Houston, Feb. 13-16).

Kok, M. V., Saracoglu, O. (2000). *Mathematical modeling of wax deposition in crude oil pipeline system*. *SPE*, 1 – 7.

Koshel K. C., Kapoor S. (1999). *Effect of Flow Improver on Indian Western Offshore Crude-carrying pipeline;* A Case Study. SPE annual Technical Conference and Exhibition. Oct. Texas USA.

Lorge O., Djabourov M., Brucy F. (1997). *Crystallisation and gelation of waxy crude oils and under flowing conditions. Revue de L'insitut Francais du Peirole*, Vol. 52, N° 2, Mars-Avril

Mahto V., Singh H. (2013). *Effect of Temperature and Pour Point Depressant on Indian waxy crude oil*. International Journal of General Engineering and Technology (IJGET) vol. 2, issue 4; 25 - 30

Miadonye A., Puttagunta V. R. (1998). *Modeling the viscosity-temperature relationship of Nigerian Niger Delta crude petroleum*. *Jour. Pet. Sci. and Tech.* 16 (5 & 6), 627 – 638.

Misra S., Baruah S., Singh K. (1995). *Paraffin Problems in crude oil production and transportation: A Review. SPE Production & Operations, 1995(1):* p. 50-54.

Oseghale C. I., Akpabio E. J., Edebor O. [(2012). *Mitigating potential risk of paraffin Wax deposition on oil pipelines in Niger Delta.* Journal of Engineering and applied sciences 7 (4) 348-352

Popoola C. A., Ayo J. A., Adedeji O. E., Akinleye O. (2015). *Triethanolamine (TEA) As Flow Improver For Heavy Crude Oils*. IOSR Journal of Applied Chemistry (IOSR-JAC), Volume 8, Issue 3 Ver. I., pp. 34-38 www.iosrjournals.org

Taiwo E. A., Fasesan S. O., Akinyemi O. P. (2009). *Rheology of Doped Nigerian Niger-Delta Waxy crude oi*l. Petroleum Science and Technology, 27, 1381-1393, Taylor and Francis group

Taiwo E. A., Otolorin J., Afolabi T. (2012). *Crude oil transportation: Nigerian Niger Delta waxy crude. Crude Oil Exploration in the World, Prof. Mohamed Younes (Ed.)*, ISBN: 978-953-51-0379-0, InTech, pp. 135-154

EXTRACTION, CHARACTERIZATION AND KINETIC MODELS OF OILS FROM LUFFA CYLINDRICA AND HURA CREPITAN SEEDS

Dagde, K. K. [1] and Okure, U. E.[2]

[1,2]Department of Chemical/Petrochemical Engineering, Rivers State University,
Port Harcourt, River State, Nigeria.

dagde.kenneth@ust.edu.ng

ABSTRACT

Present study depicts possibility of extracting oils from Hura crepitan and Luffa cylindrical seeds by soxhlet extraction process, using normal hexane as solvent at different temperature, particle size and extraction time. The oils extracted were separated from oil-solvent mixture by distillation. Physicochemical analysis of the refined oils showed saponification values of 132.45 and 290.32 mgKOH/g, acid values of 12.62 and 27.21 mg KOH/g; iodine values of 3.33 and 176.89 g/100g; viscosity (at 15 °C) of 2.43cp and 3.40cp; refractive index of 1.42 and 1.43; flash point of 128°C and 130°C; specific gravity of 0.93 and 0.94; and moisture content of 6.61% and 8.11% for Hura crepitan and Luffa cylindrical seeds respectively. These results indicated that Hura crepitan oil was highly unsaturated making it suitable for industrial applications as compared with oil from Luffa cylindrica . Maximum percent yields of oils were obtained at 60 ^{O}C, extraction time of 80 mins using 40g of grounded seeds, 0.425mm particle size and 200ml of normal hexane. The kinetics of oils extracted were derived from mass transfer rate equation and power index model and were found to fit reasonably well with the power index model kinetics with mass transfer co-efficient of 0.044min^{-1} for mass transfer model and 0.0736min^{-1} for the power index model.

Keywords: *Solvent Extraction, Characterization, Kinetics, Luffa cylinderica and Hura crepitan.*

1. INTRODUCTION

The need for diversification of the economy and calls by Nigerian citizens for the National Assembly to pass into law, the local content bill came at the right time, as the Nation's economy continue to dwindle. This desire has necessitated the Federal Government to place ban on the importation of most foreign products, including vegetable oil. Nigeria is blessed with diverse sources of vegetable oil (Dawodu, 2009). In searching for more sources of vegetable oil, *Luffa cylindrica* and *Hura crepitan* were investigated in this research.

Luffa cylindrical is commonly known as sponge gourd. It is cylindrical in shaped with smooth surface, which climbs on other plants or materials while growing and produces an average of 33 seeds per fruit. Luffa cylindrica is a sub-tropical plant, which requires warm summer temperatures and long frost-free growing season when grown in temperate regions (Partap *et al*., 2012). While the *Hura crepitan* also known as sand box is a seed from sand box trees which are commonly planted to provide shade.

The three common methods by which oil is extracted from its oil bearing higher seeds are: mechanical pressing, supercritical fluid extraction, and solvent extraction. Solvent extraction method gives higher percentage yield and less turbid oil than mechanical extraction and a low operating cost in relation to supercritical fluid extraction method (Dhellot et al., 2006). Hexane is often used as solvent for oil extraction due to its low boiling points for easy separation after extraction, its non polar nature and its comparatively low toxicity when compared to other solvents. Soxhlet extraction, percentage yield and quality of oil, characterization, kinetics and thermodynamic studies of several oil bearing seeds in Niger Delta, Nigeria have been investigated by several researchers; Akpabio *et al.* (2011), Orhevba and Jinadu (2011) did extraction of oil from *Dacryodes edulis* (Native pear) and *Persea Americana* (Avocado pear) fruits; Nwabanne (2012) did extraction on fluted pumpkin seed; Jabar *et al.*, (2015 and 2016) did extraction of *thevetia peruviana* from its oil bearing seed. Most of the oils were investigated for the production of biodiesel (Abdullah *et al.*, 2013).

This research centres on the use of soxhlet extraction method to extract oil from *Luffa cylidrica* and *Hura crepitan* seeds using hexane as the extracting solvent. The effects of temperature, extraction time, particle size on percentage yield of oils were studied. The physiochemical parameters and kinetic models of the soxhlet extraction process were investigated.

2. MATERIALS AND METHODS

2.1 Sample Collection and Preparation

The *Luffa* fruit were collected from swampy area in Ikot Akpa Inyang Village, while the *Hura crepitan* Seeds were obtained from its fruit, plucked from sandbox tree along Mbiakot road, Mbiakot village, all of Oruk Anam Local Government Area, Akwa Ibom, Nigeria. The fruits were cut open to expose the seeds and sun dried for two days. The seeds were then crushed and sieved to particle sizes of 0.425, 1.00, 1.80 and 2.80mm. The 0.425 mm particle size was divided into 20 equal portions with constant weight of 40.00g. This was done to study the effect of time and temperature.

2.2 Oil Extraction

The oil extraction was carried out in the soxhlet apparatus using n-hexane as solvent. Each of the prepared particle size was placed in the thimble of the extractor and heated via mantle to temperatures of 50, 100, 150 200 ºC and extraction times of 20, 40, 60 and 80 min, respectively.

The mixture of n-hexane and the seed oil (miscella) obtained from the extraction was transferred into distillation flask at temperature of 68 ºC to further separate the oil from the solvent. At the end of the distillation process, the weight of the oil was recorded.

2.3 Percentage Yield

The yield of oil extracted in percentage was calculated using the formula.

$$Percentage\ \ yield\ \ (Y) = \frac{weight\ \ of\ \ pure\ oil\ \ extracted\ \ [w_o]}{weight\ \ of\ \ particle\ \ [w_p]} \times 100\% \quad (1)$$

2.3.1 Characterization of the Extracted Seed Oil

Iodine value, acid value, saponification value and peroxides value were determined using AOCS (1986) method, while refractive index, flash point, viscosity and specific gravity were determined by AOCS (1990) method as in Firestone (2009).

2.3.2 Saponification Value

The Acid Value (AV) was calculated using the expression

$$SV = \frac{(B-S)\times N \times M}{w_o} \quad (2)$$

Where B = blank titre value, S = sample titre value, N = normality of KOH (0.5M), M = molar mass of KOH (56.1) and w_o = weight of oil sample.

2.3.3 Acid Value

The Acid Value (AV) was calculated using the expression

$$AV = \frac{TV \times N \times M}{w_o} \quad (3)$$

where TV is the titre value, N is the normality of KOH (0.1M), M is the molar mass of KOH (56.1) and w_o the weight of oil sample.

2.3.3 Iodine Value

The Iodine Value (IV) was calculated from the equation

$$IV = \frac{(B-S)\times N \times 12.69}{w_o} \quad (4)$$

where B is the blank titre value, S is the sample titre value, N is the normality of sodium thiosulphate and w_o the weight of oil sample.

2.3.4 Peroxide Value

The peroxide value (PV) was calculated from the equation

$$Peroxide\ Value\ (PV) = \frac{(S-B)\times N \times (1000)}{w_o} \quad (5)$$

where B is the blank titre value, S is the sample titre value, N is the normality of sodium thiosulphate and w_o the weight of oil sample.

2.3.5 Refractive Index

The refractive index was determined using Abbe Refractometer.

2.3.6 Flash Point

The flash point of oil was obtained using the Pensky Martens flash point tester.

2.3.7 Specific Gravity

The specific gravity of the oil was obtained using the expression

$$Specific\ \ gravity = \frac{Weight\ \ of\ \ Oil}{Weight\ \ of\ \ equal\ Volume\ \ of\ \ water} \quad (6)$$

2.4 Extraction Kinetics

The extraction of oil from *Hura Crepitan* and *Luffa Cylindrical* using hexane as the extracting solvent involved no chemical reaction between the oil and the solvent hence the obtained experimental data in soxhlet extraction method were investigated using mass transfer kinetic model.

2.4.1 Kinetic Model

In leaching operation, the mass transfer rate involved in solid-liquid interface has been expressed as:

$$\frac{dm}{dt} = K' \frac{A}{b}(C_s - C) \quad (7)$$

Where m is the mass of solute transferred with time (g), K' is the diffusion coefficient (cm^2/min),
A is the area of solid-liquid interface (cm^2), b is the effective thickness of liquid film surrounding the particle (cm), t is the time of solute transfer (min), C is the concentration of solute in the bulk of the solution with time (g/cm^3) and C_s is the concentration of saturated solution in contact with the particles (g/cm^3).

$$\text{But } m = VC \quad (8)$$

Where V is the volume of vessel or reactor (cm^3). In batch operation, V is constant thus from equation (7)

$$dm = VdC \quad (9)$$

Combining equations (7) and (9) gives

$$\frac{dC}{dt} = K' \frac{A}{bV}(C_s - C) \quad (10)$$

Let $$K' \frac{A}{Vb} - = k \quad (11)$$

Where k is extraction rate constant (min^{-1}), hence from equation (10), we have

$$\frac{dC}{dt} = k(C_s - C) \quad (12)$$

By integrating equation (11) using the bounding condition of t = 0 and $C = C_O \; to \; t = t \; and \; C = C$, assuming no resistance in the solid phase (pure solvent) and expressing the resulting equation in logarithmic form; also, if pure solvent is used, C_o = 0 i.e there is essentially no resistance in the solid phase for a pure material then:

$$\ln\left(\frac{C_s}{C_s - C}\right) = kt \quad (13)$$

Expressing equation (12) in terms of yield,

$$\ln\left(\frac{Y_s}{Y_s - Y}\right) = kt \quad (14)$$

A plot of $\ln\left(\frac{Y_s}{Y_s - Y}\right)$ against t gives a slope equivalent to k.
where: Y = Percentage of oil yield with time (%), Y_s = Percentage of oil yield at saturation point (%)

Further simplification of equation (13) yields

$$Y = Y_s\left(1 - e^{-kt}\right) \quad (15)$$

2.4.2 Power Index Model

The power index model is expressed in equation (16) according to Nwabanne, (2012).

$$\frac{dY}{dt} = kY^n \quad (16)$$

Where n is power index and not the order of reaction. Every other parameter in the equation remained as earlier defined.
Integration of equation (15) using boundary condition of t=0, $and \; Y = Yo$, to t = t and $Y = Y$ by separation of variable method and expressing in logarithmic form yields

$$\ln Y = \frac{1}{(1-n)}\ln[k(1-n)] + \frac{1}{(1-n)}\ln t \quad (17)$$

A plot of $\ln Y$ against $\ln t$ gives a slope equivalent to $\frac{1}{1-n}$.

3. RESULTS AND DISCUSSION

3.1 Analysis of GC –MS Chromatogram

GC –MS Chromatogram was used for the identification/analysis of the oil sample to determine the type of fatty acid, degree of saturation, and physicochemical properties. Figure 1 and 2 depicts the pressure of Palmitic, and Linoliec fatty acid in the oil sample. Pick 1 indicate Palmitic acid while pick 2 and 3 indicates Linoleic fatty acid at retention time of 20.6 min.

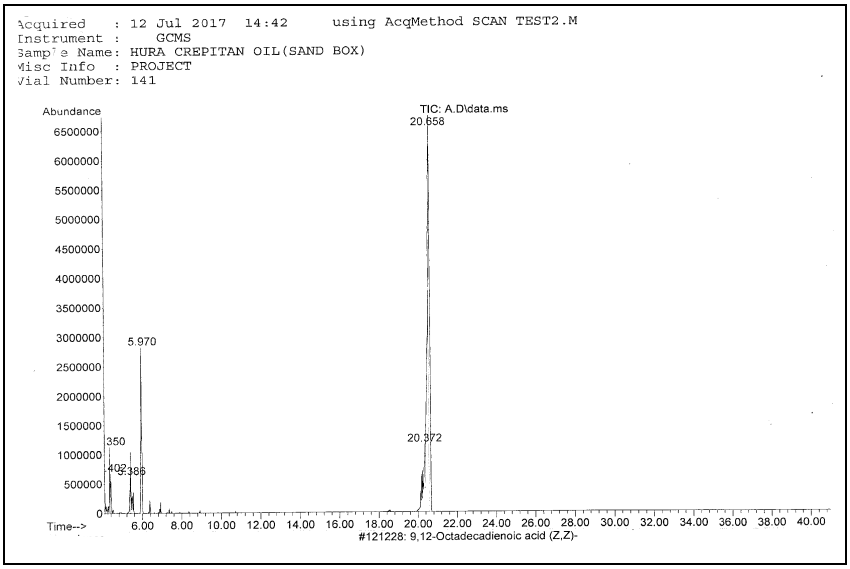

Figure 1: GC-MS Chromatogram of *Hura crepitan*Seed Oil

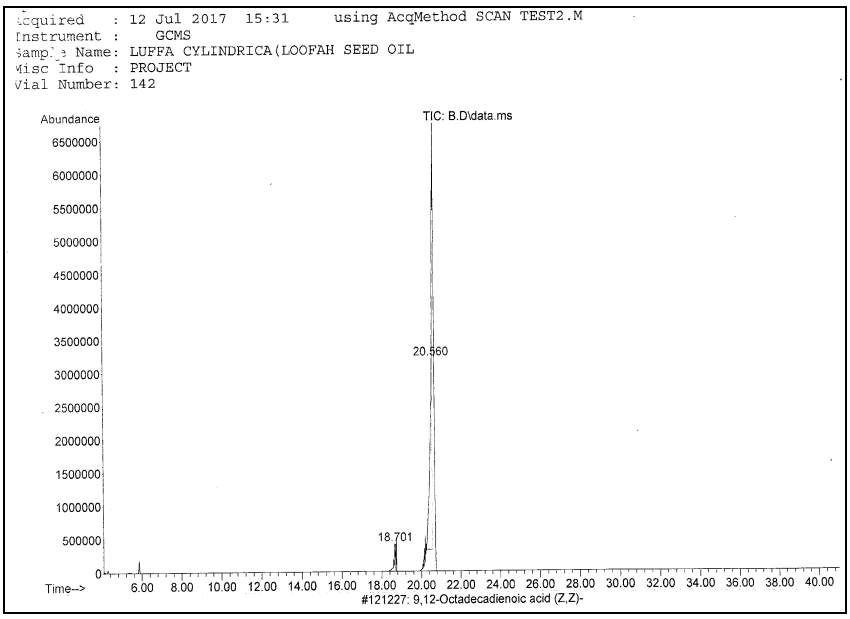

Figure 2: GC-MS Chromatogram of *Luffa cylindrical* Seed Oil Sample

Table 1 and 2 show that *Hura crepitan* and *Luffa cylindrica* seed oil Sample contain palmitic and linoleic fatty acid. Linoleic fatty acid is unsaturated with two double bonds, low melting point of about -5^0C and of very rapid reactivity to oxygen. Its ability to react with oxygen enhances its use as film forming vehicles for paints, varnishes, floor coverings, lubricants and other industrial applications.

Table 1: Analysis of GC-MS Chart Peaks of *Hura crepitan* Seed Oil Sample

Retention Time (min)	Compound	Formula	M.W	Weight (%)	Peak
5.970	Palmitic acid	$C_{15}H_{31}COOH$	256	10.01	Peak I
20.372	Linoleic acid	$C_{17}H_{31}COOH$	280	5.25	Peak II
20.658	Linoleic acid	$C_{17}H_{31}COOH$	280	66.62	Peak III

Table 2: Analysis of GC-MS Chart Peaks of *Luffa cylindrica* Seed Oil Sample

Retention Time (min)	Fatty Acid	Formula	M.W	Weight (%)	Peak
18.701	Palmitic acid	$C_{15}H_{31}COOH$	256	3.15	Peak 1
20.560	Linoleic acid	$C_{17}H_{31}COOH$	280	96.85	Peak 2

Where M.W is the molecular weight

3.2 Physicochemical Properties of Extracted Oil

The physicochemical characteristics of *Luffa cylindrica* and *Hura crepitan* oils are presented in Table 3. The physical analysis of the oil obtained gave a pH of 5.89 and 5.10 for *Luffa cylindrica* and *Hura crepitan* oils respectively which indicate that the oils are acidic in nature. A value of 1.42 and 1.43 was obtained for the refractive index, a specific gravity of 0.93 and 0.94, flash point of 128^{0}C and 130^{0}C, moisture content of 6.61 and 8.11 for *Luffa cylindrica* and *Hura crepitan* oils respectively. The oils were found to be dark brown and golden yellow in colour and have non-offensive odour.

The chemical analysis showed that the oils obtained have a saponification value of 132.45 and 290.32(mgKOH/g), acid value of 12.62 and 27.21(mgKOH/g), iodine value of 31.33 and 176.89 (g/100g), peroxide value of 10.50 and 3.75(mg eq./kg sample) for *Luffa cylindrica* and *Hura crepitan* oils respectively. The high saponification value of the *Hura crepitan* oil is indicative that it can be used for soap production and in making other cosmetic products like sampoo. The iodine number for *Hura crepitan* oil indicates high degree of unsaturation depicting the racidity and drying properties of the oil suggesting that the oil is drying in nature.

Table 3: Physicochemical Characteristics of Extracted Oils

Parameter	Value	
	Luffa cylindrical	*Hura crepitan*
Saponification Value (mgKOH/g)	**132.45**	**290.32**
Acid value (mgKOH/g)	12.62	27.21
Iodine value (g/100g)	31.33	176.89
Peroxide value (mg eq./kg sample)	10.50	3.75
Viscosity at 15 ºC (cp)	2.43	3.40
Refractive index (-)	1.42	1.43
Flash point (ºC)	128	130
Specific gravity (-)	0.93	0.94
Moisture content (%)	6.61	8.11
pH	5.89	5.10
Colour	Dark brown	Golden yellow

3.3 Percent oil yields

The percent oil yields of 42.01 and 38.9 for *Hura crepitan* and *Luffa cylindrical* oils respectively were comparable to values of 49.9% *(Melina seed)*, 46.3% *(Jatropha Curcas L seeds)*, 52.4% of *(Persea Americana)* and 56.5% of *(Dacryodes edulis)* as reported by Uzoh *et al.* (2014), Joshi *et al.* (2011), and Akpabio *et al.* (2011), respectively.

3.4 Effect of Extraction Time on Oil Yields

Effect of extraction time on the yield of oil obtained from *Luffa cylindrica* and *Hura crepitan* were studied at constant temperature and particle size. The experimental results showed that the yield of oil for both raw materials increases with time. At of 60 ºC and 0.425 mm, the yields increased from 11.40 to 35.90 % in *Luffa cylindrical* and 13.72 to 42.01% in *Hura crepitan* at time of 20 to 80 min. It could be seen that the oil yield was greater in *Hura crepitan* than in *Luffa cylindrical*.

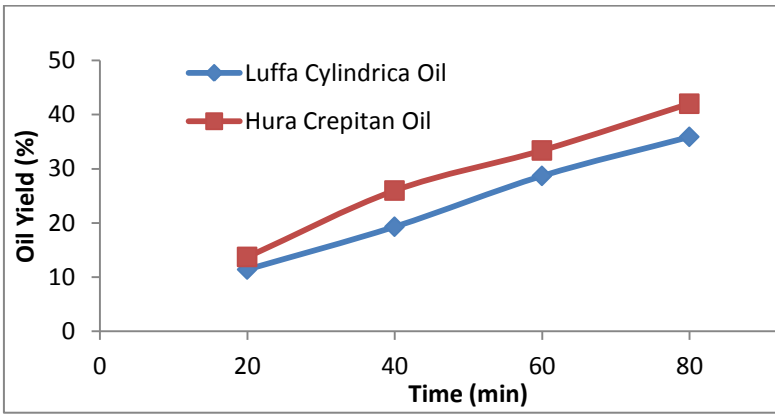

Figure 3: Comparison of *Luffa Cylindrica* and *Hura Crepitan* Oil Yield with Time

3.5 Effect of Temperature on Oil Yields

The effect of temperature on oil yields as shown in Figure 2 revealed that temperature increase improved the yield of oil for both raw materials. At 80 min and particle size of 0.425 mm, the oil yield increases from 15.62 to 35.9 % in *Luffa cylindrical* and 18.31 to 42.01 % in *Hura crepitan* at temperature of 30 to 60ºC. The percentage yield of oil from *Hura crepitan* was higher *than* that from *Luffa cylindrical*.

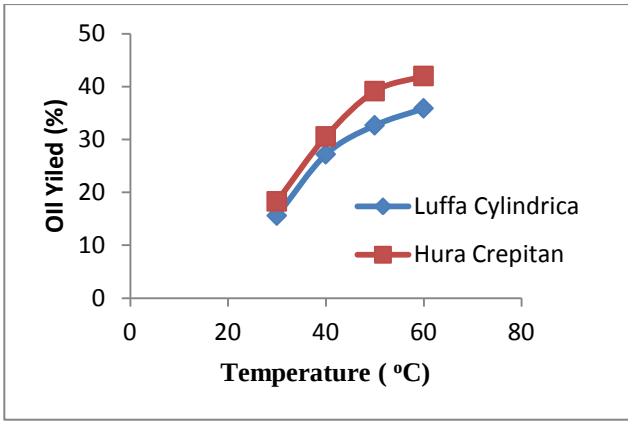

Figure 4: Comparison of *Luffa Cylindrica* and *Hura Crepitan* Oil Yield with Temperature

3.6 Effect of particle size on Oil Yield

The effect of particle size on oil yield is shown in Figure 3. At 80 min and temperature of 60 ºC, the oil yield decreases from 35.90 to 18.65 % in *Luffa cylindrical* and 42.01 to 22.68 % in *Hura crepitan* at particle size of 0.425 to 2.80 mm. But in terms of raw material, the yield under the influence of particle size was higher in *Hura crepitan than* in *Luffa cylindrical* oil.

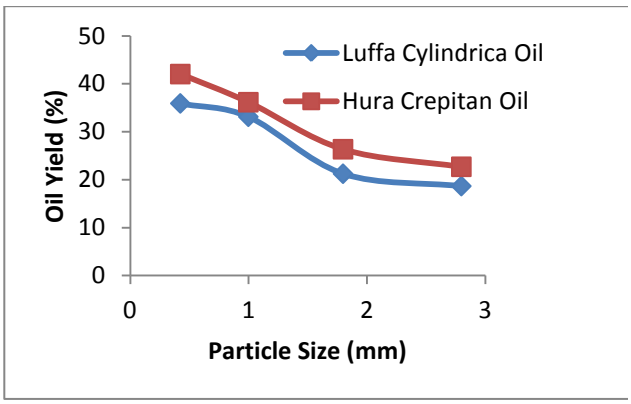

Figure 5: Comparison of *Luffa Cylindrica* and *Hura Crepitan* Oil Yield base on Particle Size

3.7 Kinetics of *Luffa cylindrical* Oil Yield

The 1st order rate kinetics of *Luffa cylindrical* oil yield shown in Figure 4 was fitted to linear regression equation and upon which, a predictive model for *Luffa cylindrical* oil yield was obtained as $Y = 35.90\left(1 - e^{-0.0261t}\right)$.

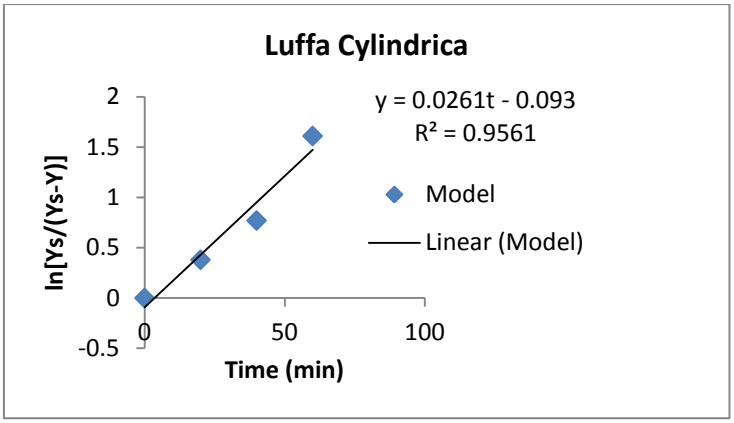

Figure 6: Determination of Kinetics Parameters for *Luffa Cylindrica*

3.8 Kinetics of *Hura Crepitan* Oil Yield

The application of 1st order rate kinetics shows that *Hura crepitan* oil yield can be predicted by the model: $Y = 42.01\left(1 - e^{-0.044t}\right)$.

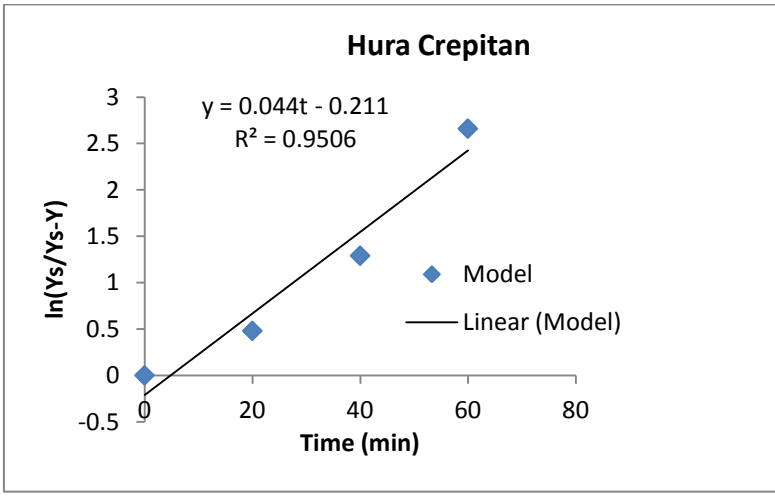

Figure 7: Determination of First order Rate Kinetic Parameters for *Hura Crepitan*

3.9 Power Index Model of *Luffa cylindrical* Oil Yield

The power index model shows that *Luffa cylindrica* oil yield can be predicted by the model: $Y = 0.8917t^{0.8436}$ with the rate constant, k = 0.7364min^{-1}.

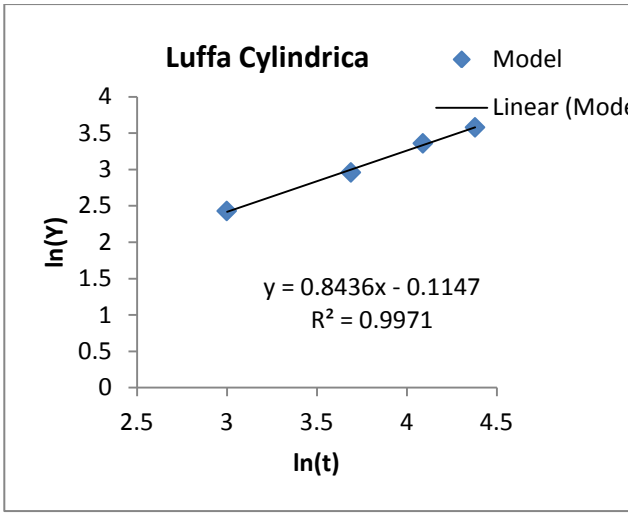

Figure 8: Power Index Rate Kinetic Parameters for *Luffa Cylindrica*

3.10 Power Index Model of *Hura Crepitan* Oil Yield

The application of power index model shows that *Hura Crepitan* oil yield could be predicted by the model: $Y = 1.2575t^{0.8056}$ with the rate constant, k = 1.0706min^{-1}.

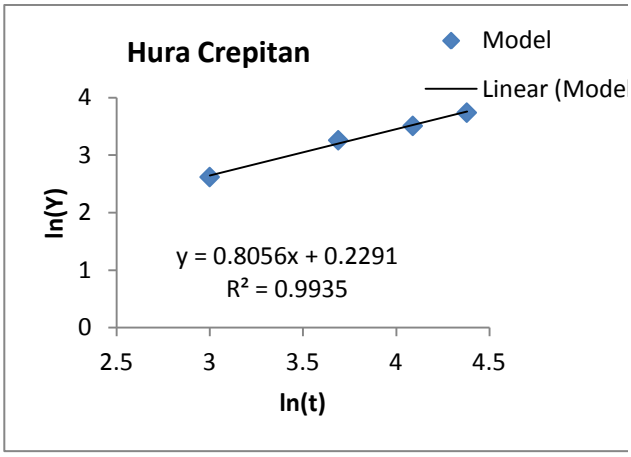

Figure 9: Determination of Power Index Rate Kinetic Parameters for *Hura Crepitan*

3.11 Comparison of Experiment and First Order Rate Kinetics for *Luffa cylindrical* Oil Yield

The experimental results for *Luffa cylindrical* oil yield was compared with the first order rate kinetics, which shows that the model values were initially higher than those of the experiment but from 60 min, their values were lower.

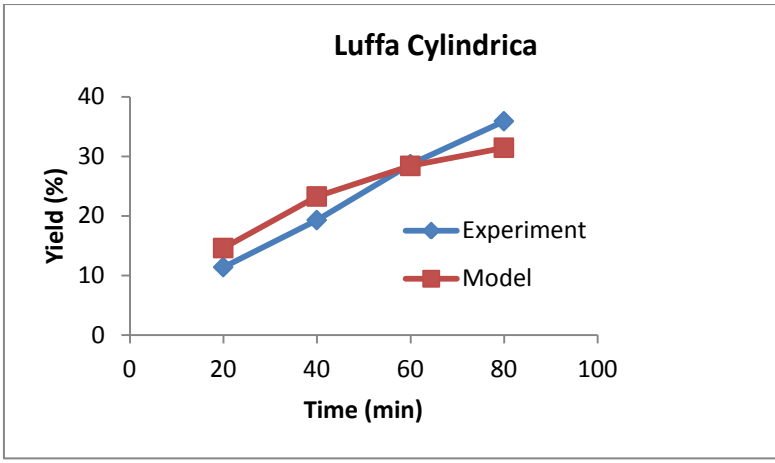

Figure 10: Comparison of Experiment and Pseudo First Order Rate Model for *Luffa Cylindrica*

3.12 Comparison of Experiment and First Order Rate Kinetics for *Hura Crepitan* Oil Yield

The experimental results for *Hura crepitan* oil yield compared with the first order rate kinetics, shows that the model values were higher than those of the experiment but nearly 80 min, their values coincided.

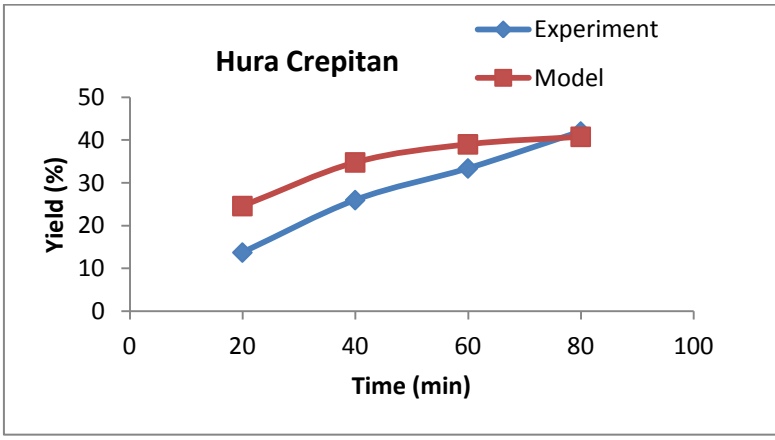

Figure 11: Comparison of Experiment and Pseudo First Order Rate Model for *Hura Crepitan*

3.13 Comparison of Experiment and Power Index Model for *Luffa cylindrical* Oil Yield

The experimental results for *Luffa cylindrica* oil yield compared with the power index rate kinetics, shows that there were no significant difference between the model predictions and the experiment results.

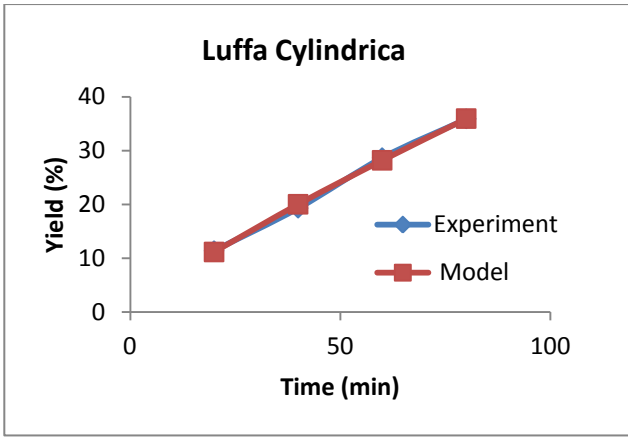

Figure 12: Comparison of Experiment and Power Index Rate Kinetic Model for *Luffa Cylindrica*

3.14 Comparison of Experiment and Power Index Model for *Hura Crepitan* Oil Yield

Figure 11 shows that the experimental results for *Hura crepitan* oil matched reasonably well with the power index rate kinetics model predictions. These show that the power index rate kinetics model is capable of predicting the percent oil yields of *Luffa cylindrical* oil and *Hura crepitan*

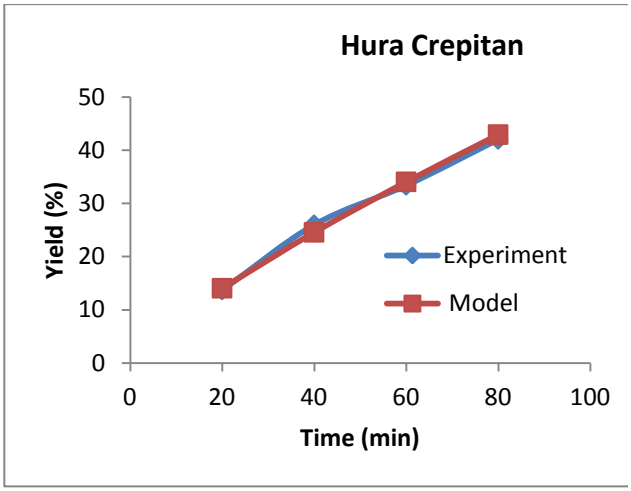

Figure 13: Comparison of Experiment and Power Index Rate Kinetic Model for *Hura Crepitan*

4.0 CONCLUSION

The extraction of inedible vegetable oil from renewable, biodegradable, abundance, environmentally friendly Luffa Cylindrica and Hura Crepitan seeds which have the potential of been an alternative to petrochemical resource have been presented. The oils especially Hura Crepitan showed high degree of unsaturation hence can be used as classified drying oil suitable for soap, paint, varnish, cosmetics, insecticides and other industrial applications. The results showed remarkable effect of parameters like temperature, particle size and extraction time on the yield of oils. The soxhlet extraction process fitted reasonable well with the power index kinetic model. Maximum percent yields of Hura Crepitan and Luffa cylindrical oils were obtained at 60^{o}C for an extraction time of 80mins using 40g of grounded Hura Crepitan and Luffa cylindrical seeds of 0.425mm particle size and 200ml of normal hexane.

5.0 REFERENCES

Abdullah, B.F., Yusop, R.M., Salimon, J., Yousif, E. & Salih, N., (2013). Physical and Chemical Properties Analysis of *Jatrophacurcas*Seed Oil for Industrial Applications, *World Academy of Science, Engineering and Technology International Journal of Chemical, Molecular, Nuclear, Materials and Metallurgical Engineering*, 7(12), 893-896.

Akpabio, U. D., Akpakpan, A. E., Matthew, I. E. & Akpan, A. U., (2011). Extraction and Characterization of Oil from Avocado Pear (*Persea Americana)* and Native Pear (*Dacryodes edulis*) Fruits, *World Journal of Applied Science and Technology*, 3(2), 27-34.

Dawodu, F. A., (2009). Physico-Chemical Studies on Oil Extraction Processes from some Nigerian Grown Plant Seeds, *Electronic Journal of Environmental, Agriculture and Food Chemistry*, 8(2), 102-110.

Dhellot, J.R., Matouba, E., Maloumbi, M.G., Nzikou, J.M., Safou Ngoma, D.G. Linder, M., Desobry, S. & Parmentier, M., (2006).Extraction, Chemical Composition and Nutrional Characterization of Vegetable Oils: Case of *Amaranthus hybridus* (var 1 and 2) of Congo Brazzaville, *African Journal of Biotechnology*, 5(11), 1095-1101.

Firestone D (2009), Official Methods and Recommended Practices of the AOCS, (6th Ed.). American Oil Chemical Society.

Gunstone, F.D., (2012). Vegetable Oils Food Technology: Composition, Properties and Uses, Blackwell Publishing Limited, CRC Press, ISNB 0-8493-2816-0.

Jabar, J. M., Lajide, L. Adetuyi, A. O., Owolabi, B. J., Bakare, I. O., Abayomi, T. G. & Ogunneye, A. L., (2015). Yield, Quality, Kinetics and Thermodynamics Studies on Extraction of *Thevetia Peruviana* Oil from its Oil Bearing Seeds, *Journal of Cereals and Oilseeds*, 6(5), 24-30.

Jabar, J.M., Lajide, L., Bakare, I. O. &Oloye, M. T., (2016). Extraction and Characterization of Vegetable Oil from *Thevetia Peruviana* and *Jatropha Curcas* Seeds, *FUTA Journal of Research in Sciences*, 12(1), 73-80.

Joshi, A., singhal, P. & Bachheti, R. K., (2011).Physicochemical Characterization of Seed Oil of *Jatropha Curcas*L. Collected from Dehradun (Uttarakhand) India, *International Journal of Applied Biology and Pharmaceutical Technology*, 2(2), 123-127.

Nwabanne, J. T., (2012). Kinetics and Thermodynamics Study of Oil Extraction from Fluted Pumpkin Seed, *Internal Journal of Multidisciplinary Science and Engineering*, 3(6), 23-27.

Orhevba, B.A. and Jinadu A.O., (2011).Determination of Physico-Chemical properties and Nutritional contents of avocado pear *(persea americana m.), Academic Research International*,1(3), 372-380.

Partap, S., Kumar, A., Sharma, N. K. &Jha, K. K., (2012).*Luffa Cylindrica*: An Important Medicinal Plant, *J. Nat. Prod. Plant Resource*, 2012, 2 (1):127-134

Uzoh, C.F., Onukwuli, O.D&Nwabanne, J.T., (2014). Characterization, Kinetics and Statistical Screening Analysis of Gmelina Seed Oil Extraction Process, *Mater Renew Sustain Energy*, 3(38). Available at: http://DOI 10.1007/s40243-014-0038-1.

REVITALIZATION OF GAS SECTOR FOR MAXIMUM UTILIZATION OF NATURAL GAS IN NIGERIA THROUGH INDUSTRIAL SYMBIOTIC SYSTEM

***Tsado, D. G. and Uwafor, O. G.**
Chemical Engineering Department,
Federal Polytechnic, Bida. Niger State. Nigeria
e-mail: davidadule@yahoo.co.uk

ABSTRACT

As a developing country, Nigeria needs industrialization to ensure wealth creation, reduce poverty and inequality gap including Nigeria's back-aching unemployment level. Any country with more industrialization will need more resources to run factories, machines, and so on; these may require the increased usage of finite natural resources, such as crude oil, natural gas, mining deposits, and so on. Therefore, solutions that secure both sustainable human and economic development need to be found. One solution combining the principles of both economic growth and sustainability is Industrial Symbiosis, and thus, the reposition of gas sector imperative for optimum economic gains. In Nigeria, less than 51% of the populations have access to electricity. And yet the natural gas is still being flared in Nigeria; where the largest single consumer of natural gas is the electricity utility. This can be translated to mean that there is no maximum utilization of natural gas. Energy supply is too essential in any country's development and experiencing consistent power failure has resulted in crippled industries in the country. Considering the existence of natural resources does not always translate to development, as these often times lead to complacency and mismanagement; Nigeria may have suffered from this. Therefore, in this presentation, the extent of production and utilization of natural gas in Nigeria is discussed. Gas utilization in the direction of electricity production which further revitalizes the gas sector and consequently drives industrialization in symbiotic manner in the country for economic development is discussed.

1. INTRODUCTION

There cannot be industrial symbiosis where industries do not exist; industrialization is fundamental to industrial symbiotic system. The term 'symbiosis' builds on the notion of mutualism in biological communities where at least two otherwise unrelated species exchange materials, energy, or information in a mutually beneficial manner. So, too, industrial symbiosis consists of place-based exchanges among different entities that yield a collective benefit greater than the sum of individual benefits that could be achieved by acting alone. Such collaboration can also increase social capital among the participants. Any country with more industrialization will need more resources to run factories, machines, and so on; these may require the increased usage of finite natural resources, such as crude oil, natural gas, mining deposits, and so on, and thus, revitalize such sector that produces the resources.

Natural Gas is a fossil fuel that exist in a gaseous state and is composed mainly of methane (CH_4) a small percentage of other hydrocarbons (e.g. ethane). The use of natural gas is becoming more and more popular as it can be used with commercial, industrial, electric power generation and residential applications.

Usually, there will be a mixture of pros and cons when it comes to industrialization (Daniel, 2015). However, a high quality of life for all humans depends on the development of sustainable production and consumption patterns and the efficient use of resources. Therefore, solutions that secure both sustainable human and economic development need to be found. One solution combining the principles of both economic growth and sustainability is Industrial Symbiosis which revitalize gas sector in Nigeria if natural gas is put at maximum utilization.

Poor energy supply is dampening the progression of industrialization in the country and the sooner it is considered an urgent discussion the better for industries and the county's economy. Energy supply is too essential in any country's development and experiencing consistent power failure has resulted in crippled industries in the country.

Currently, the largest single consumer of natural gas in Nigeria is the electricity utility, with an average consumption of 42 million standard cubic meters per day (mmscm/d) at peak production, or about 70% of

domestic consumption. Nigeria has one the lowest electricity access in Africa. Also, less than 51% of the populations have access to electricity. And yet the natural gas is still being flared in Nigeria. This can be translated that there is no maximum utilization of natural gas.

Industrialization and technological development, just like most of the other national developments, are usually the byproducts of optimal management of both human and natural resources. Any nation that fails to develop and utilize the human and natural resources, the backbone of national development, will not only be backward in terms of technological advancement, but will surely be condemned to perpetual poverty irrespective of how numerous other resources might be (Kenichi and Takahiro, 2006).

Considering the existence of natural resources does not always translate to development, as these often times lead to complacency and mismanagement; Nigeria may have suffered from this. Therefore, in this presentation, the extent of production and utilization of natural gas in Nigeria will be discussed. Gas utilization in the direction of electricity production, which will further drive industrialization in the country and thereby revitalize the Nigerian gas sector, is examined.

2. GAS UTILIZATION IN NIGERIA

Nigeria is one of the top ten nations in the world with huge natural gas reserves. Nigeria's gas reserves was estimated at 187 trillion standard cubic feet of gas (tscf), with current production estimated at 8.24 billion standard cubic feet of gas per day (scfd) as of 2012. This is made up of 98 tscf of associated gas (AG) and 89 tscf of non-associated gas. A large fraction (about 21%) of the AG produced during the production of crude oil is currently being flared, as at 2013 **(**Chijioke, 2014: NAPIMS, 2015).

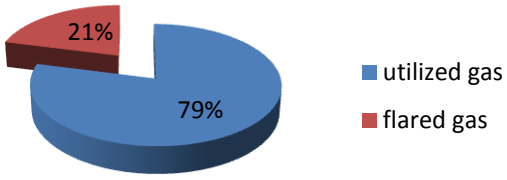

Source: Omosomi, (2014)

Figure 1: Percentage Gas Utility and Flared in Nigeria as at 2013

In order to diversify its revenue base and reduce the huge wastage of valuable resource as well as the degradation of the environment as a result of flaring, the Nigerian Government, through the NNPC, is vigorously pursuing a number of natural gas utilization projects with its joint venture partners whereby associated gas would be harnessed to achieve these objectives.

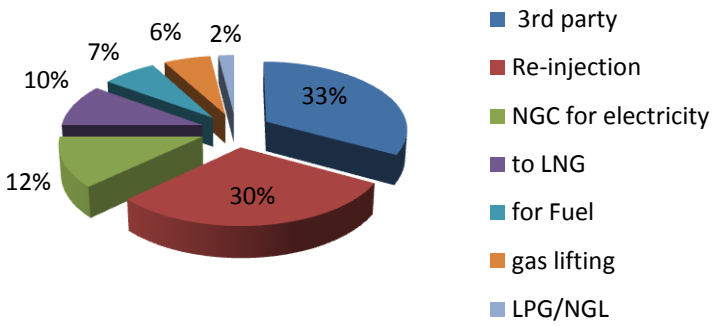

Source: Omosomi, (2014)

Figure 2: Distribution of the 79 % of the quantity utilized to various purposes- as at 2013

In the first nine months of 2013, an aggregate of 1,615.79 billion cubic feet of natural gas was produced with 79 percent of the quantity utilized. An analysis of the supply chain as conducted by Business Day Research and Intelligence unit (BRIU) revealed that 33 percent of gas utilized was sold to third parties, 30 percent was for re-injection purposes for enhanced oil recovery, while 12 percent was sold to NGC for power generation and 10 percent was for LNG. In addition, 7 percent was utilized for fuel while 6 percent was for gas lifting and the remaining 2 percent for LPG/NGL as feedstock to Eleme Petrochemical Company Limited (EPCL). Globally, Nigeria is the 6th largest producer of liquefied petroleum gas (LPG) and the second largest on the African continent (Omosomi, 2014).

Subsequently, of total gas produced from January to September of 2013, 21 percent or 331.81 billion cubic feet was flared. Gas flared in monetary terms translates to N237.73 billion. The opportunity cost is estimated to be equivalent to 792 megawatts (MW) of electricity generating potential.

Natural gas can also be used by industries as a raw material (feedstock) for the production of secondary products, such as methanol, fertilizer, gas– to- liquids (GTL); or as an industrial fuel for manufacturing firms. This has direct multiplier effect on the economy.

This means that the gas sector in Nigeria is going to be a beehive of activities, and a lot of room exists for investment in this area. Some of these are: LNG (Liquefied Natural Gas), IPP (Independent Power Plant), GTL (Gas to Liquid Conversion), NGL (Natural Gas Liquids) and Methanol. Gas supply to local industries, is indeed an industry with great potentials and future in the 21st century.

The National Gas Company (NGC) currently supplies gas for power generation, as source of fuel or as feedstock to current industries, etc and the demand is increasing. A large potential market exists for investors in this area. Domestic gas demand is about 400 million cubic feet a day (MMcf/d) which is very low compared to the size of Nigeria's population and its gas resources (Kareem *et al*., 2012).

Power sector consumes about 90% of the total gas supply, industrial 4% and the chemical feedstock about 3%, the pattern of gas consumption

Gas is a close substitute for other fuels in electricity generation, a complement to crude oil in revenue earning, a feedstock for fertilizer and petrochemical industries and environmentally friendlier, being cleaner than crude oil or coal. But natural gas in Nigeria has a problem and that is, most of it is flared (Ojinnaka, 1998). This leads to adverse effect on the environment

Currently, the largest single consumer of natural gas in Nigeria is the electricity utility, with an average consumption of 42 million standard cubic meters per day (mmscm/d) at peak production, or about 70% of domestic consumption. With an estimated electricity consumption per capita of about 150 kWh per annum in 2010 (NBS, 2012), Nigeria has one the lowest electricity access in Africa. Also, less than 51% of the populations have access to electricity. Hence one of the most important domestic uses of natural gas will be in gas-to-power projects. An earlier study in this area (Ibitoye & Adenikinju, 2007) indicated that for Nigeria to move from low to middle-income country, meet requirements of the millennium development goals and also achieve the status of an industrializing nation, per capita electricity consumption will have to rise to about 5 000 kWh by the year 2030. Most of this demand for electricity will have to be met through the use of natural gas power plants.

Another viable route for domestic gas consumption is through the extension of natural gas pipelines to industrial and commercial consumers – cement factories, pharmaceutical and petrochemical companies, food and beverages factories, etc. Demand for gas by industrial and commercial consumers could range between 28 and 42 mmscm/d (Francis, 2014). Apart from opening up more channels for gas utilization, this will also improve the economy through increased production.

Electricity generation from natural gas is accorded a high priority in the National Gas Plan. In the Strategic Gas Plan for Nigeria (ESMAP, 2004), electricity generation is projected to grow at the annual rate of 6%, and natural gas demand for this increase in electricity generation is expected to rise from 21 mmscm/d in 2010 to over 198 mmscm/d in 2040. With this, per capital electricity would increase to 771 kWh in 2040 (World Bank, 2013).

"Nigeria will require about 70 percent of gas produced to meet her power supply need". Minister of Power, Mr. Chinedu Nebo stated this in Lagos at a pre-conference workshop of the 32nd Annual International Conference and Exhibition of the Nigerian Association of Petroleum Explorationist (NAPE) with the theme ''Driving an Executable Gas Flare-out agenda for Nigeria's Oil and Gas Industry''. The Minister explained that with the number of households in Nigeria put at 29million, at an average consumption of 1MW for some 500 homes, a maturing Electricity Supply Industry in Nigeria should be producing some 60GW of power for household consumption every day, and of these, some 42 GW should be fueled by gas. The Minister maintained that opportunities abound for new IPPs in Nigeria's electricity supply industry, with a call on experts in NAPE to contribute towards making the new gas frontiers a reality for the Nigerian power sector (Adewale**,** 2014).

3. INDUSTRIAL SYMBIOTIC SYSTEM

Industrial symbiosis is part of a new field called industrial ecology. Industrial ecology is principally concerned with the flow of materials and energy through systems at different scales, from products to factories and up to national and global levels. Industrial symbiosis focuses on these flows through networks of businesses and other organizations in local and regional economies as a means of approaching ecologically sustainable industrial development. Industrial symbiosis engages traditionally separate industries in a collective approach to competitive advantage involving physical exchange of materials, energy, water, and/or by-products. The keys

to industrial symbiosis are collaboration and the synergistic possibilities offered by geographic proximity (Marian, 2012).

The term 'symbiosis' builds on the notion of mutualism in biological communities where at least two otherwise unrelated species exchange materials, energy, or information in a mutually beneficial manner. So, too, industrial symbiosis consists of place-based exchanges among different entities that yield a collective benefit greater than the sum of individual benefits that could be achieved by acting alone. Such collaboration can also increase social capital among the participants.

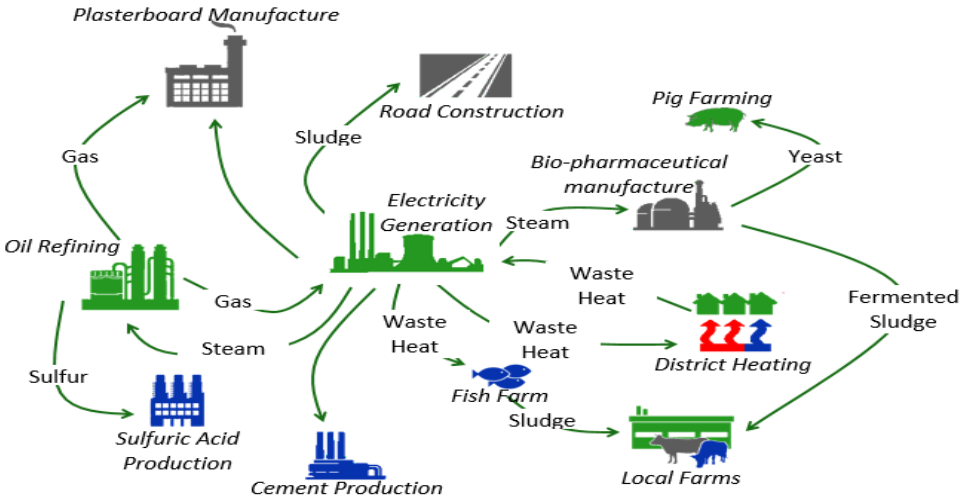

Source: http://www.energenz.com/themes/circular-economy/industrial-symbiosis/

Figure 3: Schematic Illustration of an Industrial Symbiosis

Why Industrial Symbiotic System?

- The private sector accounts for around two thirds of natural resources consumption.
- Industrial symbiosis converts negative environmental externalities into benefits.
- Industrial symbiosis promotes economic growth and at the same time reduces environmental burdens.
- While implementation generally is in a geographical distinct area, the benefits are not limited to this area but link to global issues.
- Industrial symbiosis is increasingly seen as integral part of economic and environmental policy, but its dynamics have not yet been fully understood.
- A better theoretical analysis and understanding of the network mechanisms would lead to facilitated coordination of initiatives and would help to ensure long term successful operation.

Industrial Symbiosis as Mechanism for Sustainable use of Environmental Resources

Decoupling of resources use from economic growth is one of the central challenges of pathways towards a sustainable future. In this context, industrial symbiosis holds huge potential. While increased resource efficiency is one of its central aspects, industrial symbiosis links to broader agendas in the fields of green economy, innovation, material and energy security, climate change, as well as local, regional and national welfare (Sigrid, 2015).

Industrial symbiosis encompasses initiatives in which two or more industrial entities develop mutually beneficial relationships. Most common is the case that one entity makes productive use of a material stream that is regarded as waste by another entity. Other examples of symbiotic cooperation include the shared utilization of specific equipment or facilities and the pooling of resources. Environmental benefits result from reduced consumption of resources and reduced amounts of waste and emissions. The system of exchange typically converts negative environmental externalities, mainly in the form of waste, into positive environmental externalities such as decreased pollution and reduced need for raw material (Chertow & Ehrenfeld 2012). For the industrial entities, the benefit lies primarily in economic advantages. Industrial symbiosis promotes economic growth, while at the same time it generates environmental benefits. Implementation of industrial symbiosis therefore holds huge potential to unlock powerful mechanisms that foster sustainable development.

4. GAS UTILIZATION TOWARDS ELECTRICITY GENERATION

The fastest growing use of natural gas today is for the generation of electric power. Gas power stations convert the heat energy from the combustion of natural gas into electricity, which can be used in homes and businesses. With greater operational flexibility and being cleaner burning than coal power plants, more and more gas-fired power stations are being built across the globe and, today. Natural gas therefore becomes an attractive "transition" fuel, as the energy supply moves away from polluting sources such as coal and nuclear sources and towards cleaner, renewable technologies.

Natural gas, because of its clean burning nature, has become a very popular fuel for the generation of electricity. In the 1970s and 1980s, the choices for most electric utility generators were large coal or nuclear-powered plants. However, due to economic, environmental and technological changes, natural gas has become the fuel of choice for new power plants built since the 1990s. In fact, the Energy Information Administration (EIA) estimates that between 2009-2015, 96.65 Gigawatts (GW) of new electricity capacity will be added in the U.S. Of this, over 20 percent, or 21.2 GW, will be natural gas additions

5. SITUATION OF NIGERIAN ELECTRICITY SUPPLY AND DEMAND

It is generally acknowledged that the present epileptic state of the electrical power supply situation in the country is one of the major causes (and perhaps the most important cause) of the economic underdevelopment of the country. It is the bane of the manufacturing industry in particular, and a major factor in the increased cost of doing business in all other sectors of the Nigerian economy.

Table 1 shows the electricity demand projections for the scenarios. It must be emphasized that the demand indicated for 2005 represents suppressed demand, due to inadequate generation, transmission, distribution and retail facilities. Suppressed demand is expected to be non-existent by 2010. For the 13% GDP growth rate, the demand projections rose from 5,746MW in the base year of 2005 to 297,900MW in the year 2030 which translates to construction of 11,686MW every year to meet the demand.

In modelling the Nigeria's energy case, four economic scenarios were developed and used as follows:
Reference Scenario - 7% GDP Growth; High Growth Scenario - 10% GDP Growth;
Optimistic Scenario I – 11.5% GDP Growth; and Optimistic Scenario II – 13% GDP Growth (based on Presidential Pronouncement for the desire to be among the first 20 economies by 2020).

Table 1: Electricity Demand Projections Per Scenario, MW

Scenario	Electricity Demand Projections Per Scenario, MW					
	2005	2010	2015	2020	2025	2030
Reference (7%)	5,746	15,730	28,360	50,820	77,450	119,200
High Growth (10%)	5,746	15,920	30,210	58,180	107,220	192,000
Optimistic I (11.5%)	5,746	16,000	31,240	70,760	137,370	250,000
Optimistic II (13%)	5,746	33,250	64,200	107,600	172,900	297,900

Source: (Sambo, 2008).

Using recent figures from Federal Ministry of Power (FMoP) and the Nigerian Electricity Regulatory Commission (NERC, the installed generation capacity in the country as at March 2012 was 6643MW, (Hydro Stations – 1900MW, and Thermal Plants – 4743MW); while the actual available power output was 2653MW: from the hydro stations - 522MW and from the thermal plants - 2136MW (Moses, 2014).

Putting it in context, the per capital grid-connected electricity consumption in Nigeria is one of the very lowest in the world, currently about 3,000MW for a population of 160 Million (compare this with Brazil which generates 100,000MW for a population of 201 million, and South Africa with available capacity of 40,000MW for a population of 50 Million).

6. GAS TO ELECTRICITY A PANACEA FOR INDUSTRIALIZATION AND ECONOMIC DEVELOPMENT

One of the pre-requisites of manufacturing productivity is adequate supply of electricity which is mainly utilized for driving machines for the production of various items. Manufacturing sector which is deliberate and sustained application and combination of an appropriate technology, infrastructure, managerial expertise, and other important resources has attracted considerable interest in development economics in recent times. This

is because of the critical role manufacturing sector plays in economic development. This sector acts as a catalyst that accelerates the pace of structural transformation and diversification of the economy, enables a country to fully utilize its factor endowment and to depend less on foreign supply of finished goods or raw materials for its economic growth, development and sustenance. The electricity crisis is represented by such indicators as electricity blackouts and persistence reliance on self-generating electricity. Indeed, as noted by Ekpo (2009), Nigeria is running a generator economy with its adverse effect on cost of production. The country's electricity market is dominated on the supply side by a state-owned monopoly Power Holding Company of Nigeria (PHCN) formerly called the National Electric Power Authority (NEPA) has been incapable of providing minimum acceptable international standards of electricity service that is reliable, accessible and available international standards of electricity for the past decades.

For any meaningful industrialization process to take place in any economy, electricity supply and demand must remain uncompromising elements of the process. This submission was corroborated by Iwayemi (1998) and Odell (1995). While the former argued that, for Columbia as a nation to industrialize electricity supply and demand are crucial factors in the process, the later also realize the importance of energy sector in the socio-economic development of Nigeria. He further submitted that strong demand and increased supply of electricity would stimulate increased income and higher living standards in Nigeria.

Also, in agreement with the duo of Iwayemi (1998) and Odell (1995), Ndebbio (2006), submitted that electricity supply drives industrialization process. He argued that one important indicator top show whether a country is industrialized or not is the megawatt of electricity consumed. According to him, a country's electricity consumption per capita in kilowatts per hour (KwH) is proportional to the state of industrialization of the country.

Adenikinju (2005), also supported the various arguments from Iwayemi (1998), Odell (1995), as well as Ndebbio (2006), by providing a strong argument to further support the overwhelming importance of energy supply to the Nigerian economy. The poor nature of electricity supply in Nigeria, according to him, has imposed significantly cost in the industrial sector of the economy. This argument also corroborates the survey of the manufacturers Association of Nigeria (MAN) in 2005, where it was indicated that the cost of generating power constitute about 36 percent of the production.

Ekpo (2009), in his own submission, elaborated on the cost of running a generator economy and its adverse effects on investment. He strongly opined that for Nigeria as a nation to jump start and accelerate the pace of industrialization, the country should consider fixing power supply problem.

Electric power is the engine that drives industrialization, which improves communication, helps innovation in science and Technology, provides sound healthcare delivery system and improves citizens standard of living. Since Electric power is the engine that drives industrialization, a stable Electric power supply is the key for Nigeria to becomes one of the most 20 developed economy in the world.

Unfortunately, Nigeria falls among the lowliest countries in terms of low level of electricity supply and low industrialization. The maximum quantity of electricity Nigeria has generated in decades hovers around inconsequential 4000 megawatts. That cannot drive any meaningful industrialization neither can it grow and develop the Nigerian economy.

It is of the view that by the virtue of her size and population Nigeria essentially requires a minimum of 40,000 MW of electricity to drive her national industrialization and development as recommended by energy experts. But Nigeria is still generating 4000 MW maximum! This approximately is barely 10percent of recommended required quantity. Experts now argue that because Nigeria only generates a small fraction of her minimum electricity requirement her industrialization and development capacity will continue to hover around 10percent of its real capacity. This is scary and saddening.

7. CONCLUSION

The gas sector in Nigeria, if maximally utilized, is going to be a beehive of activities, and a lot of room exists for investment in this area. Some of these are: LNG (Liquefied Natural Gas), IPP (Independent Power Plant), GTL (Gas to Liquid Conversion), NGL (Natural Gas Liquids) and Methanol. The fact still remains that the abundant existence of natural gas resource does not always translate development, but proper development of sustainable utilization patterns of the resource is very crucial to national industrialization and development.

Electric power is the engine that drives industrialization. Today, Nigeria's daily power production of some 4000MW of power of which some 3100MW is fueled by about 880MMscf/d. It is of the view that by virtue of her size and population Nigeria essentially requires a minimum of 40,000 MW of electricity to drive her national industrialization and development as recommended by energy experts. Therefore, for gas fueled IPPs to generate 40,000 MW, about 11Bcf/d of gas will be required. And if this gap is to be filled by IPPs of 150 - 200MW size capacity, over 170 of them will be built, each requiring some 60 MMscf/d, according to experts. The country's gas growth needs for power have to be met through dedicated gas developments, targeted at producing gas for power. Advantages abound for doing this which includes diversification of the sources of gas supply for domestic market use, with its strategic benefits in security of supply. Other benefit is the creation of inland industrial hubs with ancillary industries sprouting around the gas production and thermal power generation facilities. This is complete national industrialization.

But usually, when it comes to industrialization there is always a mixture of pros and cons, for instance, hallmark for modern economic growth and development; environmental harms; and increased usage of finite natural resources (such as natural gas, and so on) and so many others. However, with Industrial Symbiosis, Environmental benefits result from reduced consumption of resources and reduced amounts of waste and emissions. The system of exchange typically converts negative environmental externalities, mainly in the form of waste, into positive environmental externalities such as decreased pollution and reduced need for raw material. Industrial symbiosis also promotes economic growth, while at the same time it generates environmental benefits. Implementation of industrial symbiosis therefore holds huge potential to unlock powerful mechanisms that foster sustainable development.

Therefore, this paper has discussed gas utilization in the direction of electricity production, which will further revitalize the gas sector and consequently drive industrialization in symbiotic manner in the country for economic development.

8. RECOMMENDATIONS

1. The Federal Government should allow domestic price and fiscals that support private sector infrastructure and non-associated gas (NAG) development, like willing buyer-willing seller approach.

2. The country's gas growth needs for power have to be met through dedicated gas developments, targeted at producing gas for power.

3. Despite the vital role that cooperation between companies and industrial symbiosis have to play in a green economy, both the extent of practical implementation and the theoretical knowledge have remained underdeveloped. The following issues should be addressed with priority:

- Suitable forms to institutionalize industrial symbiosis initiatives and to facilitate implementation and coordination of projects.
- Research to improve the theoretical basis and to advance models.
- Improved economic and environmental analyses to reveal the implications at different levels (individual entities, local, regional scale, national scale) and to quantify benefits.
- Mechanisms and opportunities to bring together practitioners, policy leaders and other stakeholders.

REFERENCES

Adenikiuju, A. (2005). Analysis of the cost of infrastructure failure in a developing economy. The case of electricity sector in Nigeria. African Economic Research Consortium.

Adewale, S. (2014). Power generation: Nigeria needs 70% gas supply. *National Dailies: The Sun Newspaper*, November 11, 2014. Retrieved from http://sunnewsonline.com/new/power-generation-nigeria-needs-70-gas-supply/

Chertow, M. and Ehrenfeld, J. (2012). Organizing self-organizing systems – towards a theory of industrial symbiosis. *Journal of Industrial Ecology* 16(1), 13-27.

Chijioke, N. (2014). *Maximizing the Use of Natural Gas in Nigeria: Prospects, Constraints and Potential Solutions.* Retrieved from **http://energymixreport.com/maximizing-the-use-of-natural-gas-in-nigeria-prospects-constraints-and-potential-solutions/**

Daniel, C. U. (2015). 18th Century Versus 21st Century: Balancing Nigeria's Preparedness for an Industrial Revolution. *The economist Nigeria, (online post)*. Retrieved from http://theeconomistng.blogspot.com.ng/2013/02/18th-century-versus-21st-century.html

ESMAP. (2004). Strategic Gas Plan for Nigeria. Joint UNDP/World Bank Energy Sector Management Assistance Programme. ESM 279 Report 279/04 Washington DC: The World Bank.

Ekpo, A.H. (2009). The Global Economic Crisis and the crisis in the Nigeria Economy. *Presidential Address at the 5th Conference of the Nigerian Economic Society, Abuja, Nigeria.*

Francis, I. I. (2014). Ending Natural Gas Flaring in Nigeria's Oil Fields. *Journal of Sustainable Development*, 7(3), 13 - 22.

Ibitoye, F. I., & Adenikinju, A. (2007). Future demand for electricity in Nigeria. *Applied Energy*, 84(5), 492-504.

Iwayemi, A. (1998). Energy Sector Development in Africa. *A Background Paper prepared for the African Development Bank (ADB).*

Kareem, S.D., Kari, F., Alam, G.M., Chukwu, G.O.M. and David, M.O. (2012). Foreign direct investment into oil sector and economic growth in Nigeria. *Int. J. Applied Econ. Finance*, 6: 127-135.

Kenichi, O. and Takahiro, F. (2006). *Industrialization of Developing Countries Analyses by Japanese Economists*. National Graduate Institute for Policy Studies, Tokyo. pp. 1-5. Retrieved from http://www.grips.ac.jp/vietnam/KOarchives/doc/EB05_COE.pdf

Marian Chertow (2012). Industrial Symbiosis. The Encyclopedia of Earth.
Retrieved from http://www.eoearth.org/view/article/153824/

Moses, A. (2014). The Nigerian Electricity Supply Industry: Status, Challenges and Some Ways Forward. Retrieved from http://akindelano.com/wp-content/uploads/2014/03/Lecture-on-Nigerian-Electricity-Supply-Industry-190512.pdf

NAPIMS (2015). *Gas Utilization*. Retrieved from http://www.napims.com/gasutilisation.html

NBS. (2012). Annual Abstracts of Statistics. Abuja, Nigeria: National Bureau of Statistics.

Ndebbio, J.E.U. (2006). The structural Economic dimensions of Underdevelopment; Associated vicissitudes and imperatives: Agenda for positive change. *33rd Inaugural Lecture*, University of Calabar, Nigeria.

Odell, P. R. (1995). The Demand for energy in developing region: A case study of the Upper An cavalley in Columbia. *Journal of Development Studies*, 3, 234-254.

Ojinnaka, I.P., (1998). Energy crisis in Nigeria: The role of natural gas. *Bull. Central Bank Niger.*, 22: 8-12.
Omosomi Omomia (2014). Growth in Natural gas utilization in the last decade. Retrieved from **http://businessdayonline.com/research/growth-in-natural-gas-utilisation-in-the-last-decade/**

Sambo, A. S. (2008). *Matching Supply with Demand*. Paper presented at the National Workshop on the Participation of State Governments in the Power Sector: 29 July 2008, Ladi Kwali Hall, Sheraton Hotel and Towers, Abuja. Retrieved from https://www.iaee.org/documents/newsletterarticles/408sambo.pdf

Sigrid, K. (2015). *Industrial symbiosis: powerful mechanisms for sustainable use of environmental resources.* ScEnSers Independent Expertise, Germany. Retrieved from https://sustainabledevelopment.un.org/content/documents/635486-KuschIndustrial%20symbiosis_

World Bank (2013). Electric power consumption (kWh per capita). Retrieved on November 22nd, 2015, from http://data.worldbank.org/indicator/EG.USE.ELEC.KH.PC

EXACT APPROACH TO BIOSTIMULATION OF SOIL CONTAMINATED WITH SPENT MOTOR OIL USING COW DUNG AND POULTRY LITTER IN LAND FARMING MICROCOSM

***Abdulsalam, S., Muhammad, I. M. and Atiku, Y. M**.
Department of Chemical Engineering, Abubakar Tafawa Balewa University Bauchi, Nigeria
*Corresponding Author; email: surajudeen_abdulsalam@yahoo.com

ABSTRACT

Bio-stimulation of hydrocarbon contaminated soil using organic stimulants are usually based on proportion of contaminated soil rather than the concentration of contaminants (exact approach) and most studies carried out on bioremediation of hydrocarbon contaminated soil were based on basic proof of concept and not geared towards development of processes that could lead to development of a realistic large scale treatment technology. In view of the aforementioned, a study was carried out on bio-stimulation of soil contaminated with spent motor oil using cow dung and poultry litter as bio-stimulants employing the exact approach in land-farming microcosms adopting the Box-Behnken design of experiment and based on the design of experiment fourteen microcosms labeled S1 to S13 and a control labeled S14 were investigated. The oil and grease content (O&G) and the total heterotrophic bacteria count (THBC) were used to assess the extent of bioremediation. After eight (8) weeks of bioremediation, the efficiency of degradation in all microcosms (S1 to S14) varied from 68 - 90% except the control (S14) with 35%. S1 showed the highest response to bioremediation of 90% and bio-stimulant efficiency of 61%. The microbial counts increased in the first three weeks (1.18×10^7 – 1.02×10^9) corresponding to the period of fast removal of O&G in all microcosms. Based on the percentage removal of the O&G content (90%), the exact approach showed a great potential for the remediation of spent motor oil contaminated soil at contaminant load range of 6.2 – 12.5% and carbon-nitrogen molar ratio (C:N) chosen (15:1 – 10:1).

Keywords: *biodegradation, bioremediation, carbon-nitrogen ratio, organic stimulants, and oil and grease content.*

1. INTRODUCTION

Petroleum based products are the major source of energy for our vehicles, industry and daily life. Due to its importance as energy source, it is prone to accidental spill during exploration, production, refining, transport and storage, which is detrimental to public health and environmental safety. Therefore, there is urgent need for the restoration or remediation of hydrocarbon contaminated sites. Global production of crude oil is estimated at more than twelve million metric tons annually, it has been reported that 1.7 to 1.8 million metric tons of petroleum hydrocarbon escapes into the soil and water bodies yearly (Agamuthu and Dadrasnia, 2013). Environment free of pollutants should be the concern of every individual but with industrialization and urbanization, it is difficult to achieve (Abdulsalam *et al*., 2016). Therefore, a form of cleaning technology is inevitable to reduce the concentration of environmental pollutants to acceptable limit.

Spent motor oil is the brown-to black oily liquid removed from a motor vehicle, when the oil is changed, spent motor oil is similar to unused oil, except that it contains additional chemicals that are produced or build up in the oil, when it is used as an engine lubricant at high temperatures and pressures, as it runs due to engine wears and intrusion of dirt. Once this oil get into the soil, the soil is contaminated and therefore, altering its integrity and hence, some form of restoration becomes imperative.

The physicochemical technologies are being used to clean up contamination in the environment (Faisal *et al*., 2004), but such technologies are expensive, not environmentally friendly, destroy soil texture and characteristics and do not always lead to the complete neutralization of contaminants (Abdulsalam *et al*., 2011). Bioremediation, a treatment based on the use of microorganisms can be used to get rid (or reduced to acceptable limits) of environmental pollutants at low cost because of its simplicity in technology, environmental friendliness, and conservation of soil texture and characteristics. Bioremediation can be applied either by stimulating microorganisms present at site called biostimulation which is believed to be more economically or by the addition of genetically grown

microorganisms known as bioaugmentation (Abdulsalam *et al*., 2012). Many research works have been carried out on spent motor oil contaminated soil using biostimulation approach employing either organic or inorganic stimulants but the former has received more patronage in recent time because of its relatively low cost and environmental safety (Abioye *et al*., 2012; Adekunle, 2011).

During the process of bioremediation, which involves the activity of microorganisms to remove pollutants, environmental parameters such as temperature, pH, oxygen and moisture content, are optimized to achieve accelerated biodegradation (Adams *et al.*, 2015). A lot of work has been reported on biostimulation of hydrocarbon contaminated soils using organic wastes as stimulants but application of these stimulants are usually based on proportion of contaminated soil rather than the concentration of contaminants in the soil (exact approach). In view of the aforementioned, a study was conducted on the use of mixture of cow dung and poultry litter blended together for biostimulation of soil contaminated with spent motor oil in landfarming microcosms employing the exact approach.

2. MATERIALS AND METHOD

Sample Collection

Top soil (0 – 20 cm) contaminated with spent motor oil was collected from Bappah Master Auto-mechanic Workshop located along Railway Road Bauchi, Bauchi State in a polythene bags and kept at the Biochemical Engineering Laboratory, Department of Chemical Engineering, Abubakar Tafawa Balewa University, Bauchi. The soil prior to microbial analysis was kept at 4°C in a refrigerator. The stimulants: cow dung and poultry litter were collected from Bappah Poultry Farm located at old G.R.A Bauchi, and cattle settlement along Gubi Dam Bauchi, Bauchi State Nigeria respectively.

Methods

The contaminated soil sample was subjected to physicochemical and microbial analyses. The soil texture was determined according to method of Day (1953), pH was determined according to method of Bates (1954), organic carbon was determined according method of Walkley and Black (1934), bulk density, particle density and porosity were determined according to method of Brandy and Weil (1999), oil and grease (O&G) was determined according to method of Chang (1998), total organic content was determined according to method of Camobre *et al*. (1996) and total heterotrophic bacteria counts (THBC) was determined according to method of John (1982). All analyses were carried out in triplicate. Details of methods for determining O&G and THBC are described as follows:

Determination of oil and grease content

Five grams (5 g) each of soil sample was weighed on an electronic weighing balance and transferred into a test tube, 5 ml of n-hexane was then added. The sample mixture was shaken vigorously for 5 min, after settling, the solvent and extract was decanted into a pre-weighed 50 ml beaker. This procedure was repeated three times to bring the total solvent volume to 20 ml, the extract and the solvent obtained was evaporated on a heating mantle. The O&G residue, which is the extract, was allowed to cool and weighed on a sensitive balance to four decimal places (Chang, 1998). Results obtained was presented in mg/kg or ppm using Eq. (1):

$$O\&G(ppm\ or\ mgkg^{-1}) = \left(\frac{Weigth\ of\ oil\ in\ soil\ sample(g)}{Weigth\ of\ soil\ sample\ taken\ (g)} \times 10^{6}\right) \quad \ldots \quad (1)$$

Percentage (%) degradation (D) was calculated using the modified form of equation in Samuel (2013):

$$D = \frac{O\&G_i - O\&G_r}{O\&G_i} \times 100 \quad \ldots \quad (2)$$

where $O\&G_i$ and $O\&G_r$ are the initial and residual O&G concentrations respectively.

More so, the percentage (%) biostimulant efficiency (B.E) was calculated at the end of day-56 using modified form of equation in Samuel (2013) presented in Eq. (3).

$$\%\ B.E = \frac{O\&G_s - O\&G_u}{O\&G_s} \times 100 \quad \ldots \quad (3)$$

where $O\&G_u$ is the removal of spent motor oil in the unamended soil, and $O\&G_s$ is the removal of spent motor oil in the amended soil.

Determination of total heterotrophic bacterial count

The enumeration of the total heterotrophic bacterial count in the microcosms were determined using standard plate counting technique. One gram (1 g) of the content in S1 was placed in a test tube and diluted

to 10 fold dilution: dilutions 10^{-4}, 10^{-5} and 10^{-6} were used and later changed to 10^{-5}, 10^{-6} and 10^{-7} past week "3". Zero point one milliliter (0.1 ml) of inoculum each from each of the selected dilutions was pipetted and plated using nutrient agar (NA) and incubated at (34±2℃) for 24 h. Plate with growth within the range of 30 – 300 colonies were counted (John, 1982). The THBC was calculated using Eq. (4).

$$THBC\ (cfu/g) = \frac{number\ of\ colonies \times reciprocal\ of\ the\ dilution\ factor}{weight\ of\ contaminated\ soil} \quad (4)$$

Experimental Design and Treatment

The Box-Behnken design of experiment was employed: three independent variables or factors at three levels (-1, 0, +1) were considered. The dependent variables are oil and grease content (O&G) and total heterotrophic bacteria counts (THBC). The values and levels of the independent variables are presented in Table 1 and coded Box Behnken design for the three independent variables and their responses are presented in Table 2.

Table 1: Experimental Factors and Levels of Variables

Factor	Level		
	Low (-1)	Average (0)	High (+1)
Cow dung (C: N)	7.5:1	6.25:1	5:1
Poultry litter (C: N)	7.5:1	6.25:1	5:1
Moisture content (%)	20	25	30

The contents in Table 2 were based on calculated amounts of various parameters in Table 1 taking 5 kg of contaminated soil sample as basis.

Table 2: Coded and Actual Values of Box Behnken Design of Experiment for the Three Independent Variables Using the Exact Approach

Run	Cow Dung (kg)	Poultry Litter (kg)	Moisture Content (kg)
1	-1 (1.95)	-1 (0.98)	0 (1.98)
2	+1 (2.93)	-1 (0.98)	0 (2.23)
3	-1 (1.95)	+1 (1.47)	0 (2.11)
4	+1 (2.93)	+1 (1.47)	0 (2.35)
5	-1 (1.95)	0 (1.18)	-1 (1.63)
6	+1 (2.93)	0 (1.18)	-1 (1.82)
7	-1 (1.95)	0 (1.18)	+1 (2.44)
8	+1 (2.93)	0 (1.18)	+1 (2.73)
9	0 (2.36)	-1 (0.98)	-1 (1.66)
10	0 (2.36)	+1 (1.47)	-1 (1.77)
11	0 (2.36)	-1 (0.98)	+1 (2.50)
12	0 (2.36)	+1 (1.47)	+1 (2.65)
13	0 (2.36)	0 (1.18)	0 (2.14)
14	-	-	-

Bioremediation Experiment

Five kilograms (5 kg) of contaminated soil sample sieved and homogenized using 2 mm sieve were transferred into a container, calculated amounts of blends of cow dung and poultry litter based on their nitrogen contents and organic carbon content in the contaminated soil as suggested by Box Behnken design of experiments were used to attain the desired carbon to nitrogen molar ratio (C:N). The calculated amounts of cow dung and poultry litter were added to the container and mixed thoroughly. The well mixed content of the container was then transferred into the microcosm labelled S1 (Figure 1). The above procedure was repeated for the remaining twelve microcosms (S2 – S13). S14 was the control, therefore, no stimulant was added. Periodic sampling of content in each of the microcosms was performed on weekly basis for the eight weeks of study. Parameters determined were the oil and grease content (O&G), total heterotrophic bacterial counts and the pH regime. In addition, the moisture content in each microcosm was determined on 2-weekly basis and where the moisture content in any of the microcosms fell below the initial amount as presented

in Table 2, such value was adjusted to its initial value using distilled water.

Figure 1: Microcosms stacked with various treatments described in Table 2

3. RESULTS AND DISCUSSION

Physicochemical Properties of Soil and Organic Wastes

The physicochemical properties of the spent motor oil contaminated soil and that of the stimulants used for bioremediation are presented in Table 3. The high value of total organic carbon (8.19±0.31%) and O&G content (188 273.33±253.25 ppm) was indication that the soil was highly contaminated with spent motor oil. The O&G content was 377 folds greater than the safe limit of 500 mg/kg set by the Nigerian Federal Ministry of Environment (Abdulsalam, 2011), hence the need for the restoration of the contaminated soil for environmental safety and public health in general.

The soil pH (6.83±0.05) was within the acceptable limit of 5.5 – 8.5 for effective bioremediation (Vidali, 2001). The soil moisture content (1.700±1.015 %) was out of the range of 12 – 25% required for optimum growth and proliferation of microbes (Adams *et al*., 2015), hence there was need to argument the moisture content to acceptable limits.

The nitrogen content of the poultry and cow dung were found to be 1.4±0.00% and 0.7±0.00% respectively (Table 3). These nitrogen contents were used to obtain the exact amounts of cow dung and poultry litter added to the contaminated soil to attain the desired C:N for all the microcosms.

Table 3: Physicochemical Properties of the Samples

Parameter	Value/inference		
	Soil	Poultry litter	Cow dung
Texture	Loamy sand		
Organic Carbon (%)	8.19±0.31		
Moisture (%)	1.70±1.02		
Porosity (%)	47.98±20.14		
Water absorption capacity (%)	38.48±0.56		
Particle density (g/cm^3)	2.00±0.06		
Bulk density (g/cm^3)	1.04±0.37		
Total organic content (%)	26.00±1.36		
Oil and grease (ppm)	188 273.33±253.25		
Organic carbon (%)	8.19±0.31		
pH	6.83±0.05		
Nitrogen (%)		1.4±0.00	0.7±0.00
Phosphorus (ppm)		2396.514±34.014	393.743±93.422

Microbiological Analysis

The THBC in the test soil was found to be $6.2\pm2.52\times10^6$ cfu/g which was above the minimum microbial population of 10^5 required for effective bioremediation (Forsyth *et al.*, 1995). Considering the microbial population in the test soil, biostimulation strategy was the most appropriate option. In addition, the five microbial types identified (Table 4) were hydrocarbon degrading ((Das and Chandran, 2011; Subathra *et al*., 2013; Drzewiecka, 2016).

Table 4: Microbiological analysis of spent motor oil contaminated soil

Parameter	Value/inference
Total heterotrophic bacterial count (cfu/g)	$6.23\pm2.52\times10^6$
Bacterial identity	*pseudomonas* spp, *klebsiella* spp, *bacillus* spp, *micrococcus* spp, *proteus* spp

Bioremediation Experiments

Oil and Grease Content (O&G) for the Microcosms

According to Abdulsalam (2011), the O&G content is one of the best indices usually used to quantify biodegradation of spent motor oil since the C-H bond in the oil is low as a result of its breakdown during usage in motor engine. Hence, the O&G content was used to assess the extents of degradation in this study. The variation in O&G content for all the microcosms with time are presented in Figure 2. All the profiles were characterized with period of fast decreased in O&G contents (week 0 - 4), followed by period of slower activities (past week 4). After week 4, the O&G content started fluctuating with ± (increase/decrease) in the residual O&G contents as shown in Figure 2, this could be attributed to uneven distribution of nutrients in the microcosms. In week 4 the residual O&G contents for S1 – S14 were 14 000.0, 14 666.7, 24 000.0, 20 000.0, 29 333.3, 14 000.0, 19 333.3, 16 000.0, 24 000.0, 18 000.0, 17 333.3, 13 333.3, 36 000.0 and 83 333.3 ppm respectively corresponding to 85, 79, 74, 69, 53, 81, 78, 71, 63, 68, 65, 86, 48 and 33% biodegradation. At the end of the 56 day, the biodegradation efficiency varied from 68 – 90% except the control (S14) with 35%. In addition, bio-stimulant efficiency (B.E) varied from 48 – 61%. The control had 0% B.E since it is on its basis the biostimulants efficiency is calculated.

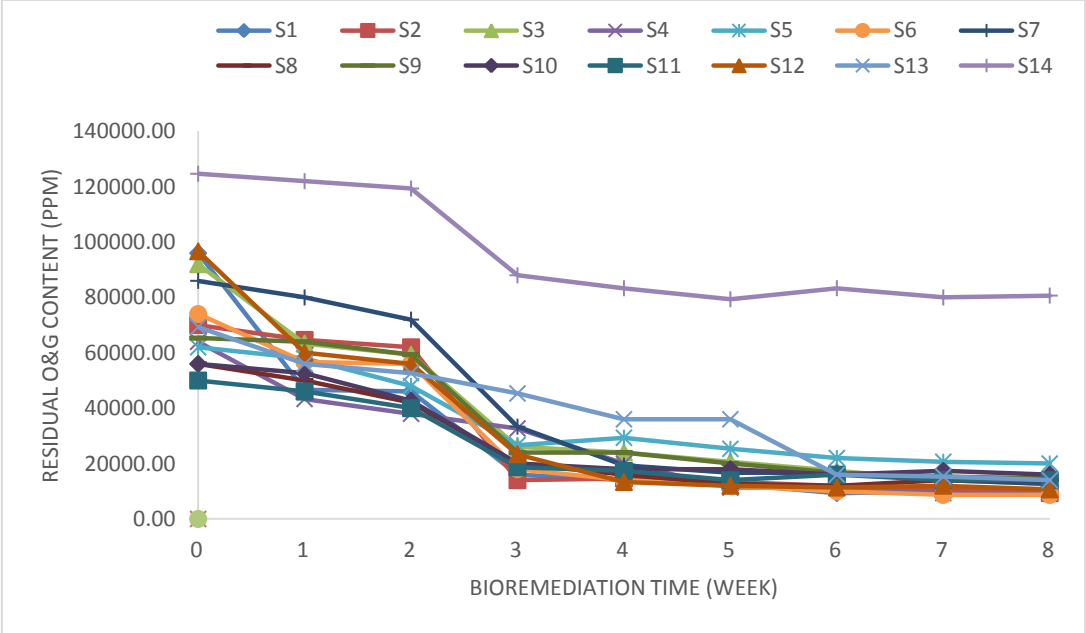

Figure 2: Variation in oil and grease content with bioremediation time

From the percentage oil and grease degradations and biostimulant efficiencies, it could be deduced that the indigenous microorganisms were able to utilize the O&G content in the spent motor oil contaminated soil as their source of carbon and energy thereby leading to biodegradation of the oil content. This observation

is in line with the findings of Samuel (2013) and Ajao *et al.* (2011).

The bioremediation and bio-stimulant efficiencies obtained in this study were superior to most of the previous studies that employed the proportion of contaminant approach: Adekunle (2011) obtained 40% degradation on soil artificially contaminated with spent motor oil at contaminant load of 5 – 12%w/w and 12%w/w organic compost over a period of 21 days. The amount of organic compost added was 0.12 weight stimulant per weight contaminated soil. In addition, Agarry and Ogunleye (2012) carried out research on bio-stimulation of spent motor oil contaminated soil using poultry manure as stimulant at contaminant load of 10%w/w over a period of forty-two (42) days. Results showed that 67.76% degradation was achieved and the amount of manure added was 0.24 weight stimulant per weight contaminated soil.

The stimulant amount used in this study ranged from 0.586 to 0.88 weight stimulant per weight contaminated soil. This stimulant range was obtained by using the carbon to nitrogen molar ratio in the range 15:1 – 10:1. From the summary of the two previous studies above, the amount of organic stimulants applied were low, although, the nitrogen content in different organic wastes are varies but using the exact approach (or C:N approach) and taking appropriate carbon-nitrogen molar ratio, the exact amount of organic stimulant required for effective degradation can be computed as was done in this study.

pH and Microbial population in microcosms

The pH values in all the microcosms ranged from 6.90±0.00 to 8.80±0.00 for the fifty-six days of bioremediation. These pH values were within the range required for effective bioremediation. Therefore, pH was not a limiting factor in this study (Vidali, 2001).

The variation in THBC and bioremediation time is presented in Figure 3. From this figure, it could be observed that the microbial growth profiles obtained for all microcosms followed typical microbial growth pattern depicting the lag, exponential, stationary and death phases (Bailey and Ollis, 1977; Abdulsalam, 2011). It could also be observed that there were fluctuations in the growth phases past week 4 which could be attributed to non-uniformity in mixing leading to un-even distribution of nutrients within the microcosms. Hence, un-even utilization of available nutrients by microorganisms, consequently the un-even growth pattern observed. This observation is in line with the finding of Samuel (2013).

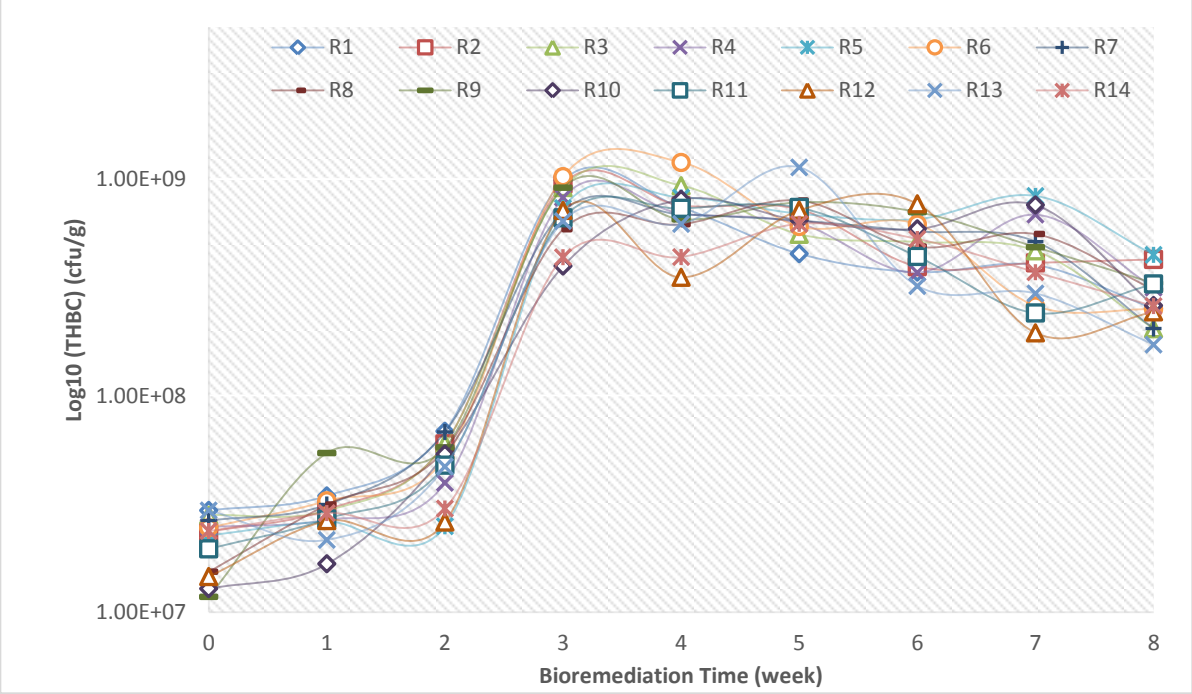

Figure 3: Variation in THBC with bioremediation time

In all the microcosms, a similar trend of lag phase or period of adaptation of microorganisms which lasted

for two weeks (week 0 – 2), followed by one week of exponential growth (between week 2 and 3) which corresponds to period of maximum microbial growth in all microcosms. The THBC for all the microcosms in week 4 (period of maximum microbial growth) ranged from 3.51×10^7 – 1.19×10^8 cfu/g, with S6 having the highest microbial growth. This period of maximum microbial growth corresponds with the period of fast removals of the O&G contents in all microcosms. Hence, it is clear that the microbial species present in the microcosms: *pseudomonas* spp, *klebsiella* spp, *bacillus* spp, *micrococcus* spp, *proteus* spp utilized the oil and grease contents contained in spent motor oil contaminated soil effectively as their source of carbon and energy. This observation agrees with the findings of Kamaluddeen *et al*. (2016).

From the aforementioned, judging from the results of O&G contents and THBC in all the microcosms, percent degradation could be improved by addition of more nutrients (i.e. two stages application of nutrient) since the activities of degradation past week "4" were very sluggish due to the slow release nature of organic wastes or stimulants. This was attested to by the profiles of O&G content attaining plateau (Figure 1) and the fact that there were no significant difference in biodegradation at past week "6" at 10% confidence level. All factors required for effective bioremediation were still present at the end of the eighth week: microbial populations (1.72×10^8 – 4.46×10^8 cfu/g), pH regime (7.04 – 7.30), residual O&G content (8 666.67 – 80 666.67 ppm) but nutrient was a limiting factor. Therefore, addition of more nutrients could drive the reaction forward and improve percent degradation.

4. CONCLUSIONS

Bioremediation of soil contaminated with spent motor oil contaminated soil was conducted using cow dung and poultry litter as organic stimulants at a soil contaminant load of 6.2 - 12.5%w/w and carbon to nitrogen molar ratio in the range of 15:1 – 10:1. Microbiological analyses of the test soil revealed that indigenous microorganisms were present in required quantity ($>10^5$ cfu/g) and type (*pseudomonas* spp, *klebsiella* spp, *bacillus* spp, *micrococcus* spp, *proteus* spp). Bioremediation studies using the Box Behnken designed of experiment revealed that the available microorganisms in all the microcosms were able to use the oil and grease content in spent motor oil contaminated soil as their sole source of carbon and energy. The biodegradation efficiency ranged from 35 – 90% and biostimulant efficiency varied from 48 – 61%. Therefore, the exact approach is an effective technique of remediating spent motor oil contaminated soil.

ACKNOWLEDGMENTS

The authors would like to acknowledge the support of Tertiary Education Trust Fund, Institutional Based Research (IBR) grant TETFUND/DESS/ATBU/BAUCHI/RP/VOL. V. Also, they would like to thank the management of Abubakar Tafawa Balewa University Bauchi-Nigeria for providing other necessary supports.

REFERENCES

Abdulsalam, Surajudeen (2011). Bioremediation of Soil Contaminated with Used Motor Oil; Concept, Process Development and Mathematical Modeling, LAP Lambert Academic Publishing GmbH & Co. KG Germany, ISBN: 978-3-8443-1234-8.

Abdulsalam, S., Adefilia, S.S., Bugaje, I.M., and Ibrahim, S., (2012). Bioremediation of soil contaminated with used motor oil in closed system .*J Bioremed, **4**(172):2155-6199.*

Abdulsalam, S. Adefia, S. S. Bugaje, I. M. and Ibrahim, S., (2011). Comparison of biostimulation and bioaugmentation for remediation of soil contaminated with spent motor oil, *Int. J. Environ. Sci. Tech.*, **8** (1): 187–194.

Abdulsalam, S., (2012). Mathematical Modeling of Bioremediation of Soil Contaminated With Spent Motor Oil. Journal of Emerging Trends Engineering and Applied Science, **3**(4):654-659.

Abdulsalam, S., Sulaiman, A.D.I., Musa, N.M., and Yusuf, M., (2016). Bioremediation of Hydrocarbon and some Heavy Metals polluted Waste Water effluent of a Typical refinery, World Academy of Science, Engineering and Technology International Journal, **10** (2):245-249.

Abdulyekeen, K. A., Muhammad, I.M., Giwa, S.O., Abdulsalam, S. (2016). Bioremediation of Used Motor Oil Contaminated Soil Using Elephant and Horse Dung as Stimulants *IOSR Journal of Environmental Science, Toxicology and Food Technology (IOSR-JESTFT) e-ISSN: 2319-2402, p-ISSN: 2319-2399, **10**(12) 73-78* www.iosrjournals.org DOI: 10.9790/2402-1012027378.

Abioye, O.P., Agamuthu, P., and Abdul-Aziz, A.R. (2012). Biodegradation of Used Motor oil in Soil

using Organic Waste Amendments. Biotechnology Research international, **8**(10):1-8.

Adams, G. O., Fufeyin, P. T., Okoro, S. E. and Ehinomen, I. (2015). Bioremediation, Biostimulation and Bioaugmention: A Review, International Journal of Environmental Bioremediation & Biodegradation, Vol. 3, No. 1, 28-39 Available online at http://pubs.sciepub.com/ijebb/3/1/5 © Science and Education Publishing DOI:10.12691/ijebb-3-1-5

Adekunle, I. M. (2011). Bioremediation of Soils Contaminated with Nigerian Petroleum Products Using Composted Municipal Wastes, *Bioremediation Journal*, 15(4): 230 – 241. ISSN: 1088 – 9868, DOI: 1080/10889868.2011.624137.

Agamuthu, P., and Dadrasnia, A. (2013). Potential of Biowastes to Remediate Diesel Fuel Contaminated Soil, *Global Nest Journal, **15**(4):* 474-484.

Agarry, S. E. and Ogunleye, O. O. (2012), Box-Behnken Design Application to Study Enhanced Bioremediation of Soil Artificially Contaminated with Spent Engine Oil using Biostimulation Strategy, *International Journal of Energy and Environmental Engineering*, Vol. 3, No. 31, pp. 1-14.

Ajao, A.T., Oluwajobi, A.O., and Olatayo V.S., (2011) .Bioremediation of soil microcosm from Auto-mechanic workshops. J. APP. SCI. Environ. Management, **15**(3):473-477, ISSN: 1119-8362.

Bates, B.G., (1954).Electronic pH Determinations John Wiley and Sons, Inc. New York.

Bailey, J. E. and Ollis, D. F. (1977).Biochemical Engineering Fundamentals, International student Edition, Mc Graw- Hill Kogakusha.LTD.Tokyo:335-356.

Brandy, N.C and Weil, R.R., (1999).The Nature and Properties of Soil, 12th Prentice-Hall Inc, U.S.A:145.

Camobreco,V.J., Richard, B.K., Steenhnis, T.S., Peverty, J.H., MC-Bride, M.B., (1996). Movement of Heavy Metals through Undisturbed and Homogenized Soil Columns. Soil Science: An Interdisciplinary Approach to Soil Research ***161**(11):*740-749.

Chang, R. (1998). *Chemistry*, 6th edition. 24: 962-963, McGraw-Hill Companies, Inc.

Das, N. and Chandran (2011), Microbial Degradation of Petroleum Hydrocarbon Contaminants: An Overview, *Biotechnology Research International*, Volume 2011 (2011), Article ID 941810. Available online @ http://dx.doi.org/10.4061/2011/941810

Drzewiecka, D. (2016). Significance and Roles of *Proteus* spp. Bacteria in Natural Environments, *Microbial Ecology*, Volume 72, Issue 4, pp 741–758.

Faisal, I.K., Tahir, H., and Ramzi, H., (2004).An overview and analysis of Site Remediation Technologies. Journnal of Environmental Management. ***71**(2004):* 95-122.

Forsyth, J. V., Tsao, Y. H. and Bleam, R. D. (1995). *Bioremediation: when is bioaugmentation needed?*, pp. 1-14. *In* R. E. Hinchee, J. Fredrickson and B. C. Alleman (ed.) Bioremediation for site remediation. Battelle Press, Columbus, Ohio.

John, P.E., Anderson (1982) .Soil Respiration In: Page A.L., Miller, R.H., and Keeney D.R. (Ed) Method of Soil Analysis, Part: Chemical and Microbial Properties, 2nd Edition American Society of Agronomy. Inc. Madison, Wisconsin USA: 832-871.

Kamaluddeen, K., Yerima, M.B., Abu, T.R., and Deeni, Y., (2016). Biostimulatory Effect of Processed Sewage Sludge in Bioremediation of Engine Oil Contaminated soils. *International Journal of Scientific and Technology Research, **5**(2):* 203-207, ISSN 2277-8616.

Samuel, E. A. (2013). Application of Carbon-Nitrogen Supplementation from Plant and Animal Sources in In-situ Soil Bioremediation of Diesel Oil: Experimental Analysis and Kinetic Modeling. *Journal of Environment and Earth Science, **3** (7):* 51-61, ISSN 2224-3216.

Subathra, M. K., Immanuel, G. and Suresh, A. H. (2013). Isolation and Identification of hydrocarbon degrading bacteria from Ennore creek, *Bioinformation*. 2013; 9(3): 150–157. doi: 10.6026/97320630009150.

Walkley, A., and Black, I.A., (1934). An Examination of the Degtjarelf Method for Determining Soil Organic Matter and proposed Modification of the Chromic Acid Method. Soil. Sci 87, 29-39.

Vidali, M. (2001). Bioremediation*:* An overview, *Journal of Applied Chemistry*, Vol. 73, No. 7, pp. 1163-1172.

DESIGN OF MODIFIED IMC-BASED PID CONTROLLERS FOR ISOTHERMAL TUBULAR REACTORS WITH AXIAL MASS DISPERSION AND FIRST-ORDER REACTION

***Williams, A. O. F. and Adeniyi, V. O.**
Department of Chemical & Petroleum Engineering
University of Lagos, Akoka, Lagos
Email: afwilliams@unilag.edu.ng; bmnpsvg@gmail.com

ABSTRACT

This paper presents the design of modified IMC-based PID-type controllers for isothermal tubular reactors carrying out first order-order reaction, and having axial mass dispersion. The partial differential equation modeling the system was lumped using the modal decomposition technique and the lumped model was then used for the controller design based on a modified Internal Model Control (IMC)-PID method earlier developed by the authors. The results of closed-loop simulations demonstrate the superior performance of the PID-type controllers so designed when compared with the Ziegler-Nichols PID tuning parameters. The PID-type controllers also show excellent robustness to plant/model mismatch.

INTRODUCTION

Chemical reactors are prevalent in the process industries and various types are found depending on the application and the specific industry. Chemical reactors are basically of three types based on operational mode: batch reactors, semi-batch reactors and continuous reactors. The continuous reactors can be further sub-divided into continuous stirred tank reactors (CSTR), tubular reactors, fixed-bed reactors and fluidized-bed reactors, to mention a few. Tubular reactors are widely employed in the process industry because they give the highest conversion per reactor volume and are easier to maintain (since there are no moving parts). They are generally applied in homogeneous gas-phase reactions. Studies relating to the efficient design and control of these reactors are therefore of practical interest.

The dynamics of tubular reactors are modeled by partial differential equations and are referred to as distributed parameter systems (DPS). There are two major approaches for the design of feedback controllers for distributed parameter systems (Ray, 1981), namely: *early* and *late* lumping approaches. Like many other processes that are modeled by partial differential equations i.e. distributed parameter systems (DPS), the control design problem for many tubular reactors can effectively be reduced to the design of PID-type controllers based on the ”early lumping” approach. The alternative approach based on ”late lumping” involves the application of distributed parameter system theory and the mathematical rigour required by this approach (cf. Ray, 1981; Zhou *et al.*, 2015) is not attractive for industrial deployment for many practical processes.

In this paper, our objective is to employ a modified Internal Model Control (IMC) approach to design PID-type controllers for the exit concentration control of the an isothermal tubular reactor with axial mass diffusion by manipulating the inlet feed concentration using the early lumping approach. The approach adopted is particularly attractive for the tubular reactor system because the peculiar structure of the system model makes it amenable to easily derive an analytical lumped parameter equivalent using the modal decomposition technique. The lumped parameter equivalent obtained in this way is then directly employed in the controller design using the modified IMC-PID method previously developed by the authors. It is to be noted that several advanced design techniques such as internal model control (IMC) and model predictive control (MPC) are available (cf. Garcia and Morari, 1982; Morari and Zafiriou, 1989; Seborg et al, 2011), however, the bulk of process control applications are still largely carried out using PID-type controllers.

The classical methods for the design of PID controllers are the semi-empirical rules of Ziegler-Nichols (1942), and Cohen and Coon (1953). These methods give controller settings which are often found to be *more under-damped* than desired in many applications (Luyben, 1990). As a result, extensive efforts have to be used (in a trial-and-error fashion) to fine-tune the controller on-line in order to obtain acceptable closed-

loop response behavior of the controlled process. Thus methods for the systematic design of PID controllers with better performance continue to be active areas of research e.g. Rivera *et al.* (1986), Morari and Zafiriou (1989), Brambilla *et al.* (1989), Williams and Adeniyi (1996), Chen *et al.* (1997) Chen *et al.* (1999), Chen and Seborg (2002), Skogestad (2003), Vilanova (2008); Skogestad and Postleithwaite (2010); Seborg *et al.*(2011); Mikhalevich *et al.*(2015a), Umamaheshwari *et al.*(2016). Viosili (2012) gives a brief survey of some of the recent research trends for PID controllers, while Yamaguchi and Kanoh (2000), Hulko and Belavy (2003), Williams and Adeniyi (2009), Alvarez *et al.*(2012) and Mikhalevich *et al.*(2015b) are some of the papers in the literature on the design or application of PID-type controllers to distributed parameter systems.

2 MODEL OF ISOTHERMAL TUBULAR REACTOR SYSTEMS WITH AXIAL MASS DISPERSION AND FIRST-ORDER REACTION

We consider the homogeneous, one-dimensional tubular reactor system in which the chemical reaction

$$A \rightarrow B \tag{1}$$

is taking place.

We make the following assumptions: (i) isothermal operation, (ii) uniform cross-sectional area, (iii) constant fluid properties, (iv) constant dispersion coefficient D, and that (v) radial gradients in velocity and concentration are negligible.

By writing a microscopic material balance for component A with first-order reaction kinetics, one obtains the mathematical model

$$\frac{\partial c_A}{\partial t'} = D\frac{\partial^2 c_A}{\partial z'^2} - v\frac{\partial c_A}{\partial z'} - kc_A \tag{2}$$

Using different mathematical arguments, Villadsen and Michelsen (1978), and Butt (1980) have shown that the appropriate boundary conditions are the following:

$$At \quad z' = 0, \quad v(c_A - c_{Ain}) = D\left(\frac{\partial c_A}{\partial z'}\right)_{z'=0}$$
$$At \quad z' = L, \quad \left(\frac{\partial c_A}{\partial z'}\right)_{z'=0} = 0 \tag{3}$$

with the following initial condition:

$$At \quad t' = 0, \quad c_A(z',0) = \bar{c}_A(z') \tag{4}$$

where D is the axial mass dispersion coefficient, an empirical quantity and c_A is the reactant concentration.

Eqs. (2 - 4) can be rewritten in the following dimensionless forms:

$$\frac{\partial x}{\partial t} = \frac{1}{Pe_M}\frac{\partial^2 x}{\partial z^2} - \frac{\partial x}{\partial z} - Dax \tag{5}$$

and the corresponding initial and boundary conditions become

$$At \quad t = 0, \quad x(z,0) = x_0(z) \tag{6}$$

$$At \quad z = 0, \quad x - \frac{1}{Pe_M}\frac{\partial x}{\partial z} = x_{in}(t); \quad At \quad z = 1, \quad \frac{\partial x}{\partial z} = 0 \tag{7}$$

where

$$z = z'/L, \quad t = \frac{v}{L}t', \quad x = \frac{c_A}{c_{ref}} \quad Da = \frac{Lk}{v} \quad and \quad Pe_M = \frac{Lv}{D}$$

The parameter, Da, known as the Damköhler number, is a measure of rate of reaction at inlet conditions; while the parameter, Pe_M, commonly used to represent the magnitude of the dispersion effects, is known as the axial Peclet number for mass transfer. The Peclet number, Pe, is the ratio of characteristic constants for convective and dispersive effects.

2.1 Lumping of the Isothermal Tubular Reactor Model

There are various methods for the lumping (discretization) of distributed parameter systems. These include classical finite difference methods (Friedly, 1972) and method of weighted residuals (Villadsen and Michelsen, 1978, Finlayson, 1980), and modal decomposition methods (Ray, 1981). In this paper, the modal decomposition method is employed because the system under consideration is linear and therefore leads to an analytical solution which can be readily written in the state-space form for analysis and controller design.

Based on the modal decomposition method (see Appendix A), the lumped model of the tubular reactor can be represented in the linear state-space form using only the first N modes or eigenfunctions of the system as follows:

$$\dot{\mathbf{x}} = \mathbf{A}_1\mathbf{x} + \mathbf{b}_1\mathbf{u} \tag{8}$$

$$\mathbf{y} = \mathbf{c}\mathbf{x} \tag{9}$$

where the system states, $\mathbf{x}$, and the matrices $\mathbf{A}_1$, $\mathbf{b}_1$ and $\mathbf{c}$ (for measurement at the exit of the reactor), are given by

$$\mathbf{x} = \left[a_1(t) \;\; a_2(t) \cdots a_N(t)\right]^T$$

$$\mathbf{A}_1 = Diag\begin{bmatrix} -(Da+\lambda_1) & -(Da+\lambda_2) & -(Da+\lambda_3) - \\ \cdots & -(Da+\lambda_N) \end{bmatrix} \quad (10)$$

$$\mathbf{b}_1 = \begin{bmatrix} B_1 & B_2 \cdots B_N \end{bmatrix}^T \quad (11)$$

$$\mathbf{c} = \begin{bmatrix} \phi_1(1) & \phi_2(1) \cdots \phi_N(1) \end{bmatrix}^T \quad (12)$$

2.2 Transfer Function Model of the Isothermal Tubular Reactor

The design of a controller using a model-based control design technique requires a model of the system to be controlled. For a SISO system, one may use a transfer function model of the form

$$\tilde{g}(s) = \frac{y(s)}{u(s)} = \frac{N(s)}{D(s)} \quad (13)$$

where $N(s)$ and $D(s)$ are numerator and denominator polynomials (in s) of $\tilde{g}(s)$, respectively. This may be obtained from the lumped parameter state-space model Eqs. 8 and 9 by Laplace transforming. from which we have

$$y(s) = \mathbf{c}(sI - \mathbf{A})^{-1}\mathbf{b}u(s) = \tilde{g}(s)u(s) \quad (14)$$

This transfer function model, $\tilde{g}(s)$, would typically be of a higher-order type for a SISO distributed parameter system.

For a diagonal A_1 given by Eq. 10, and $\mathbf{b_1}$ and $\mathbf{c}$ given by Eqs. 11 and 12, it can easily be shown that $\tilde{g}(s)$ is of the following general form:

$$\tilde{g}(s) = \sum_{i=1}^{N}\left[\frac{\phi_i(1)B_i}{s+(Da+\lambda_i)}\right] \quad (15)$$

3.PID CONTROL DESIGN/TUNING METHOD

Details of the PID-type controller design/tuning method employed are available in Williams and Adeniyi (1996). Therefore, only an overview is presented here.

Let the model of the process for which a PID controller is to be designed, be represented as

$$\tilde{g}(s) = \frac{\sum_{i=0}^{\hat{M}}\hat{a}_i s^i}{\sum_{i=0}^{\hat{N}} b_i s^i}; \quad \hat{M} < N \quad (16)$$

in which it has been assumed that any pure time delays originally present in the system model has been rationalized using, for example, a first-order Padé polynomial.

By using the IMC design method (Garcia and Morari, 1982; Rivera *et al.*, 1986; Morari and Zafiriou, 1989) to design the IMC controller g_I for Eq. (16), and then transforming this into the classical feedback controller g_c (through the equivalence: $g_c = g_I/(1-\tilde{g}g_I)$), it can be shown that the resulting controller transfer function for g_c can be simplified to the form

$$g_c = \frac{\sum_{i=0}^{N} b_i s^i}{\sum_{i=1}^{N} a_i s^i} \quad (17)$$

in which the numerator coefficients, b_i are those of the denominator of the original model, Eq. (16); while the denominator coefficients, a_i, now depend on some of the coefficients resulting from the factorization (cf. Rivera *et al., 1986*) of $\tilde{g}(s)$ into $\tilde{g}_+(s)$ and $\tilde{g}_-(s)$, and the IMC filter parameter, ε.

3.1 Reduction to a PI Controller

At low- and high-frequencies, Eq. (17) can be approximated, respectively by PI controllers, as follows:

$$g_{c_{low}} = \frac{b_1 s + b_0}{a_1 s}, \quad g_{c_{high}} = \frac{b_N s^N + b_{N-1}s^{N-1}}{a_N s^N} \quad (18)$$

Let the fraction contributed by the low-frequency approximation to the PI controller be φ, so that $(1-\varphi)$ is the fraction contributed by the high-frequency approximation, then the resulting PI controller transfer function is

$$g_{c_{(PI)}} = K_c\left(1 + \frac{1}{\tau_I}\frac{1}{s}\right) \quad (19)$$

$$K_c = \frac{b_1}{a_1}\varphi + (1-\varphi)\frac{b_N}{a_N}, \quad \tau_I = \frac{a_N b_1 \varphi + (1-\varphi)a_1 b_N}{a_N b_0 \varphi + (1-\varphi)a_1 b_{N-1}} \quad (20)$$

3.2 Reduction to Ideal PID Controllers

Through a similar procedure as above, the ideal PID controller approximation of Eq. (17) is

$$g_{c_{(PID)}} = K_c\left(1 + \frac{1}{\tau_I}\frac{1}{s} + \tau_D s\right) \quad (21)$$

$$K_c = \frac{b_1}{a_1}\varphi + (1-\varphi)\frac{b_N}{a_N}, \quad \tau_I = \frac{a_N b_1 \varphi + (1-\varphi)a_1 b_N}{a_N b_0 \varphi + (1-\varphi)a_1 b_{N-1}} \quad \tau_D = \frac{b_2 a_N}{a_N b_1 \varphi + (1-\varphi)a_1 b_N} \tag{22}$$

Expressions for the parameters of practical PID controllers (i.e. an ideal PID controller cascaded with a first-order filter) have also been derived from the low- and high-frequencies approximations of Eq. (17) but these are not presented here for brevity. For details see Williams and Adeniyi (1996).

3.3 Controller Tuning

For a given system, $\tilde{g}(s)$, the PI and PID controller parameters given above depend on both the filter parameter, ε (which is implicit in a_i's) and the parameter, φ which determines the fraction of the low- and high-frequency approximations of Eq. (17) included in the PI and PID controllers. Thus apart from ε, the parameter $\varphi(0 \le \varphi \le 1)$ provides an additional way of influencing the closed-loop response provided by the PI and PID controllers.

Now, it is obvious that the approximation of the full controller, g_c, given by Eq. (17), by a PI or PID-type controller will result in performance degradation from that attainable with Eq. (17), and may even lead to closed-loop stability problems when implemented on the original higher-order system. Thus to ensure closed-loop stability and acceptable performance, an appropriate value of the filter parameter, ε must be chosen. The maximum closed-loop amplitude ratio criterion as proposed in Williams and Adeniyi (1996) was also employed in this paper, and is stated as follows:

For a given value of φ, choose ε^* such that

$$F = \max_{0 \le \omega \le \omega_\infty} \left| \frac{\tilde{g}(j\omega) g_c(j\omega, \varepsilon^*, \varphi)}{1 + \tilde{g}(j\omega) g_c(j\omega, \varepsilon^*, \varphi)} \right| - M^* = 0 \tag{23}$$

where M^* is the desired maximum closed-loop amplitude ratio. This problem can be easily solved using for example the Interval Bisection Method (cf. Forsythe *et al.* , 1977).

4. APPLICATION TO THE TUBULAR REACTOR SYSTEM

4.1 Transfer Function of the 4th-order Lumped Equivalent System

For this system, dynamic simulation studies show that a 4th-order lumped model obtained by modal decomposition is a good representation of the exact system response. Consequently, we shall use this 4th-order lumped model to carry-out PID-type controller design to control the exit reactor concentration.

For the nominal system parameter ($Da = 2$, $Pe_M = 1$), the lumped, state-space matrices of this tubular reactor system with the reactor exit concentration as the measured/controlled variable, are as follows:

$$\mathbf{A}_1 = Diag\begin{bmatrix} -3.17196 & -14.02186 & -43.70038... \\ ... & -93.06362 \end{bmatrix}$$

$$\mathbf{b}_1 = \begin{bmatrix} 0.92139 & 1.34462 & 1.39336 & 1.40458 \end{bmatrix}^T$$

and

$$\mathbf{c} = \begin{bmatrix} 1.5192 & -2.21691 & 2.29726 & -2.31576 \end{bmatrix}^T$$

from which the system transfer function is obtained as

$$g_r = \frac{N(s)}{D(s)}$$

where

$$N(s) = -1.6329595s^3 - 51.224635s^2 - 2364.005645s + 48292.157813$$

$$D(s) = s^4 + 153.95782s^3 + 6462.887936s^2 + 76008.636272s + 180883.304678$$

This transfer function relates the effect of the manipulated variable (the inlet feed concentration) to the controlled variable which is the exit reactor concentration of the reactant.

4.2 Factorization of g_r

Solving for the roots of the numerator of the system transfer function g_r using any of the severally available software applications (e.g. Matlab, Scilab, Mathematica or even good, old FORTRAN), it can easily determined that the the transfer function g_r has a RHP zero at $s = 1/\beta$ = 14.141392.

Using the Type II factorization (Garcia and Morari, 1982, Williams and Adeniyi, 1996) to factor out this RHP zero, it is straightforward to show that the full-order, classic feedback controller equivalent to the IMC controller for g_r is given by

$$g_{rc} = \frac{C_n}{C_d} \tag{24}$$

where

$$C_n = s^4 + 153.95782s^3 + 6462.887936s^2 + 76008.636272s + 180883.304678$$

$$C_d = 23.0923133\varepsilon^2 s^4 + [1050.945093\varepsilon^2 + 23.092313(2\varepsilon + \beta)]s^3 + [48292.15707\varepsilon^2 + 1050.945093(2\varepsilon + \beta)]s^2 + 48292.1570(2\varepsilon + \beta)$$

Putting this in the form of Eq. 17, we obtain that

$$b_4 = 1.0,\ b_3 = 153.95782,\ b_2 = 6462.887936,\ b_1 = 76008.636272,\ b_0 = 180883.304678$$

$$a_4 = 23.0923133\varepsilon^2,\ a_3 = [1050.945093\varepsilon^2 + 23.092313(2\varepsilon + \beta)]$$

$$a_2 = [48292.15707(2\varepsilon^2 + 1050.945093(2\varepsilon + \beta)],\ a_1 = 48292.15707(2\varepsilon + \beta)$$

Using the appropriate equations in Section 3, the PI and PID-type controller parameter expressions follow directly from the relevant coefficient a_i's and b_i's given above.

4.3 Closed-Loop Simulation Results

4.3.1 Nominal Performance

For a unit step change in setpoint, Figure 1 shows a comparison of the new PI controller design and that of a PI controller designed according to the Ziegler-Nichols tuning method. The corresponding plots for rejection of a unit step change in concentration disturbance in the reactor feed, and comparison with a Ziegler-Nichols PI controller, are shown in Figure 2, respectively.

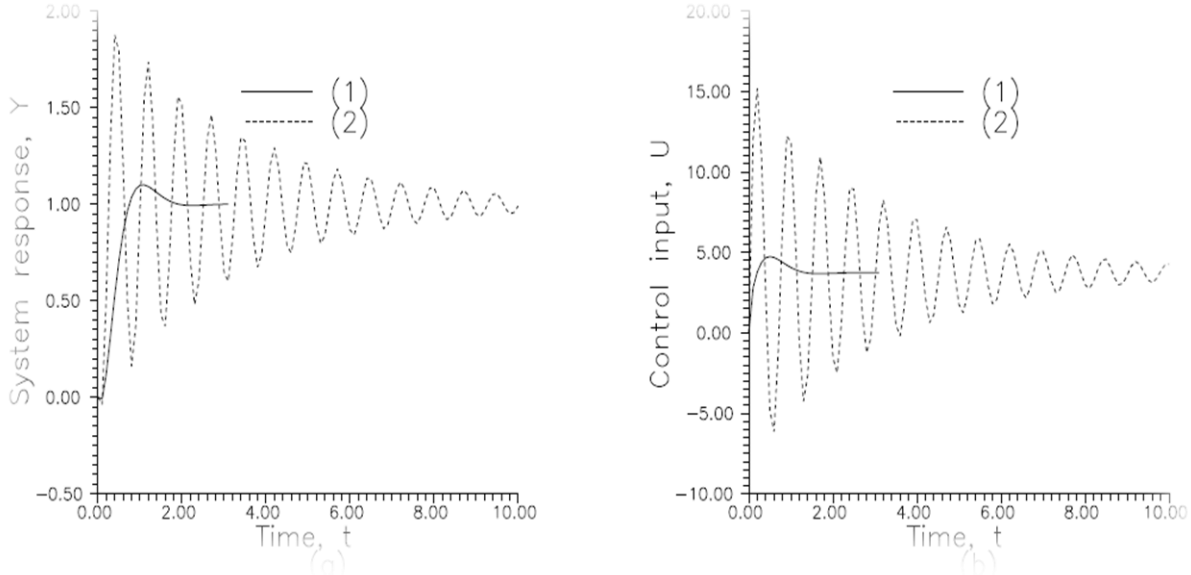

Figure 1: Comparison of performance of new PI controller with $\varphi = 0.9$ (solid line) and ZN PI Controller (short-dashed line) for a unit step change in setpoint. (a) Left: Controlled variable response, (b) Right: Control input response

.

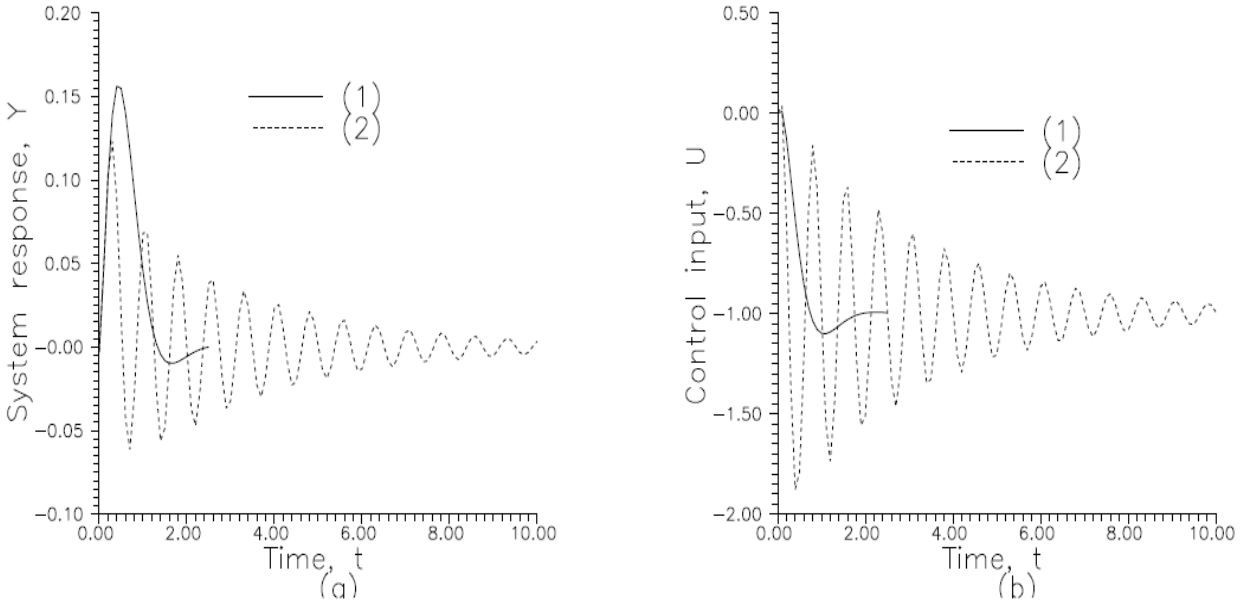

Figure 2: Comparison of performance of PI controllers for a unit step change in concentration disturbance at reactor inlet. Legend: 1, New PI controller with $\varphi = 0.9$; 2, ZN PI Controller. (a) Left: Controlled variable response, (b) Right: Control input response.

For the same step change in setpoint as above, Figure 3 shows a comparison plot of the system response for the new, ideal PID and Type A practical PID controllers for unit step change in setpoint, while Figure 4 is a comparison of the performance of the ideal and the Type A practical PID controllers with performance of the ZN-PID controller for unit step change in disturbance at the inlet to the reactor.

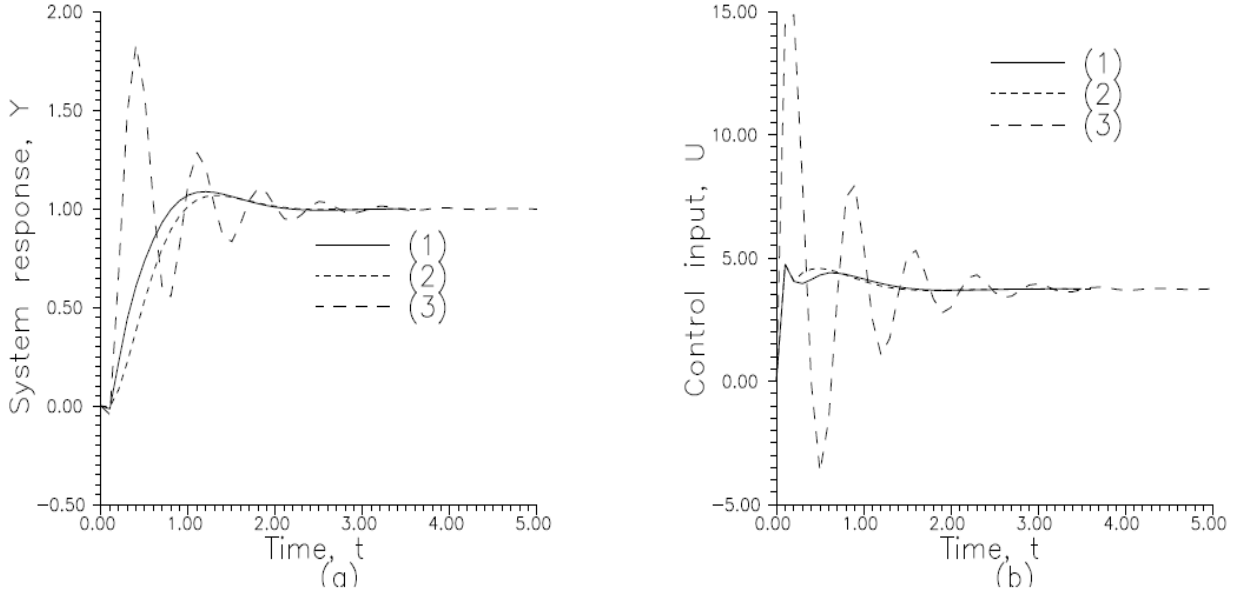

Figure 3: Comparison of response of System to a unit step change in setpoint. Legend: 1, new ideal PID controller with φ = 0.9; 2, new Type A practical PIDcontroller with φ = 0.9; and 3, ZN ideal PID design, respectively. (a) Left: Controlled variable, (b) Right: Control input

.

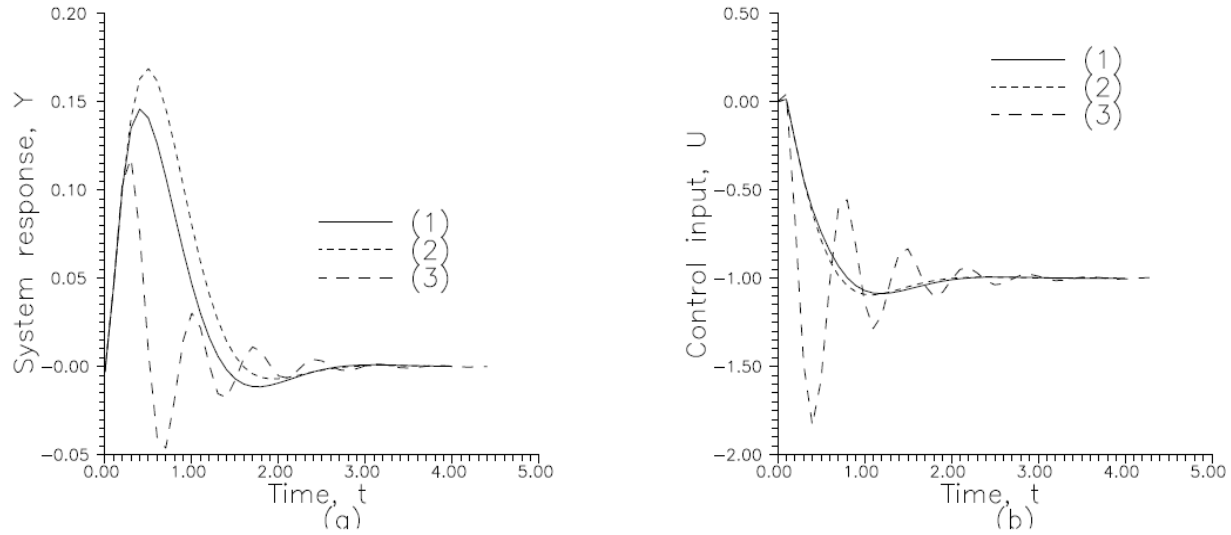

Figure 4: Comparison of performance of new PID-type controllers with ZN PID controller for a unit step change concentration disturbance at reactor inlet. Legend: 1, New PID controller at φ = 0.9; 2, new Type A practical PID controllers at φ = 0.9; 3, ZN-PID controller. (a) Left: Controlled variable response, (b) Right: Control input response.

The foregoing nominal closed-loop simulation results (i.e. Figures 1-4) demonstrate the vastly superior performance (smoother responses, shorter settling time etc) of the PID controllers designed using the modified IMC method of Williams and Adeniyi (1996), compared with those based on the classical Ziegler-Nichols tuning parameters.

4.3.2 Effect of φ

For three selected values of φ, Figure 5 shows the plots of the simulated response of the new PI controller designs for unit step change in setpoint, while, Figures 6 shows the response for a unit step change in disturbance at the reactor inlet.

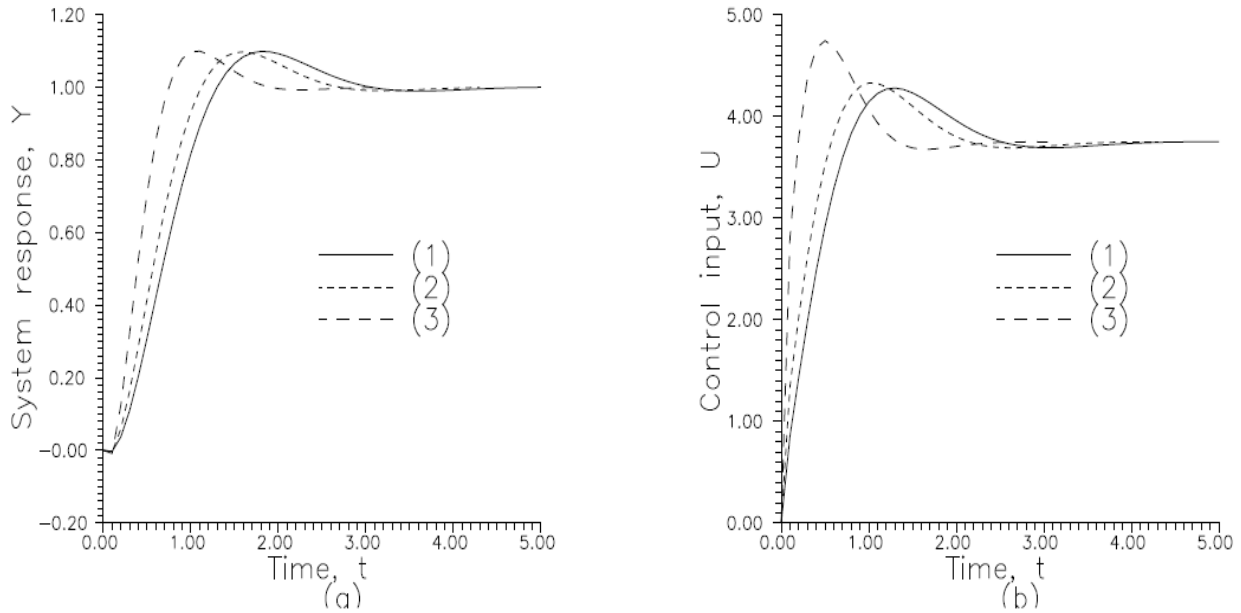

Figure 5: Response of System to a unit step change in setpoint. Legend: 1,2,3 new PI design with φ = 0.3,0.6,0.9 ,respectively. (a) Left: Controlled variable, (b) Right: Control input

.

From these plots, we see that the effect of increasing φ is to speed up the response of the controllers for both setpoint tracking and disturbance rejection. Although not presented (due to page limit consideration), similar trend was observed for closed-loop response of the PID-type controllers as φ is increased. Note that it is possible to determine an optimal value of φ which minimizes an objective function such as the Integral Square Error (ISE) or the Integral Absolute Error (IAE). However, this is not considered in this paper.

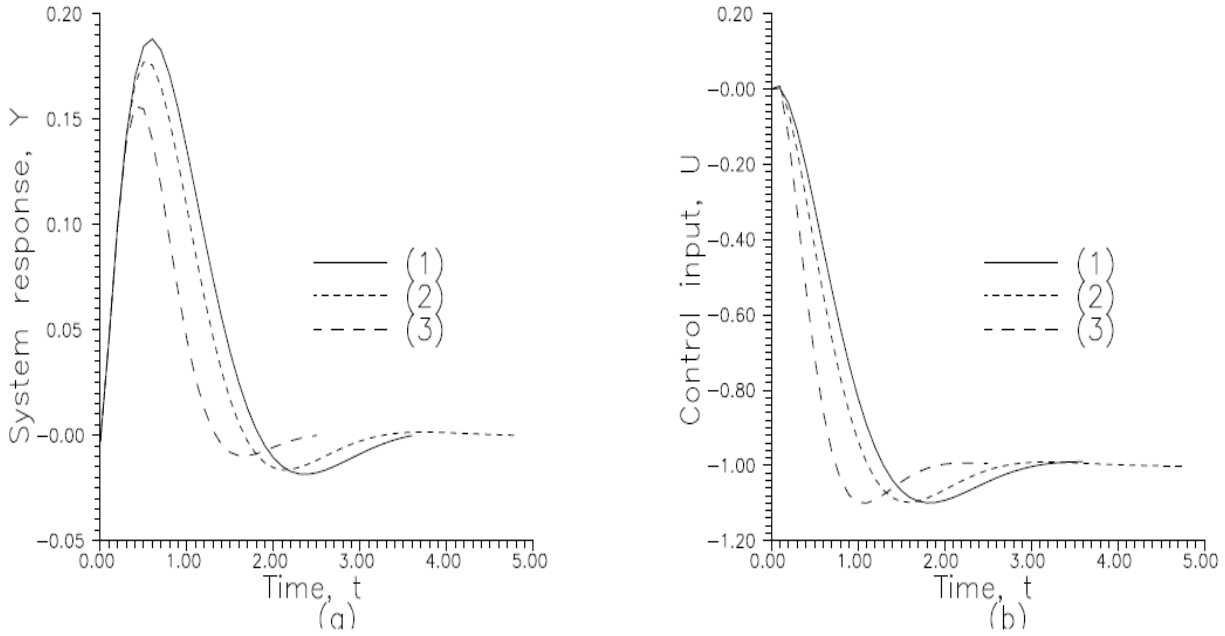

Figure 6: Response of System to a unit step change in concentration disturbance at reactor inlet. Legend: 1,2,3 new PI design with $\varphi = 0.3, 0.6, 0.9$,respectively. (a) Left: Controlled variable, (b) Right: Control input

.

4.3.3 Effect of Model/Plant Mismatch

The foregoing simulations were carried out on the 4th-order model employed for controller design i.e. we assumed no model/plant mismatch. In order to investigate effect of model/plant mismatch on the performance of the new PID designs, they were all simulated on the 6th-order lumped model of the reactor system, which we then assumed to be the plant.

Figures 7 and 8 show the comparison of the plots of the performance of the new PI controller designs on the 4th-order model and the plant for both unit step change in setpoint, and regulation of a unit step change in concentration disturbance at the reactor inlet, respectively. Similar plots were obtained for the case of the PID-type controllers.

From these plots, we see that the controllers exhibit very good robustness for the plant/model mismatch.

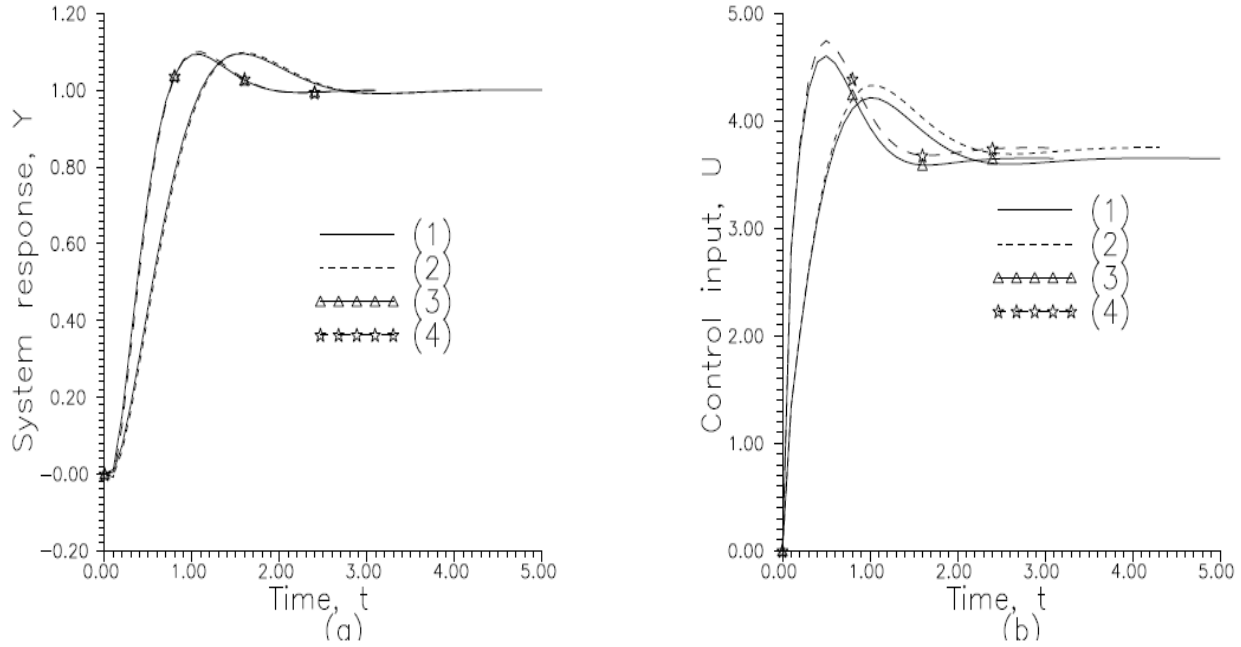

Figure 7: Comparison plot of response of new PI controller on both model and plant to a unit step change in setpoint. Legend: 1, plant and 2, model for controller at φ =0.6; 3, plant and 4, model for controller at $\varphi = 0.9$. (a) Left: Controlled variable, (b) Right: Control input.

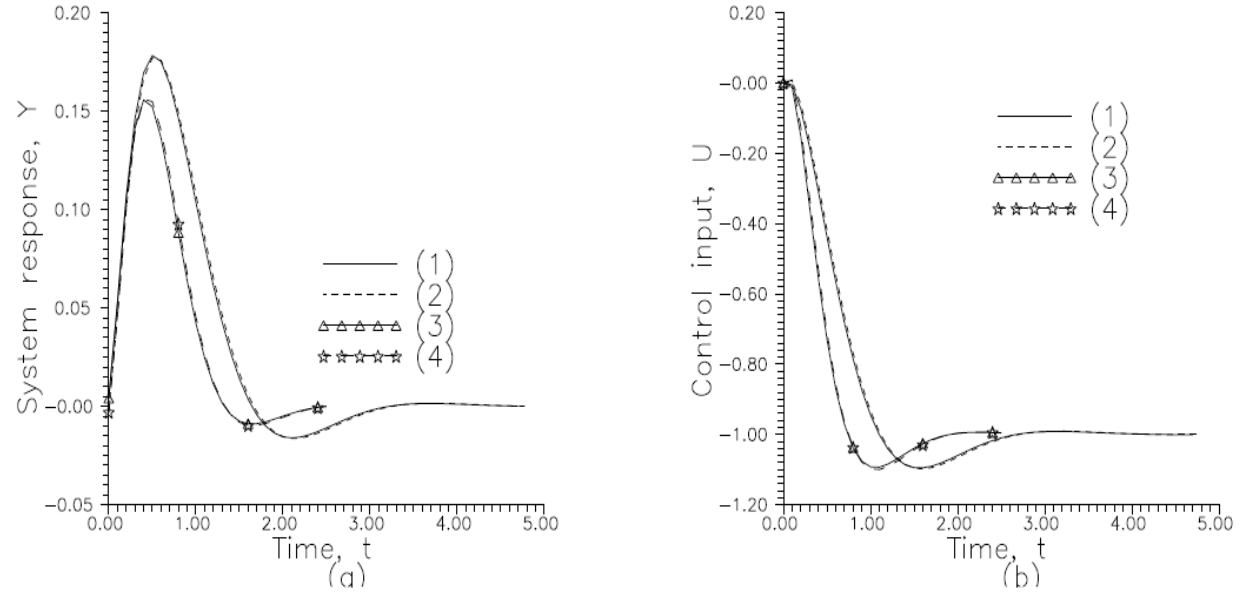

Figure 8: Comparison plot of response of new PI controller on both model and plant to a unit step change in concentration disturbance at the reactor inlet. Legend: 1, plant and 2, model for controller at φ =0.6; 3, plant and 4, model for controller at $\varphi = 0.9$. (a) Left: Controlled variable, (b) Right: Control input.

5. CONCLUSION

High performance PID-type controllers have been designed for an isothermal tubular reactor system with axial disperson and first-order kinetics using the early lumping approach. The partial differential equation modelling the system was lumped using the modal decomposition technique method and the lumped model was then used for the controller design based on the modified IMC-PID method earlier developed by the authors. Simulation results show the superior performance of the designed PID-type controllers compared with PID controllers based on the Ziegler-Nichols tuning method. Simulations were carried out to explore the effect of one of the controller design parameters and to demonstrate the robustness to plant-model mismatch.

REFERENCE

Alvarez , J. D., Normey-Rico, J. E. and Bereguel, M. (2012). Design of PID Controllers with Filter for Distributed Parameter Systems, *IFAC Proceedings*, **Vol. 45**, Issue 3, pp. 495 – 500.

Brambilla, A., C. Scali and S. Chen (1989). Tuning of conventional controllers for robust performance, *Proc. IFAC Low Cost Automation*, Milan, Italy.

Butt, J. B., *Reaction Kinetics and Reactor Design*, Prentice-Hall, Inc., Englewood cliffs, New Jersey, (1980).

Chen, C-L., H-P. Huang and H-C. Lo (1997). Tuning of PI controllers for self-regulating process, *Trans. Chinese Inst. Chem. Engrs* **Vol. 28** (No. 5).

Chen, C-L., S-H. Hsu and H-P Huang (1999). Tuning of PI/PID controllers based on gain/phase margins and maximum closed-loop magnitude, *Trans. Chinese Inst. Chem. Engrs* **Vol. 30** (No. 1).

Chen , D., Seborg D. E. (2002). PI/PID controller design based on direct synthesis and disturbance rejection. *Ind Eng Chem Res.*, **41**:pp. 4807- 4822.

Cohen, G.H., and G. A. Coon (1953). Theoretical Considerations of Retarded Control, *Trans. ASME*, **Vol. 75**, p. 827.

Forsythe, G. E., M. A. Malcolm and C. B. Moler (1977). *Computer methods for mathematical computations*, Prentice-Hall, Inc., Englewood Cliffs, N. J.

Garcia, C. E. and M. Morari (1982). Internal model control. 1. A unifying review and some new results, *Ind. Eng. Chem. Process Des. Dev.*, **Vol. 21**, pp. 308–323.

Hulko , G. and Belavy, C. (2003). PID Control of Distributed Parameter Systems, IFAC Proceedings, **Vol. 36**, Issue 18, Sept. pp. 101–106.

Luyben, W. L. (1990). *Process modeling, simulation and control for chemical engineers*, Second edition, McGraw-Hill Book Company, New York.

Mikhalevich, S. S., Baydali, S. A. and Manenti, F. (2015a). Development of a Tunable Method for PID Controllers to Achieve the Desired Phase Margin, *J. Proc. Control*, **25**, pp. 28–34.

Mikhalevich, S. S., Rossi, F., Manenti, F. and Baydali, S. A. (2015b). Robust PI/PID Controller Design for the Reliable Control of Plug Flow Reactor, *Chemical Engineering Transactions*, **43**, pp. 1525 – 1530

Morari, M. and E. Zafiriou (1989). *Robust process control*, Prentice-Hall Inc., Englewood Cliffs, N., J.

Ray , W. H., (1981). *Advanced Process Control*, McGraw-Hill Book Company, New York.

Rivera, D. E., M. Morari and S. Skogestad. (1986). Internal model control. 4. PID controller design, *Ind. & Eng. Chem. Process Des. Dev.*, **Vol. 25**, pp. 252–265.

Seborg, D. E, Edgar T. F., Mellichamp, D. A. (2011). *Process Dynamics and Control*, 3rd ed. Wiley, New York.

Skogestad, S. (2003). Simple analytic rules for model reduction and PID controller tuning. *J Process Control.* **13**, pp. 291-309.

Skogestad, S., and Postlethwaite, I. (2010). *Multivariable Feedback Control: Analysis and Design*, 2nd ed., Wiley, New York.

Umamaheshwari, G., Nivedha, M., Psci Dorritt., J (2016). Design of Tunable Method for PID Controller for Higher Order System, *Inter. J. of Eng. and Comp. Sci*, **5**, Issue 7, July, pp. 17239-17242.

Villadsen, J., and M. L. Michelsen (1978). *Solution of Differential Equation Models by Polynomial*

Approximation, Prentice-Hall Inc., Englewood Cliffs, N. J.

Vilanova, R. (2008) IMC based Robust PID design: Tuning guidelines and automatic tuning, *J Process Control.* ; **18**(1), pp. 61-70.

Williams, A. O. F., and V. O. Adeniyi (1996). A New method for the design of PID-Type controllers, *Proc. 13th. IFAC World Congress* San Francisco, USA, June 30–July, 6, 1996.

Williams, A. O. F. and V. O. Adeniyi (2009). PID Control Design for a Distributed Parameter Heat Conduction System, *e-Proceedings of the 29th. Annual Conference of the Nigerian Society of Chemical Engineers*, Abuja, Nigeria.

Yamagushi, N. and Kanoh, H. (2000). Design of Robust PID Parameters for Distributed Parameter Processes, *IFAC Proceedings*, **Vol. 33**, Issue 24, Sept., pp. 221–226.

Ziegler, J. C. and N. B. Nichols (1942). Optimum settings for automatic controllers, *Trans ASME*, **Vol. 64**, pp. 759–768.

Zhou, W., Hamroun, B., Le Gorrec, Y., and Couenne, F. (2015). Dissipative Boundary Control Systems with Application to an Isothermal Tubular Reactor, *IFAC Papersonline*, **Vol. 48**-13, pp. 150-153.

APPENDIX A

To solve the dynamic system model, Eq. (5) subject to the initial and boundary conditions given by Eqs. (6) to (7), by modal decomposition technique, these are first re-defined using the Dirac delta function to obtain

$$\frac{\partial x}{\partial t} = \frac{1}{Pe_M}\frac{\partial^2 x}{\partial z^2} - \frac{\partial x}{\partial z} - Dax + \delta(z)u(t) \quad \text{(A.1)}$$

$$\text{At} \quad z = 0, \quad \frac{\partial x}{\partial z} = Pe_M x, \quad \text{At} \quad z = 1, \quad \frac{\partial x}{\partial z} = 0 \quad \text{(A.2)}$$

Assuming solutions of the form

$$x(z,t) = \sum_{k=1}^{\infty} a_k(t)\phi_k(z), \quad \delta(z)u(t) = \sum_{k=1}^{\infty} b_k(t)\phi_k(z) \quad \text{A.(3)}$$

Ray (1981) has shown that

$$\phi_k(z) = B_k e^{Pe_M z/2}\left[\cos\omega_k z + \frac{Pe_M}{2\omega_k}\sin\omega_k z\right], \quad \text{(A.4)}$$

$k = 1,2,\ldots$

in which

$$B_k = \left[\int_0^1 \left(\cos\omega_k z + \frac{Pe_M}{2\omega_k}\sin\omega_k z\right)^2 dz\right]^{-1/2} \quad \text{(A.5)}$$

$k = 1,2,\ldots$

where ω_k, are the roots of the transcendental equation

$$\tan\omega_k = \frac{Pe_M\,\omega_k}{\omega_k^2 - \left(Pe_M/2\right)^2} \quad k = 1,2,\ldots \quad \text{(A.6)}$$

and the system eigenvalues, λ_k are given by

$$\lambda_k = \frac{1}{Pe_M}\left(\omega_k^2 + \frac{Pe_M^2}{4}\right) \quad \text{(A.7)}$$

From the orthogonality property of the eigenfunction $\phi_k(z)$, we have

$$b_k = \int_0^1 \delta(z)\phi_k^*(z)u(t)dz = B_k u(t) \quad \text{(A.8)}$$

where

$$\phi_k^* = \exp^{-Pe_M z/2}\phi_k$$

is the adjoint eigenfunction.

From Eqs. (A.8) and (A.33):

$$x(z,t) = \sum_{k=1}^{\infty}\left[e^{-\theta_k t}a_k(0) + \frac{b_k}{\theta_k}\left[1 - e^{-\theta_k t}\right]\right]\phi_k(z) \quad \text{(A.9)}$$

in which $\theta_k = Da + \lambda_k$

Let the initial steady-state concentration profile for a steady-state input $\bar{u}$ be $\bar{x}(z)$, then

$$a_k(0) = \int_0^1 \phi_k^*(z)\bar{x}(z)dz \quad \text{(A.10)}$$

If a step change in the input is now made from u_1 to u_2, then

$$b_k = B_k u_2$$

and the system step response at various axial distances can then be computed from Eq. (A.9). This requires that we first compute B_k, λ_k and $a_k(0)$ given by Eqs. (A.5), (A.6) and (A.10), respectively.

BIOSYNTHESIS OF IRON OXIDE NANOPARTICLES USING CENTRAL COMPOSITE DESIGN OF RESPONSE SURFACE METHODOLOGY

***Alaya-Ibrahim, S[1,2]., Kovo, A. S[1,2]., Abdulkareem A. S[1,2]., and Adeniyi, O. D[1,2].**

[1]Nanotechnology Group, Centre for Biotechnology and Genetic Engineering, Federal University of Technology, PMB 65, Minna, Niger State, Nigeria;

[2]Chemical Engineering Department, Federal University of Technology, PMB 65, Minna, Niger State, Nigeria.

*Corresponding author email: neekyai@yahoo.com 08032877199

ABSTRACT

Central Composite Design (CCD) of Response Surface Methodology has been applied in optimizing the size of iron oxide nanoparticles (FeONPs) synthesised by studying the effects of three (3) important elements which are reaction time, reaction temperature and extract volume. The quadratic model was selected and fitness of the model was studied using sequential model of sum of squares and model of summary statistics. The effects and interaction between the elements studied on the size of synthesised FeONPs were investigated using analysis of variance (ANOVA), 2D contour plots and 3D surface plot. ANOVA showed that the time of reaction has the greatest effect on the size of FeONPs synthesised and the 3D surface plots revealed that to obtain the smallest size of FeONPs, the reaction time and the reaction temperature has to be set at 15 mins & 25 ^oC respectively.

Keywords*. Iron oxide nanoparticles, Biosynthesis, CCD. RSM*

1. INTRODUCTION

Iron oxide nanoparticles (FeONPs) are considered as one of the most multipurpose and safe nanoparticles because of their biodegradability, biocompatibility, ease of surface modification and magnetic properties which enable them to be controlled by external magnetic field. Thus, they are useful in various biomedical applications such as targeted drug delivery, cell sorting, contrast agents for magnetic resonance imaging (MRI) and hyperthermia (Meyyappan *et al*., 2015; Al-Ruqeish *et al*.,2016). They also play important role in environmental remediation circle, as it is used in removal of both organic and inorganic heavy metal pollutants from polluted water (Balamurugan *et al*., 20l4).

However, the antibacterial and the catalytic activities of FeONPs just like any other metal nanoparticles are relatively dependent on their sizes, structure, shape, size distribution & chemical-physical environment. Hence, it is of paramount importance to have control over the size distribution and this is often achieved by specifically varying the system methods, reducing agents and stabilizer (Abou El- Nour *et al*., 2010).

Response Surface Methodology (RSM) is a mathematical tool which aids in better understanding & optimizing the response of an experiment (Fisher, 1920) by basically feeding the software with information which in turn provide an accurate prediction of response. RSM was purposely designed to replace experimental response with predictive one by studying the various effects of parameters that will result to optimum response (Neda *et al*., 2002). Thus, it is widely applied in optimizing many processes which include; chemical & pharmaceutical, biological/biomedical, food sciences, production engineering, air quality analysis & toxicological research, and simulation studies (Ray, 2006; Montegometry, 2005; Carley *et al*., 2004; Neda *et al*., 2002; Allen and Yu, 2000). This is due to numerous advantages of RSM over conventional method as follows; (1) ability to efficiently predict values from numerical or practical experiments at discrete data points (2) it minimizes cost of analysis methods, the associated resources & high numerical data analysis (3) it also reduces the process development (Cira *et al*., 2016; Ray, 2006) and (4) it estimates the interactions between the process parameters (Asadi and Zilouei, 2017)

In this study, Central Composite Design (CCD) of Response Surface Methodology was employed in optimizing the particle size of iron oxide nanoparticles (FeONPs) through investigations of influence of the major synthesis parameters such as reaction time, reaction temperature and the extract volume.

2. MATERIALS AND METHODS

Materials

$FeCl_3$ and $FeCl_2$. $4H_2O$ salts used in this work are of analytical grade, manufactured by BDH, England. Deionized water was used throughout the study and the mango leaves was collected from Tunga area of Minna, Niger state, Nigeria.

Preparation of Mango Leaves Extract

The mango leaves collected were washed thoroughly with distilled water to remove dust from their surfaces before drying them under shade at room temperature for 18 days. After drying, they were crushed using porcelain mortar and pestle.

40 g of crushed mango leaves was boiled in 400 ml of deionized water for 15 mins. The mixture was allowed to cool & centrifuged at 6600 rpm for 30 mins, it was decanted, filtered using Whattman filter paper. The filtrate was collected as the MLE and stored in a bottle at a temperature of 4 ^oC for further experimental use.

Biosynthesis of FeONPs

Certain volume of MLE was reacted with 5 ml of 0.01 M of $FeCl_3$ and $FeCl_2$. $4H_2O$ (ratio 2:1) in a water bath shaker at specific temperature & reaction time based on the optimization parameters generated by Design Expert 10 using CCD of RSM. This procedure was carried out on all the samples and upon completion of their reaction time, samples were withdrawn from the shaker for UV-Visible Spectroscopy (UV) analysis (the UV result is in the main work) and the sizes were calculated from TEM analysis using Zeiss Auriga HRTEM

Table 1. Alpha ($\propto$) values of the factors studied and their coded form

Name	Coded factors	Units	Low	High	-alpha	+alpha
Time	A	Minute	5	15	1.59104	18.409
Temperature	B	Celsius	25	80	6.2507	98.7493
Extract volume	C	millilitre	5	14	1.93193	17.0681

Optimization Process

The rotatable CCD of RSM was employed because of its flexibility. Central Composite Design (CCD) is a combination of 2 level factorial design, centre points which is usually replicated and axial or star points. The distance of each axial points from the centre is called alpha ($\propto$). The value of $\propto$ is subject to the number of factors considered as well as some desired properties. Also, the star points are usually twice the number of factors in the design and it's a representation of extreme values for each factor in a design (minimum & maximum) (http://www.itl.nist.gov/div898/handbook/, 2017). In CCD, the centre points determine the orthogonality as well as the rotatability of a design.

- Orthogonality is a property of RSM that allows the model terms & block effects to be estimated independently by minimizing the variation in the regression coefficient.
- Rotatability is the measure of the variance of the predicted response at any point "x" which depends on the distance of x from the design center point. This property of RSM improves the precision of prediction (Asadi and Zilouei, 2017; Box and Draper, 1987).

Thus, for rotatable design, the alpha ($\propto$)= $[2^k]^{1/4} = 2^{3/4}$ = 1.682, for this design, where k is number of factors = 3.

The ($\propto$) values of the factors studied and their coded form are shown in Table 1

The factors studied are reaction time, reaction temperature and the plant extract volume which are coded as A, B & C respectively. A total number of 20 runs was generated for the optimization of the size of FeONPs and after the experiments, the various sizes obtained are shown in Table 2.

Characterization Techniques

The FeONPs synthesized were characterized using UV-Visible Spectroscopy and Transmission Electron Microscopy (TEM)

Table 2. Experimental Design and Response Factor of Response Surface Analysis for FeONPs

Experimental Run	Time (min)	Temperature (Celcius)	Extract Volume (ml)	Size (nm)
1	5	25	14	0
2	10	52.5	9.5	8.11
3	5	80	5	0
4	15	25	14	0
5	15	80	5	10.11
6	15	80	14	0
7	15	25	5	9.37
8	5	25	5	0
9	5	80	14	0
10	10	52.5	9.5	8.11
11	10	52.5	9.5	8.11
12	10	52.5	9.5	8.11
13	18.41	52.5	9.5	12.21
14	1.51	52.5	9.5	0
15	10	52.5	9.5	8.11
16	10	98.75	9.5	0
17	10	52.5	1.93	18.11
18	10	6.25	9.5	0
19	10	52.5	9.5	8.11
20	10	52.5	17.07	6.25

UV-Visible Spectrum analysis: The syntheses of FeONPs were monitored using UV-Vis spectra by sampling 1 ml of FeONPs solution in 10 ml of distilled water using Shimadzu UV-visible spectrophotometer 1800 at the range of 190-800 nm.

Transmission Electrons Microscopy (TEM) analysis: The formation and sizes of the FeONPs synthesized were determined using Zeiss Auriga High Resolution Transmission Electrons Microscopy **(**HRTEM). 0.02 g of the FeONPs was suspended in 10 ml of methanol which was ultra- sonicated until there was complete dispersion of the FeONPs. A drop of the slurry was dropped on the holey carbon grid and photo light was used to dry the sample. The dried sample was loaded onto the sample holder and the electron microscope was operated for imaging

3.0. RESULTS AND DISCUSSIONS

UV-Vis spectra

Iron oxide nanoparticles was synthesised using different volume of plants extract with 5 ml of $FeCl_3$ & $FeCl_2$ (ratio 2:1) at different temperatures and reaction time as illustrated in Table 2 based on CCD of Response Surface Method of optimization. An immediate colour change was observed from light yellow to black colour, as soon as the Mango Leaves Extract (MLE) was added to the salt in all cases. This is an indication of formation of iron oxide nanoparticles, as the colour change is the easiest & commonest form of identification of nanoparticle formation (Balamurugan *et al*., 2014). The change in colour is due to the excitation of the Surface Plasmon Vibrations in the Iron oxide nanoparticles (Song and Kim, 2009; Sneha Shah *et al*., 2014). The wavelength obtained from the synthesis of FeONPs ranges from 199 nm–267 nm which is of typical spectra of FeONPs (Pattanayak and Nayak, 2013; Sranvanths et al., 2016) as shown in Figure 1

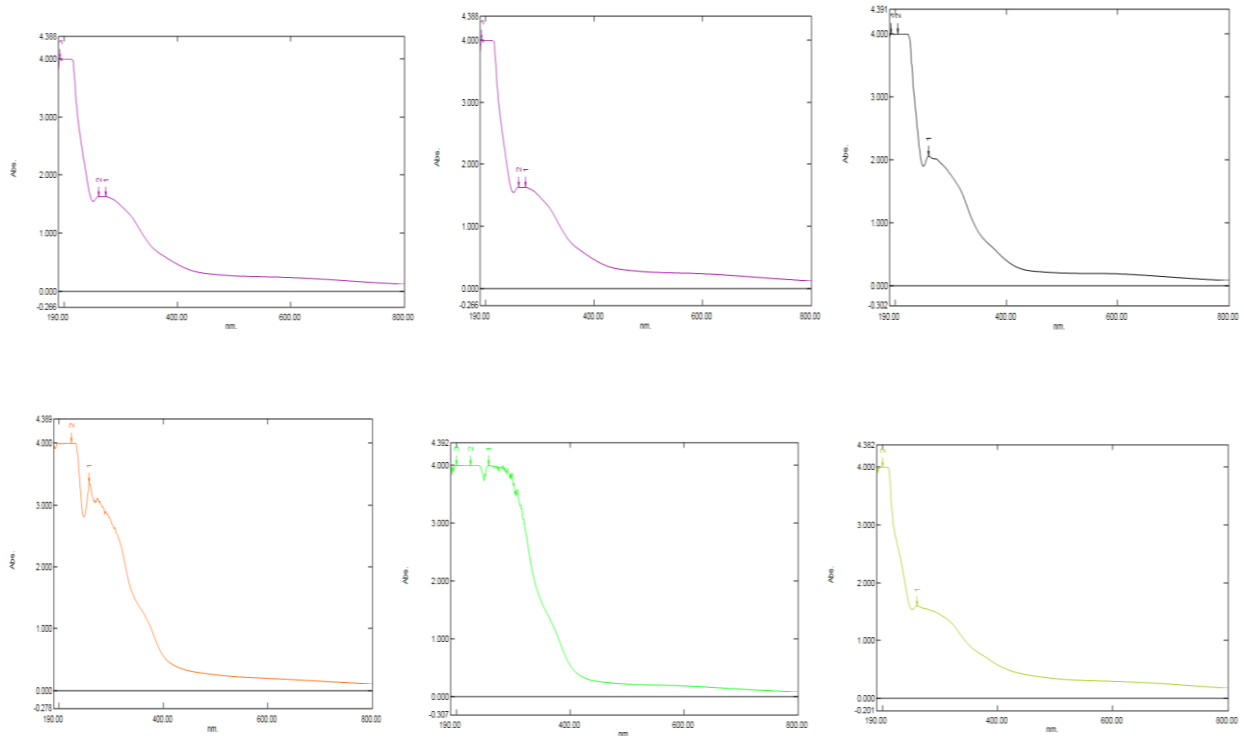

Figure 1. UV-vis spectra of FeONPS

High Resolution TEM

The HRTEM of FeONPs synthesized with MLE are shown in Figure 2. A well dispersed spherical FeONPs are reveal as shown Figures 2a, b and f while that of Figures 2c, d & e are clustered. The clustering is attributed to the magnetic nature of FeONPs due to their large surface to volume ratio, thereby having high surface energies (Balamurugan et al., 2014) The average sizes were calculated to be in the range of 6.25-18.11 nm.

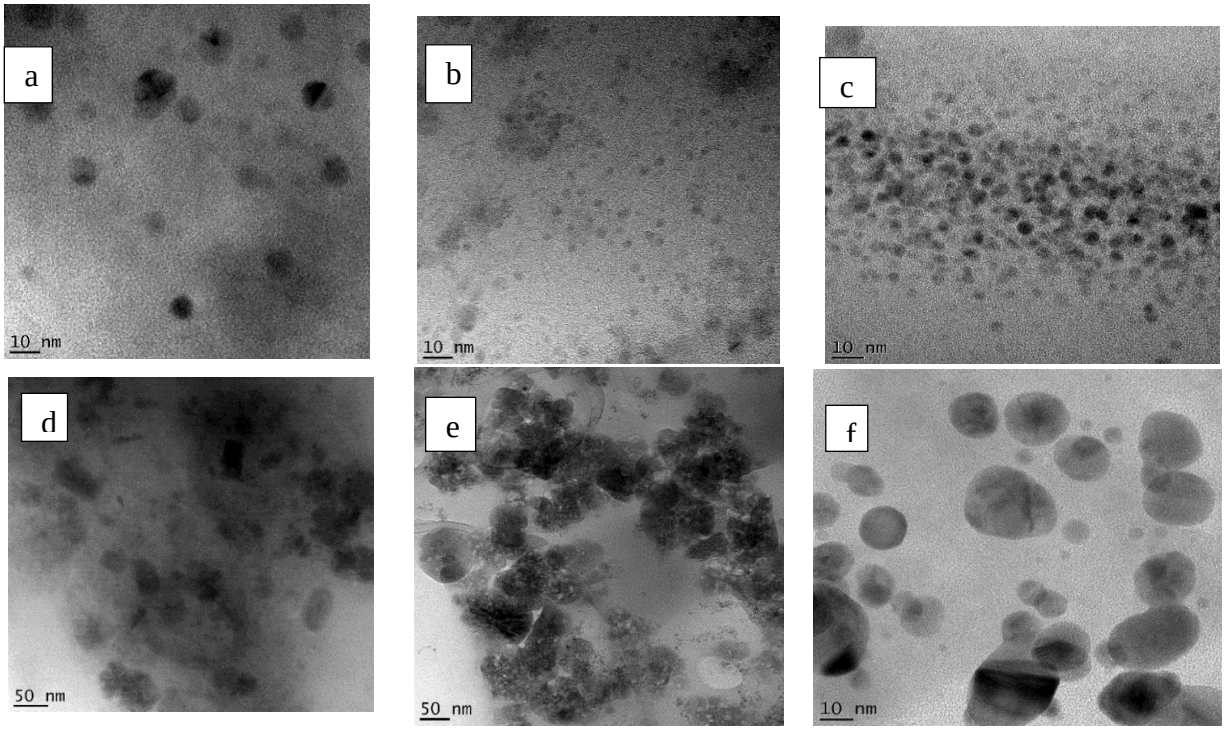

Figure 2. HRTEM images of FeONPs

Response Surface Method (RSM) Design

Central Composite Design (CCD) of Response Surface Method was employed in this study as earlier sated. The various response obtained from the interaction of studied parameters on the sizes of FeONPs synthesised are shown in Table 2. The sizes of FeONPs obtained ranges from 0 to 18.11 nm. The obtained size is in line with those obtained in previous work; 6.30 nm & less than 20 nm of FeONPs were synthesised using Desmodium gangaticum & Ocinum sanctum extracts respectively (Meyyappan *et al*., 2014; Balamurugan *et al*., 2014). In addition, nanoparticles have been defined as a nanocrystalline material with a size range of 1-100 nm (Dhermedra *et al*., 2008; Panda *et al*., 2015). However, not all the synthesises resulted to formation of FeONPs as shown by TEM analysis through which the sizes were calculated (results in the main work). This is an indication that UV analysis is not enough to ascertain the formation of FeONPs as all were assumed to form according to the UV results. Hence, further analysis such as TEM is recommended. The zero values as shown in the table are as a result of non-formation of those FeONPs. This can be attributed to the fact that at those combined optimization parameters, synthesis of FeONPs were not favoured and could also be as a result of presence of some unidentified impurities which might have suppressed the formation of FeONPs.

The Response analysis was carried out using Excel 2016 and Design Expert 10 (Trial version). For all the analysis, the p-values (Prob > F), the F-value, predicted and adjusted R-Squared, sum of squares were estimated and their effects on the experimental response were obtained. For a model to be selected, certain condition must be satisfied; p-values (Prob > F) must be lower than 0.05. the difference between the adjusted & predicted R-Squared must be less than 0.2. The p-value is the smallest variance which can nullify the selection of a particular model, if its condition is not satisfied. The predicted & adjusted values are the values predicted by the software & the experimental values respectively.

Selection of the Response Surface Model

Quadratic model with two-factor interaction (2FI) was selected in this study and the fitness of evaluation was done using sequential model of sum of squares & model of summary statistics as illustrated in Table 3 & Table 4. Sequential model of sum of squares examines the significance of each model for p-value (Prob>F) lower than 0.05. Although, the (Prob>F) of Linear vs Block Model is 0.03, however, that of Quadratic vs 2FI Model of < 0.0001 is lower

Table 3. Sequential Model of Sum of Squares

Source	Sum of Squares	Df	Mean Square	F-Value	p-value Pro> F
Linear vs Block	231.1	3	77.03	3.89	0.0305
2F! vs Linear	47.57	3	15.86	0.76	0.5358
Quadratic vs 2FI	229.2	3	76.4	34.55	<0.0001

On the other hand, Table 4 shows the model summary of statistics, the Quadratic Model has the lowest standard deviation, highest coefficient of regression (R^2) value and the difference between the predicted R^2 & adjusted R^2 is 0.19, which is less than 0.2. A model is said to be fitting the data & can reliably be used, if the difference between the predicted R^2 & adjusted R^2 is lower than 0.2. Hence, Quadratic Model was selected and the Model equation in coded form is;

$$X = 8.55 + 2.93A + 0.054B - 2.8C + 0.093AB - 2.43AC - 0.092BC - 1.50A^2 - 3.65B^2 + 0.65C^2 \quad 1$$

where X is size (nm

Table 4. Model Summary of Statistics

Source	Std. Dev	R-Squared	Adjusted R-Squared	Predicted R-Squared
Linear	4.45	0.4379	0.3255	0.1102
2FI	4.56	0.5280	0.292	0.3890
Quadratic	1.49	0.9623	0.9246	0.7384

Analysis of Variance (ANOVA)

The adequacy of the selected model was established using ANOVA test as illustrated in Table 5. The table shows that p-value (Probability > F) for the Quadratic Model is lower than 0.05, thus it is significant. Also, the coefficient of regression (R- squared) is 0.9623 which is close to 1, which is an indication that the experimental

& predicted responses are well correlated; and adequate precision of 15.565 is an indication of strong signal that the model can be used for optimization as its value is higher than 4

Table 5. Analysis of Variance (ANOVA) of selected Response Model

Source	Sum of Squares	df	Mean Square	F- Value	p-value Prob>F
Model	507.87	9	56.43	25.52	<0.0001
A-Time	117.24	1	117.24	53.03	<0.0001
B-Temperature	0.04	1	0.04	0.018	0.8958
C-Extract volume	113.82	1	113.82	51.48	<0.0001
AB	0.068	1	0.068	0.031	0.8642
AC	47.43	1	47.43	21.45	0.0012
BC	0.068	1	0.068	0.031	0.8642
A	32.19	1	32.19	14.56	0.0041
B	192.21	1	192.21	86.94	<0.0001
C	6.14	1	6.14	2.78	0.1301
Std. Dev	1.49		R-Squared	0.9623	
Mean	5.24		Adjusted R	0.9246	
			Predicted R	0.7384	
			Adequate Precision	15.565	

The correlation between the actual and predictive size of FeONPs was also examined using predictive vs actual plot as shown in Figure 3. There is close agreement between the predicted and actual size of synthesised FeONPs as shown by points of the data, which are not too far apart.

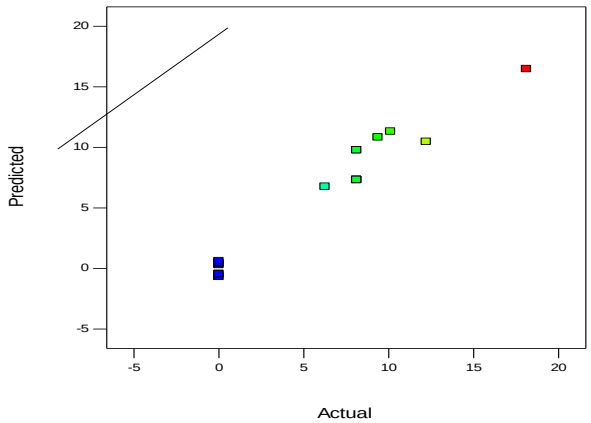

Figure 3. Predicted vs Actual values

Effects of Reaction Time, Reaction Temperature and the Extract volume on the Size of the Synthesised FeONPs

After the adequacy of the model has been established, the effects &interaction between the model terms on the response of the model was studied using ANOVA, 2D contour plot and 3-D surface plot.With reference to Table 5 (ANOVA) It can be deduced that time & extract volume are significant factors which influences the size formation of FeONPs with their p-value (Prob >F) of < 0.0001 & < 0.0001 respectively, while temperature has insignificant effect. Also, the interaction between time & extract volume has significant effect on the response of the model and its p-value (Prob >F) is < 0.0012. The F-Values of time, temperature & extract volume were found to be 53.03, 0.018 & 51.48 respectively. This is an indication that time has the highest influence on the size formation of FeONPs with highest F-value of 53.03. Thus, increasing the reaction time results to bigger size of FeONPs and vice versa.

Figure 4a and Figure 4b shows the 2D contour of temperature vs time & that of extract volume vs time respectively. Figure 4a examines the effect of temperature and time on the size formation of FeONPs synthesised. It could be deduced that keeping temperature constant and increasing the reaction time leads to increased size of the FeONPs. For instance, at temperature of 36 ^{o}C and reaction time of 6.03 min, a size of 3.98 nm was obtained while at the same temperature, with increased reaction time of 8.12 min, a size of 5.91nm was obtained. This is in support of ANOVA result identifying temperature as an insignificant.

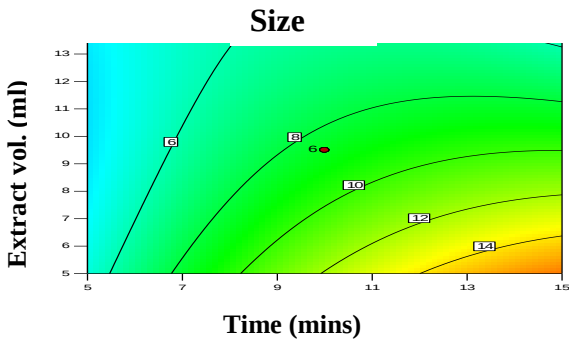

Figure 4a. 2D Contour Plot of Temperature vs Time

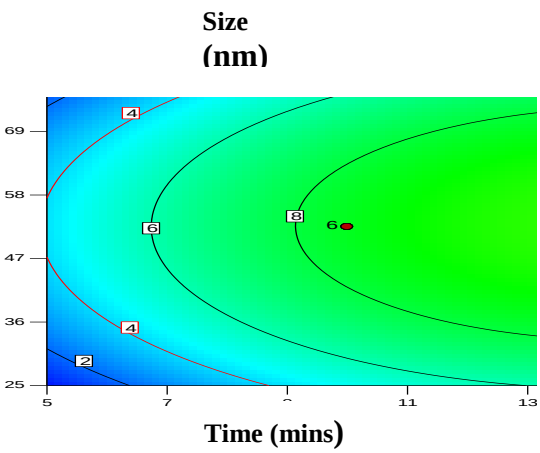

Figure 4b. 2D Contour Plot of Extract Volume vs Time

On the other hand, figure 4b relates the effect of extract volume and time as a function of size. The plot shows that lowering the volume of extract at constant reaction time produces a bigger size of FeONPs.

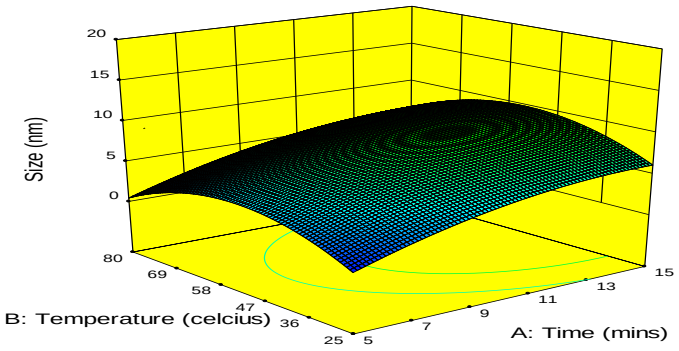

Figure 5. 3D Surface plot of Temperature & Time with Extract volume at the Central

The effects of reaction temperature and reaction time on the size of FeONPs with the extract volume at the central level is shown in Figure 5 The figure shows that in order to obtain the smallest size of FeONPs, the reaction time and the reaction temperature has to be set at 15 mins & 25 ^{o}C respectively

Numerical Optimization for Desirability of the Response

Numerical optimization was employed by the Design Expert software to determine the desirability of the size of FeONPs synthesised. The actual values of the operating variables (time, temperature & extract volume) as well as the response (size) were set, ranging from the minimum to maximum values. The software then proffers solution of their various optimal values and determine the desirability of the response (size). Desirability ranges from zero to one (1), desirability value of 1 is an ideal case and that of zero does not fit well. Thus, the desirability test was conducted on the FeONPs experimental variables & the obtained sizes as illustrated with Ramp view in Figure 6.

The figure shows that the optimal reaction time temperature and extract volume for obtaining FeONPs are,

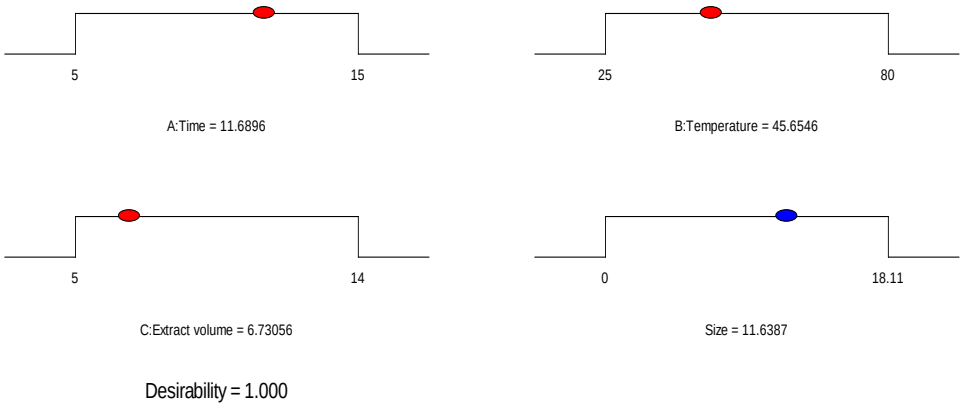

Figure 6. Ramp View of desirability of Size of Synthesized FeONPs

11.69 mins, 45.65 ^{o}C and 6.73 ml respectively, with their combined desirability of 1. The results of the desirability analysis as shown in Table 6, show different combinations of predicted synthesis parameters (time, temperature & extract volume) and their corresponding sizes of the FeONPs as well as their desirability value. They all fitted well with desirability value of 1, however, the Ramps result was confirmed as the best combinations.

Table 6. Results of Desirability Analysis

Number	Time (min)	Temperature (^{o}C)	Extract volume (ml)	Size (nm)	Desirability
1	11.69	45.66	6.73	11.64	1
2	5	80	5	1.63	1
3	5	25	5	1.52	1
4	10	52.5	9.5	8.55	1
5	15	80	14	1.72	1
6	5	25	14	0.8	1
7	15	80	5	12.55	1
8	15	25	14	1.61	1
9	5	80	14	0.54	1
10	9.68	62.2	11.55	6.8	1

Hence the optimum experimental parameters for the synthesis of FeONPs by RSM are **11.69 mins 6.73 ml & 45.66 ^{o}C** for reaction time, extract volume and reaction temperature respectively

4.0. CONCLUSIONS

The CCD of RSM has been successfully used in optimizing the size of FeONPs and it was found to be an effective tool. Time and extract volume were found to have significant effect on the size formation of FeONPs, with time having the greater effect, the 3D surface plot of temperature & time with extract volume at the central level shows that in order to obtain the smallest size of FeONPs, the reaction time and the reaction temperature has to be set at 15 mins & 25 ^{o}C respectively.

REFERENCES

Abou El- Nour, K.M.M., Eftaiha, A., Al-Warthan, A., Ammar, R.A.A. (2010). Synthesis and applications of silver nanoparticles. *Arabian Journal of Chemistry* 3: 135-140. Doi: 10.1016/j-arabjc.2010.04.08

Allen, T. and Yu, L. (2000). A method for and from simulation, optimization, proceeding of 2010

Al-Ruqeishi, M.S., Mohiuddin, T., and Al- Saadi, L.K. (2016). Green synthesis of iron oxide nanorods from deciduous Omani mango leaves for heavy oil viscousity treatment. *Arabian Journal of Chemistry.* http//.dx.doi.org/10.1016/j-arabjc2016.04.003

Asadi, N. and Zilouei, H. (2017). Optimization of organosolv pretreatment of rice straw for enhanced biohydrogen production using Enterobacter aerogenes. *Bioresources Technology* 227:335-344. Doi: 10.1016/j.biotech.2016.12.073

Balamurugan, M.G., MOhanraj, S., Kodhaiyolii, S., and Pulgalenthi, V. (2014). Ocinum sanctum leaf extract mediated green synthesis of iron oxide nanoparticles: spectroscopic and microscopic studies. *Journal of Chemical & Pharmaceutical Sciences special issue* 4: 201-204

Box, G.E.P. and Draper, N.R. (1987). Empirical Model Building and Response surfaces. *John Wiley and Sons.* New York. Pp 477

Carley, K.M., Kamneva, N.Y. and Ramingo, J. (2004). Response Surface Methodology, Centre for computational Analysis of social and organisational systems- *Technical Report* cmu-ISRI-04-136

Cira, S.C., Dag, A., and Karakus, A. (2016). Application of Response Surface Methodology and Central Composite Inscribed Design for Modelling and Optimization of Marble Surface Quality. *Advance in Material and Engineering* 2016:13. http://dx.doi.org/10.1155/2016/2349476

Dhermedra,K.T., Behari, J., and Prasengt, S., (2008). Application of nanoparticles in waste water treatment. *World Applied Sciences Journal* 3(3): pp 417-433.

Fisher, R.A. (1920). Design of Experiment, 8th edition, Published by *Oliver & Biyd*, pg 245

Meyyappan, A., Banu, S.A. and Kurian, G.A. (2015). One step synthesis of iron oxide nanoparticles via chemical and green route- an effective comparison. *International Journal of Pharmacy and Pharmacy Sciences* 7(1): 70-74

Montgometry, D.C. (2005). Design and Ananlysis of Experiment, 6th edition, *John Wiley*, New York

Neda, Z., Alireza, A., Lye, L. and Popescu, R. (2002). Application of RSM in Numerical Geotechnical Analysis, *55th Canadian Society for Geotechnical Conference*, Hamilton, Ontario, Canada. http://www.engr.mum.ca/~llye/indexl.htm

NIST/SEMATECH e –Handbook of statistical methods, http://www.itl.nist.gov/div898/handbook/ cited on the 5th of September, 2017.

Ray, S. (2006). Response Surface Methodology; A statistical process tool for optimization. *The Indian Textile Journal* cited at www.indiantextilejournal.com/articles/F.Adetails.asp?id=393

DEVELOPMENT OF MODELS FOR SIMULATION OF FLUIDIZED BED REACTOR FOR COAL GASIFICATION.

***Dagde, K. K., Iregbu, P. O. and Iminabo, J.**
Department of Chemical/Petrochemical Engineering
Rivers State University, Nkpolu Oroworukwo, Port Harcourt, Nigeria
Email: dagde.kenneth@ust.edu.ng.

ABSTRACT

A model describing the steady state behaviour of a fluidized bed reactor for coal gasification has been developed. The model was developed based on the principle of conservation of mass and the hydrodynamics specifications of Kunii and Levenspiel was adopted for the fluidized bed reactor models. The reaction kinetics of the gasification reactions were obtained from literature. The models consist of eight (8) ordinary differential equations which were integrated numerically using the fourth order Runge-Kutta algorithm implemented in MATLAB. The results obtained compared reasonably well with literature data with a percentage deviation ranging from -0.2% to 8.8%. Simulation of model at various operating parameters gave the optimum yield at 1 bar total pressure, 1135K temperature, 0.0257m bubble diameter and 0.0301m/s superficial velocity. Sensitivity analysis showed that the superficial velocity, bubble diameter, temperature and pressure are some of the process variables that affect the yields of synthesis gas (CO and H_2), carbon (iv) oxide (CO_2), and methane (CH_4).

Key Words: *Modeling and Simulation, Fluidized Bed Reactor, Coal, Gasification, MATLAB*

1.0 INTRODUCTION

Owing to the dwindling supply of energy and raw materials since mid-seventies, everyone is aware that a rational and economic use of resources, particularly energy resources, is the real challenge facing the world economy. The decline in the availability and affordability of domestic reserves of petroleum and natural gas fuels, coupled with the increasing reliability problems in the supply of imported fuels has generated a renewed interest in the utilization of coal reserves in Nigeria. The concept of coal conversions to produce a more useful or convenient form of energy has been known for many years, and various processes have been explored to accomplish this task. Thermal gasification has been proposed as one technical option for the conversion of coal to gaseous fuels and/or chemicals. Although many contacting devices have been proposed for coal gasification, fluidized beds are widely used because of their advantageous characteristics, such as high rates of heat transfer and excellent gas solid contacting. The main approaches for converting coal into an improved non-polluting energy source are: Coal combustion to produce heat, steam, and/or electricity; Coal pyrolysis to produce gas, pyrolytic liquids, char, and chemicals; Coal gasification to produce low or intermediate BTU gas and Coal liquefaction to produce liquid fuels. The different ways of converting solid coal into liquid are non-catalytic liquid phase dissolution or solvent extraction, direct catalytic hydrogenation pyrolysis, etc. The term gasification signifies the thermal reaction of solid fuels with air, oxygen, steam, carbon dioxide, or mixture of these, to yield a gaseous product that is suitable for use either as a source of energy or as a raw material for the synthesis of chemicals, liquid fuels, or other gaseous fuels. Thus, gasification yields a product that can be handled with maximum convenience and minimum cost, and in addition, greatly extends the uses to which solid fuels may be put. For both technical and economic reasons, most gasification processes for synthesis gas production or for the production of energy as gaseous fuel, strive for total gasification of the solid fuel. As the price of our petroleum and natural gas resources increase and supplies diminish, increased emphasis will be placed upon the development of alternative sources of energy. Today, petroleum and natural gas account for over 90% of the total energy consumption in Nigeria. Furthermore, about 80% of our petroleum products are imported (NBS, 2016). It is, therefore, essential that alternative sources of energy be developed in order that the country's economic growth of energy consumption can be maintained. As much there is a pressing need to conserve known supplies of crude oil and established processes for the production of synthetic liquid fuels and gases.

Coal is clearly one of our most abundant fossil resources and must play a key role in supplying energy and chemicals for the remainder of this and all of the next

century. As such the conversion of the nation's vast resources of coal to liquid and gaseous fuels has been envisioned as a major contributor to the energy picture in the near future. There is an urgent need for a strong, balanced energy program involving the direct combustion of coal and the conversion of coal to gaseous and liquid fuels. In addition, new and improved technology in these areas must assure environmental protection.

For coal to play a significant role in our energy future utilization cannot be restricted to the use of only premium coal; that is, the types of coal with low sulphur, low ash, and non-caking characteristics. Research must be pursued into the utilization of our total coal reserves.

Various processing options are being explored to convert coal into fuels and useful chemicals. The most important factor concerning the potential utilization of coal is its conversion flexibility. Although coal is relatively stable as a storehouse of energy and chemicals, it can be treated in a few different but basically simple ways in order to release these values usefully. The science and technology of the complete gasification of coal have advanced significantly due to the considerable expansion in basic research on the fundamental chemistry and physics of gasification reactions, and on gasification and purification processes. Most research work on coal gasification considered the de-volatilization reaction that occurred immediately the coal enters the reactor due to increased temperature (Rajan and Wen, 1980), but this research considered the secondary reactions which takes place after the de-volatilization reactions, which represents the main gasification reactions.

2.0 REACTOR MODEL

Gasification of coal in a fluidized bed reactor involves chemical reactions as well as mass transport which are profoundly affected by the hydrodynamics in the reactor. Figure 1 shows the hypothetical representation of a two phase fluidized bed reactor comprising of the bubble and emulsion phases. The emulsion phase consists of coal particles and the gas flow rate is equivalent to minimum fluidization velocity. The flow rate of gas in the bubble phase is in excess of the minimum fluidization velocity.

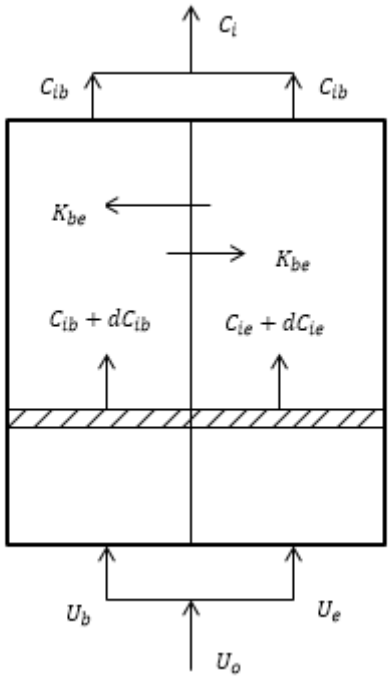

Figure 1: Two Phase Fluidized Bed Reactor for Coal Gasification.

2.1 Model Assumptions

This model will be based on the two phase theory of fluidization with the following assumptions (Davidson and Harrison, 1963):

1. The fluidized bed consists of two phases,' namely, bubble and emulsion phases, which are homogeneously distributed statistically.
2. The voidage of the emulsion phase remains constant and is equal to that at incipient fluidization.
3. The bed can be characterized by an equivalent bubble size, and the flow of gas in the bubbles is in plug flow.
4. The emulsion phase is well mixed.
5. The bed operates at under steady state and isothermal condition.
6. No reaction takes place in the bubble phase.

2.1.1 Material Balance Equation

(a) Bubble phase: Application of the law of conservation of mass to gases in the bubble-phase, with the assumptions of no accumulation and without gasification reactions, gives the material balance on species *i* over an elemental volume of $A_b\Delta h$ as:

$$\frac{\partial C_{ib}}{\partial t} = -U_b \frac{\partial C_{ib}}{\partial h} + D_{ib} \frac{\partial^2 C_{ib}}{\partial h^2} - K_{be}(C_{ib} - C_{ie}) \qquad (1)$$

Expressing equation (1) in dimensionless form and assuming steady state yields

$$0 = -\frac{U_b \partial y_{ib}}{H \partial Z} + \frac{D_{ib} \partial^2 y_{ib}}{H^2 \partial Z^2} - K_{be}(y_{ib} - y_{ie}) \qquad (2)$$

Since dispersion causes a decrease in the overall yield of the process, neglecting the dispersion term $\frac{D_{ib}\partial^2 y_{ib}}{H^2\partial Z^2}$, the resulting equation takes the form of a plug flow as;

$$\frac{dy_{ib}}{dZ} = -\frac{HK_{be}}{U_b}(y_{ib} - y_{ie}) \quad (3)$$

Equation (3) represents the bubble phase model.

(b) For the Emulsion phase

Application of the law of conservation of mass with gasification reactions in the emulsion-phase on species *i* over an elemental volume of $A_b\Delta h$ based on the above assumptions gives

$$\frac{\partial C_{ie}}{\partial t} = -\frac{U_e}{\varepsilon_{mf}}\frac{\partial C_{ie}}{\partial h} + \frac{D_{ie}}{\varepsilon_{mf}}\frac{\partial^2 C_{ie}}{\partial h^2} + \frac{A_b K_{be}}{A_e \varepsilon_{mf}}(C_{ib} - C_{ie}) + \frac{r_{ie}}{\varepsilon_{mf}} \quad (4)$$

Writing the model in dimensionless form and assuming steady state condition we have;

$$\frac{dy_{ie}}{dZ} = \frac{HA_b K_{be}}{A_e U_e}(y_{ib} - y_{ie}) + \frac{Hr_{ie}}{C_e U_e} \quad (5)$$

Equation (5) represents the model for the emulsion phase.

2.2 Hydrodynamic Relationships

Functional relationships among the parameters and variables that depend on the hydrodynamics of the fluid-bed are given as follows:

Bubble and Emulsion Phase Velocities

The bubble phase velocity U_b can be estimated using the formula (Kunii and Levenspiel, 1991):

$$U_b = U_o - U_{mf} + U_{br} \quad (6)$$

where $U_{br}\,represents$ the rise velocity of a single bubble in the bed and is given by

$$U_{br} = 0.711\ (gd_b)\text{^}\frac{1}{2}$$

where, d_b represents the bubble diameter

The emulsion phase velocity $U_e = U_{mf}$ (7)

where U_{mf} is the minimum fluidization velocity

Bed Fraction in the Bubble Phase

Levenspiel (2001) gave the volumetric gas flow in the bubble phase as:

$$U_b f_b = U_o - U_{mf} \quad (8)$$

$$f_b = \frac{U_o - U_{mf}}{U_b} \quad (9)$$

$f_b = 0.1\ to\ 0.001$ by experiment (Levenspiel, 2001).

Interchange Transfer Coefficient

This is estimated using Kunii and Levenspiel (2001) correlation;

(a) Bubble – Cloud Transport Coefficient (K_{bc})

$$K_{bc} = 4.5\left[\frac{U_{mf}}{d_b}\right] + 5.85\left[\frac{D^{\frac{1}{2}}g^{\frac{1}{4}}}{d_b^{\frac{5}{4}}}\right] \quad (10)$$

where d_b is the bubble diameter, D is the diffusivity; g is the acceleration due to gravity;

(b) Cloud – Emulsion Transport coefficient (K_{ce})

$$K_{ce} = 6.78\left(\frac{\varepsilon_{mf} D U_{br}}{{d_b}^3}\right) \quad (11)$$

Where, ε_{mf} is the void fraction at minimum fluidization

(c) Bubble – Emulsion Transport Coefficient (K_{be})

K_{be} is obtained by the addition of the two parallel resistances.

$$\frac{1}{K_{be}} = \frac{1}{K_{bc}} + \frac{1}{K_{ce}} \text{ i.e } K_{be} = \frac{K_{bc}.K_{ce}}{K_{bc}+K_{ce}} \quad (12)$$

Bubble Diameter

The bubble diameter d_b is estimated using Mori and Wen (1975) correlation;

$$d_b = D_{bm} - (D_{bm} - D_{bo})exp\left(-0.3\frac{x}{D}\right)^1 \quad (13)$$

$$D_{bm} = 0.652\{A(U_o - U_{mf})\}^{0.4} \quad (14)$$

$$D_{bo} = 0.00376(U_o - U_{mf})^2 \quad (15)$$

where D_{bo} is the initial bubble diameter and D_{bm} is the maximum bubble diameter.

The equivalent bubble diameter (Kunii and Levenspiel, 1969) is calculated at the middle of the total bed height,

$$h = \frac{H}{2} \quad (16)$$

2.3 Kinetic Model

Gasification of coal has numerous chemical reactions, but for the purpose of this research char gasification reactions would be considered;

Reaction (1)

$$C + H_2O \xrightarrow{k_1} CO + H_2 \quad (17)$$

Reaction (2)

$$C + CO_2 \xrightarrow{k_2} 2CO \quad (18)$$

Reaction (3)

$$C + 2H_2 \xrightarrow{k_3} CH_4 \quad (19)$$

Rate Kinetics Evaluation

The general expression for coal char gasification reaction rate is given by Carberry, (1976) as;

$$(r_i) = k(C_g, T)C_j \quad (20)$$

where, k is the apparent gasification reaction rate constant, which include the effect of temperature (T) and the effect of the gasifying agent (C_g), and C_A is the concentration of coal char. However, the concentration of the gasifying agent remains constant during the process, hence *k* only depends on temperature. Also, the H_2O, CO_2, $2H_2$ are assumed to be in excess resulting in a competitive reaction for carbon.

This implies that; $(r_i) = k(T)C_j$ (21)

And from Arrhenius Equation

$k(T) = k_o exp(\frac{-E_j}{RT})$ (22)

Therefore, $(r_i) = k_o exp(\frac{-E_j}{RT})C_j$ (23)

here, $C_j = C_{jO}(1 - X_j)$ (24)

So, $(r_i) = k_o exp(\frac{-E_A}{RT})\, C_{jO}(1 - X_j)$ (25)

where, k_o = pre-exponential factor, E_A = activation energy of coal and X_A = desired degree of conversion of coal.

Hence;

For Coke (A); $(-r_A) = (k_1 + k_2 + k_3)C_{AO}(1 - X_A)$ (26)

For CO+H_2 (B); $(r_B) = k_1 C_{AO}(1 - X_A)$ (27)

For CO (C): $(r_C) = k_2 C_{AO}(1 - X_A)$ (28)

For CH_4 (D): $(r_D) = k_3 C_{AO}(1 - X_A)$ (29)

Since there is no chemical reaction in the bubble phase; equations for each component gives;

$\frac{dy_{Ab}}{dZ} = -\frac{HK_{be}}{U_b}(y_{Ab} - y_{Ae})$ (30)

$\frac{dy_{Bb}}{dZ} = -\frac{HK_{be}}{U_b}(y_{Bb} - y_{Be})$ (31)

$\frac{dy_{Cb}}{dZ} = -\frac{HK_{be}}{U_b}(y_{Cb} - y_{Ce})$ (32)

$\frac{dy_{Db}}{dZ} = -\frac{HK_{be}}{U_b}(y_{Db} - y_{De})$ (33)

The kinetic models equations (26), (27), (28) and (29) are incorporated into the emulsion-phase reactor models equations (5) to give

$\frac{dy_{Ae}}{dZ} = \frac{HA_bK_{be}}{A_eU_e}(y_{Ab} - y_{Ae}) + \frac{H(k_1+k_2+k_3)C_{AO}(1-X_A)}{C_eU_e}$ (34)

$\frac{dy_{Be}}{dZ} = \frac{HA_bK_{be}}{A_eU_e}(y_{Bb} - y_{Be}) + \frac{HK_1C_{AO}(1-X_A)}{C_eU_e}$ (35)

$\frac{dy_{Ce}}{dZ} = \frac{HA_bK_{be}}{A_eU_e}(y_{Cb} - y_{Ce}) + \frac{HK_2C_{AO}(1-X_A)}{C_eU_e}$ (36)

$\frac{dy_{De}}{dZ} = \frac{HA_bK_{be}}{A_eU_e}(y_{Db} - y_{De}) + \frac{HK_3C_{AO}(1-X_A)}{C_eU_e}$ (37)

Equations (30-37) represent the Fluidized Bed Reactor models.

The exit concentration from the bubble and emulsion phases could be linked together by using the formula developed by Dagde and Puyate (2012) as:

$y_i = \beta y_{ib} + (1 - \beta)y_{ie}$ (38)

where i = A, B, C and D representing Coal (carbon), CO+H_2, CO and CH_4 respectively,

Substituting:

$y_A = \beta y_{Ab} + (1 - \beta)y_{Ae}$ (39)

$y_B = \beta y_{Bb} + (1 - \beta)y_{Be}$ (40)

$y_C = \beta y_{Cb} + (1 - \beta)y_{Ce}$ (41)

$y_D = \beta y_{Db} + (1 - \beta)y_{De}$ (42)

where $\boldsymbol{\beta}$ = 1- $\frac{U_{mf}}{U_o}$ (43)

The kinetic parameters for the coal gasification reactions are presented in Table 1

Table1: Kinetic parameters for coal gasification reactions, Yoon (1977)

Reaction	Activation Energy (Ej) kJ/kmole	Frequency Factor (kj) S^{-1}
$C + H_2O \xrightarrow{K1} CO + H_2$	121417	5.0*10^2
$C + CO_2 \xrightarrow{K2} 2CO_2$	360065	0.2*10^9
$C + 2H_2 \xrightarrow{K3} CH_4$	230274	0.75*10^3

2.4 Operating Parameters

The model equations developed contain certain unknown hydrodynamic and kinetic parameters such as the reaction rate constants for the various reaction paths (K_{ij}), the fluidized bed hydrodynamic parameters, (K_{be}), (U_e), (U_b), (U_{br}), etc. These constants have to be determined before integration of the models equations (30-37).

Table 2: Operating and Hydrodynamic parameters (Debashis, 1981)

Parameters	**Values**
Area of bubble phase	500 m^2
Area of emulsion phase	700m^2
Superficial gas velocity, U_o	0.18 – 0.14 m/s
Minimum fluidization velocity, U_{mf}	0.12 – 0.09 m/s
Bubble velocity, U_b	0.556 m/s
Bubble diameter, d_b	0.0487 m
Bed height, H	9.8 m
Mass transfer interchange coefficient	4.92 s^{-1}
Mass transfer interchange coefficient between The cloud and emulsion phase, K_{ce}	3.00 s^{-1}
Mass transfer interchange coefficient between the bubble and emulsion phase, K_{be}	1.86 s-1
Temperature, T	833 - 1133 K
Universal gas constant	8314 J/mol. K

2.5 Solution Techniques

The model equations (30-37) were solved using MATLAB 7.5 ODE 45 solver from Mathworks by employing the 4th order Runge Kutta algorithm in solving the resultant ordinary differential equation (ODE). The initial and boundary condition for the dimensionless height used in solving the model equation were between 0 to 1 at an interval of 0.05 i.e z = 0 to 1; $\Delta Z = 0.05$. The initial and boundary condition for mass fractions of each component used in solving the equation for the bubble and emulsion phase were between 0 to 1.

3.0 RESULTS AND DISCUSSION

Table 3 shows a comparison between literature data and model predictions (Equations 30-37) indicating that the predicted data agree reasonably well with deviations ranging from -2.2 to 8.8 percent from literature data. The predictions of synthesis gas which is the major advantage of this process matches the literature data very closely with a percentage deviation of -0.2%.

Table 3: Comparison of Model Predictions with Literature Data.

Component	Plant Data	Model Prediction	% Deviation
Syn gas (CO and H_2)	0.05	0.0499	-0.2
CO_2	0.065	0.0713	8.8
CH_4	0.087	0.089	2.2

$$\%\ Deviation = \frac{Model\ Prediction - Plant\ Data}{Model\ Prediction}$$

Figure 2 shows the variation of the yields of products with the mass fraction of the reactant (coal). The results across the bed height, while the yield of synthetic gas (CO and H_2), CO_2, and CH_4 increased throughout the catalyst height of the reactor.

The mass fraction of species A decreased from 0.59 to 0.39, while the yields of B, C, and D increased from 0 to 0.499, 0.0713, and 0.089% respectively, along the catalyst bed height of the reactor. These increase in species B, C, and D were as a result of the depletion of species A.

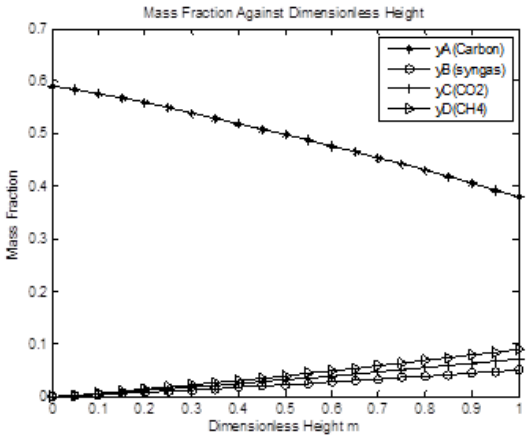

Figure 2: The variation in mass fraction of each component along the reactor dimensionless height.

3.1 Sensitivity Analysis

A sensitivity analysis was performed to determine the effects of superficial gas velocity, bubble diameter, reaction temperature and total pressure on the yield of products.

3.1.1 Effect of Superficial Gas Velocity

From Figure 3, the decrease in the yield of B, C, and D is attributed to low residence time of the coal (carbon) at high superficial velocity and low conversion of A due to channelling and by-passing effect inherent in fluidized bed at higher superficial velocity (Carberry, 1976). At lower superficial velocity the feed spends a longer time in the fluidized bed. So, the mass fraction of A increased as the superficial velocity increased but the mass fraction of species B, C, and D decreased as the superficial gas velocity increased with the mass fraction of D decreasing the most.

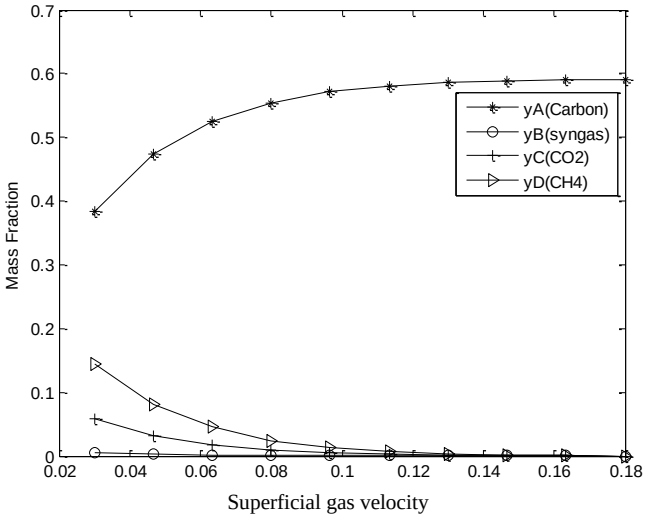

Figure 3: Superficial gas velocity variation with mass fractions of each component.

3.1.2 Effect of Bubble Diameter

The influence of bubble diameter is a very important factor that affects the mass fraction of each component. The bubble diameter profile is shown in Figure 4. From Figure 4, the decrease in yield of B, C, and D can be attributed to slugging effect and the fact that the bubble size causes the bubble to move upward in a piston-like manner, then disintegrates and rains down thereby creating a local space velocity different from the overall space velocity (Cheremisionff and Cheremisionff, 1984).

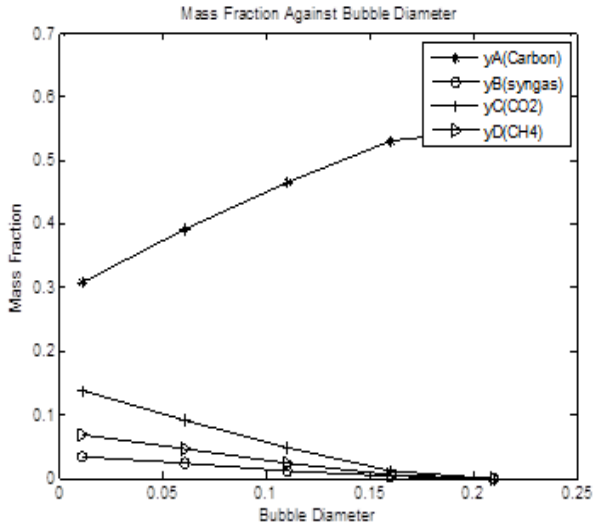

Figure 4: Bubble diameter variations with mass fraction of each component.

Thus, the mass fraction of A increases as the bubble diameter increases along the height of the reactor.

3.1.3 Effect of Temperature

Temperature is a very important parameter in coal gasification. Most times, the rate of conversion is governed by the temperature of the reactor. The temperature profile is shown in Figure 5.

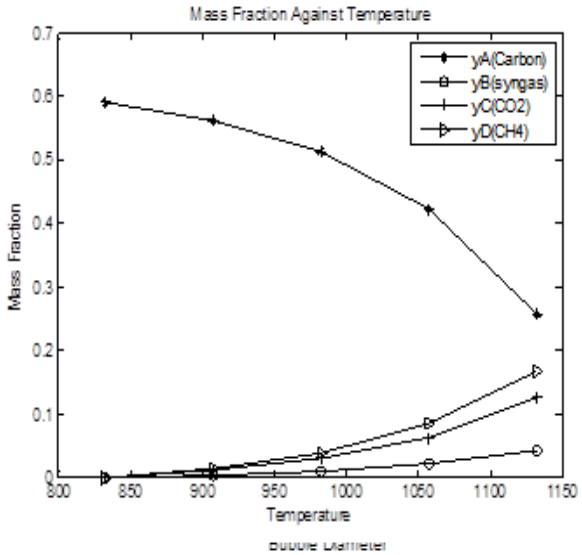

Figure 5: Temperature variations with mass fraction of each component.

From Figure 5, the mass fraction of species A decreased as the temperature increased because the temperature in the bubble phase increased from the distributor to the top of the bed, leading to increase in the mass transfer and the rate of combustion reactions. Also, from Figure 5, the mass fraction of B, C, and D increased as the temperature increased along the height of the reactor in accordance with Arrhenius rate law.

3.1.4: Effect of Pressure

The effect of the total pressure on the performance of the fluidized bed coal gasification reactor is shown in Figure 6. From Figure 6, the mass fraction of A decreased as the pressure increased while the yields of B, C, and D increases as the pressure increased along the height of the reactor in accordance with Raoult's law.

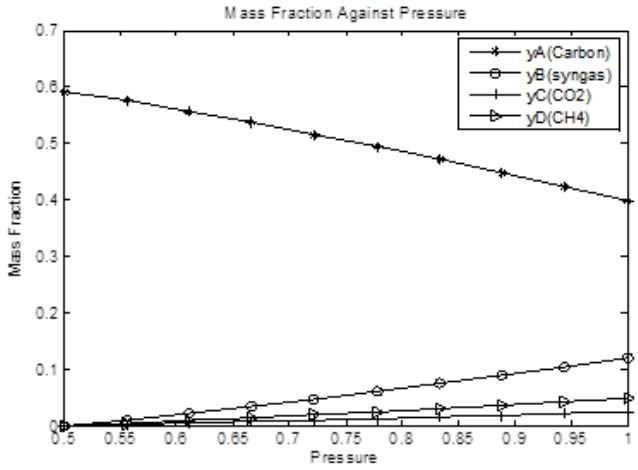

Figure 6: Pressure variations with mass fraction of each component

4.0 CONCLUSIONS

A mathematical model, incorporating the dominant mechanistic features to describe the gasification of coal in a fluidized-bed reactor has been developed. The models do not include the Initial coal devolatlzation because reactions were assumed to proceed almost instantaneously which includes only the secondary reactions. The kinetic parameters were obtained from literature. The sets of ordinary differential equations evaluated numerically using Runge-Kutta algorithm adapted in Matlab ODE45 solver. The comparison of the model predictions with literature data showed reasonable agreement especially the yield of synthesis gas which is the interest of the present analysis. Simulation results depicts that reaction temperature, pressure, bubble diameter of various components, and superficial velocity of coal, are major variables that affect the performance of the coal gasification fluidized bed reactor. To optimize the yields of the process, the temperature and pressure must be high, bubble diameter and superficial velocity must be maintained low.

REFERENCES

Alexeyev A.D. (2010). *Physics of coal and mining processes. Kiev: Naukova dumka*, 423.

Carberry, J. J. (1976). *"Chemical and Catalytic Reaction Engineering", McGraw Hill Books Co., New York, P: 556 – 557.*

Cherenisnoff, N. P. and Cherenisnoff, P.N (1984) "Hydrodynamics of Gas – Solid Fluidization", Guff publishing company Book Division, Houston, P: 138 – 164.

Davidson, J.F. and D. Harrison, (1963). *"Fluidized Particles", Cambridge University Press, New York.*

Dagde, K. K. and Puyate, Y. T., (2012) "Modelling Catalyst Regeneration in an Industrial FCC Unit", *American Journal of Scientific and Industrial Research*, 4 (3): 294 – 305.

Debashis Neogi, (1981). "Coal gasification in an experimental fluidized – bed reactor", *Indian Institute of technology, Ktoragpur, India.*

Falyushin P.L., Dudarchik V.M., Krayko V.M., Anufriyeva E.V., Smolyachkova E.A. (2010). Temperature Resistance of Brown Coal of Lelchytsy Deposit// *Prirodopolzovanie. 21, 305-311.*

Gordon,A.L.; Amundson,N.R., (1976). "Modelling of Fluidized Bed Reactors-IV: Combustion of Carbon Particles", *Chemical Engineering Science, 31, (12), 1163-1178.*

Gulmaliyev A.M., Golovin G.S., Gladum T.G. (2003). *Theoretical Foundations of Coal Chemistry. M.: Publishing House of Moscow State Mining University, 556.*

Howard,J.B.; Williams,G.C.; Fine,D.H., (1972). "Kinetics of Carbon Monoxide Oxidation in Postflame Gases", *14th Symposium (International) on Combustion, Pittsburgh, Pennsylvania, Aug. 20-25, 975-986.*

Kunni, D. and Levenspiel, O., (1991). *"Fludization Engineering, 2nd edition, Butterworth – Heinment, Boston*.

Kunil, D. and 0. Levenspiel, (1969). *"Fluidization Engineering", Chapter 4, Wiley, New York.*

Mehdi Mehrpooya, Cyrus Rahbari and S.M. Ali Moosavian (2017). Introducing a Hybrid Multi-Generation Fuel Cell System, Hydrogen Production and Cryogenic CO_2 Capturing Process, *Chemical Engineering and Processing: Process Intensification, 120, 134*.

Mori, S. and C.Y. Wen, (1975). "Estimation of Bubble Diameter in Gaseous Fluidized Beds," *AIChE Journal*, 2, 109-115.

Mustafa Ozer, Omar M. Basha, Gary Stiegel and Badie Morsi (2017). Effect of Coal Nature on the Gasification Process, *Integrated Combined Cycle (IGCC) Technologies. 257-304.*

National Bureau of Statistics (NBS), 2016.

Rajan,R., and Wen,C.Y., (1980). "A Comprehensive Model for Fluidized Bed Coal Combustors", *AIChE Journal*, 26(4), 642-655.

Shevkoplyas V.N. (2007). Calculation of Basic Kinetic Parameters of Solid Fuels, according to the Derivatographic Analysis // *Issues of Chemistry and Chemical Technology. 2, 179-183*.

Yoon, H., Wei J., and Denn, M.M. (1977). "Modeling and Analysis of Moving Bed Coal Gasifiers," AF-590, Volume 1, Technical Planning Study 76-653, Research Project 986-1, Final Report, Nov.

Yuncai Song, Jie-Feng, Yalong Jia, Wenying Li and Yitian Fang (2014). Influence of Ash Agglomerating Fluidized Bed Reactor Scale-up on Coal Gasification Characteristics. *AlChE Journal*, 60(5), 1821-1829.

MODELLING THE EFFECT OF TEMPERATURE ON DRYING MECHANISM OF CATFISH CRACKER

[*]Adeyi, A. J. [1], Adeyi, O. [2], Oke, E.O [3]. , Salaudeen, M. [4] and Ezekiel M.O [4]

[1]Mechanical Engineering Department, Ladoke Akintola University of Technology Ogbomoso, Oyo-State, Nigeria
[2]Chemical Engineering Department, Landmark University, Omu Aran, Kwara State, Nigeria
[3]Chemical Engineering Department, Micheal Okpara University of Agriculture, Umudike, AbiaState, Nigeria
[4]Nigerian Institute for Oceanography and Marine Research, Victoria Island, Lagos Nigeria
*Corresponding Author e-mail:adeyi.abiola@yahoo.com

ABSTRACT

The drying characteristics of 2 mm slices of formulated catfish cracker were investigated at 40, 50 and 60 °C and at a fixed air velocity of 1.5 m/s using a convective oven dryer. The samples were dried up to equilibrium moisture content. It was apparent from the results that the drying time reduced as the drying temperature increased. The experimental drying data of the formulated fish cracker were fitted to three semi-empirical thin layer drying models: Page's, Henderson and Pabis and Logarithmic. Statistical parameters of R^2, X^2 and RMSE were used to determine the suitability and for identification of best performing model for describing the drying kinetics of formulated catfish cracker slices. The Logarithmic model gave the best prediction when compared with other tested models. From the results obtained, two different falling rates periods were observed, and the effective moisture diffusivity ($Deff$) values were found to range between 2.26495 E-08 - 4.49344E-08 m^2/s and 4.21387E-09 - 8.7924 E-09 m^2/s for the first and second falling rate periods respectively. Increasing drying temperature also caused an increase in $Deff$ values. The activation energies were also found as 29.63 kJ/mole and 31.82 kJ/mole for first and second falling rate periods respectively. The Logarithmic model can, therefore, be employed to understand the mechanism of catfish cracker drying, the design of the drying process, and the design of drying equipment, prediction and control of the process.

***Keyword**: Catfish, Cracker, Diffusivity, Activation Energy, Thin-layer modelling*

1. INTRODUCTION:

Fish is a high-protein, low-calorie food and an important source of omega-3 fatty acids and minerals, such as calcium and phosphorus (Okereke and Onunkwo, 2014). Fish is the most easily accessible animal protein especially in the developing countries. Nowadays, fish cracker, a product of fish utilization process, is gaining a widespread acceptability in Nigeria as an entertaining ready-to-eat snack. The snack is easy to make because it is sold as an intermediate food product leaving only the deep frying aspect to the consumer to perform. Fish cracker, also represents a route to which stunted fishes with low economic values have an economic benefit to the fish farmer (aqua culturist). Although fish cracker can be made in different ways, they are usually produced by mixing flesh of a specific fish, food starch, monosodium glutamate (MSG) and other spices. Other ingredients can be added to enhance better acceptability and improved properties; this is dependent on the producer (Mbaeyi-Nwaoha and Itoye, 2016). The ingredients after mixing are steamed/boiled, refrigerated, sliced into small piece and then dried first before frying (Mbaeyi-Nwaoha and Itoye, 2016; Nurul *et al.,* 2009). Drying of the cracker is necessary to reduce its moisture content for preservation, storage, marketing and post processing (deep frying). Most commercial and locally formulated (homemade) crackers conform to 1-3 mm slices (Mbaeyi-Nwaoha and Itoye, 2016; Netto *et al.,* 2014) perhaps to enhance fast drying of the product. In Nigeria, because of the availability of sun energy, drying of formulated fish cracker is usually done through sun drying which is not too predictable and constitutes a limitation in improving the fish cracker production from small scale to large scale production. The importance of the choice of drying route and optimization is, therefore, significant in fish cracker processing and development. In this sense, the understanding of products' drying kinetics, mathematical modelling, and evaluation of related thermodynamic parameters will improve the product quality and assists in equipment design.

Drying is a dual process that involves the internal penetration of the sample by heat energy and outward diffusion of moisture from the sample. Control of drying process in food or agricultural product is necessary to avoid unwanted product and destruction of

micro nutrients. Drying is an energy intensive unit operation and long drying periods tend to increase the energy requirements for the production of the dry product (Agarry *et al.,* 2013). Hence process optimization is necessary for the economic drying of specific products. Drying in Africa is usually carried out through natural sun drying. However, because of its unhygienic implications, the use of aided technologies is rapidly becoming acceptable, especially with emerging strict laws on food processing from the government agencies. Drying of materials is a complicated process involving simultaneous heat and mass transfer (Okereke and Onunkwo, 2014). Generally, the drying process takes place in two stages; the first stage happens at the surface of the drying material at a constant drying rate and is similar to the vaporization of water into the ambient. The second stage drying process takes place with decreasing drying rate (Okereke and Onunkwo, 2014) as heat energy passes from the surface to the core of food.

Mathematical modelling and simulation of drying curves under different conditions are important to obtain a better control of drying unit operation and an overall improvement of the quality of the final product (Hazbavi and Samadi, 2013). The mathematical modelling allows the food researchers to choose the most suitable operating conditions either to describe the drying equipment or minimize the drying times for the final product specifications (Gamll, 2011). The thin-layer drying models can be categorised as theoretical, semi-theoretical and empirical models. The semi-theoretical model based on the theory and the drying kinetics experimental, is derived from the simplification of Fick's second law of diffusion or modification of the simplified model, which has been widely used to describe the drying characteristics (Guan *et al.,* 2013). Drying should also progress in a regular manner because spontaneous drying may lead to case-hardening of the sample. Page model had been investigated for studying the drying characteristics of some fruit and vegetables such as pepper (Akpinar *et al.,* 2003), apricot (Mirzaee *et al.,* 2010), purslane (Demirhan and Özbek, 2010) and mango fruits (Kabiru *et al.,* 2013). Other empirical models used for fitting kinetic data of agricultural products include Midilli model (Mirzaee *et al.,* 2010), Wand and Singh model (Hamdami *et al.,* 2006; Mirzaee *et al.,* 2010), Logarithm, Henderson and Pabis, Tow term and Newton models (Mirzaee *et al.,* 2010). All the empirical models consist of drying rate and equation constants which must be obtained from the fitting of the experimental kinetic data to the models. The statistical parameters such as coefficient of determination (R^2), chi-square (χ^2) and root mean error (RMSE) are frequently used for determining the suitability of each model in describing the experimental kinetic data.

The moisture diffusivity is an important parameter in material characterization, and the knowledge of moisture diffusivity enables the proper choice of drying and or process conditions for specific foods. Molecular diffusion is the main water transport mechanism in dehydration and to predict the water transfer in food materials, diffusion models based on Fick's second law are frequently used (Okereke and Onunkwo, 2014). Basically, in the application of Fick's law to evaluate moisture diffusivity of infinite slab of thin layer, assumptions such as moisture migration being by diffusion, one-dimensional moisture movement, uniform initial moisture distribution, negligible shrinkage, constant moisture diffusivity, and negligible external resistance to heat and mass transfer are usually made. Effective moisture diffusivity describes all possible mechanisms of moisture movement within the foods, such as liquid diffusion, vapour diffusion, surface diffusion, capillary flow and hydrodynamic flow (Okereke and Onunkwo, 2014). It is therefore expected that moisture diffusion will increase with moisture content especially when the sample is fresh, progressively decrease and later remain constant. Other frequently studied products' thermal property frequently measured is activation energy and this is because of its usefulness in ideal dryer design (Aghbashlo *et al.,* 2008).

The objectives of this study are as follows. For catfish cracker dried in a conventional oven, (1) Obtaining the drying kinetic data for mass/moisture transfer during the convective oven drying process of catfish cracker, (2) determination of the thin layer drying model that best fits the drying data, (3) estimation of the effective diffusivities at drying temperatures and (4) estimation of the activation energy of the drying operation. The study aims to understand the drying behaviour of catfish cracker for process design, equipment design, and optimization.

2.0 MATERIALS AND METHODS

2.1 Materials

Fresh catfish of about 500 g was purchased from a local food market in Lagos, Nigeria. Other ingredients such as corn starch, pepper, salt and magi were purchased from a supermarket in Lagos. The dryer used for the experiment is a convective oven dryer equipped with

fan, temperature regulator and timer. The dryer is 1m by 2 m rectangular shaped drying chamber with relatively high capacity loading. The dryer was also equipped with two strategically positioned heating elements (1.5 kW) at the top and bottom for total heat coverage of the chamber. The door of the dryer was made of transparent material for easy visual monitoring of the product. A primerie model weighing balance with accuracy of 0.01 g was used for the experiment. Knife was used for fish deboning, degutting and filleting. Pestle and mortal was used for mashing of the deboned fish flesh. Steaming pan and refrigerator were also used for the production process.

2.2 Methods

2.2.1 Preparation of Catfish Cracker Sample

The recipe and method of Okereke and Onunkwo (2014) were adopted for the preparation of catfish cracker. The pre-fish processing was done according to the method of Okereke and Onunkwo (2014). In brief, the catfish was washed, gutted, filleted and de-headed manually using a sharp knife. The flesh was further washed with running tap water. 35 g of filleted and deboned catfish flesh was mashed using the attrition pepper grinder and was mixed with 25 g of corn starch, a cube of magi, 0.01 g of pepper and 0.05 g of salt. The mixture was rolled out into a cylindrical shape using a tin mould and then steamed for 45 minutes. After, samples were kept in the refrigerator at -4 ^{O}C before the drying experiments. Multiple 5 g of thinly sliced fish cracker (2 mm) samples were made and selected for each batch of the experiment. The experiment was designed to be a one at a time experiment through which variable inputs temperature (40, 50 and 60 ^{O}C), air velocity of 1.5 m/s and constant thickness of 2 mm (based on local producers' standard practices) were used for the investigation. Moisture loss output/responses were taken at constant intervals in agreement with previous studies.

2.2.2 Determination of Initial Moisture Content

The initial moisture content of the fish cracker was determined by using oven drying method (AOAC, 1984). About 5 g of samples were oven dried at 70 ^{O}C for 12 h. The initial moisture content was established on a dry basis (d.b.). The experiments were conducted in triplicates and the initial moisture content of the fish cracker was reported as the average of three experimental trials. The relationship below (Equation 1) was used to establish the initial moisture content.

$$Initial\ Moisture\ Content\ (db.) = \frac{Wet\ Weight - Dried\ Weight}{Dried\ Weight} X\ 100\ (\%) \quad (1)$$

2.2.3 Determination of Moisture Loss and Associated Parameter

The samples were defrosted by allowing the fish cracker slices to reach the room temperature (25^{o}C) before drying experiments proceeded. Hazbavi and Samadi (2013) method was used for the drying experiment, where the change in moisture was recorded at an interval of time. The effect of temperature variation was studied as a function of time at an air velocity of 1.5 m/s. The selected temperatures were 40, 50 and 60 ^{O}C. However, before the drying experiment, the dryer was allowed to work at the set experimental temperature for 30 min such that the temperature throughout the oven chamber was uniform. At each set temperature, the 5 g of 2 mm thinly sliced sample is placed on a mesh holder and inserted in the oven chamber. The moisture loss was recorded at 5 min time intervals during the experiment with an accuracy of 0.01 g. The investigation continues until there was no difference between four successive recordings (equilibrium). The drying process was carried out to final moisture content of about 2 - 2.3 % from an initial moisture content of about 151.5 % (db.).

Furthermore, the moisture loss values were converted to a suitable format for use in kinetics modelling. Specifically, instantaneous moisture losses were converted to moisture ratio using the established relationship and assumptions. The relationship is as in Equation 2

$$MR = \frac{Mt - Me}{Mo - Me} \quad (2)$$

from the relation, MR represent moisture ratio, M_t represents the moisture content of the product after drying time t, M_e represents the stable or equilibrium moisture content of the product and M_0 represents the initial moisture content of the sample. It can be easily seen that the equation will naturally reduce to the ratio of present moisture content to original moisture content as in Equation 3.

$$MR = \frac{Mt}{Mo} \quad (3)$$

Drying rate was also determined to understand the rate at which the material losses moisture over time. The mathematical relationship used for calculating the drying rate is expressed in Equation (4).

$$DR = \frac{Xt + \Delta t + Xt}{\Delta t} \quad (4)$$

Where $Xt + \Delta t$, is the moisture content at a future time, Xt is the moisture content at the present time and Δt is the change in time.

2.2.4 Fitting of Empirical Models

Three semi-empirical models were fitted to the experimental moisture ratio data to better understand the mechanism of drying of the developed catfish cracker. The used models were Page model (Equation 5), Henderson and Pabis model (Equation 6) and Logarithmic model (Equation 7).

$$MR = Exp.(-K.t^n) \quad (5)$$

$$MR = a.Exp.(-K.t) \quad (6)$$

$$MR = b.Exp(-K.t) + C \quad (7)$$

where n and b are exponent specific to each model: a, K and C are model constants and t is the drying time

Curve fittings for the chosen semi empirical models were performed using the solver function in Microsoft Excel adopting the generalized reduced gradient (GRG2) nonlinear optimization code to determine the drying parameters. The suitability of each model was judged using the statistical parameter values of coefficient of determination (R^2) (Equation 8), root mean square error (RMSE) (Equation 9) and reduced chi square (X^2) (Equation 10). A high value of coefficient of determination coupled with low values of root mean square and chi-square signifies a better model.

$$R^2 = 1 - \left(\sum_{i=1}^{N} \frac{(\text{MRpre,i} - \text{MRexp,i})^2}{(\text{MRpre,i} - \text{AverageMRexp})^2}\right) \quad (8)$$

$$X^2 = \frac{\sum_{i=1}^{n}(\text{MRexp,i} - \text{MRpre,i})^2}{N-Z} \quad (9)$$

$$RMSE = \sqrt{\frac{\sum_{i=1}^{n}(\text{MRexp,i} - \text{MRpre,i})^2}{N}} \quad (10)$$

where, N is the number of observations, Z is the number of constants, MRexp and MRpre are the experimental and model predicted moisture ratios, respectively.

2.2.5 Determination of Coefficient of Diffusivity and Activation Energy

Fick's second law of diffusion was used to calculate the moisture diffusivity of catfish cracker. The analytical solution of second Fick's law given by Rayaguru and Routray (2011) is represented in Equation 11 as:

$$MR = \frac{8}{\pi^2}\sum_{n=0}^{\infty}\frac{1}{2n+1}\exp\left[-(2n+1)^2\frac{\pi^2}{4L^2}Deff * t\right] \quad (11)$$

where MR is the moisture ratio, $Deff$ is the effective moisture diffusivity in m^2s^{-1}; L is the half thickness of the product in meter (m) and t is time in second (s). For long drying period, the Equation (11) can be simplified to Equation (12) as follows:

$$ln\,(MR) = ln\,(\tfrac{8}{\pi^2}) - Deff\,(\tfrac{\pi}{2L})\,\text{^2} * t \quad (12)$$

The effective moisture diffusivity was determined using Fick's law during the falling rate period. Briefly, the effective diffusivity was determined from the slope (Equation 13) of a straight line obtained by plotting natural logarithm of experimental drying data ($ln(MR)$) against time (t).

$$Slope = \frac{\pi^2\,Deff}{4L^2} \quad (13)$$

The relation between temperature and the effective moisture diffusivity can be described by an Arrhenius-type relationship in Equation 14 (Guan *et al*., 2013)

$$Deff = D_o\,Exp\,(\tfrac{E_a}{RT_a}) \quad (14)$$

where D_o is the pre-exponential factor for Arrhenius equation (m^2/s) and E_a is the activation energy for moisture diffusion (kJ/mole), R is the gas constant (kJ/mole.K) and T_a is the absolute temperature in kelvin (K). The activation energy was obtained from the slope (Equation 15) of the straight line by plotting $ln(Deff)$ versus the reciprocal of the temperature ($1/T_a$)

$$Slope = -\frac{Ea}{R} \quad (15)$$

3 RESULT AND DISCUSSION

3.1 Effect of Drying Temperature and Time on Catfish Cracker Moisture Ratio

Figure 1 shows the effect of drying temperature and time on the moisture ratio (MR) of the formulated catfish cracker at an air velocity of 1.5 m/s. As expected, the MR of the formulated catfish cracker decreased with increased drying time. This was although pronounced at the beginning of the experiment when moisture was being rapidly removed from the surface of freshly prepared cracker due to the availability free moisture which was rapidly removed and became less obvious as the drying experiment progressed. The decreased moisture removal at the latter end of the experiment may be as a result of decreased moisture content or case hardening of the catfish cracker which prevented the heat from entering the core of the product. The same observation was reported for the drying behaviour of some agricultural products such as onion slices (Revaskar *et al.*, 2014), kiwi fruit slices (Shahi *et al.*, 2014), *Pandanus amaryllifolius* leaves (Rayaguru and

Routray, 2011), Okra (Afolabi and Agarry, 2014) and Fish fillets (Ikrang *et al.*, 2014).

Drying temperature also had a great effect on the drying behaviour of the cracker. The relative positions of the drying profiles showed that the MR decreased with increased temperature due to increased drying rate. This is in accordance with the report of Nag and Dash (2016) on mathematical modeling of thin layer drying kinetics and moisture diffusivity study of elephant apple. For instance, when the drying temperature was increased from 40 to 60 ^{O}C, the drying time reduced by 49 % which implied a faster moisture removal at the higher temperature. However, too high a temperature will lead to case hardening phenomenon, denaturing and even burning.

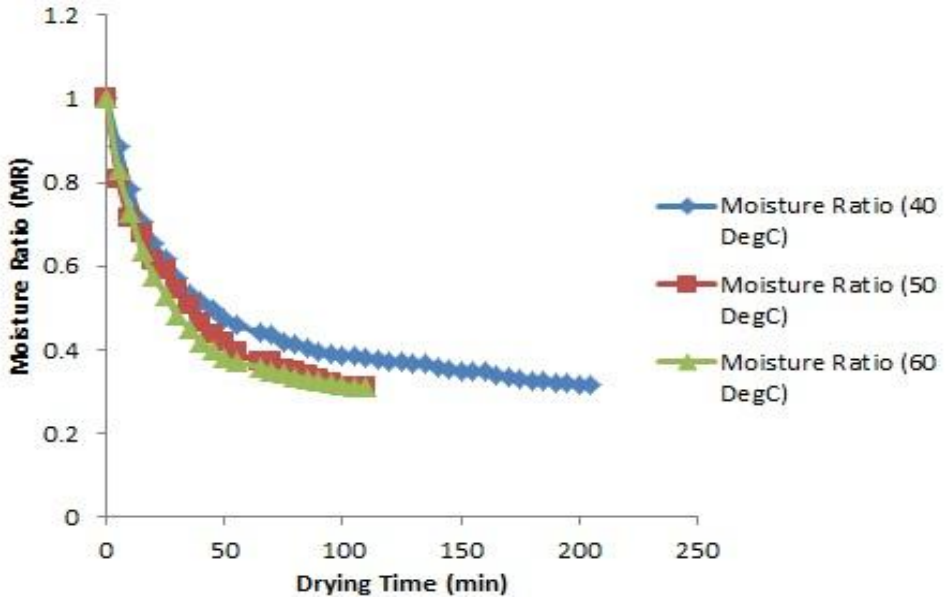

Figure 1: Graph of Moisture Ratio versus Drying Time for the drying of fish cracker

Figure 2 shows the graph of drying rate against drying time. The drying rate increased rapidly at the onset of drying and reached the peak in 5 min before it later fell. This indicated that 5 min was enough to remove all the free moisture on the surface of catfish cracker before the further inward-to-outer moisture removal began. The drying rate however, continued to reduce afterwards and this may be due to the slow internal outward moisture movement which implied that catfish cracker may not be too porous for easy movement of moisture. The drying rate clearly showed its dependency on temperature and it increased as the temperature increased.

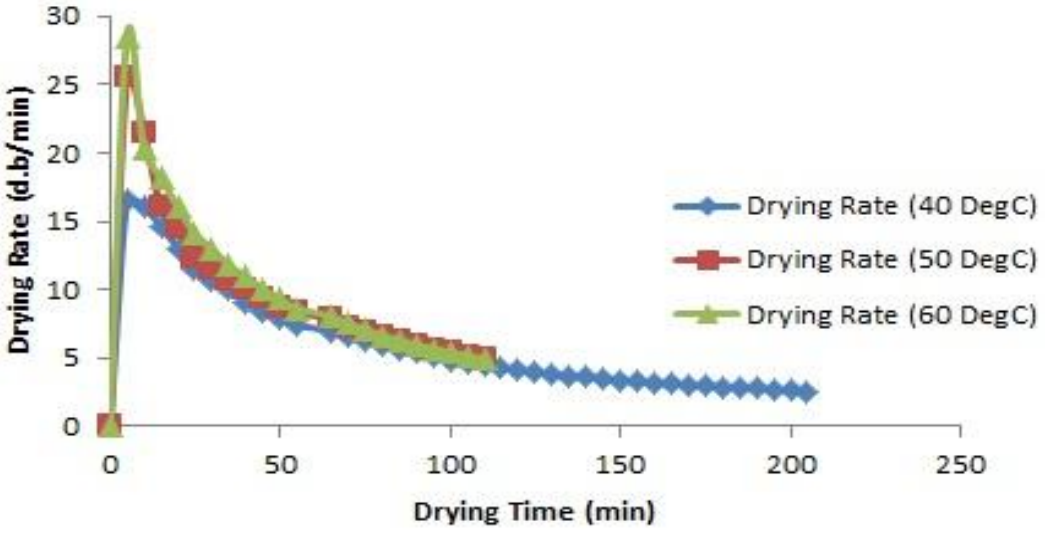

Figure 2: Graph of Drying Rate versus Drying Time for the drying of fish cracker

3.2 Modelling of the Drying Kinetics

In order to describe the effect of temperature on the kinetics of the formulated fish cracker, three semi-empirical thin-layer drying kinetic models were considered as detailed in Equations 5 – 7. Among the examined models, Logarithm model was judged the most appropriate for the description of experimental kinetic data at all temperatures with highest R^2 values, and lowest χ^2 and RMSE values. The estimated model parameters at different drying conditions are as illustrated in Table 1.

Table 1: Comparison of different models with parameters for drying of formulated catfish cracker

Model Name	Temperature (^OC)	Constants	R^2	χ^2	$RMSE$
Page	40	**k**= 0.1825 **n** = 0.528	0.9413	0.00213	0.04503
Henderson and Pabis	40	**a** = 0.7661 **k** = 0.029	0.7901	0.00547	0.07213
Logarithmic	40	**b** = 0.7352 **k** = 0.1578 **c** = 0.3412	0.9909	0.00024	0.01501
Page	50	**k** = 0.1437 **n** = 0.722	0.9599	0.00146	0.03646
Henderson and Pabis	50	**a** = 0.8951 **k** = 0.061	0.9202	0.00291	0.05148
Logarithmic	50	**b** = 0.7775 **k** = 0.1744 **c** = 0.2973	0.9903	0.00037	0.01797
Page	60	**k** = 0.1672 n = 0.684	0.9265	0.00271	0.04970
Henderson and Pabis	60	**a** = 0.8766 **k** = 0.064	0.8662	0.00500	0.06745
Logarithmic	60	**b** =0.8454 **k** = 0.233 **c** = 0.3137	0.9986	0.00005	0.00685

Observations from Table 1 indicate that the parameters of Logarithm model increased as temperature increased. The implication is that with the increase in temperature, the drying curve becomes steeper meaning an increase in drying rate. From the graphs in Figure 3, it is qualitatively obvious that the Logarithmic model outperformed the other models that were used in the modelling of the experimental data.

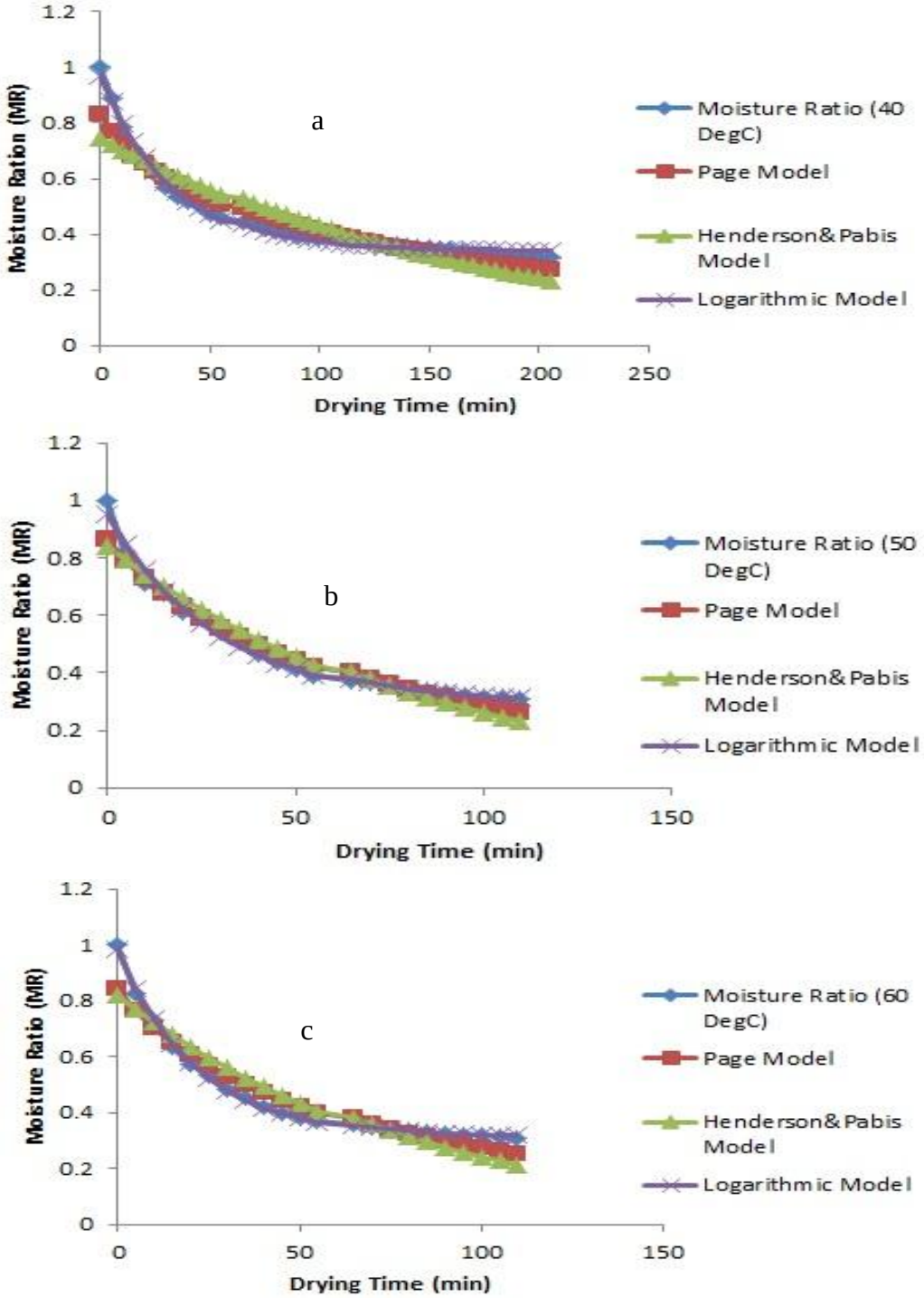

Figure 3: Prediction of experimental moisture ratio as a function of drying time using thin layer semi empirical drying models at (a) 40 ^{O}C (b) 50 ^{O}C (c) 60 ^{O}C.

3.3 Effect of Temperature on the Coefficient of Moisture Diffusion

The diffusivity was evaluated through linear regression from the slope of the ln (MR) versus time relationship as depicted in Figure 4. From Figure 4, it is apparent that the drying of fish cracker at all the three temperatures occurred in two distinct falling rate periods. A similar observation was reported by Motevali *et al.* (2012) in the thin-layer modelling of Jujube. Therefore, for a specified constant temperature, two different diffusivities must be established for the two observed falling rates periods accordingly.

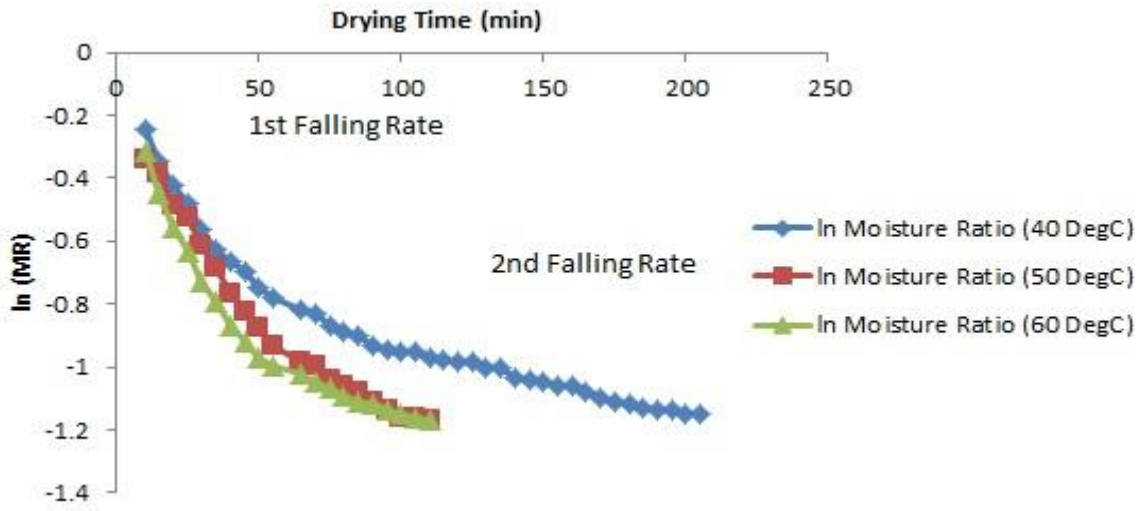

Figure 4: Plot of ln (MR) against Time

The effective moisture content values for various drying temperatures were determined and presented in Table 2. The range of moisture diffusivity values for the first falling rate period was from 2.26495E-08 to 4.49344E-08 m^2/s and that for the second falling rate period varied from 4.21387E-09 to 8.7924E-09 m^2/s. Observations indicated that the moisture diffusivity of the first and second falling rate periods increased with increased temperature. A similar range of moisture diffusivity was reported for agricultural products. Mariem *et al.* (2014); reported a range 10^{-9} and 10^{-8} m^2/s for tomato samples, while Guan *et al*. (2003) reported a range of 10^{-8} - 10^{-12} m^2/s for food materials.

Table 2: Diffusivity values at different temperatures and rate periods

	Diffusivity (m^2/s)	
Temperature (^OC)	**1st Falling Rate Period**	**2nd Falling Rate Period**
40	2.26495E-08	4.21387E-09
50	3.051E-08	5.8751E-09
60	4.49344E-08	8.7924E-09

Equations 16 and 17 are the regressed relationships between effective moisture diffusivity and drying temperatures for the first and second falling rates respectively.

$Deff$ = 3E-11T^2 - 2E-09T + 6E-08 first falling rate (16)

$R^2 = 1$

$Deff$ = 6E-12T^2 - 4E-10T + 1E-08 Second falling rate (17)

$R^2 = 1$

3.4 Effect of Temperature on the Activation Energy

The activation energy (Ea) was determined from the slope of the linearized Arrhenius equation. A graph of ln ($Deff$) versus 1/ T was made and Ea was evaluated according to the method of Mariem and Mabrouk (2014). Figures 5 showed the relationship between ln($Deff$) versus 1/ T for the first and second falling rate periods respectively.

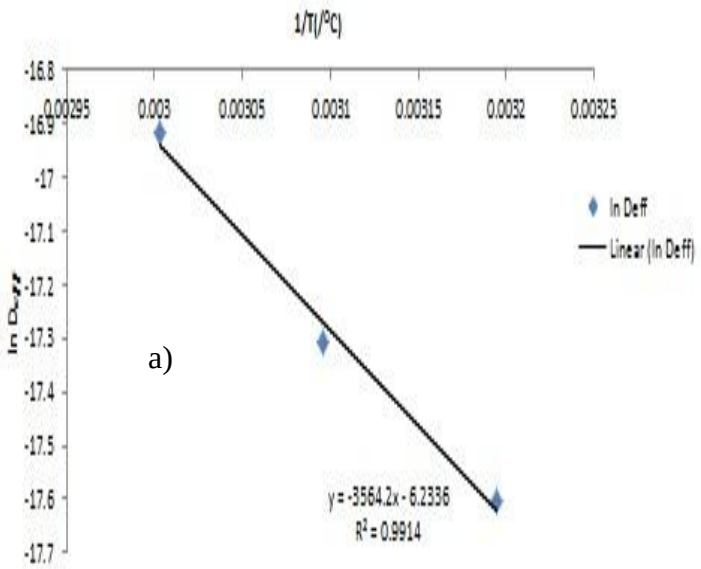

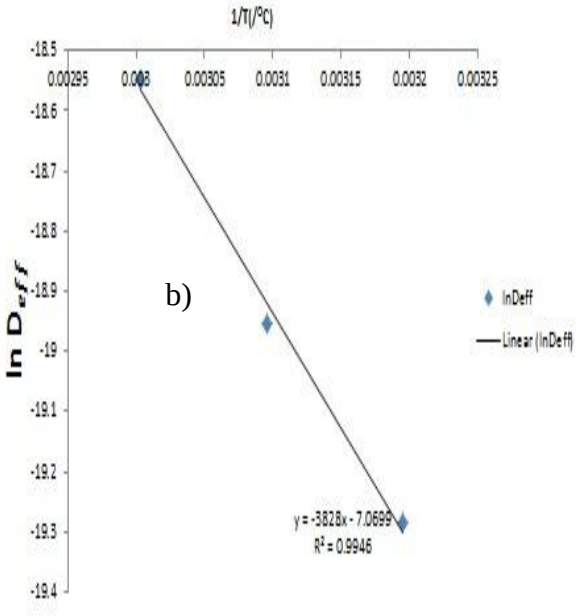

Figure 5:Graph of ln ($Deff$) versus inverse of absolute temperature for (a) first falling rate period (b) second falling rate period

Ea for the first and second falling rate periods as previously shown in Figure 4 was determined to be 29.63 kJ/mol and 31.82 kJ/mol respectively. The results were in close agreement with the values of 24.94 kJ/mol and 28.40 kJ/mole reported for tomato slices and green peas respectively (Mariem *et al.*, 2014).

4 CONCLUSION

The thin layer drying of formulated fish crackers was investigated. The experimental drying data were fitted to some semi-empirical thin layer models. Thermodynamic parameters such effective moisture diffusivity and activation energy were also determined. The moisture ratio of the formulated catfish cracker decreased with increased drying time and temperature. Drying proceeded in falling rate periods only till equilibrium was reached. The Logarithmic equation had the highest R^2 and lowest chi-square and RMSE values and was the most suitable thin layer model for describing the drying kinetics of the formulated catfish cracker. The effective moisture diffusivities and the activation energies were found to be in the range 2.26495E-08 - 8.7924E-09 m^2/s and 29.63 - 31.82 kJ/mol for the first and second falling rate periods respectively. The results obtained can be well used for analysis, design, understanding, and prediction of mechanisms involved in the drying of catfish cracker.

Acknowledgement

The authors appreciate Nigerian Institute for Oceanography and Marine Research for the provision of Laboratory facilities for the completion of this project.

Nomenclature

a, b, c	Model coefficient
d.b.	Dry basis
SE	Standard error
RMSE	Root mean square error
SST	Sum of square
k	Drying rate constant (min^{-1})
M	Moisture content (% d.b.)
MR	Moisture ratio
M_0	Initial moisture content (% d.b.)
M_e	Equilibrium moisture content (% d.b.)
$MR_{exp,i}$	ith Experimental moisture ratio
$MR_{pre,i}$	ith Predicted moisture ratio
n	Exponent
R^2	Coefficient of determination
t	Time (min)
D_{eff}	Effective diffusivity, m^2/s
D_0	Pre-exponential factor of Arrhenius equation, m^2/s
E_a	Activation energy, kJ/mol
k_0	Slope
R	Gas constant
L	Half slab thickness

REFERENCES

Afolabi, T. J., and Agarry, S. E. (2014). *Thin Layer Drying Kinetics and Modelling of Okra (Abelmoschus esculentus (L.) Moench) Slices under Natural and Forced Convective Air Drying. Food Science and Quality Management*, 28, 35-49.

Agarry, S.E., Ajani, A.O. and Aremu, M.O. (2013). *Thin Layer Drying Kinetics of Pineapple: Effect of Blanching Temperature – Time Combination. Nigerian Journal of Basic and Applied Science.*

Aghbashlo, M., and Samimi-Akhijahani, H. (2008). *Influence of Drying Conditions on the Effective Moisture Diffusivity, Energy of Activation and Energy Consumption During the Thin-Layer Drying of Berberis Fruit (Berberidaceae). Energy Conversion and Management*, 49(10), 2865-2871.

Akpinar, E. K., Bicer, Y., and Yildiz, C. (2003). *Thin Layer Drying of Red Pepper. Journal of food engineering*, 59(1), 99-104.

A.O.A.C. (1984). *Official Methods of Analysis of the Association of Official Analytical*
Chemist s' 14 th Ed. Published by the Association of Official Analytical Chemist s', Arlington, Virginia, 22209 USA.

Demirhan, E., and Özbek, B. (2010). *Drying Kinetics and Effective Moisture Diffusivity of Purslane undergoing Microwave Heat Treatment. Korean Journal of Chemical Engineering*, 27(5), 1377-1383.

Gamlı, Ö. F. (2011). *Effective Moisture Diffusivity and Drying Characteristics of Tomato Slices during Convectional Drying. GIDA-Journal of Food*, 36(4), 201-208.

Guan, Z., Wang, X., Li, M., and Jiang, X. (2013). *Mathematical Modelling on Hot Air Drying of Thin Layer Fresh Tilapia Fillets. Polish Journal of Food and Nutrition Sciences*, 63(1), 25-33.

Hazbavi, I., and Samadi, S. H. (2013). *Using of Semi-Empirical Models and Fick's Second Low for Mathematical Modeling of Mass Transfer in Thin Layer Drying of Carrot Slice. Global Journal of Science Frontier Research*, 13(4).

Hamdami, N., Sayyad, M., and Oladegaragoze, A. (2006). *Mathematical modelling of Thin Layer Drying Kinetics of Apples Slices. In 13th World Congress of Food Science and Technology* 2006 (pp. 324-324).

Kabiru, A. A., Joshua, A. A., and Raji, A. O. (2013). *Effect of Slice Thickness and Temperature on the Drying Kinetics of Mango (Mangifera indica). International Journal of Research and Review in Applied Sciences*, 15(1), 41-50.

Ikrang, E. G.,Okoko, J. U., Obot, M. S. and Akubuo,C. O (2014) *Modelling of Thin Layer Drying Kinetics of Salted Fish Fillets (Tilapia Zilli) in a Direct Passive Solar Dryer. IOSR Journal Of Environmental Science, Toxicology and Food Technology (IOSR-JESTFT)*, Volume 8, Issue 1, 18-24.

Mariem, S. B., and Mabrouk, S. B. (2014). *Drying Characteristics of Tomato Slices and Mathematical Modeling. International Journal of Energy Engineering*, 4(2A), 17-24.

Mirzaee, E., Rafiee, S., and Keyhani, A. (2010). *Evaluation and Selection of Thin-Layer Models for Drying Kinetics of Apricot (cv. NASIRY). Agricultural Engineering International: CIGR Journal*, 12(2), 111-116.

Motevali, A., Abbaszadeh, A, S. Minaei, S., Khoshtaghaza., M. H and Ghobadian, B. (2012). *Effective Moisture Diffusivity, Activation Energy and Energy Consumption in Thin-layer Drying of Jujube (Zizyphus jujube Mill). J. Agr. Sci. Tech.*

Mbaeyi-Nwaoha, I.E. and Itoje, C.R (2016) ***Quality Evaluation of Prawn Crackers Produced from Blends of Prawns and Cassava (Manihot esculenta), Pink and Orange Fleshed Sweet Potato (Ipomoea batatas (L) Lam) Starches. African Journal of Food Science and Technology.*** **Vol. 7(4) pp. 051-059.**

Nag, S., and Dash, K. K. (2016). *Mathematical Modelling of Thin Layer Drying Kinetics and Moisture Diffusivity Study of Elephant Apple*.

Netto, J. D. P. C., Oliveira Filho, P. R. C. D., Lapa-Guimarães, J., and Viegas, E. M. M. (2014). *Physicochemical and Sensory Characteristics of Snack made with Minced Nile tilapia. Food Science and Technology (Campinas)*, 34(3), 591-596.

Nurul, H., Boni, I., and Noryati, I. (2009). *The Effect of Different Ratios of Dory Fish to Tapioca Flour on the Linear Expansion, Oil Absorption, Colour and Hardness of Fish Crackers. International Food Research Journal*, 16, 159-165.

Okereke A.N and Onunkwo D.N, (2014). *Acceptance of Fish Crackers Produced From Tilapia and Catfish. IOSR Journal of Environmental Science, Toxicology and Food Technology.*

Revaskar, V. A., Pisalkar, P. S., Pathare, P. B., and Sharma, G. P. (2014). *Dehydration Kinetics of Onion Slices in Osmotic and Air Convective Drying Process. Research in Agricultural Engineering*, 60(3), 92-99.

Rayaguru, K. and Routray, W (2011) *Microwave Drying Kinetics and Quality Characteristics of Aromatic Pandanus amaryllifoliusleaves. International Food Research Journal* 18(3): 1035-1042

Shahi, M. M. N., Mokhtarian, M., and Entezar, A. (2014). *Optimization of Thin Layer Drying Kinetics of Kiwi Fruit Slices using Genetic Algorithm. Advances in Natural and Applied Sciences*, 8(11), 11-19.

PHYSICOCHEMICAL CHARACTERIZATION OF *DELONOX REGIA* OIL AND HETEROGENEOUS CATALYST SYNTHESIS FROM THE HUSK FOR BIODIESEL PRODUCTION USING RESPONSE SURFACE METHODOLOGY (RSM) DESIGN APPROACH

***Aransiola, E. F. [1], Omotayo, M. T. [1], Alabi-Babalola, O. D. [1] and Solomon, B. O.[1]**

[1]Department of Chemical Engineering, Biochemical Engineering Laboratory, Obafemi Awolowo University, Ile-Ife, Osun-State.

Corresponding Author; aransiolaef@gmail.com and +2347051487171

ABSTRACT

This study investigated the synthesis of heterogeneous catalyst using Delonix regia husk for biodiesel production from its seed oil. This was with a view to developing renewable fuel from cheap under-utilized raw material. The extracted Delonix regia seed oil (DRSO) was characterized for its physicochemical properties and fatty acid composition. The heterogeneous catalyst was synthesized via impregnation process. The husk and the synthesized catalyst were characterized for their morphology, elemental composition and functional groups. Two-step transesterification method was used to convert the oil into biodiesel. The effect of the catalyst on conversion of DRSO into biodiesel was carried out before optimization study. The KOH to carbonized char (CC) ratio at where the maximum biodiesel yield was attained was used for the optimization study. The kinematic viscosity and acid value of the oil were 51.22 m^2/S and 19.08 at 25^oC respectively. The optimum values were statistically predicted as methanol-oil ratio of 18:1, reaction time of 90 min, reaction temperature of 60^oC and KOH to CC ratio of 3:1 at a catalyst loading of 9% w/w with biodiesel yield of 88.06%.

From the results it can be concluded that Delonix regia could serve as a potential source of cheap raw material for heterogeneous catalyst synthesis for biodiesel production.

***Keywords**: Heterogeneous catalyst, Delonix regia husk, Delonix regia seed oil, Biodiesel, Transesterification, Response Surface Methodology.*

1. INTRODUCTION

The world's teeming population, industrialization and urbanization have led to a tremendous increase in energy utilization. This ever-increasing energy demand, gradual depletion of conventional energy reserves coupled with the negative environmental impacts associated with the exploitation, exploration and use of fossil fuel have rekindled researchers' interest in the area of renewable energy globally (Aransiola *et al.*, 2012). This quest for alternative energy sources can also be a significant tool for bio-economy diversification of developing countries.

Biofuel has been identified as one of the most promising sources of alternative to fossil fuel due to its environment-friendly properties like bio-degradability, renewability and ease of combustion. Researches in this aspect focus on two major fuels: bioethanol which could be made from crop grains, sugarcane, lignocellulosic wastes among others and biodiesel produced from algae, vegetable oils; and animal fats obtained from tallows (Bugaje, 2006; Bobboi *et al*., 2007).

Both edible and non-edible oils from oilseeds have been successfully utilized in the production of biodiesel. To date, edible oils such as soybean oil in the USA, rapeseed oil in Europe, and palm oil in southeastern Asia have been used to produce biodiesel (Guoqing and Katsuki, 2012). However, the growing human demand of edible oils does not encourage their use for biodiesel production. To deal with this concern of food versus fuel, there is need to identify more plant oils that are non-edible and under-utilized such as oil from *Delonix regia*.

Delonix regia also known as the Royal Poinciana or Flamboyant tree is a specie of flowering plant. According to traditional classification of medicine, it belongs to *Caesalpiniaceous* family but according to the phylogenetic classification, it belongs to *Fabaceae fa*mily (subfamily of *Leguminaceae*). This tree, which is native to Madagascar is an ornamental medium-sized tree, widely planted in avenues and gardens. It is consistently voted among the top five most beautiful flowering trees in the world (Aminu, 2012). *Delonix regia* popularly known as" Pansheke or Apapanla" in

Yoruba language is known in Nigeria as a fast growing tree with usually low, widely spreading branches producing a flat broad crown. The leaves are about 18 inches long with very numerous closely crowded opposite leaflets about 0.5 inches long arranged along 11 – 12 pairs of pinnae. The fruits are large flat pods up to 2 feet long by 2 – 3 inches. They are green and flaccid when young; broad, almost black when dry, hard and woody, hanging conspicuously for a long time on trees and eventually splitting open and constituting a waste to the environment (Aminu, 2012).

Most of the commercial production of biodiesel worldwide uses homogeneous base catalysts, which are corrosive and non-reusable and produces waste that needs to be neutralized in order to mitigate the potential deleterious environmental impact. Heterogeneous catalysis can overcome the limitations of homogeneous catalysis through easy separation and reuse of catalyst. However, mass transfer diffusional resistance becomes prominent in heterogeneous catalysis and thus lowers the rate of reaction. To minimize this resistance, structure promoter or catalyst support plays a vital role because it can provide both maximum surface area and sufficient number of active sites for reaction. (Zabeti, 2009).

The development of low cost renewable heterogeneous catalyst support will act as alternative to homogeneous catalyst, which can further reduce the overall cost of biodiesel and make it competitive with the conventional diesel. Such a novel catalyst support can either be prepared from biomass or waste generated in households. Activated carbon can meet the desirable properties of green catalysts because of its highly effectiveness as catalyst support in liquid and vapor phase reactions (Sumit *et al*., 2015). The appreciable micro-porous surface of activated carbon makes it suitable to be used as catalyst support in transesterification reaction. Hence, conventional homogeneous catalyst like KOH and NaOH can easily be dispersed onto the surface of activated carbon possessing high surface area and low ash content (Sumit *et al*., 2015).

Potassium hydroxide is extensively used, as catalyst in the transesterification of vegetable oils and its applicability is favorable at industrial level due to high activity and low cost. It has been found that nearly 90% conversion can be achieved using potassium hydroxide impregnated palm shell carbon as catalyst in the transesterification of palm oil (Baroutian *et al*., 2010).

Very few researchers have worked on activated carbon as catalyst support in biodiesel production. Some of them include: Leclercq *et al*., (2001), Baroutian *et al*., (2010), and Dehkhoda *et al.*, (2010) and hence the need to explore other sources of activated carbon as is being carried out in this study

Dehkhoda *et al*., (2010) had used a carbon based solid acid catalyst by bio-charring sulfonated material for conversion of canola oil into biodiesel and reported 92% of yield at 60 ^{o}C , alcohol to oil ratio 15:1, catalyst loading 5 wt% and reaction time of 1 hour. Among various carbonaceous supports, flamboyant husks have been chosen as precursor in this work to develop catalyst support due to its availability, zero cost, high surface area and impressive micropore volume (Sarojini and Manavalan, 2012).

2. MATERIALS AND METHODS

The Flamboyant seeds used for this work were collected from ornamental trees (Plates 1a and 1b) grown along Road 1 in Obafemi Awolowo University, Ile-Ife, Osun State, Nigeria The dried fruit pods were split open to collect the seeds (Plate 1c). The impurities were removed using a screen mesh; the seeds were subsequently cleaned and dried in an oven at 110 ^{0}C for 6 hours. Milling using a milling machine followed this. The milled seeds were sieved to reduce the particle size. All chemical reagents used in this work were of analytical grades.

Plate 1a: *Delonix regia* tree in its flowering season

Plate 1b: *Delonix regia* tree showing its fruit pods

Plate 1c: *Delonix regia* seeds

2.1 Proximate Analysis of the Oil Seed and the Flamboyant Husk

The proximate analysis for moisture content, ash content, crude fibre and crude protein of the oil seed was carried out by the methods stipulated in AOAC (2006) while the moisture content, volatile matter, ash content and fixed carbon (weight %) of the flamboyant husks were carried out according to the methods described in ASTM D 121.

2.2 Catalyst Preparation

The flamboyant husks were properly cleaned with distilled water to remove fines and dirt and dried in hot air oven at 105 ^{o}C for 24 hours. Dried samples were broken into smaller pieces and then grinded to reduce the size in the range of 300 - 425 µm. These were placed in horizontal cylindrical shelled muffle furnace (RHF 1600, Bomford, Sheffield, England) maintained at a temperature of 400 ^{o}C for one hour to form carbonized char.

The carbonized char (CC) was impregnated with potassium hydroxide solution by mixing 10 g of it in four different solutions of initial concentration 10 g, 20 g, 30 g and 40 g of KOH per 100 ml of deionized water giving four different KOH to CC ratios of 1:1, 2:1, 3:1, 4:1. Carbonized Char with KOH solution was agitated in an orbital shaker at 200 rpm at constant temperature of 30 ^{o}C and impregnated for 24 hours. The solid catalyst was then calcined in a muffle furnace at 250 ^{o}C, and then dried at room temperature for 24 hours.

2.3 Characterization of Carbon-based Catalyst

The impregnated catalyst (Plate 2) was characterized using Scanning Electron Microscope (SEM), Atomic Absorption Spectroscopy (AAS) and Fourier Transform Infrared (FTIR).

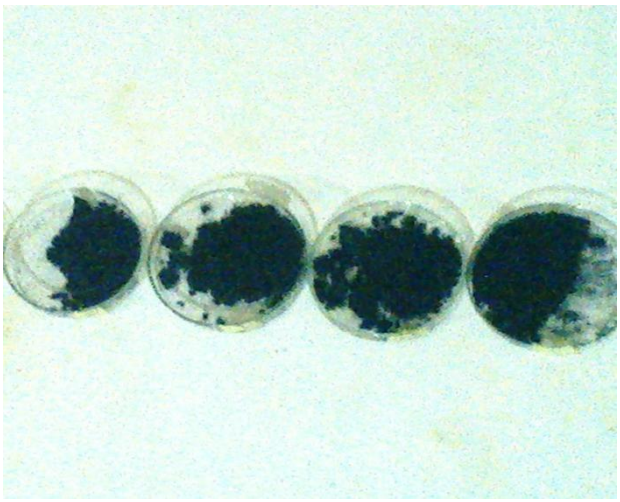

Plate 2: Synthesized Carbon-based Catalyst

2.3.1 Surface morphology

Scanning Electron Microscopy (SEM) analysis was used to study the surface morphology of the catalyst. The topographical images of the sample were captured by SEM machine (ASPEX 3020 Type-I, Japan). About 0.1 g sample was stocked to the mounting plate and was fastened to the stage using screw. Sample was below the top of the drawer. The sample drawer was held in snug with the right hand, the lever pulled down with the left hand and held snuggly for about 20 – 30 mins. At a pressure of approximately $5x10^{5}$ torr, vaccum pump was started and the drawer held up. Magnification was increased to the desired factor. Moreover, brightness /contrast and spot size were adjusted for optimum resolution and signal. The images and spectra obtained were saved.

2.3.2 Elemental analysis

Elemental analysis was carried out using Atomic Absorption Spectroscopy (AAS) with Perkin-Elmer Analyst 400 (Optical Emission Spectrometer).

2.3.3 Functional group analysis

This functional group analysis of the catalyst was carried out using Fourier Transform Infrared (FTIR). Sample weighing 0.1 g was mixed with 1 g of Potassium bromide, spectroscopy grade (Merk, Darmstadt, Germany), in a mortar. Part of this mix was introduced in a cell connected to a piston of a hydraulic pump giving a compression pressure of 15 kPa/cm^2. The mix was converted to a solid disc, which was placed in an oven at 105 ^{o}C for 4 hours to prevent any interference with any existing water vapor or carbon dioxide molecules. Then it was transferred to the analyzer and a corresponding spectrum was obtained showing the wavelengths of the different functional groups in the sample against transmittance. Comparing with those in literatures then identified the peaks.

2.4 Oil Extraction Procedure

A 5-litre Soxhlet apparatus and n-hexane as solvent were used for this study. Initially, the apparatus was charged with a known weight of grinded *Delonix regia* seeds in a muslin cloth placed in a thimble of Soxhlet apparatus. A round bottom flask containing known volume of n-hexane was fixed to the end of apparatus and a condenser was tightly fixed at the bottom end of the extractor. The whole set up was heated up using a water bath maintained at a temperature of 70 ^{o}C. Heating on a heating mantle at temperature of 70 ^{o}C recycled the excess solvent in the oil after the extraction. The quantity of oil extracted was determined gravimetrically and stored in a plastic bottle for further processing. The oil yield was evaluated as the ratio of the weight of the extracted oil to the weight of the oilseed powder sample.

$$\% \text{ Oil Yield (w/w)} = \frac{Weight\ in\ gram\ of\ extracted\ oil}{Weight\ in\ gram\ of\ grinded\ sample} \quad (1)$$

2.5 Physicochemical Properties and Fatty Acid Composition of *Delonix Regia* Seed Oil (DRSO)

The physiochemical properties of the extracted oil such as refractive index, moisture content, viscosity, acid value, saponification value, specific gravity, % free fatty acid (FFA) and pH were determined by the methods of AOAC (1990). All the parameters were determined in duplicate and average values were recorded.

A gas chromatographic (GC) machine from Shimadzu, hyphenated to a mass spectrometer MSD 5975C, England, equipped with an auto-sampler GC789OA and auto-injector was used for the fatty acid composition determination. Oil sample of 25 mg was dissolved into 0.5 ml of n-hexane and the resulting sample solution was filled into the GC auto sampler vial and injected into the GCMS for the analysis and identification of the fatty acid composition of the oil sample.

2.6 Biodiesel Production Process via Heterogeneous Catalysis

A two-step process was used for this biodiesel production. The esterification reaction process was first carried out in order to reduce the FFA of the oil to almost 1% before the transesterification reaction process.

2.6.1 Solid-catalyzed esterification step

Twenty-five milliliters of DRSO was measured into a 250-ml three-neck glass reactor well equipped with a thermometer and a water-cooled condenser and heated to 60 ^{o}C on a magnetically stirred hot plate. Then, 2 g of $Fe_2(SO_4)_3$ was added to the oil in the reactor and stirred for 5 min before the addition of methanol in a methanol:oil ratio of 15:1. The reaction was stopped after 1 h and the esterified oil was transferred into a separating funnel, which was allowed to stand for 2 h to facilitate separation of the methanol-water layers formation at the top, which was decanted. The excess methanol in the pretreated oil was removed by distillation prior to the determination of the acid value.

2.6.2 Solid-catalyzed transesterification step

The same experimental setup described for the esterification process, except that methanol to oil molar ratio (12:1) was employed. The reacting mixture, which consists of the methanol and oil were added together and the temperature was controlled by hot plate magnetic stirrer maintained at 600 rpm and 60 ^{o}C. Two grams of the different ratios of the prepared carbon based catalysts were added to the mixture. After 1 hour of reaction, the mixture was cooled to room temperature and transferred to separating funnel in order to separate the biodiesel produced from the glycerol. The upper layer; biodiesel, was washed with 50 ml deionized water twice and the final organic layer was separated. The biodiesel yield was calculated using Equation 2 for each variation

$$Biodiesel\ yield = \frac{Weight\ of\ biodiesl\ produced}{Weight\ of\ oil\ used} \quad (2)$$

2.7 Optimization Study of *Delonix regia* Biodiesel Production

In this study, an investigation was conducted on the optimization of the transesterification reaction of fatty

acids of DRSO to fatty acids methyl esters (biodiesel) using Response Surface Methodology. The KOH to CC ratio at where the maximum yield of biodiesel was attained in the previous section was used. Response Surface Methodology (RSM) was used to test the influence of methanol-to-oil ratio, reaction time and temperature on the conversion of pretreated DRO to biodiesel. A Box–Behnken factorial design with three factors and three levels including 12 factorial points and three center points was used for fitting a second-order response surface. Selected factors for the transesterification reactions were methanol-to-oil: X_1, temperature (^oC): X_2 and time (min): X_3. Tables 1 and 2 show the independent factors and their levels for Box-Behnken design, and the combinations of three independent variables in a Box-Behnken experimental design. The experiment was designed using Design Expert software package, version 9.0.3 (Stat-Ease Inc., Minneapolis, MN, USA).

The fitted quadratic response model is described by:

$$Y = b_o + \sum_{i=1}^{k} b_i X_i + \sum_{i=1}^{k} b_{ii} X_i^{\,2} + \sum_{i<j}^{k} b_{ij} X_i X_j + e \qquad (3)$$

Where: Y is the response factor (biodiesel yield), b_o is the intercept value, b_i (i= 1, 2,…,k) is the first order model coefficient, b_{ij} is the interaction effect, and b_{ii} represents the quadratic coefficients of X_i and e is the random error.

The experimental data obtained were subjected to multiple regression analysis using Design Expert software package, version 9.0.3 (Stat-Ease Inc., Minneapolis, MN, USA) to obtain the coefficients of the polynomial model of the response. The quality of fit of the model was evaluated using test of significance and analysis of variance (ANOVA).

2.8 *Delonix regia* Biodiesel Characterization

The produced biodiesel propeties such as density, moisture content, viscosity and flash point were carried out according to ASTM standard procedure.

Table 1: Coding of Experimental Factors and Levels for Biodiesel Synthesis.

Variable	Symbol	Coded factor levels		
		-1	0	+1
Methanol-to-oil ratio	X_1	6	12	18
Reaction time (min)	X_2	60	90	120
Temperature (^oC)	X_3	60	65	70

Table 2: Box-Behnken Experimental Design Matrix for the three Independent Variables

Standard run	X_1	X_2	X_3
1	-1	-1	0
2	1	-1	0
3	-1	1	0
4	1	0	0
5	1	0	-1
6	-1	0	-1
7	-1	0	1
8	1	-1	1
9	0	1	-1
10	0	-1	-1
11	0	-1	1
12	0	1	1
13	0	0	0
14	0	0	0
15	0	0	0

3. RESULTS AND DISCUSSION

3.1 Proximate Analysis of the *Delonix regia* Husk

The proximate analysis of *Delonix regia* husk is highlighted in Table 3. It can be observed that the fixed carbon quantity in the biomass was 31.23% while moisture content was 3.03%, volatile matter 58.65% and ash content 7.09%. Thus, the relatively moderate fixed carbon quantity indicates that the husks could be a promising source towards the preparation of carbonized char, which may be used as a catalyst support. This fixed carbon obtained is higher than the one reported by Sugumaran *et al.* (2012) who reported a fixed carbon content of 5.20%.

Table 3: Proximate Composition of *Delonix regia* Husk

Constituents	Percentage composition (%)
Ash content	7.09
Moisture content	3.03
Fixed carbon content	31.23
Volatile matter	58.65

3.2 Analysis of the Synthesized Catalyst from *Delonix Regia* Husk

Elemental analysis of KOH impregnated carbon catalyst, carried out by atomic absorption spectroscopy is as presented in Table 4. Quantitatively, this result showed that maximum percentage of potassium (79.44 %) exists on the surface followed by calcium (16.06%), sodium (2.21%) and magnesium (1.82%). The percentage composition of iron, manganese and zinc were below 1%.

The Scanning Electron Micrograph (SEM) images of carbonized char and KOH impregnated carbon were taken and depicted in Plates 3 and 4. From the micrograph, it is revealed that the impregnated KOH crystal is capable of modifying the surface structure of the carbonized char. The impregnation was effective in developing microspores on the surface and hence, high surface desirable for good catalyst was obtained. Plate 4 shows significant dispersion of KOH onto the surface of the carbonized char confirmed by the blockage of the pores as compared to Plate 3.

Fourier Transform Infrared Spectroscopy (FTIR) was performed to check the presence and change in functional group characteristics in carbonized char and KOH impregnated carbon as presented in Figures 1 and 2. The surface functional groups present in the carbonized char were the bands at 2920.08 cm^{-1} corresponds to aliphatic C-H stretching; two sharp peaks 2359-2342 cm^{-1} correspond to triple carbon-carbon bond bending; a band around 1436 cm^{-1} is due to the presence of aromatic nitro compound NO_2 symmetric stretching; and a band from 875 cm^{-1} is attributed to C-H bending. Figure 2 clearly indicates the presence of hydroxyl groups on the surface of KOH impregnated carbon and confirmed by an elongated broad u-shaped peak at a wavelength of 3215.26 cm^{-1}. Moreover, the bands at 1558.66 cm^{-1} and 1506.50 cm^{-1}, which were not present in the infrared spectroscopy of carbonized carbon may be attributed to the aromatic carbon–carbon stretching vibration and the short peak at 1048.40 cm^{-1} corresponds to –C-H bend. Thus, the presence of hydroxyl group was confirmed from the FTIR study.

Table 4: Elemental Composition of *Delonix regia* Husk

Elements	Concentration (mg/l)	% Maa Fraction
Calcium	30 533	16.06
Iron	705	0.37
Magnesium	3450	1.82
Manganese	125	0.07
Sodium	4206	2.21
Potassium	151 000	79.44
Zinc	60	0.03

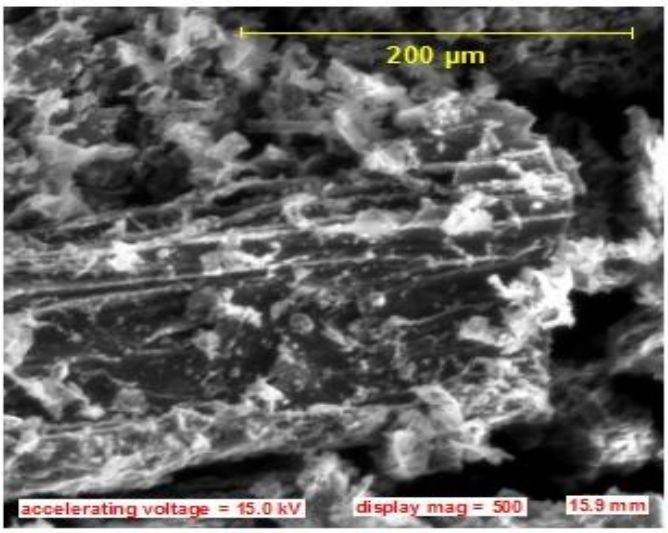

Plate 3: Micrograph of Carbonized Char at 500 magnifications.

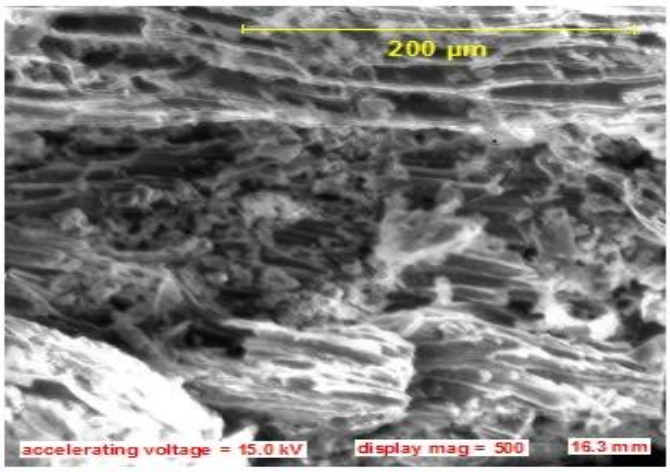

Plate4: Micrograph of KOH Impregnated Carbon at 500 magnifications

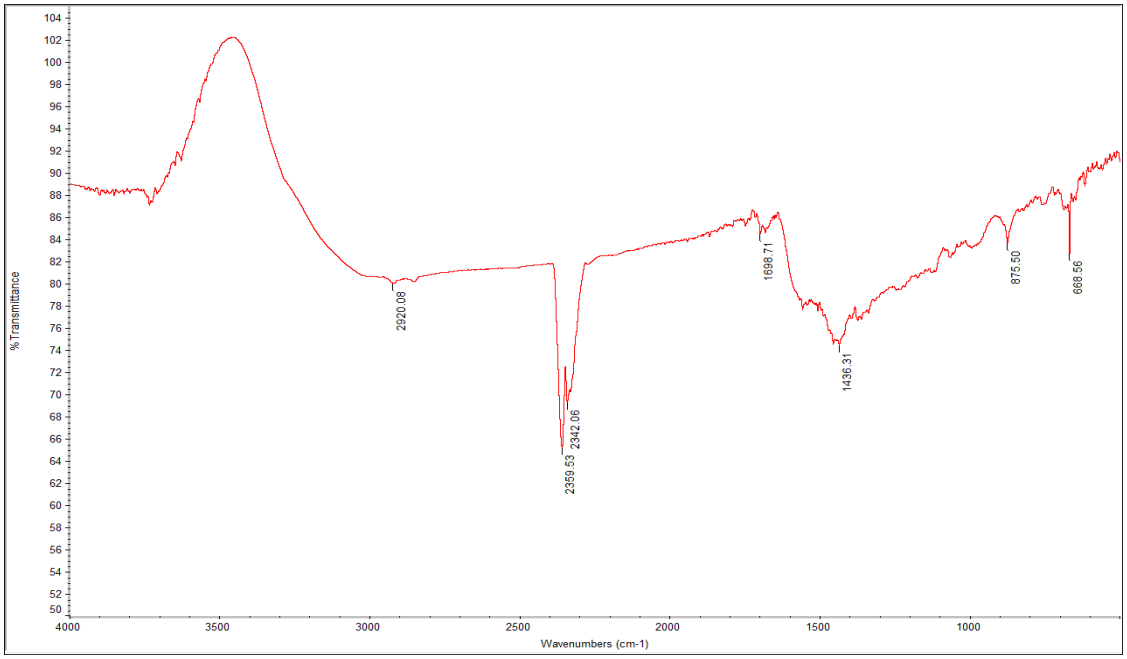

Figure 1: FTIR of Carbonized Char

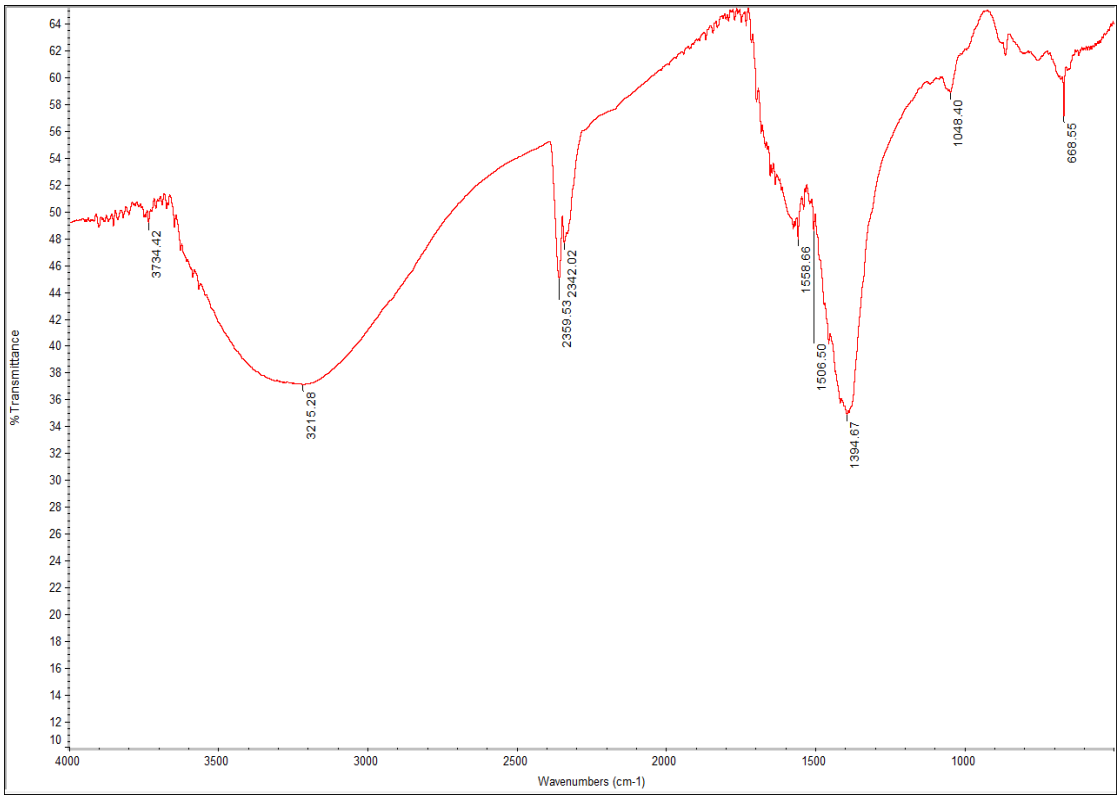

Figure 2: FTIR of KOH Impregnated Carbonized Char

3.3 Quality Characterization of *Delonix regia* Seed Oil (DRSO)

The physical and chemical properties of the oil are as shown in Table 5 and these have been used for the assessment of the quality of the DRSO.

Table 5: Physico-Chemical Properties of *Delonix regia* Seed Oil (DRSO)

Parameters	Mean Values
Colour	Brownish Yellow
State at room temperature	Liquid
Moisture content (%)	0.005
Acid value	19.08
Fatty acid (%)	9.54
Density (25 ^{o}C) g/cm^3	0.8838
Kinematics Viscosity (25 ^{o}C) (mm^2/s)	51.22
Refractive index (30 ^{o}C)	1.4689
Saponification value (mg KOH/ g oil)	172.2
Iodine value (g I_2/100 g)	96.20

3.3.1 Physical Properties of DRSO

It was observed that the oil (liquid at room temperature) obtained was brownish-yellow in colour, having a refractive index of 1.4689, which is very comparable to the refractive indices of 1.442 and 1.4549 reported by Adewuyi *et al.,* (2010) and Krishnan *et al.,* (2015) respectively. The oil also had moisture content of 0.005% with a specific gravity of 0.8838 and kinematic viscosity, which is a measure of the resistance of oil to shear, was 51.22 mm^2/s. Okey and Okey (2014) reported 0.893 for specific gravity and 38.45 mm^2/s for kinematic viscosity.

3.3.2 Chemical Properties of DRSO

The percentage free fatty acid (%FFA) of DRSO in this present work was 19.08%. Adewuyi *et al.,* (2010) reported FFA of 20.8% while Krishnan *et al.,* (2015) reported 9.76% for the oil respectively. The significant difference observed could be due to the variation of species in the oilseed types.

A saponification value of 172.2 mg KOH/g was obtained for DRSO in this work indicating high concentration of triglycerides. The saponification value also suggests that the main fatty acids present in the DRSO were of high molecular mass, which was confirmed by the results from the fatty acid composition. The Iodine value, which indicates the level of unsaturation of oil or a fat (Knothe, 2002), for the DRSO (96.20 g I_2/100 g oil) shows a good level of unsaturation. Krishnan *et al.,* (2015) and Adewuyi *et al*., (2010) reported iodine values of DRSO of 117.46 g I_2/100 g and 127.7 g I_2/100 g respectively.

The European standard as described by the requirements and test methods (EN 14214) suggested maximum iodine value of 120 g I_2/100 g oil for biodiesel. The value obtained for DRSO indicates that it is a good feedstock for biodiesel production. These results showed that the oil was highly unsaturated with the main fatty acids as palmitic (16.366%) and linoleic (83.634%).

The standard also recommends that the linolenic acid and polyunsaturated methyl ester (≥4 double bonds) contents in biodiesel should not be greater than 12% and 1%, respectively (Akintunde *et al*., 2015). This confirms that DRSO with no linolenic acid content and no presence of polyunsaturated fatty acid with ≥4 double bonds should be a good candidate for biodiesel production.

Delonix regia seed oil fatty acid percentage composition was obtained to consist of 16.37% Palmitic acid (C 16:0), 83.63% Linoleic acid, and while stearic, oleic, linolenic acid are detected only in trace amounts.

3.4 Effect of Catalyst Loading on Yield of Biodiesel.

The effect of varying the amount of KOH impregnated in the catalyst on conversion of DRSO into biodiesel was studied**.** The yield of biodiesel was plotted against impregnation ratio as presented in Figure 3. It can be observed that maximum yield of 78% biodiesel was attained at KOH to CC ratio of 3:1 at a catalyst loading of 9%. Sumit *et al.,* (2015) in their work on the transesterification of *Hevea brasiliensis* oil, at a temperature of 60 ^{o}C, methanol to oil ratio of 15 : 1, a time of 60 minutes at 750 rpm, reported a maximum yield of 89.37%, at 3.5 wt% catalyst concentration.

Moreover, Liu *et al*., (2008) studied the conversion of soybean oil to biodiesel using CaO as a heterogeneous catalyst reported a biodiesel yield of 95% when the reaction was carried out for 3 hours using 8wt% catalyst concentration. Garcia *et al*. (2008) also worked on the transesterification of soybean oil using sulfated zirconia with catalyst concentration ranging from 2 - 5wt%. They reported that the highest conversion was achieved with 5wt% catalyst. The relatively lower yield recorded from this study might therefore be as a result of the shorter reaction time.

3.5 Optimization of *Delonix regia* Biodiesel Production

In this optimization study, Table 6 depicts the coded factors considered with experimental results, predicted values as well as the residual values obtained. Design Expert 8.0.3 software was employed to evaluate and determine the coefficients of the full regression model equation and their statistical significance.

Table 7 shows the results of test of significance for every regression coefficient. The results show that the p-values of the model terms are significant, i.e. $p< 0.05$. In this case, the three linear terms (X_1, X_2, X_3), three cross products (X_1X_2, X_1X_3, X_2X_3) and two quadratic terms (X_1^2, X_2^2) were all remarkably significant model terms at 95% confidence level. Figure 4 shows the parity plot of the predicted values against actual values.

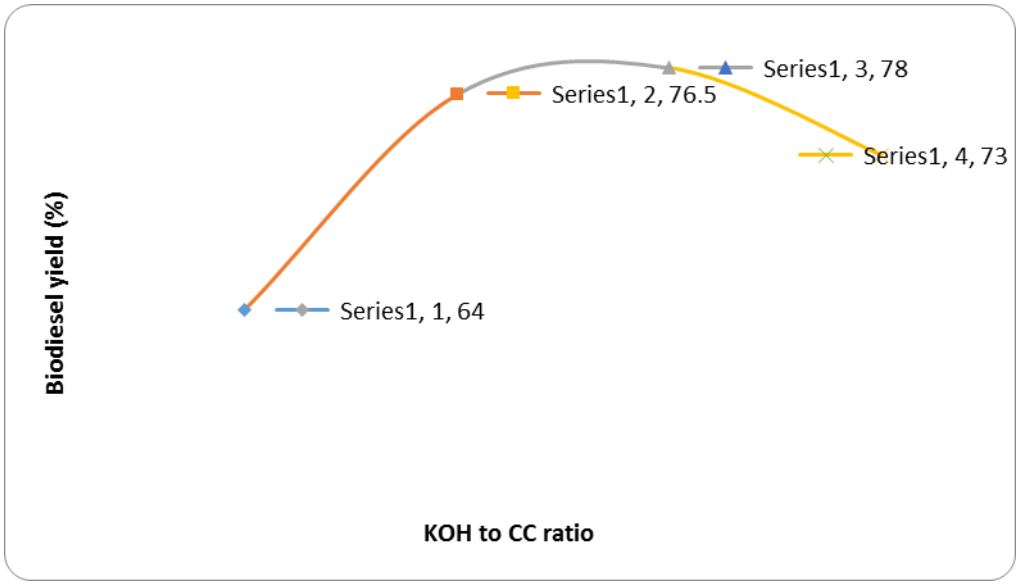

Figure 3: Plot of Biodiesel yield against Impregnation ratio

Table 6: Actual, Predicted Yield and Residual Values for biodiesel production

Std Order	Run Order	X_1,	X_2,	X_3	Experimental Yield % (w/w)	Predicted Yield % (w/w)	Residual
3	1	-1	1	0	69.270	69.179	0.091
11	2	0	-1	1	71.690	71.504	0.186
13	3	0	0	0	80.220	79.443	0.777
5	4	-1	0	-1	67.620	67.525	0.095
15	5	0	0	0	80.220	79.443	0.777
14	6	0	0	0	77.890	79.433	-1.553
12	7	0	1	1	84.070	84.069	0.001
9	8	0	-1	-1	79.540	79.541	-0.001
6	9	1	0	-1	88.150	88.057	0.093
4	10	1	1	0	84.570	84.476	0.094
1	11	-1	-1	0	72.530	72.624	-0.094
10	12	0	1	-1	70.240	70.426	-0.186
2	13	1	-1	0	77.490	77.581	-0.091
2	14	1	0	1	80.360	80.455	-0.095
7	15	-1	0	1	80.640	80.733	-0.093

All p-values are less than 0.05 except X_3^2 implying that the model proves to be suitable for the adequate representation of the actual relationship among the selected factors (X_1, X_2, and X_3).

Table 8 shows the analysis of variance of regression equation model. The model F-value of 1378.58 implied that the model was significant. The data obtained best fit a quadratic model, exhibiting low standard deviation and high "R-Squared" values. The goodness of fit of the model was checked by the coefficient of determination (R^2). Guan and Yao (2008) reported that a R^2 should be at least 0.80 for the good fit of a model. In this case, the R^2 value of 0.9996 indicated that the sample variation of

99.96% for transesterification reaction is attributed to the independent factors (methanol-oil-ratio, reaction time (min) and reaction temperature (^oC) and only 0.04% of the total variation was not explained by the model. The predicted determination of coefficient (pred. R^2) value of 0.9955 is in reasonable agreement with the adjusted determination of coefficient (Adj. R^2) of 0.9989. The "Lack of Fit F-value" of 1.27 implies the Lack of Fit is not significant relative to the pure error. In this case, a non-significant lack of fit is good. Therefore, it could be used in theoretical prediction of the transesterification reaction.

The final equation in terms of coded factors for the Box Behnken response surface quadratic model is expressed in equation 4 below:

$$Y = 80.11 + 5.06375X_1 + 0.8625X_2 + 1.40125X_3 + 2.58500X_1X_2 - 05.2025X_1X_3 + 5.42000 X_2X_3 - 0.66875X_1^2 - 3.47625X_2^2 - 0.2487X_3^2 \quad (4)$$

Table 7: Test of Significance for Every Regression Coefficient

Source	Sum of Squares	df	Mean Square	F-value	P-value
Model	524.52	9	58.28	1378.58	
X_1	205.13	1	205.13	4852.34	<0.0001
X_2	5.95	1	5.95	140.77	<0.0001
X_3	15.71	1	15.71	371.57	<0.0001
$X_1 X_2$	26.73	1	26.73	632.26	<0.0001
$X_1 X_3$	108.26	1	108.26	2560.95	<0.0001
X_2X_3	117.51	1	117.51	2779.55	<0.0001
X_1^2	1.65	1	1.65	39.06	0.0015
X_2^2	44.62	1	44.62	1055.45	<0.0001
X_3^2	0.23	1	0.23	5.40	<0.0001

The low values of standard error (< 0.1) observed in the intercept and all the model terms show that the regression model fits the data well, and the prediction is good (Table 9). The variance inflation factor (VIF) obtained in this study shows that the center points are orthogonal to all other factors in the model.

A graph can provide a visual method to observe responsive value and to test parameter level relation. Figure 5 shows the response surface plots representing the effect of reaction time and methanol/oil ratio interaction on FAME yield while keeping reaction temperature constant at zero level. Figure 6 shows the response surface plots representing the effect of reaction temperature and methanol/oil ratio interaction on FAME yield while keeping reaction time constant at zero level while Figure 7 shows the response surface plots representing the reaction temperature and reaction time interaction on FAME yield while keeping methanol/oil ratio constant at zero level.

The optimal condition values of the independent variables selected for the extraction process were found by applying regression analysis to Equation (4) using the Design Expert software package version 8.0.3 (Stat-Ease Inc., Minneapolis, MN, USA**).** The optimum values were statistically predicted as methanol-oil ratio of 18:1, reaction time of 90 min and reaction temperature of 60 ^oC with a corresponding biodiesel yield of 88.06%.

Applying the optimum values to three independent experimental replicates validated the model and the average value of biodiesel yield obtained was 88.15 %. This is a confirmation of the effectiveness of the RSM model in describing the transesterification reaction.

Table 8: Analysis of Variance (ANOVA) of Regression Equation

Source	Sum of Squares	df	Mean Square	F-value	P-value
Model	524.52	9	58.28	1378.58	<0.0001
Residual	0.21	5	0.042		
Lack of Fit	0.14	3	0.046	1.27	0.4680
Pure Error	0.073	2	0.036		
Cor Total	524.73				

$R^2 = 0.9996$

Adjusted $R^2 = 0.9989$

Predicted R^2 = 0.9955
Adeq Precisor = 122.305

Table 9: Regression Coefficients and Significance of Response Surface Quadratic

Factor	Coefficient Estimate	df	Standard Error	95% CI Low	95%CI High	VIF
Intercept	80.11	1	0.12	79.80	80.42	
X_1	5.06	1	0.073	4.88	5.25	1.00
X_2	0.86	1	0.073	0.68	1.05	1.00
X_3	1.40	1	0.073	1.21	1.59	1.00
$X_1 X_2$	2.59	1	0.10	2.32	2.85	1.00
$X_1 X_3$	-5.20	1	0.10	-5.47	-4.94	1.00
$X_2 X_3$	5.42	1	0.10	5.16	5.68	1.00
X_1^2	-0.67	1	0.11	-0.94	-0.39	1.01
X_2^2	-3.48	1	0.11	-3.75	-3.20	1.01
X_3^2	-0.25	1	0.11	-0.52	-0.026	1.01

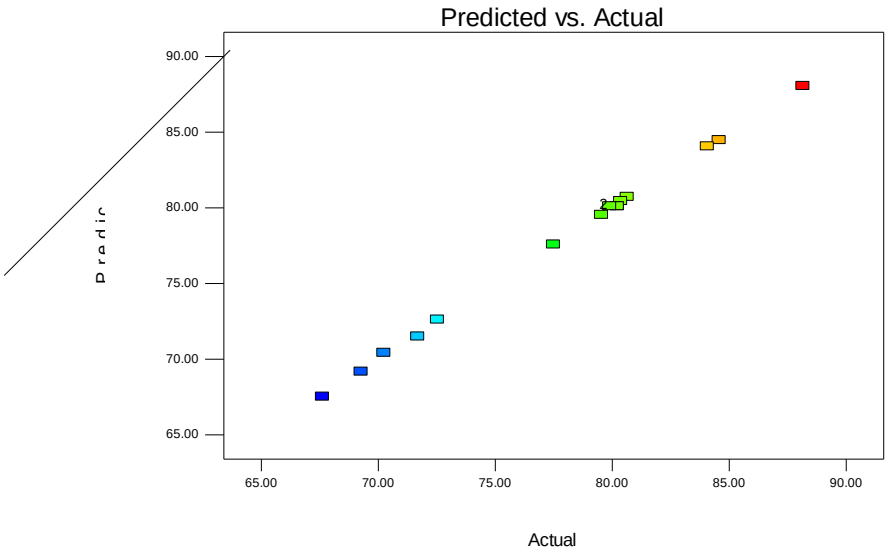

Figure 4: Parity plot showing the predicted values against actual values

.

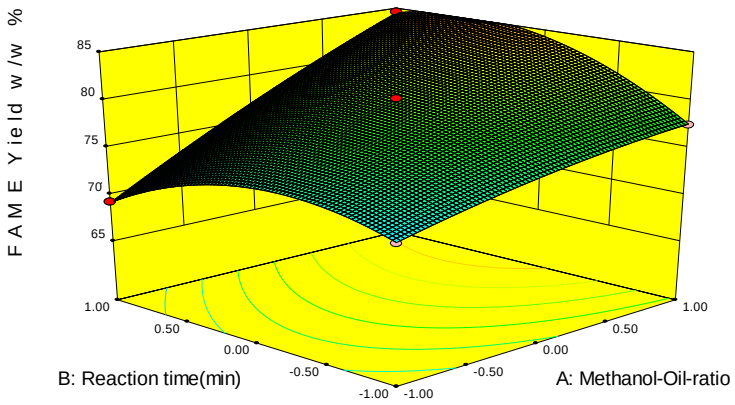

Figure 5: The response surface plot for interactive effect of reaction time and Methanol/Oil ratio on the biodiesel yield.

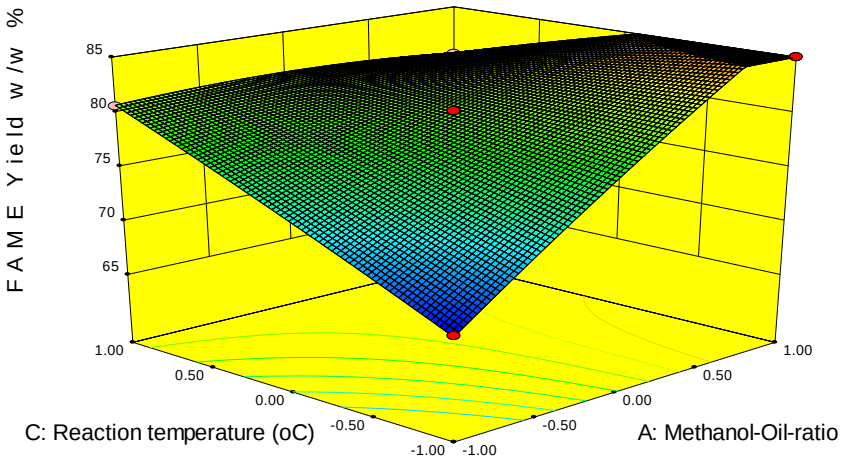

Figure 6: The response surface plot for interactive effect of reaction temperature and Methanol/Oil ratio on the biodiesel yield.

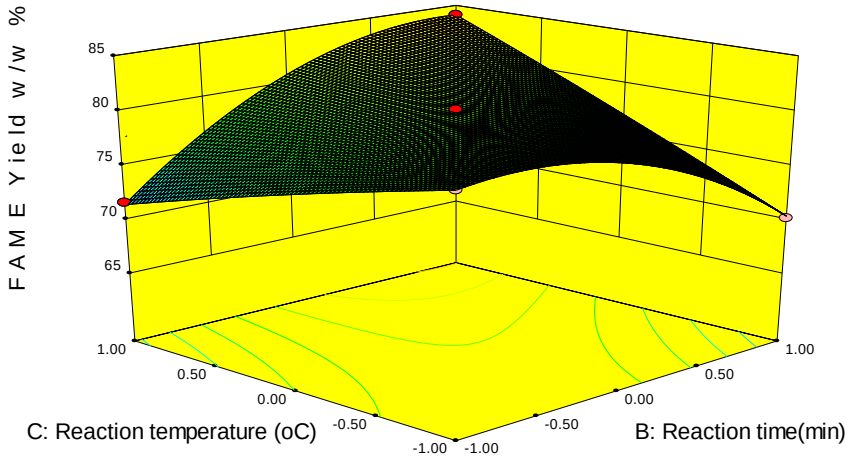

Figure 7: The response surface plot for interactive effect of reaction temperature and reaction time on the biodiesel yield.

3.6 Biodiesel Characterization

The biodiesel prepared from DRSO using carbon based heterogeneous catalyst was characterized to check its properties viz. density, viscosity, flash point, moisture content following ASTM (American Society for Testing and Materials) standards. Numerical values of the properties of generated biodiesel are enumerated in Table 10. It can be seen that all the determined properties are in the range specified by ASTM for biodiesel.

Table 10: Properties of Biodiesel obtained from *Delonix regia* seed oil

Parameters	Mean Values Obtained from The Study	ASTM Biodiesel Specifications
Density at 25°C (kg/m^3)	0.862	0.80- 0.90
Moisture content (%)	0.02	max. 0.05
Viscosity (mm^2/s)	4.5	1.9 – 6.0
Flash point (° C)	128	min 130

4.0 CONCLUSION

The physicochemical properties and fatty acid profile of DRSO indicate that *Delonix regia* oilseeds can serve as a potential feedstock for industrial uses such as biodiesel production, soap making, paint making among others. The results showed that the oil was highly unsaturated with the main fatty acids as linoleic acid (83.63%) and palmitic (16.37%) acid.

The potassium hydroxide catalyst impregnated on the flamboyant husk carbonized char in this study shows a significant performance in catalyzing the conversion of *Delonix regia* seed oil into biodiesel. A maximum biodiesel yield of 78% was obtained at KOH to CC ratio of 3:1 at a catalyst loading of 9% w/w while studying the effect of catalyst loading on the biodiesel yield. The optimum values were statistically predicted as methanol-oil ratio of 18:1, reaction time of 90 min and reaction temperature of 60 ^{o}C with a corresponding biodiesel yield of 88.06%.

This study concludes that *Delonx regia* tree, as a biomass, if properly explored could be feedstock for the non-edible oil as well as a heterogeneous catalyst support for the transesterification of the bio-oil into biodiesel.

REFERENCES

Adewuyi, A., Oderinde, R. A., Rao, B. V. S., Prasad, R. B. N. and Anjaneyulu, B. (2010). Chemical component and fatty acid distribution of *Delonix regia* and *Peltophorum pterocarpum* seed oils. *Food Science and Technology Research,* 16: 565- 570.

Akintunde A. M., Ajala O. S., Betiku E. (2015). Optimization of *Bauhinia monandra* seed oil extraction via artificial neural network and response surface methodology: A potential biofuel candidate. *Industrial Crops and Products*, 67: 387-394.

Aminu M., (2012). Different pre-germination treatments for *Delonix regia* seeds, JORIND 10(2) www.transcampus.org./journals, www.ajol.info/journals/jorind accessed on 12/07/2015.

AOAC – Official methods of analyses of the Association of Official Analytical Chemists (1990). 15th Edition, Washington DC, USA.

Aransiola, E. F., Ojumu, T. V., Oyekola, O. O. and Ikhuomoregbe, D.I.O. (2012). A study of biodiesel production from non-edible oil seeds: A comparative study. *The Open Conference Proceedings Journal*, 3, 18-22.

Annual Book of ASTM Standards 2006, Vol. 5.04, ASTM D 6751-03

Baroutian, S., Aroua, M. K., Raman, A. A. A. and Sulaiman, N. M. N.(2010). Potassium hydroxide catalyst supported on palm shell activated carbon for transesterification of palm oil. *Fuel Process Technology*, 91:1378 – 1385.

Bugaje, I. M., (2006). Renewable Energy for sustainable development in Africa: a review. *Renewable and Sustainable Energy Review*, 10: 603-612.

Bobboi, U., Usman, A. M. and kwanjo, V.A. (2007). Advances in biodiesel production, use and quality assessment. University of Maiduguri, Faculty of Engineering Seminar. 4:1 – 110.

Dehkhoda, A. M., West and A. H., Ellis, N. (2010). Biochar based solid acid catalyst for biodiesel production. *Applied Catalysis*, 382:197–204.

Garcia, C. M, Teixeira, S., Marciniuk, L.L. Schuchardt, U. (2008). Transesterification of soybean oil catalyzed by sulfated zirconia, *Bioresources Technology,* 99: 6608–6613.

Guoqing, C. and Katsuki, K. (2012). Biodiesel production from waste sludge by acid-catalysed esterification. *International Journal of Biomass and Renewable*, 1: 1 - 5

Krishnan, P. R., Kumar, G.R., Sakthi. S. and Swaminathan, K. (2015). Lipase catalyzed biodiesel production from *Delonix regia* oil. *International Journal of Energy Resources and Science and Technology*, Vol. 4, No. 2.

Liu, X., He, H., Wang, Y., Zhu, S., Piao, X. (2008). Transesterification of soybean oil to biodiesel using CaO as a solid base catalyst. *Fuel*, 87(2): 216-221.

Okey E. N. and Okey P. A. (2013). Optimization of biodiesel production from non-edible seeds of *Delonix regia* (Gul Mohr), *International Journal of Bioresource Technology*, 1(1): 1-8.

Sugumaran P, Susan V. P., Ravichandran P, Seshadri S. (2012). Production and characterization of activated

carbon from banana empty fruit bunch and Delonix regia fruit pod. Journal of Sustainable Energy & Environment, 3: 125–32.

Sumit, H. D., Tarkeshwar K., Gopinath H. (2015). Central composite design approach towards optimization of flamboyant pods derived steam activated carbon for its use as heterogeneous catalyst in transesterification of *Hevea brasiliensis* oil. *Energy Conversion and Management*, 100:277-287.

Zabeti M., Daud W., Aroua M. K. (2009). Optimization of the activity of CaO/Al2O3 catalyst for biodiesel production using response surface methodology. *Applied catalysis*, 366:154-9

KINETICS STUDY OF CORROSION OF MILD STEEL IN SULPHURIC ACID USING *MUSA SAPIENTUM* PEELS EXTRACT AS INHIBITOR

***Salami, L[1]. and Umar, M.[2]**

Environmental Engineering Research Unit, Department of Chemical and Polymer Engineering, Lagos State University, Epe, Lagos State, Nigeria

Department of Chemical Engineering, Federal University of Technology, Minna, Niger State, Nigeria

*Corresponding author: SalamiLukumon@yahoo.com

ABSTRACT

The use of inhibitor is a way of minimizing the rate of corrosion of materials. This work was carried out to study the kinetics of corrosion of mild steel in sulphuric acid using Musa Sapientum peels extract as inhibitor. The rates of corrosion of the mild steel were computed using the method of Bradford. The results of the study revealed that the weight loss is inversely proportional to the concentration of the inhibitor. The concentration of inhibitor is also inversely proportional to the rate of corrosion of mild steel but the rate of corrosion of the mild steel is directly proportional to the weight loss of mild steel. The kinetics of mild steel in sulphuric acid using Musa Sapientum peels extract inhibitor followed a first order with rate constant of 4.874 g/mm^2 yr. The half life of the mild steel was found to be 0.142 mm^2 yr/g. This study has shown that Musa Sapientum peels extract can be used as corrosion inhibitor for mild steel in sulphuric acid and the kinetics model for the process is $r = 4.874C$.

Keywords: *Kinetics, corrosion, mild steel, sulphuric acid and Musa Sapientum extract.*

I.0 INTRODUCTION

Corrosion is the gradual destruction of materials usually metals by chemical reaction with its environment which means electrochemical oxidation of metals in reaction with an oxidation such as oxygen (Salami *et al*., 2012). Mild steel is extensively used in industries and as a result corrodes when exposed to various industrial environment and conditions (Inemesit and Nnanake, 2013). The application of inhibitors has been said to be amongst the most practicable ways for protection of metals against corrosion especially in acidic media (Desai and Kapapara, 2009; Fouda *et al*., 2011; Mathur and Vasudevem, 1982: Inemesit and Nnanake, 2013 and Singh *et al*., 2008).

Extensive works on corrosion inhibitors of mild steel have been reported in the literature. Salami *et al*. (2012) studied the corrosion inhibition of mild steel in sulphuric acid using Musa Sapientum peels extract. The results of the study revealed that as the concentration of inhibitor increased, the rate of corrosion decreased. Moreover, Hmimou *et al.* (2012) studied the corrosion inhibition of mild steel in acidic medium using 2–propargyl-5-p-chloro-phenyltetrazole compound as an inhibitor. The studied showed that the compound has a good inhibiting property for mild steel corrosion in acidic medium with inhibition efficiencies value of ninety eight percent. In 2013, Inemesit and Nnanake, investigated the inhibition of mild steel corrosion in hydrochloric acid using ciprofloxacin drug as inhibitor. The investigation revealed that the drug has a promising inhibitory action against corrosion of mild steel in the acidic medium.

Olasehinde *et al*. (2013), studied the thermodynamics and kinetics of *Nicotiana tabacum* extracts used as corrosion inhibitors of mild steel in hydrochloric acid. The study revealed that the inhibition efficiency increased with an increase in inhibitor concentration but decreased with rise in temperature and exposure time. Jerome *et al.* (2014) investigated the kinetics of corrosion of mild steel in petroleum water mixture using ethyl ester of lard as an inhibitor. The investigation proved that the inhibition efficiency increased as the inhibition concentration increased but decreased with temperature. Ejikeme *et al*. (2015) worked on the inhibition of mild steel and aluminium corrosion in sulphuric acid using leaves extract of Africa bread fruit as inhibitor. The work revealed that the corrosion rate decreased in the presence of the extract compound to the one without the inhibitor.

In this work, the aim and objective is to study the corrosion of mild steel in sulphuric using *Musa Sapientum* (banana) peels extract as inhibitor with a view of establishing the kinetics model for the process. The establishment of kinetics model for the corrosion of mild steel in sulphuric acid using *Musa Sapientum* peels

extract as inhibitor will help chemical engineers and corrosion engineers to predict the characteristics and mechanism of the process which justifies this study.

2.0 THEORY

Chemical kinetics is the study of chemical system whose composition changes with time. It major concern is the measurement of reaction rate and their interpretation. The kinetics of corrosion of mild steel in sulphuric acid using *Musa Sapientum* peels extract as inhibitor can be represented by:

$$r = kC^n \quad (1)$$

where r = corrosion rate of mild steel

k = rate constant for the process

n = order of reaction for the process

C = inhibitor concentration

The rate constant has the following characteristics:

- Rate constant is a measure of the rate of reaction. The greater the value of the rate constant, the faster is the reaction.
- At a particular temperature, each reaction has a definite value of the rate constant.
- The value of the rate constant for the same reaction changes with temperature.
- The value of the rate constant of a reaction does not depend upon the concentration of the reactants
- The units of the rate constant depend upon the order of reaction

Linearising equation (1), it gives:

$$\ln r = \ln k + n \ln C \quad (2)$$

From equation (2), a plot of ln r against ln C gives a straight line with slope equal to n and intercept on y axis from which k can be evaluated.

3.0 METHODOLOGY

3.1 Preparation of Coupons

The mild steel used in this study was obtained from Owode market in Ketu area of Lagos State and the analysis of the chemical composition of the mild steel was carried out in the chemistry laboratory of University of Lagos. The chemical composition of the mild steel is presented in Table 1. A sheet of mild steel was cold – cut into small sheets of length 100 mm, width 50 mm and 13 mm thickness. A hole of same diameter was drilled from the top of each coupon, midway along the width for passage of a thread. Each of the five coupons used has a weight of 35 .5 g. The coupon were mechanically polished with silicon carbide abrasive paper, degreased with acetone, washed in distilled water and finally dried.

3.2 *Musa Sapientum* Extract

2 kg of fresh samples of *Musa Sapientum* peels were collected from Ayetoro market in Epe area of Lagos State and were washed carefully with distill water to remove any form of dirt from the peels. The peels were dried under the sun and weighed at intervals until a constant weight of 1.20 kg was attained. The dried Musa Sapientum peels were ground using an industrial scale grinder to powdered form. The powdered Musa Sapientum peels was then run through 200 mesh size sieve to obtain very fine powdered samples and to separate the shaft of the peels. The fine powdered were completely soaked in ethanol solution for 96 h after which the mixture was stirred properly in order to have homogenous solution and then filtered. The filtrate was subjected to evaporation process to remove the ethanol in the filtrate. The inhibitor was obtained in its pure form at the end of the evaporation process. The stock solution of the extract obtained were used in preparing different concentrations of the extract by dissolving 0.2, 0.4, 0.6 and 0.8 g of the extract in 1 litre of 2.0 M H_2S0_4 respectively.

3.3 Weight Loss Method

Five beakers each containing 200 ml of 2.0M H_2SO_4 were labeled A, B, C, D and E. 0.0 , 0.2, 0.4, 0.6 and 0.8 g/L of inhibitor solution were added to the beakers respectively. Each of the five mild steel coupons was put in each beaker and remained in the beaker for 72 hours after which the coupons were removed from the beakers and weighed. It was ensured all solution dropped from the coupons before weighing. The experiments were performed at ambient temperature.

3.4 Measurement of Corrosion Rate

The method of Bradford (1993) is used to calculate the corrosion rate. The corrosion rate is calculated using equation (3):

$$r = \Delta M \times 3.45 \times 10^6 \Big/ \ell A t \quad (3)$$

where ΔM = weight loss (g) of coupon

A = total surface area of the coupon (cm^2)

ℓ = density of the coupon (g/cm^3)

t = time (hours)

The weight loss and total surface area of the coupon are calculated using equations (4) and (5) respectively:

$$\Delta M = M_0 - M_F \quad (4)$$

$$A = 2(LW + WT + LT) \quad (5)$$

where M_0 = initial weight of the coupon

M_F = final weight of the coupon

L = length of the coupon
T = thickness of the coupon
W = width of the coupon

4.0 RESULTS AND DISCUSSION

Table 1 showed the composition of the mild steel used in this study while Table 2 presented the concentration of inhibitor, initial and final weight of coupons as well as loss in weight of the coupons. Table 3 showed the concentration of inhibitor and rate of mild steel coupon while Figure 1 depicted a graph of ln r against ln C.

Table 1. Chemical composition of mild steel used in the study

Element	C	Si	Mn	S	Pt	Sn	Cr	Cu	Fe
Composition (wt %)	0.14	0.2	0.42	0.25	0.85	0.05	0.01	0.05	98.03

Table 2. Initial and final weight of coupons as well as loss in weight of the coupons in different concentrations of Musa Sapientum extract.

Concentration of inhibitor (g/L)	Initial weight of coupon (g)	Final weight of coupon (g)	Loss in weight of coupon (g)
0.00	35.50	35.25	0.25
0.20	35.50	35.32	0.18
0.40	35.50	35.35	0.15
0.60	35.50	35.39	0.11
0.80	35.50	35.42	0.08

Table 3. Concentraion of inhibitor and corrosion rate of mild steel coupons

Concentration of inhibitor (g/L)	r (mm/yr)	ln C	ln r
0.20	10.067	- 1.61	2.3093
0.40	8.3894	- 0.91	2.1270
0.60	6.1522	- 0.51	1.8168
0.80	4.4743	-0.22	1.50

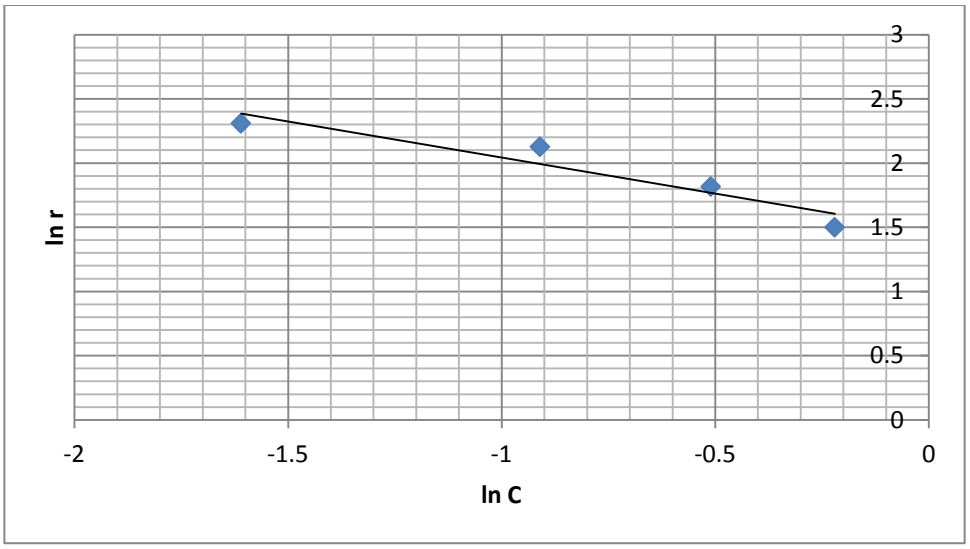

Fig. 1. A graph of ln *r* against ln *C*

It is cleared from Table 2 that the weight loss when zero *Musa Sapientum* extract (inhibitor) was added was the highest. The weight loss decreased as the concentrations

of inhibitor solution increased. This revealed that the concentration of inhibitor is inversely proportional to the weight loss. This is in agreement with the previous works of some researchers who have used inhibitors different from *Musa Sapientum* peels extract (Jerome *et al*., 2014; Inemesit and Nnanake, 2013; Ashassi and Nabavi, 2000; Ebenso and obot, 2010; Eddy *et al*., 2008; Eddy *et al*., 2009 and Kinani and Chtaini, 2007). The rate of corrosion of mild steel in inhibitor solution decreased as the concentrations of inhibitor increased. The rates of corrosion of mild steel in *Musa Sapientum* extract inhibitor solution shown in Table 3 were generated using equation (3). From Table 3, the rates decreased as the concentration of inhibitor increased.

The graph of ln r against ln C shown in Figure 1 was plotted using the values from Table 3. From Figure 1, the slope was approximately 1 which indicated that the order (n) for this study is 1. The rate constant was obtained from Figure 1 to be 4.874 g/mm^2 yr. Hence the kinetics of corrosion of mild steel in sulphuric acid using Musa Sapientum peels extract as inhibitor can be represented as:

$$r = 4.874C \quad (6)$$

For a first order reaction, the relationship between rate constant and half life can be written as (Umoren et al., 2008 and Jerome et al., 2014):

$$t_{1/2} = 0.693/k \quad (7)$$

Hence the half life of the mild steel in sulphuric acid using Musa Sapientum peels extract inhibitor is 0.142 mm^2 yr/g.

5.0 CONCLUSION

This study has shown that the *Musa Sapientum* peels extract can be used as corrosion inhibitor of mild steel in sulphuric acid. The weight loss of mild steel is inversely proportional to the concentrations of the inhibitor. Moreover, the rate of corrosion of mild steel in sulpuric acid is also inversely proportional to the concentrations of the inhibitor. However, the weight loss of mild steel in sulphuric acid is directly proportional to the rate of corrosion of mild steel using *Musa Sapientum* peels extract inhibitor. The kinetics of the rate of corrosion of mild steel in sulphuric acid with respect to the concentrations of inhibitor followed a first order with rate constant of 4.874 g/mm^2 yr with half life of 0.142 mm^2 yr/g.

ACKNOWLEDGEMENT

The authors thank Emeritus Professor A.A. Susu for his mentorship and leadership role in the pursuit of our academic carrier and for establishing Environmental Engineering Research unit of the Department of Chemical and Polymer Engineering, Lagos State University, Epe, Lagos State, Nigeria.

REFERENCES

Ashassi-sorkhabi, H. and Nabavi-Amri, S. A. (2000). ''Corrosion inhibition of carbon steel in petroleum mixture by N-containing compound''. *Acta Chimica Slovenica,* Vol.47(4): 507 – 518.

Bradford, S. A. (1993). "Corrosion control".Van Nostrand, New York.

Desai, P. S., and Kapopara, S. M. (2009). ''Inhibiting effect of anisidines on corrosion of aluminium in hydrochloric acid''. *India Journal of Chemical Technology,* Vol.16(6):486 – 491.

Ebenso, E.E. and Obot, I. B. (2010). ''inhibitive properties, thermodynamic characterization and quantum chemical studies of secnidazole on mild steel corrosion in acidic medium''. *International Journal of Electrochemical Science,* Vol. 5: 2012 – 2035.

Eddy, N. O., odoemelam, S.A. and odiongenyi, A.O. (2008). ''Ethanol extract of Musa acuminate peelas eco-friendly inhibitor for the corrosion of mild steel in acidic medium''. *Advanced national Applied Science*, Vol. 2(1): 35 – 42.

Eddy, N. O., odoemelam, S.A. and odiongenyi, A.O. (2009). ''Inhibitive adsorption and synergistic studies on ethanol extract of Gnetum aricana as green corrosion inhibitor for mild steel in acidic medium''. *Green Chemical,* Vol. 2(2): 111 – 119.

Ejikeme, P. M., Umana, S. G., Menkiti, M. C. and Onukwuli, O. D. (2015). ''Inhibition of mild steel and aluminium corrosion in sulphuric acid by leaves extract of African Breadfruit''. *International Journal of materials and Chemistry,* Vol. 5(1): 60 – 67.

Fouda, A .S., Elewady, G.Y. and El-Haddah, M.N. (2011). ''Corrosion inhibition of carbon steel in acidic

solution using some azodyes''. *Canadian journal on scientific and Industrial Research*, Vol.2(1): 1-18.

Hmimou, J., Rochidi, A., Touir, R., Ebn, M., Rifi, E.H., El Hallaoui, A., Anouar, A. and Chebab, D. (2012). ''Study of corrosion inhibition of mild steel in acidic medium by 2 – propargl -5 –p - chlorophenyltetrazole'' *Journal of Material Environment*, Vol.3(3):543 – 550.

Inemesit, A . A., and Nnanake, A .O. (2013). ''inhibition of mild steel corrosion in hydrochloric acid solution by ciprofloxacin drug'. *International Journal of Corrosion*, dxdoi. Org/10.1155/2013/3016.

Jerome, A.U., Ternenge, J.C., Abubakar, M. and Chigozie, O. (2014). ''Kinetics of the corrosion of mild steel in petroleum water mixture using ethyl ester of lard as inhibitor''. *African Journal of Pure and Applied Chemistry*, Vol. 8(3): 60 – 67.

Kinani, L. and Chtaini, A. (2007). ''Corrosion inhibiton of titanium in artificial saliva containing fluoride''. *Leonardo Journal of Science*, Vol. 6(11): 33 – 40.

Mathur, P.B. and Vasudevan, T. (1982). ''Reaction rate studies for the corrosion of metals in acid''.*Corrosion*, Vol. 38(3): 171 – 178.

Olasehinde, E.F., Olusegun, S.J., Adesina, A.S., Omogbehin, S.A., Momoh-Yahayah, H. (2013). ''Inhibitory action of Nicotiana tabacum extracts on the corrosion of mild steel in acidic medium''. *Nature and Science*, Vol. 11(1): 83 – 90.

Salami, L., Wewe, T.O.Y., Akinyemi, O.P. and Patinvoh, R.J. (2012). ''A study of the corrosion inhibitor of mild steel in sulphuric acid using Musa Sapientum peels extract''. *Global engineers and technologists review*, Vol. 2(12): 1 – 6.

Singh, M. R. and Nabavi-Amri, S. A. (2008). ''The inhibitory effect of diethanolamine on corrosion of mild steel in sulphuric acid medium''. *Portugaliae Electrochemical acta*, Vol. 26: 479 – 492.

TECHNIQUE FOR TREATING WASTEWATER WITH LOCALLY MODIFIED ADSORBENT

[*] Ujile, A. A. and Okwakwam, C.

Department of Chemical/Petrochemical Engineering, Rivers State University, Port Harcourt, Nigeria.

[*]Corresponding Author's email: ujile.awajiogak@ust.edu.ng; Tel: +2348033398876

ABSTRACT

This work details the techniques for heavy metal removal from wastewater using modified adsorbent. An aqueous wastewater sample at standard atmospheric condition and neutral pH from an oil and gas facility effluent section containing amongst other organic and inorganic contaminants was treated. An adsorbent locally produced in the course of this work from a 2000g of dry empty oil palm bunch (DEOPB), an agricultural waste material obtained from a local oil palm processing mill was used to treat the effluent. The adsorbent was subjected to pyrolysis and chemically activated using a 0.1mol hydrochloric acid (HCl). The adsorption behaviors of iron, copper and cadmium were found to obey Pseudo Second Order kinetic model and the Langmuir isotherm model was used to fit the iron, copper and cadmium adsorption isotherm onto the DEOPB activated carbon with their equilibrium capacities agreeing with experimental data except for the lead component that showed no effect. The heavy metals contaminants investigated using this technique was found to have been removed from the wastewater stream in the following percentage removals; iron; 57%, copper; 99.6% and cadmium; 90% but was ineffective in the removal of the lead component as its concentration remained unchanged throughout the experiment. The locally produced activated carbon was subjected to laboratory analysis and its properties (Density; 0.369g/m^3, Particle Size; 0.18mm, Ash Content; 5.73%ww, Porosity; 90%, Surface Area; 691 m^2/g) was found to favorably compare with commercial activated carbon.

***Key words**: biosorbent, kinetics, oil palm bunch, chemical activation*

1. INTRODUCTION

The hazardous and non-degradable inorganic compounds present in industrial effluent waste water causes very severe problems to aquatic environment where they are mostly discharged into. These inorganic compounds/heavy metals present in this effluent stream are termed very hazardous because of their high solubility in water and can early be absorbed by living organisms, thereby causing severe and in most cases hereditary diseases in animals Agunwamba, et al (2002). It is with this resolve that various researches are being carried out to investigate the most safe and economically viable techniques in removing these hazardous compounds from Industrial effluent before discharge into water bodies. The effective removal of these metallic compounds from an aquatic environment is still a big problem as most methods/techniques employed in turn create more problems in releasing chemical sludge to the environment.

Adsorption amongst other methods/techniques like co-precipitation, bio-sorption, electro coagulation, ultra-filtration, employed for the treatment and removal of heavy metals from industrial effluent streams have been found to be less expensive and a better alternative in handling these hazardous compounds Salfuddin and Kumaran (2005).

Heavy metals are mostly generated as effluent waste from various industrial activities such as electroplating and metal surfaces treatment, Printed Circuit Board (PCB) manufacturing, wood processing industries, petroleum refining etc. All these industrial activities produce different heavy metals that can be categorized as hazardous waste requiring extensive waste treatment in large quantities of waste waters, residues and sludge (Sorme and Lagerkvist, 2002) and (Kadirvelu et al, 2001)

The conventional methods of heavy metals removal from industrial waste water include many processes such as chemical precipitation, flotation, adsorption, ion exchange and electrochemical desorption. In the recent past chemical precipitation was the most used methods in removing/treating heavy metal laden effluent waste water. Wang et al, 2004 represented the conceptual mechanism for chemical precipitation as:

$$M^{2+} + 2(OH^-) \leftrightarrow M(OH)_2 \downarrow$$

Where M^{2+} and (OH^-) represent the dissolved metals ions and the precipitant respectively, while $M(OH)_2$ is the insoluble metal hydroxide. The adsorbability of a compound increases with: increasing molecular weight, a higher number of functional groups such as double bonds or halogen compounds, increasing polarisability of the molecules (Ujile, 2014). It has also been established that the adsorption force is the sum of all the interactions between all the atoms. The short range and additive nature of these forces results in activated carbon having the strongest physical adsorption forces of any known materials.

Chemical activation method of producing activated carbon involves the addition of substances such as phosphoric acid, zinc chloride, potassium sulphide etc. which restrict the formation of tar to the carbon aqueous material after it is carbonized. Activated carbon via this method has very good adsorption properties and makes use of low temperature, shorter hold times, simplicity and good porous structure when compared to activated carbon obtained via physical activation (Bernado (1997). It is worth noting that chemical activating agents may include phosphoric acid (H_3PO_4), phosphorus pentoxide (P_2O_5), (Izquierdo et al, 2011); zinc chloride ($ZnCl_2$), (Cronje et al, 2011); potassium hydroxide (KOH), (Krol et al, 2011). But for the purpose of this research work, hydrochloric acid (HCl) was used.

The kinetic models have been used to investigate the mechanism of sorption and the potential rate controlling steps, which is an important tool used in selecting optimum operating conditions for full scale batch processes of adsorption. The notable models that have been used are the Pseudo-First order, Psuedo-second order, intra-particle and Langmuir. The removal of Cu (II) ion from aqueous solutions using sago waste as adsorbent, (Aksu and Isoglu, 2005); phenol removal from aqueous systems by tender leaf refuse (Abdelwahad, 2007); Adsorption of Phenol and dye from aqueous solution using chemically modified date peat activated carbon (Ahmedna, 2007); chromium (VI) removal from aqueous solution and industrial waste water by modified date pal trunk (Sunil et al, 2014); amongst other researchers have all applied this various models in their studies Gupta, et al (2001).

Dhiraj et al, (2008) having studied and investigated the conventional techniques for removal of toxic metal contaminants generated from ever growing industrial activities, found that these techniques were not economical as it was too expensive and will further generate huge quantity of toxic chemical sludge.
Toles, et al, (2000) compared the various techniques in modern day heavy metal contaminated effluent waste water treatment at the same water pH and temperature. At the end of their investigation, they were able to state the limitation of the various techniques and came up with the conclusion that the amount of contaminant removal from stream by adsorption was higher making it (adsorption) the most viable of all. They used almond shell for the activation process.

Sandhga et al, (2003), reviewed the technical feasibilities of various low cost adsorbent for removing heavy metal contaminated waste water which included expensive materials like zeolites, chitesan chemical activated carbon and locally made activated carbon. The results obtained were compared with that of chemical activated carbon showed/demonstrated that these low cost materials has high adsorption capacities and remove more heavy metal impurities Babel and Kurniawan (2003); Sud, et al (2008).

Apart from adsorption method using activated carbon adsorbent for removal of heavy metal contaminants from waste water/aqueous solutions, other methods were also investigated. Nural et, al (2014), studied the removal of heavy metals ions from mixed solutions via polymer enhanced ultra-filtration using standard as water soluble bio polymer. It was found at the end of the study that only zinc, Zn (II) and chromium Cr(III) and (IV) gave higher rejection (ie removed by the starch based polymer recovery than lead, (Pb) which was among the contaminants in the stream, thereby making this techniques deficient as compared to adsorption.
Barakat, (2011), was of contrary opinion as to the work done by Nural et al, (2014), in his article, where recent development and technical applicability of various treatment of heavy metals contaminants removal from industrial effluent waste water such adsorption on new adsorbents, electro dialysis photocatalysis, and membrane filtration was reviewed. His work was able to establish that amongst of the mentioned techniques, only adsorption and membrane filtration handled these contaminants optimally.

Activated carbon with surfaces modification was studied and found to be most suitable for the removal of heavy metals from waste water when compared to conventional and expensive methods (Eleni et al, 2015). Other studies were also able to show that surface modification is of great advantage to adsorption process

as it decreases the adsorption equilibrium time (Chingombe, et al, 2005). Adsorption has advantages over other methods for remediation from waste water because its design is simple. It is sludge-free and can be of low capital intensive except that its manufacturing cost is quite high (Pataule, 2005).

Adsorption process reduces energy consumption, increases yield, selectivity, non-generation of toxic sludge etc. It is for these reasons that researchers have gone into these areas with a view to looking at the ways of producing low cost adsorbent. This research work involves developing minimum cost adsorbent obtained from empty dry oil palm bunch (an agricultural waste) and the mass-transfer process involved in removing these metals from process plant effluent.

2. EXPERIMENTAL PROCEDURE

Materials used in carrying out this research work are dry empty oil palm bunch (DEOPB), effluent waste water and industrial chemicals & apparatus such as magnesium oxide (MgO), Hydrochloric acid (HCl), distilled water, methyl blue, litmus papers, cylindrical beakers, laboratory test sieves, crucibles, burners, gas cylinder, locally manufactured pyrolizer, retort stand, analytical weighing balance, atomic adsorption spectrophotometer (AAS), ball roller mill crusher, industrial oven, thermometer, digital weighing balance.

Methods

Experiment was performed to produce carbonaceous materials from dry empty oil palm bunch (DEOPB) using the methods of pyrolysis before activating using HCl and modified with magnesium oxide. The results obtained were analyzed and studied using computer programming software to determine the kinetic parameters.

Sample Collection and Preparation

Empty Palm bunch

Dry empty oil palm bunches were collected in large quantity from a local palm oil processing mill where they (dry empty oil palm bunch) were littered and thus, constituting environment hazards in Obelle community in Emohua local government area in Rivers State. The sample so collected was properly washed, cut into bits and air dried before taking into the laboratory for further processes to obtain the "activated carbon as the adsorbent, this was subjected to chemical treatment with 0.1mol magnesium oxide as the modifier.

Industrial Effluent Waste Water

Waste water sample was collected from one of the major process industries operating in Rivers State and subjected to chemical analysis.

Sample preparation

The air dried empty oil palm bunch cut into bits was pyrolyzed at controlled temperature range 600 to 800^{o}C in the laboratory of the department of Chemical/Petrochemical Engineering Rivers State University of Science and Technology Nkpolu Port Harcourt, for chemical activation and then modified with 0.5mol magnesium oxide (MgO), which was used as the adsorbent.

Production of the Activated Carbon

Production of the activated carbon adsorbent from the dry oil palm bunch was achieved by the pyrolysis method.

Experimental Procedure

A 10gram of the locally produced activated carbon equivalent to 10cm in length was used as the packed bed in the cylindrical beaker as set up in the laboratory. This was then modified with 10ml of 1.0mol magnesium oxide (MgO). A 150mls of the effluent water sample was then poured into the set-up and with the help of the control valve, the AC packed bed and stopper. The sample was able to retain at various times of interest (10mins, 20mins, 30mins, 40mins, 50mins, 60mins & 70mins) with the entire content emptied out with the concentrate collected after each run and replaced with fresh bed of AC.

The results of the various concentrations of the heavy metals of interest (Iron; Fe, Copper; Cu, Cadmium; Cd, and Lead, Pb) in the aqueous effluent sample before and after the treatment with the locally produced activated carbon adsorbent from dry empty oil palm bunch modified with magnesium oxide was determined using an Atomic Absorption spectrophotometer (AAS), model; Analyst 200 and make; Perkins Elmer at various holding time and packed bed length is shown in the Table 1.

Mass transfer model developed from the removal of heavy metal from effluent stream as computed in course of this research (Okwakwam, 2017) is:

$$C_A = C_{Ao}\left[1 - \frac{2\sqrt{D_{AB}t}}{\pi y}\left(1 - e^{-\frac{y^2}{4D_{AB}\,t}}\right)\right] \qquad (1)$$

where C_A, C_{AO}, D_{AB}, y are the concetration of component A at time t (ppm), initial concentration of component A (ppm), mass diffusivity of component A into the adsorbent B (cm/s), mass of adsorbate adsorbed, (g) respectively.

Equation (1) is the model equation describing the concentrations of the heavy metals remaining in the effluent stream after adsorption with time at constant bed height.

The adsorption rate constants for all the metal contaminants were obtained from the expressions Ho and Meckay, (1998) :

$$\frac{1}{q_t} = \frac{1}{K_2 q_e^2 t} + \frac{1}{q_e} \qquad (2)$$

Characterization of Adsorbent

An elementary analysis was performed on the adsorbent thus produced to determine its physical and activity properties, such as bulk-density particle size, surface area, porosity, ash content, hydrogen and sulphur contents. The following values were obtained;

$$Bulk\ Density = \left(\frac{Mass\ of\ Sample}{Volume\ of\ Sample}\right) \qquad (3)$$

Bulk density = 0.369g/ml

$$Ash\ content = \frac{(weight\ of\ crucible + sample\ before\ ashing) - (weight\ of\ crucible + sample\ after\ ashing)}{(weight\ of\ crucible + sample\ before\ ashing)} \times 100$$

(4)

Ash Content = 5.73% w/w

Particle size: a particle size distribution of 1.18mm to 1.40mm was used for effective adsorption. This was achieved using a "Laboratory Test Sieve, Appeture 1.18/1.40mm, ENDECOTT LTD, London England, No. 66724" after mill crushing using a "Ball Mill Roller Crusher, Pascal Energy Company Ltd, No. 14429" in the Chemical Engineering Laboratory of the Rivers State University of Science and Technology, Nkpolu, Port Harcourt.

Porosity: A 200ml of activated carbon sample was weighed using an Analytical Weighing Balance, Denver Germany, model AE223, 03/2015 and poured into a 300ml cylindrical beaker. A measure of 100ml of distilled water using a measuring cylinder was poured into a calibrated cylinder. The water was then slowly poured into the beaker containing the activated carbon until the water got to the surface of the activated carbon which was obtained to be 270ml. The value was recorded and input into the mathematical expression below:

$$\%Porosity = \left(\frac{Volume\ of\ Water\ added}{Total\ Volume\ in\ AC}\right) \times 100$$

(5)

$$\%Porosity = \left(\frac{270}{300}\right) \times 100$$

% Porosity = 90%

Surface Area: The Brunauer Emmett Teller (BET) theory which is based on the concept that an adsorbed molecule is not free to move over the surface, and which exerts no lateral forces on adjacent molecules of the adsorbate. But that different numbers of adsorbed layers are allowed to build up on different parts of the surface.

$$\frac{P}{V(P^0 - P)} = \frac{1}{CV_m} + \frac{C-1}{CV_m} \cdot \frac{P}{P^0}$$

$C = e^{(q_1 - q_L)/RT}$ (C: constant)

Vm: Monolayer adsorption amount

V: Adsorption amount at the equilibrium pressure P

(Richardson et al, 2002)

P = saturated vapour presure

$$S_{BET} = \frac{Vm}{22414} \cdot 6.02 \times 10^{23} \cdot \sigma \cdot 10^{-18} \qquad (6)$$

N = (Avogadro's number) = 6.025 x 10^{23} molecules/mol

σ = (X-Sectional Area of N_2 Molecule) = 0.162 nm^2

(One molecule of nitrogen adsorbed on alumina or activated carbon occupies 0.162 nm^2)

Most adsorbents are highly porous materials, and adsorption takes place primarily on the walls of the

pores or at specific sites inside the particle. Because the pores are generally very small, the internal surface is in order of magnitude greater than the external area and is often 500 to 1,000 m^2/g (McCabe et al, 2005).

The various sample extracts collected at the different 'run time' intervals were sent to the laboratory and subjected to further analysis using the Atomic Adsorption Spectrophotometer (AAS), Analyst 200 model made by Perkins Elmer to determine the various concentration of the heavy metal of interest (Fe, Pb, Cd, Cu) present in the aqueous sample extracts and the result tabulated below

3. RESULTS

Table 1: Effect Of Time On Adsorption Capacity Of Fe, Cu, Pb, Cd With 1o Cm Bed And 10g Weight Of Adsorbent

S/N	Time (min)	Iron conc (ppm)	Copper conc (ppm)	Lead conc (ppm)	Cadmium conc (ppm)	Length of Activated carbon bed (cm)	Weight of Activated Carbon used (g)
1	0	0.1400	0.0438	0.0038	0.0020	10	10
2	10	0.1100	0.0021	0.0038	0.0020	10	10
3	20	0.0800	0.0021	0.0038	0.0018	10	10
4	30	0.0700	0.0017	0.0038	0.0013	10	10
5	40	0.0600	0.0017	0.0038	0.0009	10	10
6	50	0,0600	0.0017	0.0038	0.0006	10	10
7	60	0.0600	0.0017	0.0038	0.0002	10	10
8	70	0.0600	0.0017	0.0038	0.0002	10	10

Table 1 shows that the adsorbent produced from the dry empty palm bunch could remove iron, copper and cadmium from industrial effluent, except lead.

Table 2: Experiment and model results of heavy metals concentrations in liquid phase

Time (min)	Fe Concentration (mg/L)		Cu Concentration (mg/L)		Cd Concentration (mg/L)	
	Experiment	Model	Experiment	Model	Experiment	Model
0	0.1400	0.1400	0.4380	0.4380	0.0020	0.0020
10	0.1100	0.1114	0.0042	0.2751	0.0018	0.0013
20	0.0800	0.0987	0.0021	0.2060	0.0013	0.0010
30	0.0700	0.0891	0.0019	0.1531	0.0009	0.0008
40	0.0600	0.0810	0.0017	0.1087	0.0006	0.0006
50	0.0600	0.0739	0.0017	0.0695	0.0004	0.0004
60	0.0600	0.0675	0.0017	0.0341	0.0002	0.0003
70	0.0600	0.0616	0.0017	0.0017	0.0002	0.0001

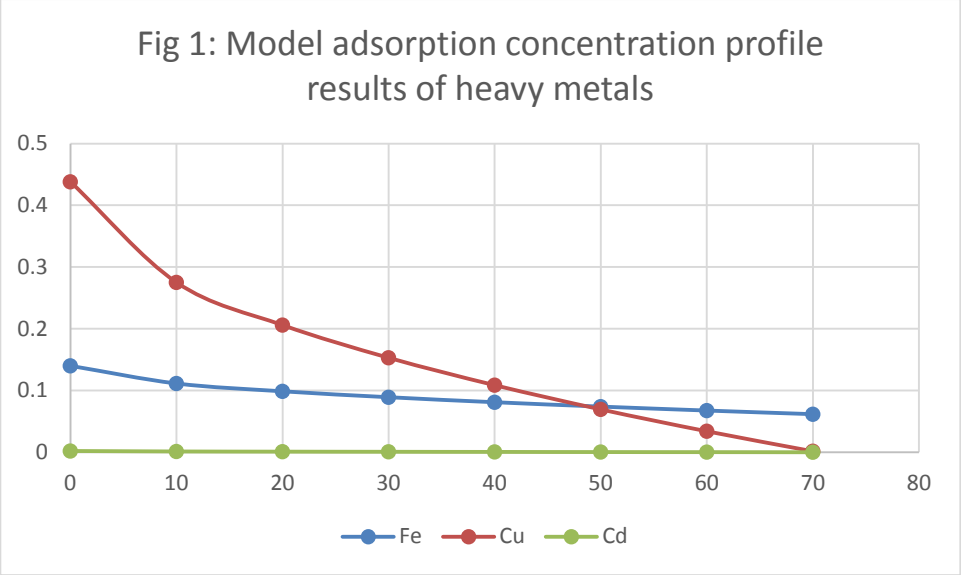

From the profile of the graph in figure 1 it will be observed that the adsorption of cadmium (Cd) onto the dry empty oil palm bunch sourced activated carbon modified with magnessium oxide remained unchanged initially and gradually progressing with time before attaining equilibruim at 60mins. From figure 2 it can be seen that the method is more effective in removing copper components from the wastewater stream as compared to iron and cadmiun. From profile, it was observed that the value of iron concentration in the model decreased at the same rate as that of experiemental value within the first 10 minutes. However, beyond which time the values of the iron concentration for the model were above those of the experiment but the different between the values of model and experiment was relatively insignificaant at the 70th minutes as can be seen in convergence in the profile.

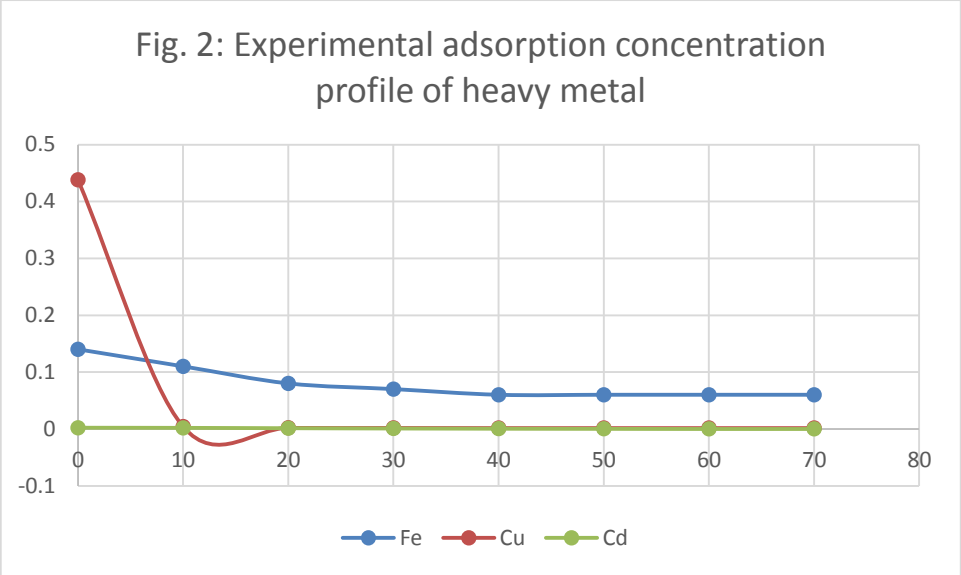

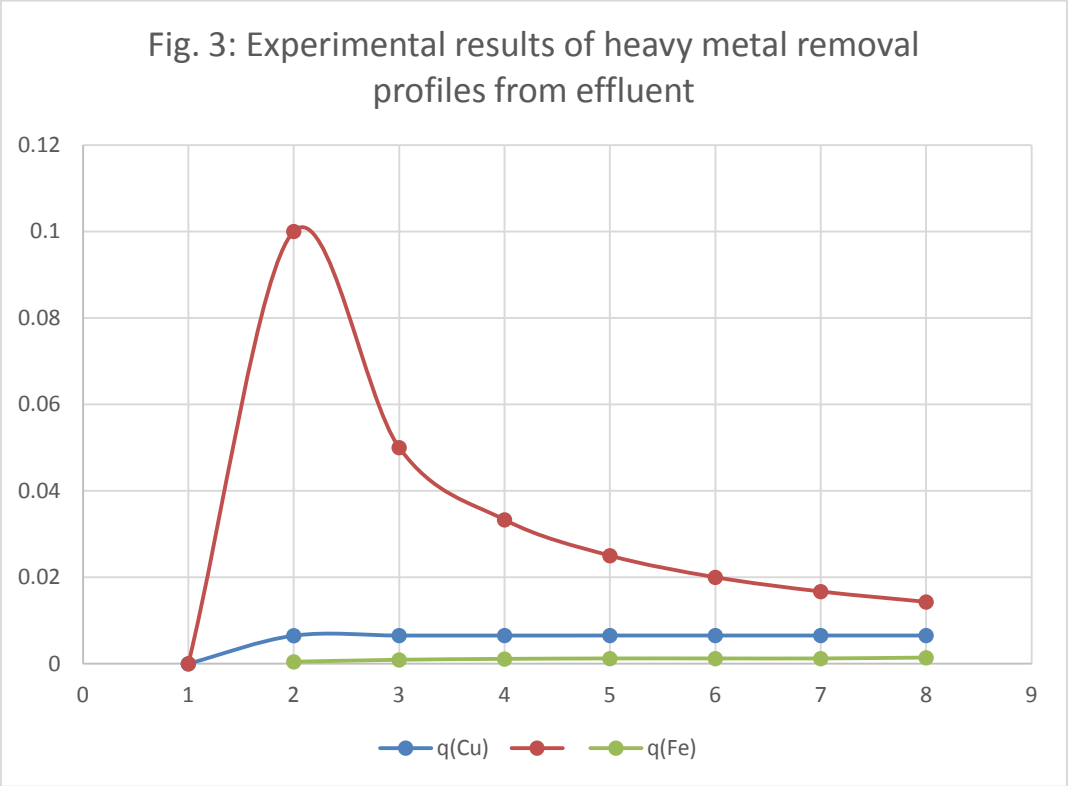

4. CONCLUSION

Based on the results of the experimental study of the techniques for removing heavy metal contaminants from industrial wastewater using activated carbon adsorbent locally produced from dry empty oil palm bunch modified with magnesium oxide, the following conclusions were drawn;

1. The locally produced activated carbon adsorbent was found to possess the characteristics and qualities of a commercial activated carbon when subjected to characteristics analysis.
2. The techniques of using the locally made activated carbon adsorbent modified with magnesium oxide was found to effectively remove iron, copper and cadmium traces but had no effect on the lead contaminant present in the wastewater stream.
3. The type of modifier used was found to play an important role in the kind/type of heavy metal contaminant of interest to be removed present in the wastewater stream.
4. The results obtained from the experimental analysis was validated with the model so developed and was found to favorably predict the progress of the adsorption process with time. The profiles as shown in figures 2, 3 and confirm this assertion.
5. Adsorption technique was found to conform to Pseudo Second Order Kinetics.

Acknowledgement

The authors acknowledge the Department of Chemical/Petrochemical Engineering of the Rivers State University of Science and Technology for the use of laboratory facilities and technologists. We appreciate the support from the Head of Department Dr. C. P Ukpaka that enhanced the completion of the research.

REFERENCES

Abdelwahab, O. (2007). Kinetic and isotherm studies of copper (II) Removal from waste water using various Adsorbent. *Egyptian Journal of Aquatic Research*, 33(1), 125-143.

Agunwamba, J.C., Ugochukwu, U.C & Imadifon, E.K. (2002). Activated carbon from maize cob part 1: removal of lead. *Int. Jour. Eng. Sc. & Tech*., 2.(2), 5-13

Ahmedna, M., Johnson, M., Clarke, S.J., Marshal, W.E & Rao, R.M. (2007). Potential of agricultural by-product

based activated carbon for use in raw sugar decolorisation. *Food Agric*. 75: 117-124.

Aksu, Z. and Isoglu, I. A. (2005): Removal of copper (II) ions from aqueous solution by biosorption onto agricultural waste sugar beet pulp, Process Biochemistry, 40, 3031-3044.

Babel, S., Kurniawan, T.A (2003). Various Treatment technologies to remove arsenic and mercury from contaminated ground water; an overview in: proceeding of the first international symposium on southeast Asian water environment, Bangkok, Chailand, 24-25 October, .433-440.

Bernado, E.C., Egashira, R. & Kawasako, J. (1997). Deco Jourisation of Molasses Waste water using Activated carbon prepared from can bagasse carbon, 35(9); 1217-1221.

Barakat, M.A. (2014), New trends in removing heavy metals from industrial waste water, *Arabian Journal of chemistry*,.4 (4), 361-377.

Binay, K. D. (2007). *Principles of mass transfer and separation processes*. University Tekndogi Petronas Malaysia. PHI Learning Private Limited New Delhi 110001

Chingombe, P., Saha, B. & Wakemam, R.J. (2005). Surface modification and characterization of a coal-based activated carbon. *Carbon*, 43(15), 3132-3143, 008-6223

Chirenj, T., Lena, Q. & Liping (2009). *Retention of Cd, Cu, Pb, Zn by Wood Ash, Line and the Fume Dust Soil*, Water Science Department, University of Florida

Cronje, K.L, Chetty, K., Carsky, M., Sahu, J.N. & Meikap, B.C. (2011). Optimization of Chromium (vi) Soprtion Potential using Developed Activated Carbon from Sugarcane Bagasse with Chemical Activatation by Zinc Chloride. *Destination*, 275(1-3) 276-2814.

Dhiraj, S. F.; Garima, M & Kaur, M.P. (2008). "Agricultural waste material as potential adsorbent for sequestering heavy metal ions from aqueous solution – A review", *Bioresources technology* 99(14): 6017-6022.

Eleni, A.D., George, Z.K, Kostas, S.T, & Kortas. A.M. (2015). "Activated carbon for removal of heavy literature focused a systematic review of recent literature focused on lead and Arsenic, *chemical engineering Journal*, 21: 699-708.

Gupta, V, K., Gupta. M. & Sharma, S. (2001). Process Development for Removal of Lead and Chromium from Aqueous Solution using red-mud- An aluminum industry waste: *Water Res*., 35(5), 1125-1134.

Ho, Y.S. & Mekay, G. (1998). Pseudo-Second-Order Model for sorption process, process Biochem, 34: 451.
http://www.microtrac-bel.com/en/tech/seminar03.html assessed on 26/06/2017.

Izquierdo, M.T, Marline-de-Yuso, A., Rubio, B. & Pino, M.R. (2011). Conversion of Almond Shell to Activated Carbon: Methodical Study of the Chemical Activation based on an Experimental Design and Relationship with their Characteristics. *Biomass Bioenergy*, 35(3): 1235-1244, 961-9534.

Kadirvelu,K., Thamaraiselvi, K. & Namasivayam, C. (2001). *Removal of Heavy Metal from Industrial Wastewaters by adsorption onto activated carbon prepared from an agricultural*

Krol, M., Grygiewicz, G. & Machnikowski, J. (2011). KOH Activation of Pitch-Derived Carbonaceous Materials effect of Carbonization degree Field Process Technol, 92 (1) 158-165, 0379-3820.

McCabe, W. L., Smith J. C. and Harriott, P. (2005): Unit Operations of Chemical Engineering. Seventh Edition. Mc Graw-Hill Chemical Engineering Series. International Edition.

Nural, H.B., Nik, M.N.S. & Mohamed, K.A. (2014). "Removal of heavy metals ions from mixed solution via polymer-Enhance Ultra-Filtration, using starch as a water soluble Biopolymer., Dept of Chem Engineering Univ. of Malaysia, 50603 Kuala Lumpur, Malaysia.

Okwakwam, C. O. (2017): Development of Technique for Heavy Metal Removal from Wastewater using Modified Adsorbent. M.Tech. Dissertation, Rivers State University, 2017

Pataule, D. & Kalibantonga (2005). *Adsorption of Heavy Metals from solution by South African Industrial Clays*, Department of Chemical and Metallurgical Engineering, Tshwane University of Technology of Paints, Varnishes and Lacquers.

Richardson, J. F., Harker, J. H. and Backhurst, J. R. (2002): Coulson & Richardson's Chemical Engineering. Vol. 2. Fifth Edition. Elsevier

Salfuddin, N. & Kumaran, P. (2005). Removal of heavy metal from industrial wastewater using chitosan coated oil palm shell charcoal, Elect. *Jour. of biotech.* 8 (1): 43-53.

Sandhya, B., Tonni, T. & Kurniawan (2003). Low cost adsorbents for heavy metals uptake from contaminated water a review; *Journal of hazardous materials*, 976: 249-243.

Sorme, L, Lagerkvist, R. (2002). Sources of heavy metals in urban waste water in Stockholm. Sci, Total Environ, 278.131-145.

Sud, D. Mahajan, G. & Kaur, M. (2008). Agricultural Waste Materials as Potential Adsorbent solid waste. Bioresour. Technol, 76: 63-65.

Sunil, K.R., Shishir, S, & Dhruv, K.S. (2014). Chromium (iv) Removal from Aqueous solution and industrial waste water by modified Date Palm Trunk, Department of Chemistry, Analytical Research Laboratory, Harcourt Butter Technological Institute, Kanput, India.

Toles, A., Marshal, E., Johnson, M., Wantell, H., Mealoon, A. (2000). Acid activation carbon from almond shells, physical, chemical and adsorptive properties, and estimated cost of product. Bioresourse Technol 71, 87-92.

Ujile, A. A. (2014): Chemical Engineering Unit Operations, Synthesis and Basic Design Calculations. Vol 1 Bomn Prints

Wang, L.K, Vaccani, D.A, Li Hung, Y.T, & Shammas, N.K. (2004). Chemical precipitation: In Wang, L.K., Hung, Y.T., Shammas, N.K. (Eds), physiochemical Treatment Processes, Humana Press New Jersey, 3: 141-198.

LETTERS TO THE EDITOR

Below are the effected complaints based on letters received from authors:

1. The correct title for the paper on Page 95 of the Journal of the Nigerian Society of Chemical Engineers, Vol. 33 No. 1 2018 is **REMOVAL OF CONGO RED AND METHYLENE BLUE DYES IN AQUEOUS SOLUTION USING COPPER (II) OXIDE NANOPARTICLES.**

2. The correct author names for the paper titled **OIL FIELD CHEMICALS FROM MACROMOLECULAR RENEWABLE RESOURCES IN NIGERIA: AN INTEGRATION OF HYDROCARBON RECOVERY WITH BIORESOURCE UTILIZATION page 85** of the Journal of the Nigerian Society of Chemical Engineers, Vol. 33 No. 1 2018 are: **Adewole, J, K.[1], Muritala, K.B.[2] and Sunmonu, M, O.[3]**

ANNOUNCEMENT

As from the next edition (March/April 2019), a fee will be charged for paper review and publication; and this will be borne by the authors. Full details will be given later.

JOURNAL OF THE NIGERIAN SOCIETY OF ENGINEERS
INSTRUCTION TO AUTHORS

1. TYPES OF PUBLICATION

The Journal of the Nigerian Society of Chemical Engineers will publish articles on the original research on the science and technology of Chemical Engineering. Preference will be given to articles on new processes or innovative adaptation of existing processes. Critical reviews on current topics of Chemical Engineering are encouraged and may be solicited by the Editorial Board. The following types of articles will be considered for publication:

a. Full length **articles or review papers**.
b. **Communication** – a preliminary report on research findings.
c. **Note** – a short paper describing a research finding not sufficiently completed to warrant a full article.
d. **Letter to the Editor** – comments or remarks by readers and/or authors on previously published materials.

The authors are entirely responsible for the accuracy of data and statements. It is also the responsibility of authors to seek ethical clearance and written permission from persons or agencies concerned, whenever copyrighted material is used.

2. MANUSCRIPT REQUIREMENTS

a. The **Manuscript** should be written in clear and concise English and typed in Microsoft Word using double spacing on A4-size paper, Times New Romans font and 12 point. A full length article or review should not exceed 15 pages. Margin should be Normal (i.e. 2.54cm for Top, Bottom, Left & Right margins).
b. The **Manuscript** should be prepared in the following format: Abstract, Introduction, Materials and Methods, Results, Discussion, Conclusion, Acknowledgements, and References..
c. The **Manuscript** must contain the full names, address and emails of the authors. In the case of multiple authorship, the person to whom correspondence should be addressed must be indicated with functional email address. As an examples, authors' names should be in this format:
Momoh, S. O., Adisa, A. A. and **Abubakar, A. S.**
If the addresses of authors are different, use the following format:
***Momoh, S. O.[1], Adisa, A. A.[2]** and **Abubakar, A. S.[3]**
Use star * to indicate the corresponding author.

d. **Symbols** should conform to America Standard Association. An abridged set of acceptable symbols is available in the fourth edition of Perry's Chemical Engineering Handbook. Greek letters, subscripts and superscripts should be carefully typed. A list of all symbols used in the paper should be included after the main text as **Nomenclature**.
e. All **Units** must be in the SI units (kg, m, s, N, etc).
f. The **Abstract** should be in English and should not be more than 200 words. The Abstract should state briefly the purpose of the research, methodology, results, major findings and major conclusions. Abstracts are not required for Communications, Notes or Letters.
g. **Citation** must be in the Harvard Format i.e. (Author, Date). Examples are (Smith, 1990) or (Jones et al, 2011). (Kemp, 2000) demonstrated that …..; (Mbuk, 1985; Boma, 1999; Sani, 2000) if more than two authors. (Telma, 2001a), (Telma, 2001b); etc if the citation have the same author and year of publication.
For more information on **Harvard Referencing Guide,** visit http://www.citethisforme.com/harvard-referencing.
h. **References** must also be in the Harvard Format i.e. (Author, Date, Title, Publication Information). References are listed in alphabetical order. Examples are shown below:
Haghi, A. K. and Ghanadzadeh, H. (2005). A Study of Thermal Drying Process. *Indian Journal of Chemical Technology*, Vol. 12, November 2005, pp. 654-663
Kemp, I.C., Fyhr, C. B., Laurent, S., Roques, M. A., Groenewold, C. E., Tsotsas, E., Sereno, A. A., Bonazzi, C. B., Bimbernet, J. J. and Kind M.(2001). Methods for Processing Experimental Drying Kinetic Data. *Drying Technology*, 19: 15-34.
i. **Tables** should contain a minimum of descriptive materials. Tables should be numbered in Arabic numerals (1, 2, 3, etc), and should be placed at the referenced point with captions (centralised) placed at the top of the table.
j. **Figures**, charts, graphs and all illustrations should be placed at the referenced point, numbered in Arabic numerals (1, 2, 3, etc) and incorporated in the text. Caption for Figures should be placed at the bottom of the Figure (centralised). Lettering set or symbols should be used for all labels on the figures, graphs, charts, photographs even when drawn in colours. (Note that figures drawn in colours may be unreadable if printed in black and white).
k. **Equations** should be typed using MS Word Equation Editor and should be centred with number (in Arabic numeral) at the right margin.
l. Wherever possible, **Fractions** should be shown using the oblique slash. E.g. x/y
m. **Footnotes** should not be incorporated in the text.
n. **Acknowledgements** should appear at the end of the paper, before the list of references.

Instruction to Authors

3. SUBMISSION OF MANUSCRIPTS

Manuscripts should be submitted by sending a Microsoft Word document (taking into account the Manuscript Requirements described in section 2 above) to the following email address: nschejournal@yahoo.com and copy stevmomoh@yahoo.com**.**
All correspondences are directed to the Editor-in-Chief using the submission emails addresses: nschejournal@yahoo.com and copy stevmomoh@yahoo.com.

4. ACCEPTED PAPERS

On acceptance, authors will be required to submit a copy of their manuscripts using Microsoft Word by emails to nschejournal@yahoo.com and copy stevmomoh@yahoo.com.

The following additional information should be observed for accepted papers: (i) Typed in Microsoft Word using 1.15 spacing on A4-size paper, Times New Romans font and 10 point; (ii) Margin should be 2.54cm for Top & Bottom; 2.20cm for Left & Right margins; (iii) The abstract should be one column document while the body of the manuscript should be double columns with 0.5cm gutter spacing except some tables and figures that may have to go in for one column document.

5. PUBLICATION

Full NSChE Journal edition in hard copy will be published twice annually.

6. REPRINT

Reprints are available on request at a moderate fee per page. Orders must be placed before the paper appears in Print.

7. READER'S INFORMATION

The papers are wholly the view of their author(s) and therefore the publishers and the editors bear no responsibility for such views.

8. SUBSCRIPTION INFORMATION

The subscription price per volume is as follows:

a. Individual Reader - ₦3,000.00
b. Institutions, Libraries, etc. - ₦5,000.00
c. Overseas Subscription - $100.00

Request for information or subscription should be sent to the Editor-in-Chief through the following emails addresses: nschejournal@yahoo.com and copy stevmomoh@yahoo.com.

9. COPYRIGHT NOTICE

Copyright of published material belongs to the journal

10. PRIVACY STATEMENT

The names and email addresses entered in this journal site will be used exclusively for the stated purposes of this journal and will not be made available for any other purpose or to any other party**.**